Contraintes GPS sur la tectonique actuelle du sud-ouest de la Bulgarie, de la Grèce du nord et de l'Albanie

Krasimir Matev

UNIVERSITÉ DE GRENOBLE

THESIS

To obtain the degree of

DOCTOR OF UNIVERSITY OF GRENOBLE

Speciality: **Terre, Univers, Environnement**

Arrêté ministériel: 7 août 2006

Presented by

Krasimir MATEV

Thesis directed by **François JOUANNE** and **Ivan GEORGIEV**

prepared in **Institut des Sciences de la Terre**
in **Doctoral School TUE**, Chambery, France
and **Department of Geodesy**, **NIGGG – BAS**, Sofia, Bulgaria

GPS CONSTRAINS ON CURRENT TECTONICS OF SOUTWEST BULGARIA, NORTHERN GREECE, AND ALBANIA

JURY

M. Bertrand MEYER	UPMC, Paris	Examiner
M. Pierre BRIOLE	ENS, Paris	Examiner
M. Joseph MARTINOD	LMTG, Toulouse	Reporter
M. Philippe VERNANT	UM2, Montpellier	Reporter
M. François JOUANNE	LGCA, Chambéry	Director of thesis
M. Ivan GEORGIEV	NIGGG, Sofia	Director of thesis
M. Dimitar DIMITROV	NIGGG, Sofia	Examiner
M. Christian BECK	LGCA, Chambéry	Examiner

Chambéry, 2011

Abstract

The investigation in the present thesis is focused on the South Balkan extensional region using Global Positioning System (GPS) technique. The GPS-derived velocity field from 230 episodic and continuous GPS stations covering the territory of Central and East Mediterranean for the period 1996-2009 has been analysed and discussed in the context of present-day tectonic block models.

The geodynamic processes in the region of South-western Bulgaria (SWB) and Northern Greece (NG) are investigated by means of GPS measurements acquired during a 12-year (1996-2008) period. SWB and NG are recently active tectonic and seismotectonic regions. The SWB is the most active seismic region on Bulgarian territory - in the Krupnik – Kresna region occurred in 1904 one of the most catastrophic earthquakes in continental Europe during the last two centuries. NG is an area with widespread seismic activity ranging from low to high with destructive earthquakes of $M \geq 6.0$ from historical to recent times. The obtained velocity field of the Earth's crust is represented by 34 points in SWB and 21 points in NG encompassing the region. The results show southward displacements between 2-10 mm/yr. The strain rates for the region obtained by GPS measurement are presented and discussed along with seismological events. In comparison with the geological and seismotectonic data, the results obtained from GPS observations confirm present-day activity of the fault structures and the dominating extension to the north-south. This extension is in agreement with the regional tectonic model of the East Mediterranean.

The current tectonics of Albania is documented by neotectonics indices and by a large number of medium size earthquakes. The focal mechanisms suggest the existence of current shortening across the external Albanides whereas the internal Albanides are affected by E-W to N-S extension. To investigate the kinematics of the Albanides, we integrate continuous and episodic GPS measurements with focal mechanisms from the Regional Centroid Moment Tensor catalogue. This study has allowed distinguishing a western Albania affected by westward motions relative to the Apulia microplate, illustrating the ongoing collision of external Albanides, whereas inner Albanides present southward motion relative to both

Apulia and stable Eurasia. The Skutar-Pesh Fault Zone, between Dinarides and Albanides, is identified as the possible northern limit of an area including Albania and western Greece, affected by a clockwise rotation relative to Apulia, and also the northern limit of the Balkans (inner Albanides, Macedonia, Bulgaria), affected by southward motion relative to Apulia and stable Eurasia. The other transverse fault zone of the Albanides, the Diber-Elbasani fault, appears to be affected mainly by a moderate extension. Compilation of the published GPS data with our data set allows to identify the external-inner Albanides limit as the western border of the domain (inner Albania, northern Greece, Macedonia, Bulgaria) affected by southward displacements relative to stable Eurasia, whereas Skutar-Pesh fault probably forms also its northern limit.

The analysis of the velocity field for the whole studied area leads to the hypothesis of a continuous deformation to the detriment of local deformation at the borders of stable blocks.

Keywords: *crustal deformations, GPS, time series, East Mediterranean*

Résumé

Dans cette thèse, nous présentons une quantification de la déformation en cours du sud des Balkans et de la Méditerranée centrale et orientale par GPS. Le champ de vitesses a été déduit de l'analyse de données issues de 230 stations GPS permanentes ou épisodiques pour la période 1996-2009. Ce champ de vitesse est analysé et discuté pour essayer de déterminer si le champ de vitesse est continu ou si, au contraire, des blocs stables peuvent être individualisés.

La déformation actuelle du sud-ouest de la Bulgarie et du nord de la Grèce a été particulièrement étudiée à partir de mesures réalisées de 1996 à 2008. Cette région est particulièrement active comme le montre la sismicité historique et en particulier le séisme de Krupnik en 1904 (sud-ouest de la Bulgarie) qui fut un séisme parmi les plus destructeur en Europe continentale au cours des deux derniers siècles. Le nord de la Grèce est quant à lui caractérisé par des séismes destructeurs de $M > 6$.

Les résultats obtenus montrent l'existence de déplacements vers le sud par rapport à l'Eurasie stable s'accroissant du nord (2mm/an) vers le sud de la région étudiée (10 mm/an). Les tenseurs de taux de déformation sont présentés et discutés à la lumière de la déformation exprimée lors des séismes. Ces deux types d'information montrent tous deux une prédominance d'une extension nord-sud en accord avec les données géologiques (présence de grabens est-ouest) et les modèle proposés pour la Méditerranée centrale et orientale.

A l'ouest des Balkans, la déformation actuelle de l'Albanie s'exprime par des nombreux indices néotectoniques et une sismicité importante présentant de nombreux séismes historiques destructeurs. Données géologiques et sismotectoniques montrent d'une part l'existence d'un raccourcissement dans les Albanides externes et d'autre part une extension Est-Ouest et Nord –Sud dans les Albanides internes.

Les vitesses de déplacements ont été quantifiées par GPS continu et épisodiques à partir de 2003. Ces vitesses ainsi que les mécanismes au foyer montrent un raccourcissement en cours à travers l'Adriatique (déplacements des Albanides externes vers l'ouest par rapport à la plaque Apulie), et un déplacement vers le sud des Albanides internes à la fois par rapport à la plaque Apulie et à la plaque Eurasie. La zone de failles Skutar-Pesh entre Albanides et

Dinarides semble former la limite nord de la zone affectée par un déplacement vers le sud par rapport à l'Eurasie comprenant l'est de l'Albanie, la Macédoine, la Bulgarie et la Grèce.

Les Albanides externes semblent être segmentées par des failles transverses actives (faille de Lezhë et de l'ile d'Othoni et du col de Dhërmi) associées à une importante sismicité historique. Les Albanides internes sont affectées à la fois par une extension nord-sud le long de la faille d'Elbasani-Diber, du graben de Korca et par une extension est-ouest de part et d'autre du graben d'Ohrid. Le domaine affecté par un déplacement vers le sud est donc limité à l'ouest par la transition antre les Albanides externes et les Albanides internes et au nord-ouest par la faille de Skutar-Pesh qui se poursuit en Macédoine.

Sur l'ensemble du domaine étudié, notre analyse du champ de vitesse nous conduit à privilégier l'hypothèse d'une déformation continue au détriment d'une déformation localisée aux frontières de blocs stables.

***Mots-clés**: déformations crustales, GPS, séries temporelles, Méditerranée Orientale*

Резюме

Настоящата дисертация фокусира своето изследване върху екстензионния регион на Южните Балкани като използва техниката на Глобалната Позиционна Система (ГПС). Полученото поле на скоростта за периода от 1996 до 2009 г. от 230 епизодични и перманентни ГПС станции, покриващи територия на Централното и Източното Средиземноморие беше анализирано и дискутирано в контекста на съвременните тектонски модели.

Геодинамичните процеси и района на Югозападна България (ЮБ) и Северна Гърция (СГ) бяха изследвани чрез ГПС наблюдения получени за периода 1996-2008г. ЮБ и СГ са съвременно активни тектонски и сеизмотектонски региони. ЮБ е най-сеизмичния район за територията на цяла България. През 1904г. в района на Крупник-Кресна се е случило едно от най-катастрофалните земетресения на континентална Европа за последните две столетия. СГ е район с широко разпространена сеизмичност от порядъка между ниска и висока сеизмичност с деструктивни земетресения с магнитут $M \geq 6.0$ в историческо и сегашно време. Полученото поле на скоростта на Земната кора представено от 34 точки за ЮБ и 21 точки за СГ покриващи района. Резултатите показват премествания в посока юг между 2-10 мм/г. Получените напрежения получени от ГПС измерванията за изследвания район са представени и дискутирани заедно със сеизмоложки събития. В съответствие с геоложки и сеизмотектонски данни получените ГПС резултати потвърждават съвременната активност на разломните структури и доминираща екстензия в посока от север към юг и са в добро съгласие с регионалните тектонски модели на Източното Средиземноморие.

Съвременната тектоника на Албания е представена от неотектонски процеси която се характеризира с голям броя силни и средни земетресения. Фокалните механизми показват съществуването на компресия настъпваща във външните Албаниди докато вътрешните Албаниди са под влиянието на екстензия в посока от И-З до С-Ю. За изследването на кинематиката на Албанидите са използвани ГПС наблюдения от перманентни станции съшито както и данни от кампании заедно със фокални

механизми взети от каталога на Регионалния Центроиден Моментен Тензор. Това изследването позволява да се разграничи влиянието на Апулийската микроплоча върху западна Албания породено от движение в посока запад представено с съществена колизия върху външните Албаниди, и от друга страна вътрешните Албаниди представят движение в посока юг спрямо Апулия и Евразия. Скутар-Пеш разломната зона, между Динаридите и Албанидите се явява вероятната северна граница на област включваща Албания и Западна Гърциям която е повлияна от завъртане по часовниковата стрелка спрямо Апулия и също така северна граница на Балканите (вътрешни Албаниди, Македония, България) повлияни от югозападно движение спрямо Апулия и Евразия. Друга възседна разломна зона на Албанидите, Дибер-Елбасани разлом, изглежда да е повлияна главно от средна екстензия. В комбинация с други публикувани ГПС данни, резултатите позволяват да се идентифицира външни-вътрешни Албаниди, като западна граница на областта (вътрешни Албаниди, Северна Гърция, Македония, България) повлияна от премествания в посока юг спрямо Евроазиатската плоча, докато разлома Скутар-Пеш формира вероятната северна граница.

Ключови думи: *деформации на земната кора, GPS, временни редове, Източно Средиземноморие*

Acknowledgements

I would like to express my gratitude to my supervisors, Associate Professor François Jouanne and Associate Professor Ivan Georgiev for their guidance and support during my study. Special thanks to Professor Pierre Briole from ENS, Paris and Associate Professor Dimitar Dimitrov from NIGGG-BAS, Sofia, who gave me the opportunity to start this doctorate research and helped me in its realization.

I would like to thank the entire staff of the Laboratory of Alpine Belts Geodynamics, University of Savoie, Chambery, France and the Department of Geodesy, NIGGG – BAS, Sofia, Bulgaria.

I gratefully acknowledge the scholarship provided by the Ministry of National Education (France) and the Ministry of Education, Youth and Science (Bulgaria). Many thanks to the responsible institutions and individuals from IGS, EPN, UNAVCO, RING, HemusNet, Corinth, Albania, Greece, Macedonian Agency of Cadastre that support the GPS data used in the present study. Most of the figures were obtained by employing the GMT freeware package by Wessel and Smith (1998).

The study was accomplished in the framework of the bilateral project RILA (3/29, 2007-2008) between Bulgarian Ministry of Education, Youth and Science and Ministère de l'Enseignement Supérieur et de la Recherché, France.

Gratitude to Maya Ilieva, Dr. Georgi Marinov, Dimitar Georgiev, Dr. Antonios Mouratidis, Dr. Aurélien Van Welden, Dr. Eva-Luz Garcia-Lara, Dr. Riccardo Vassallo and Pascale Bascou for their friendship, encouragement and inspiring discussions throughout the rough times during the doctorate.

I am deeply grateful to my lovely wife Radost Mateva for her great support, encouragement and patience during my PhD study.

Contents

List of figures

List of tables

Chapter I

Introduction

Most of the studies in the East Mediterranean focus on the area to the south of the North Anatolian fault (Figure 1.1) and its westward continuation to one of the most rapidly deforming Aegean region (20-35 mm/yr). Not so much is known about the active deformation in the regions to the North. The South Balkans extensional region (SBER) is situated to the north of the west part of the North Anatolian fault zone and to the south of a poorly defined boundary that extends from North Bulgaria to the west of the Adriatic coast (McKenzie, l972; Burchfiel et al., 2006, 2008; Kotzev et al., 2006, 2008).

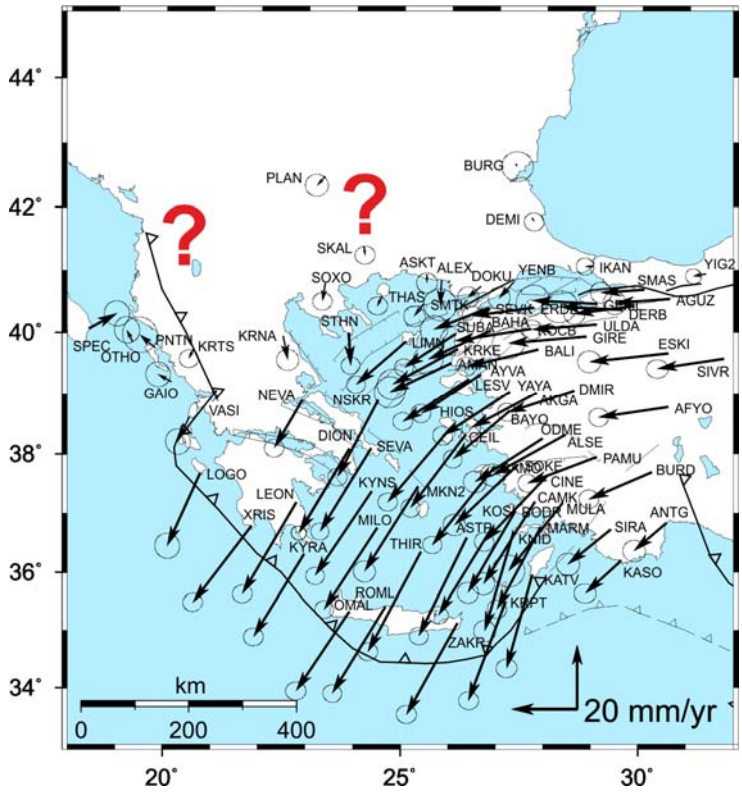

Figure 1.1. *GPS horizontal velocities in a Eurasia-fixed reference frame for the period 1988-1997 published by McClusky et al., (2000).*

South-west Bulgaria and North Greece are part of the most deformational system in the East Mediterranean. Several publications have been made in the last 30 years based on seismological data, active fault distributions and seafloor bathymetry in order to study better tectonic evolution in the East Mediterranean region (McKenzie, 1972, 1978; Le Pichon and Angelier, 1979, 1981; McKenzie and Jackson, 1983; DeMets et al., 1990; Taymaz et al., 1991; Jestin et al., 1994; Goldsworthy et al., 2002). The current kinematics of the south part of the South Balkans region and the Aegean has became better known due to the availability of the GPS (Billiris et al., 1991; Le Pichon et al., 1995; Davies et al., 1997: Clarke et al., 1998; Cocard et al., 1999; Briole et al., 2000; McClusky et al., 2000; Kotzev et al., 2001; Ayhan et al., 2002; Meade et al., 2002; Flerit et al., 2003; Le Pichon et al., 2003; Kotzev et al., 2006; Burchfiel et al., 2006; Georgiev et al, 2006). The present thesis describes horizontal movements and strain rates in the region of SWB and NG, obtained by GPS observations for the period 1996-2008. The data in SWB are collected from a geodynamic network which was established by Central Laboratory of Geodesy at the Bulgarian Academy of Sciences (CLG-BAS) for monitoring of present-day crustal motion on the territory of SW Bulgaria. The points of the network cover the main tectonic structures in the region and have been selected after geological study of the arrea. The present study gives detailed information on the displacements in SWB and especially in NG where a lack of sufficient GPS observations exists so far.

The current tectonics in Albania are characterized by significant microseismicity, small and medium earthquakes and a few large events as shown by the occurrence of six earthquakes with Ms magnitudes exceeding 6 during the last century (1905, Shkodra earthquakes Ms 6.6, 1911 Ohrid lake earthquake Ms 6.7, 1920 Tepelena Ms 6.4, 1926 Durres earthquake Ms 6.2, 1967 Dibra earthquake Ms 6.6 and 1979 Montenegro earthquake Ms 6.9). The focal Mechanisms (Sulstarova et al., 1980, Louvari et al. 2001, Pondrelli et al., 2002, 2004, 2006 and 2007), as well as the neotectonic studies (Aliaj et al, 2000; Carcaillet et al, 2009) underline the existence of a current E-W shortening across the external Albanides whereas the internal Albanides experience an E-W to N-S extension (Tagari et al., 1993). The Albanides are crossed by two transversal faults, the Vlora-Elbasani-Dibra and the Shkodra-Pesh (Scutari-Pesh) fault zones (Roure et al., 2004). The latter fault zone seems to be the north boundary of the Albania-Northern Greece zone characterized by NNW-SSE structural direction and by the significant post Miocene rotation as it is shown by Speranza et al., 1995 and van Hinsbergen et al., 2005. To the North of the Scutari-Pesh or Shkoder-Pesh fault, the Dinarides have not experienced such rotation and they are characterized by NW-SE structural directions.

Chapter II

Tectonic settings

2.1. Eastern and Central Mediterranean

The tectonic settings of the Mediterranean Sea are characterised mainly by the collision of the Arabian and the African plates with the Eurasian plate (McKenzie, 1970; Jackson and McKenzie, 1984; 1988). In a generalized scheme, the major tectonic processes occured within the large-scale kinematic framework of the Mediterranean-Alpine region and

Figure 2.1. *Geodynamic framework of the Mediterranean region. The major tectonic structures are adopted from Hollenstein 2006. The arrows represent plate motion relative to Eurasia (McClusky et al., 2000). NAF: North Anatolian Fault; EAF: East Aegean Fault; NAT: North Aegean Trough; KFZ: Kefalonia Fault Zone; GDZ: Gargano–Dubrovnik zone;*

can be described as a consequence of the sea-floor spreading in the Atlantic Ocean, the Read Sea and the Gulf of Aden. The higher spreading rates in the South Atlantic as compared to those in the North Atlantic induces a gradual counter clockwise rotation of the African plate, resulting in a north-westward directed push against Eurasia (Plag et al., 1998). The Africa-Eurasia convergence started in late Cretaceous (~90 Ma ago) (Dewey et al., 1989), causing compression and shortening between those two plates. More than 1000 km of African lithosphere has been subducted since that time. Figure 2.1 illustrates major tectonic regime in the Mediterranean. The observation of the topography and bathymetry and the distribution of the seismicity in the Mediterranean (Figure 2.1 and Figure 2.2) reveals that the convergence regime is manifested by the continental collision in correspondence of the Magrebides, the Alps, and further east the Dinarides, Albanides further to the east until Hellenides in Greece, and through two fronts of the subduction along the Calabrian Arc and Hellenic Arc.

2.1.1. Eastern Mediterranean

The region of the Eastern Mediterranean is characterized as a very complex region in the aspect of kinematics and dynamics because of the wide variety of tectonic processes including: (1) continental collusion with various stages such as Zagros, Caucasus and Black Sea (Figure 2.1), (2) subduction of oceanic lithosphere and the associated back-arc spreading as Cyprus, Hellenic, Calabrian Arcs, Aegean and Tyrrhenian Seas, (3) continental extension in the western Turkey, Marmara Sea, Aegean extensional domain and Gulf of Corinth, (4) continental “escape” of Anatolian plate, (5) major continental strike-slip faults such as right-lateral strike-slip motion along the North Anatolian fault (NAF) into the North Aegean Trough (NAT), the left-lateral strike-slip of the East Anatolian Faults (EAF), the left-lateral strike-slip of the Dead Sea Fault and the right-lateral strike-slip along the Kefalonia Fault Zone (KFZ) into the Ionian Sea, (6) a variety of smaller-scale processes associated with African-Arabian-Eurasian plate interactions. All of these processes are contained within an area with linear dimensions of roughly 2000 km.

The tectonic plate models (DeMets et al., 1990; Jestin et al., 1994) based on geological and seismological analyses show that the Arabian plate moves in north-northwest direction with respect to the Eurasian one with a velocity of about 18-25 mm/yr, averaged for a period of 3 million years. These models also show that the African plate moves to the north with respect to the Eurasian one with a velocity of about 10 mm/yr.

Figure 2.2 shows the seismicity with magnitude larger than 3 in the Mediterranean region for the period 1973-2008. It clearly demonstrates that Aegean Sea is presently the most

active area of the Mediterranean-Alpine zone at the present. Apart from this concentration of seismicity around the Aegean microplate, the distribution of the earthquakes outlines mainly

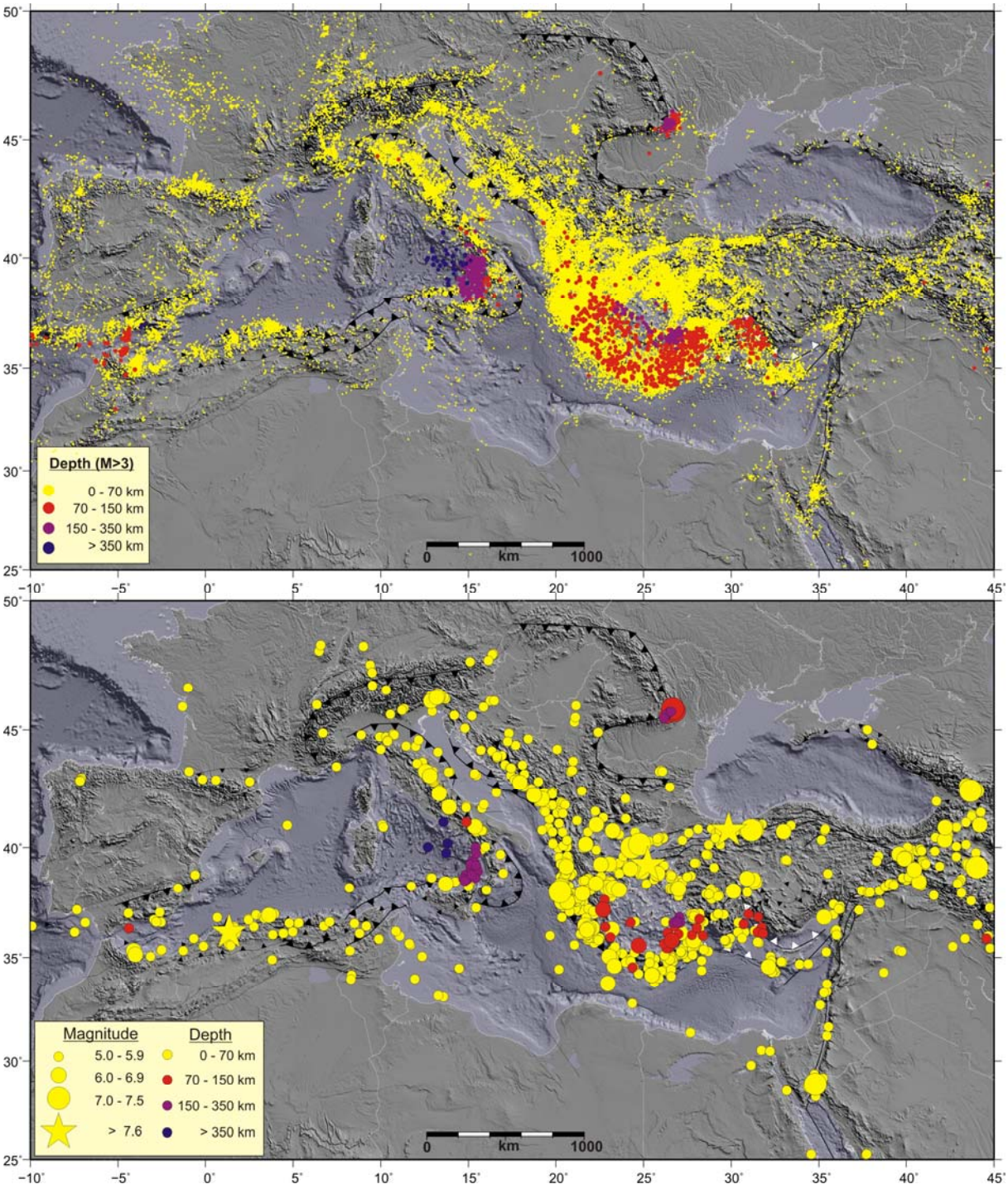

Figure 2.2. *Seismic events of the Mediterranean for the period 1973-2009 according to USGS-NEIC (National Earthquake Information Center of the U.S. Geological Survey,* http://neic.usgs.gov/neis/epic/epic_global.html*). Top: earthquakes with magnitude M≥3; Bottom: earthquakes with magnitude M≥5.*

the following orogenic belts: the Betics, the Pyrereenes, the Alps, the Apennines, the Dinarides and the Hellenides. Most of these areas are characterized by occurrence of shallow earthquakes. Deep earthquakes are observed in relation with subducted African slabs, mainly in the Aegean and the Tyrrhenian back-arc basins also in the area of Cyprus Arc. There is a cluster of deep earthquakes in the eastern Carpathians connected to the deformation of a vertical slab below the Vrancea area.

The highest concentration of large (M>6) and very large (M>7) earthquakes is observed along the continuation of the boundary between the Anatolian and Aegean plates and the Hellenic arc (Figure 2.2). In Eastern and Northern Turkey, the seismic activity is primarily associated with the East Anatolian transform Fault and the North Anatolian Fault. The region around the Hellenic arc exhibits the highest tectonic movements related to the continental Europe – 30-35 mm/yr (McClusky et al., 2000). The seismic activity in the North Aegean region and East Turkey is associated mainly with the North Aegean Trough and the North Anatolian Fault.

2.1.1.1. Aegean region

The Aegean region is one of the most rapidly deforming parts of the continents, with velocity differences of 20–40 mm/yr developed across its 700×700 km extent. The region has a prominent place in the study of continental tectonics because there are good records of seismic activity and Quaternary faulting; many of the active faults have limestone footwalls that resist erosion, so form prominent scarps (e.g., Goldsworthy and Jackson, 2000, 2001), and the record of large earthquakes ($Mw \geq 5.8$) is reasonably complete over the past 120 years (Ambraseys and Jackson, 1990; Jackson and McKenzie, 1988; Shaw and Jackson, 2010). These observations, along with geodetic measurements of crustal displacements on the time scales between a century (Billiris et al., 1991; Davies et al., 1997; Veis et al., 1992) and a decade (e.g., Avallone et al., 2004; Briole et al., 2000; Clarke et al., 1998; Hollenstein et al., 2008; Kahle et al., 2000; McClusky et al., 2000; Reilinger et al., 2006) have contributed importantly to the development of ideas about the kinematics and dynamics of continental deformation.

Recent studies of the kinematics of the region, particularly those using the Global Positioning System (GPS) to measure crustal velocities, have interpreted the tectonics in terms of the relative motions of rigid microplates or blocks (e.g., McClusky et al., 2000; Nyst and Thatcher, 2004; Reilinger et al., 2006). Early studies of the kinematics, however, which were based largely upon the evidence from earthquake focal mechanisms and active faulting,

recognized the relative motion of rigid bodies, or microplates, but also emphasized that significant parts of the region deform in a diffuse fashion (e.g., Jackson and McKenzie, 1988; McKenzie, 1970, 1972); see Le Pichon et al. (1995) for a comparable view based on geodetic velocities. Other geodetic studies of the kinematics suggested that a large proportion of the crust of the region is straining at several tens of nanostrain (nstrain) per year (e.g., Billiris et al., 1991; Clarke et al., 1998; Davies et al., 1997; Hollenstein et al., 2008). Analysis of this distributed strain has generated several important insights into continental deformation, for example the relations between normal faulting, elevated heat flux and subsidence are now understood in terms of distributed thinning of the lithosphere (McKenzie, 1978a, 1978b). Equally, the relations among slip vectors of earthquakes, paleomagnetic rotations, and finite displacements on faults can be explained by analyzing how crustal blocks accommodate a velocity field that is coherent over a length scale much larger than the blocks themselves (e.g., Jackson et al., 1995; McKenzie and Jackson, 1983, 1986; Taymaz et al., 1991). The predominantly westward-to-southwestward movement of Turkey and Greece relative to Eurasia may reflect the difference in gravitational potential energy between the thick crust in eastern Turkey and the thin crust of the ocean floor of the eastern Mediterranean (McKenzie, 1972); additional forces resulting from the sinking of the subducting slab or from instabilities of the lithosphere may also influence this motion (Le Pichon, 1982; McKenzie, 1978b). The dynamics are linked to the kinematics through the question of whether the continental lithosphere as a whole deforms in response to these forces, in which case the distribution of strain rates should reflect the large-scale distribution of stress within the lithosphere (e.g., Hatzfeld et al., 1997; McKenzie, 1978b; Sonder and England, 1989), or whether deformation is confined to a few narrow weak zones, in which case motions of the lithosphere will resemble those of a set of rigid microplates (e.g., McClusky et al., 2000; Nyst and Thatcher, 2004; Reilinger et al., 2006). As a result of GPS measurements during the period 1988-1997 McClusky et al. (2000) (the red arrows on Figure 2.3) provided evidence for the existence of an Anatolian plate moves away with ~24 mm/yr respected to Eurasian one from the zone of convergence in eastern Turkey, and an Aegean plate that moves at the different velocity producing extension in the Aegean domain. Central and southern Aegean move as a rigid plate to south-southwest with respect to Eurasia with a velocity of ~35 mm/yr. Nyst and Thatcher (2004), using data from six GPS networks in the Eastern Mediterranean, propose that contemporary deformation in Aegean is due to the relative motion of 4 microplates: Anatolian moving WSW at 15-25 mm/yr relative to Eurasia, South Aegean moving SSW at ~30 mm/yr, Central Greece rotating clockwise at ~4°/Myr around pole in southernmost Albania, and South Marmara moving WSW at 23 mm/yr relative to Eurasia (Figure 2.3).

The most resent study by Floyd et al. (2010) in the region of Greece and the Aegean Sea presents a new velocity field for based on 254 survey-mode and continuous GPS (CGPS) sites, using it to test models for the deformation based on the relative motion of between 4 and 15 rigid blocks, and upon a smoothly varying field of strain rate. The obtained velocities by Floyd et al. (2010) are inconsistent with models for the tectonics of Greece and the Aegean that divide the region up into a small number of microplates (e.g., Nyst and Thatcher, 2004).

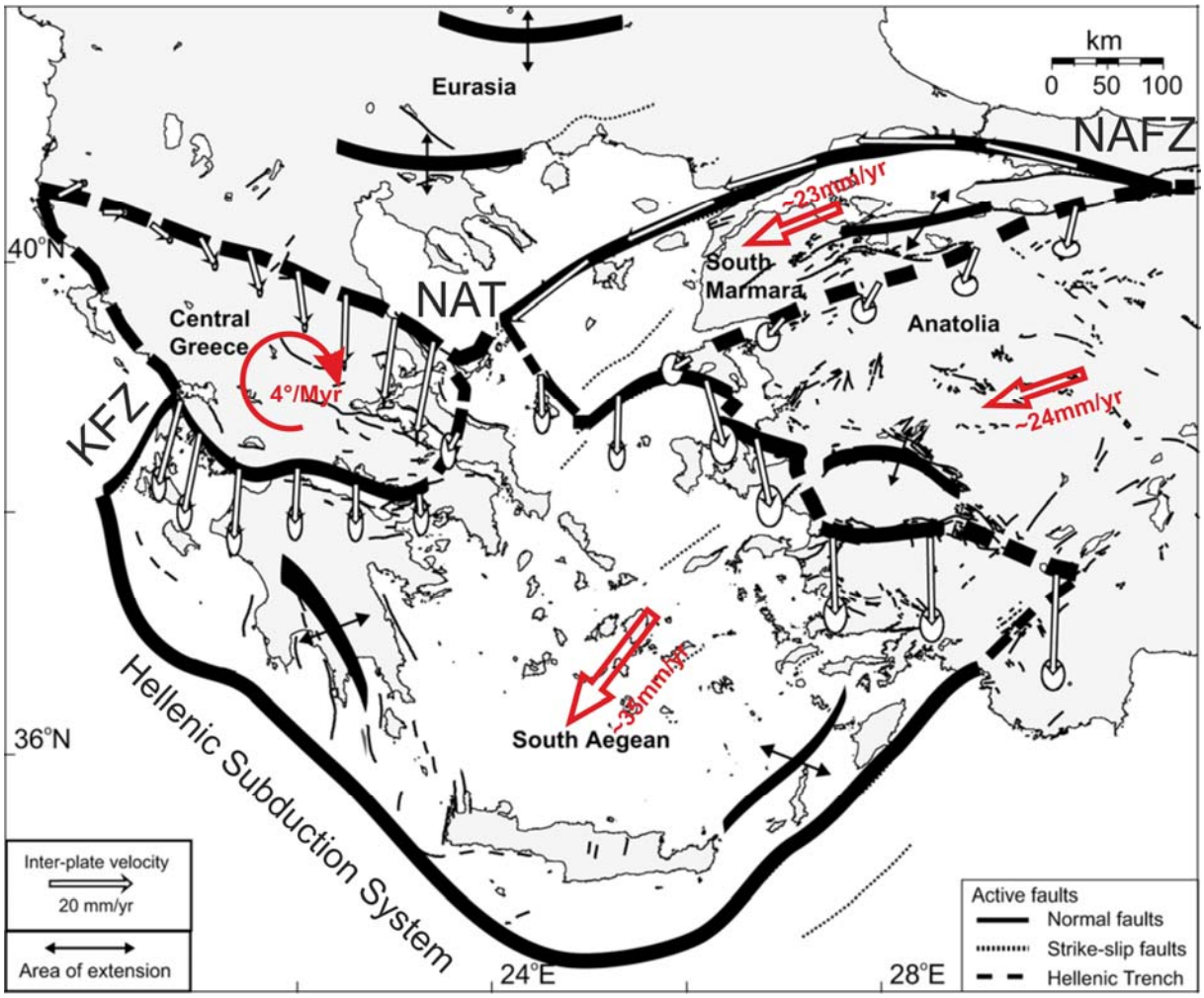

Figure 2.3. *Schematic mapping of stable microplates and their approximate boundaries inferred from GPS results, active fault distribution, and earthquake fault plane solutions. Predicted relative motions across microplate boundaries are shown by arrows that indicate the motion of the south bounding block with respect to the north bounding block. The red arrows show observed direction of motion relative to Eurasia; NAFZ: North Anatolian fault zone, NAT: North Aegean trough; KFZ: Kefalonia fault zone (after Nyst and Thatcher 2004).*

Rigid blocks with linear dimension ≈400 km or greater misfit the observed velocities by up to 15 mm/yr (4–5 mm/yr RMS), and the distributions of active faults and large earthquakes show that deformation is required in the interiors of such blocks. Decreasing the size of the

blocks, and thereby increasing their number, improves the fit of block models to the observations. The reported velocities by Floyd et al. (2010) can be fit to within about 2–3 mm/yr RMS by the relative motions of 10 or more rigid blocks that are of scale ≈1–200 km on a side. These velocities are fit equally well by a field of velocity gradients that is locally uniform on the scale of 100–200 km but varies smoothly on larger scales, though such a field underestimates the strain rates in the western Gulf of Corinth. Although continuous and block models fit the GPS velocities comparably well, the continuously varying field of velocity gradients offers the advantage of explaining the locations of, and sense of slip on, the major faults and earthquakes of the region. The authors agree with previous authors who have suggested that the extension of the Aegean region (which is clearly expressed in the seismicity, the active faulting, and the Quaternary geomorphology, as well as in the geodesy) is explained by the difference in gravitational potential energy between the continental lithosphere of the Greece and Turkey and the oceanic lithosphere to the south and southwest of the region (e.g., Davies et al., 1997; Hatzfeld et al., 1997; Le Pichon, 1982; Le Pichon et al., 1995; McKenzie, 1972).

2.1.2. Central Mediterranean

The central Mediterranean region is a complex tectonic patchwork of arcuate collisional mountain belts (Alps, Dinarides), old unsubducted Tethyian oceanic lithosphere (Ionian Sea), young oceanic rift basins (Tyhrrenian Sea), active (Calabrian Arc) and aborted subduction zones, accretionary prisms (Appenines), and microplates (Figure 1.2). The central Mediterranean displays an assemblage of lithospheric blocks with different structural and kinematic features and a variety of geodynamic processes, including subduction, backarc spreading, rifling, thrusting, normal and strike-slip faulting (Mantovani et al. 1997), trapped between the relatively undeformable African and Eurasian plates, for which the NUVEL-1A plate motion model predicts a northwest-southeast convergence at about 7 mm/yr (DeMets et al. 1994). Seismotectonic investigations in the Mediterranean region had a central role in the development of the microplate concept (McKenzie, 1970), in the description of distributed deformation (McKenzie and Jackson, 1983), and in the confirmation of early microplate hypotheses by space geodesy (e.g., Smith et al., 1994; McClusky et al., 2000).

2.1.2.1. Adriatic microplate

The tectonic evolution of the central Mediterranean is closely related to the kinematics of the Adriatic Block, but its relative motion with respect to the African Plate has been a long-

debated issue in the geological and geophysical literature (Mantovani et al. 1990; Mele 2001; Wortmann et al. 2001). The stratigraphic and paleomagnetic studies have described the Meso-Cenozoic geological evolution of the central Mediterranean, as the boundary between the Eurasian and African plates, has been largely controlled by the paleogeographic inheritance of the African and Eurasian margins (Argand, 1924). The most relevant feature is the Adriatic, a large piece of continental crust of African affinity (Channell et al., 1979), which colliding with the Eurasian plate formed the orogenic belts that now surround the Adriatic Sea. The reconstruction of past relative plate positions (Dewey et al., 1989; Mazzoli and Helman, 1994; Wortmann et al., 2001; Rosenbaum et al., 2002) and the absence of differential paleomagnetic rotations (Channell, 1996; Van der Voo, 1993; Rosenbaum et al., 2004) have been used as arguments to support the hypothesis of the Adriatic region behaving as a rigid promontory of the African plate.

McKenzie (1972) first proposed the existence of an Adriatic microplate that moves independently of both Africa (Nubia) and Eurasia in the Mediterranean. Anderson and Jackson's (1987) analysis of earthquake slip-vectors determined for the large (mb>5.5) earthquakes that rimmed the deforming edges of the aseismic Adriatic coreshowed consistent NE–SW extension in the Apennines, N–S shortening in northern Italy, and NE–SW shortening in Croatia and Albania, suggesting the presence of a microplate rotating counter-clockwise about a nearby pole. The large-scale tectonic features of the peri-Adriatic domain are quite well described by the counter-clockwise rotation of Adria with respect to the Eurasian Plate around a pole located in the western Alps (Anderson & Jackson 1987). Despite this relatively coherent slip-vector pattern, the microplate model was not widely accepted, in part, because it is at odds with Neogene geologic features that indicate recent convergence across the Apennines and Alps (e.g., Platt et al., 1989; Selvaggi and Amato, 1992; Favali et al., 1993; Italiano et al., 2000; Wortel and Spakman, 2000).

Space geodetic data support the hypothesis of an Adriatic microplate, independent, or partially independent, from the African Plate (Ward 1994; Calais et al. 2002; Oldow et al. 2002; Nocquet & Calais 2003; Battaglia et al. 2004, Serpelloni et al. 2005, D'Agostino et al. 2008, Weber et al. 2010), in agreement with other seismotectonic observations (McKenzie 1972; Anderson & Jackson 1987; Westaway 1990). The Adriatic Sea is surrounded on its eastern, northern and western margins by actively deforming belts, the Albanides and Dinarides, the Alps, and the Apennines, respectively. Ward (1994), using VLBI data, published the first space geodetic study of the Adria microplate. Calais et al. (2002) simultaneously inverted GPS velocities from only two continuous GPS sites in the Po Plain, UPAD and TORI, together with Anderson and Jackson's (1987) slip vector data set, deriving

an Adria–Eurasia angular velocity vector similar in position to Anderson and Jackson's (1987) pole of rotation. Calais et al. used this constraint, together with the inferred curved western Adria–Eurasia boundary (Figure 1), to explain the unexpected dextral shear and extension that they observed geodetically in the western Alps, where clearly collision and thrusting seem to have ceased. Battaglia et al. (2004) used ~50 circum-Mediterranean GPS sites to simultaneously study Adria motion and elastic strain along model edges, and to test whether Adria could be separated into two blocks north and south of the Gargano–Dubrovnik zone (Figure 2.1) (the Adria microplate and the Apulia microplate). The counter-clockwise rotation of the Adriatic region relative to Eurasia results in increasing convergence rates across the Alps from W to E with ≈2 mm/a of N-S shortening in the Eastern Alps (Grenerczy et al., 2005; D'Agostino et al., 2005). Baselines crossing the western Alps do not show significant shortening in agreement with seismological information showing extension along the crest of the Alps and right-lateral strike slip on NE-SW faults (Calais et al., 2002; Sue et al., 1999; Delacou et al., 2004; Thouvenot and Fréchet, 2005). Strike-slip motion and shortening occur in Slovenia and along the Dinarides with limited information due to the few available GPS stations. Increasing extension rates up to 3–4 mm/a of extension are observed from NW to SE along the crest of the Apennines (D'Agostino et al., 2001; Hunstad et al., 2003). A significant change in crustal motion occurs between Sicily and the Calabrian Arc (Pondrelli et al., 2004) across the region near the Messina Straits (D'Agostino and Selvaggi, 2004). Crustal motion in southern Sicily are clockwise rotated relative the predicted motion of Nubia and 4–5 mm/a of Eu-Nu convergence are probably accommodated offshore north of Sicily (Hollenstein et al., 2003; Goes et al., 2004) in the southern Tyrrhenian Sea. Grenerczy et al. (2005) and Serpelloni et al. (2005) performed similar wide-aperture GPS studies; and D'Agostino et al. (2008) and Devoti et al. (2008) presented recent robust kinematic analyses and developed models using data from a large number of GPS sites. Battaglia et al.'s (2004) and D'Agostino et al.'s (2008) analyses suggested an Adria-southern microplate (Apulia) boundary in the central Adriatic along the Gargano–Dubrovnik seismic belt (Figure 2.1). Oldow et al. (2002) however presented a very different and testable view of Adriatic kinematics. By combining GPS velocities from their Italian Peri-Tyrrhenian Geodetic Array (PTGA) and the EUREF network with those from the eastern Adriatic CRODYN network (Altiner, 2001), they reproposed that the Adriatic is an African (Nubian) promontory that is fragmenting along a complex boundary into a Eurasia-attached northwestern block and a Nubia-attached southeastern block. Weber et al. (2010) follow Battaglia et al. (2004) and D'Agostino et al. (2008) studied the motion of the Adriatic microplate using Eurasian-referenced GPS-derived velocities from Istria Peninsula (Slovenia, Croatia) and Po Plain (Italy) sites and earthquake

slip vectors around its edges from a Regional Centroid Moment Tensor catalogue. Weber et al. (2010) treat only the northern segment of Adriatic lithosphere north of the Gargano–Dubrovnik zone. Weber et al. (2010) best-fitting GPS Adria–Eurasia angular velocity vector (Euler pole) comes from 7 Istria Peninsula (Slovenia, Croatia) and 10 Po Plain (Italy) sites, it locates at 45.03°N, 6.52°E, with a 0.297±0.116°/Myr counter-clockwise rotation rate. An Adriatic microplate interpretation is at odds with Neogene geologic features that indicate recent convergence across the Apennines and Alps. The neotectonics–geology mismatch probably signals the recent birth of the Adria microplate upon termination of the Nubia–Eurasia Alpine collision and Adria slab break-off beneath the Apennines.

2.2. South Balkans

The Southern Balkan extensional system is north of the western part of the North Anatolian fault zone and south of a poorly defined boundary that extends through northern Bulgaria west to the Adriatic coast (McKenzie, l972; Burchfiel et al., 2006, 2008; Kotzev et al., 2006, 2008). The active deformation in extensional region in South Balkan is not well known and it has been separated from the main Aegean regime since ~6-10 Ma by the propagation of the North Anatolian fault zone into the northern Aegean Sea (Armijo et al., 1996; Sengor et al., 2004). After that deformational event, the Aegean region to south of the North Anatolian fault zone began to move SSW as a single plate and the extension within the South Balkan region became more N-S oriented and with a lower rate than southward movement of the Aegean plate.

Geological investigation (Burchfiel et al., 2000, 2003; Nakov et al, 2001) suggest that the northern boundary of the Aegean extensional regime passes through north central Bulgaria, and their analysis of young and active faulting has indicated that much of the Balkan Peninsula has been characterized by extensional tectonism which refer to the southern Balkan extensional regime. GPS results from 25 stations in Macedonia measured in 1996 and 2000 (Burchfiel et al., 2006), and GPS results between 1996 and 2004 in western Bulgaria define an approximately ESE-trending extensional boundary that marks the northernmost extent of Aegean extensional domain.

2.2.1. Southwest Bulgaria

The region of Southwest Bulgaria has the most pronounced tectonic and seismotectonic activity on the whole Bulgarian territory (Shanov et al. 2001). The

investigated area exhibits diverse relief structures, which are subjected to horizontal and vertical movements of various intensity (Zagorchev, 2001). Southwest Bulgaria falls within a zone of contemporary extension of the Earth's crust with complex interaction between horizontal and vertical movements of the geological structures (Zagorchev 1992, 2001).

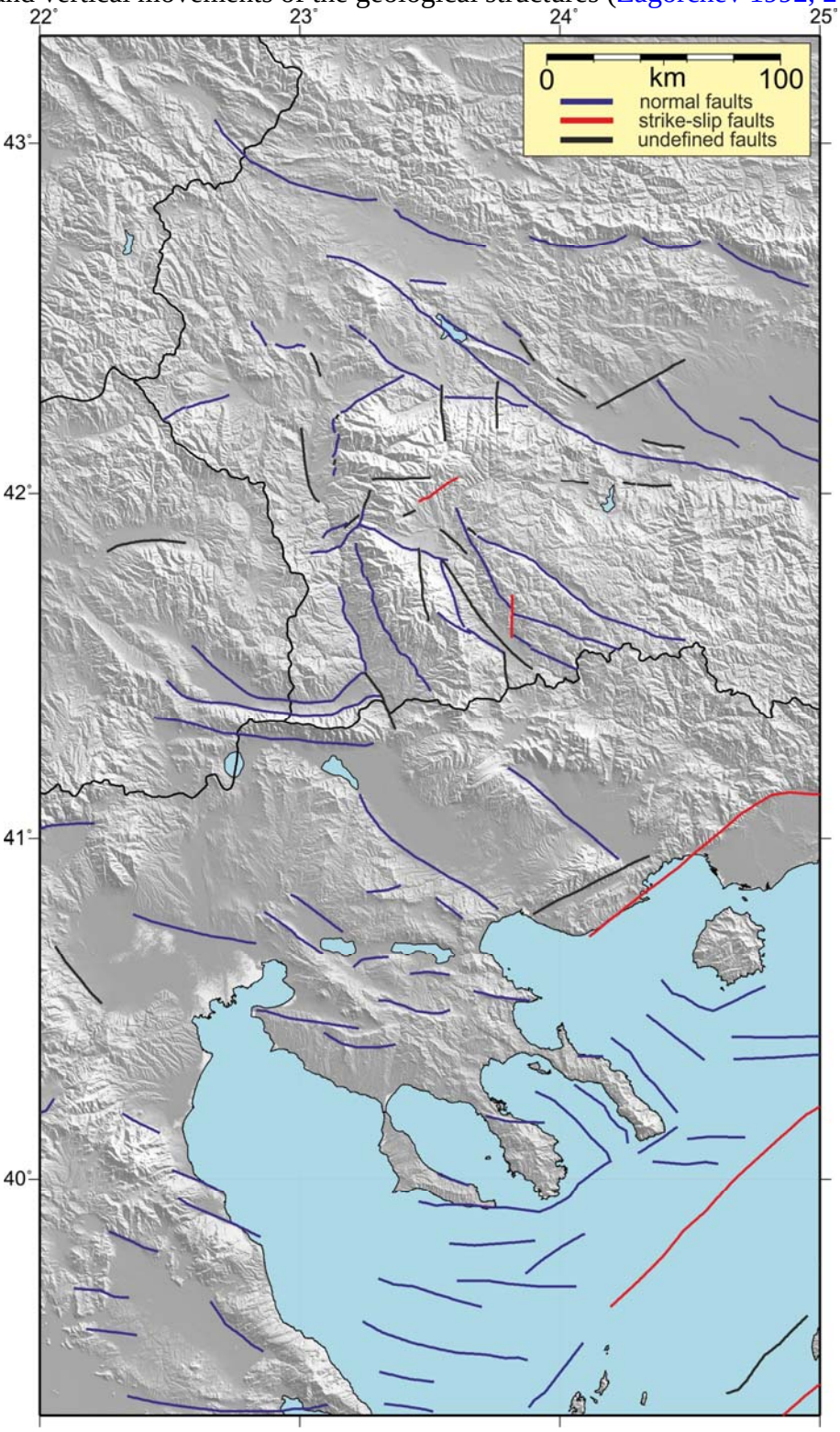

Figure 2.4. *Scheme of the active and potentially active faults in the region of SW Bulgaria and Northern Greece according Geodynamic map of the Mediterranean (Barrier et al., 2004).*

The analysis of the geological data provides evidence for contemporary activity of the fault structures formed during the Late Neogene and the Quaternary (Tzankov et al. 2000). Figure 2.4 illustrates the active and potentially active faults on the territory of the studied region from geological data and active faults according Geodynamic map of the Mediterranean (Barrier et al., 2004). The contemporary tectonic activity is also closely related with the high seismicity of this area. The strongest earthquake during the last two centuries in Europe occurred in 1904 in the region of Krupnik-Kresna (Vatsov, 1905). The magnitude of the earthquake was estimated to be between 7.3 and 7.8 by Gutenberg and Richter (1954) and Christoskov and Grigorova (1968) or M=7.5–7.9 (Ranguelov et al., 2001). Using satellite imagery and geological data Meyer et al. (2002) found that the possible rupture of the Krupnik fault compatible with their observations would account for a magnitude 6.9 significantly smaller than the previous estimates. Results determining the seismic risk for Southwest Bulgaria show potential seismic hazard for the whole region (Bonchev et al. 1982, Papazachos et al. 1996).

2.2.2. Northern Greece

Northern Greece is an intracontinental region behind the Hellenic subduction zone with widespread seismic activity ranging from low to high with destructive earthquakes of M≥6.0 in historical to recent times. Geological and seismological data indicate that recent seismic activity is mainly localized along, inherited, faults zones, affecting Northern Greece since Oligocene-Miocene times. These data also indicate that seismic activity in Northern Greece is concentrated along normal faults of several kilometres (Mountrakis et al., 2006). Figure 2.4 shows the active fault in Northern Greece according (Barrier et al., 2004). Northern Greece is characterized by small rates of crustal motion. The results show that the velocities significantly differ from the motion of Eurasia. We obtained southward to south–southeastward movements of 2–6 mm/yr. They represent the same kinematic regime as found in the regions farther north (Hollenstein et al., 2008).

2.2.3. Albania

Current Tectonics of Albania is documented by neotectonics indices and by a large number of medium size earthquakes. Focal mechanisms suggest the existence of current shortening across the external Albanides whereas internal Albanides are affected by E-W to N-S extension. The recent tectonics of Albania (Figure 2.5) is characterized by an important microseismicity, small and medium size earthquake and a few large events as shown by the

occurrence of 6 earthquakes with Ms magnitudes exceeding 6 during the last century (1905, Shkodra earthquakes Ms 6.6, 1911 Ohrid lake earthquake Ms 6.7, 1920 Tepelena Ms 6.4, 1926 Durres earthquake Ms 6.2, 1967 Dibra earthquake Ms 6.6 and 1979 Montenegro earthquake Ms 6.9). Focal Mechanisms (Sulstarova et al., 1980, Louvari et al. 2001, Pondrelli et al., 2002, 2004, 2006 and 2007), as well as neotectonics investigations (Figure 2.5) (Aliaj et al, 2000; Carcaillet et al, 2009) underline the existence of a current E-W shortening across

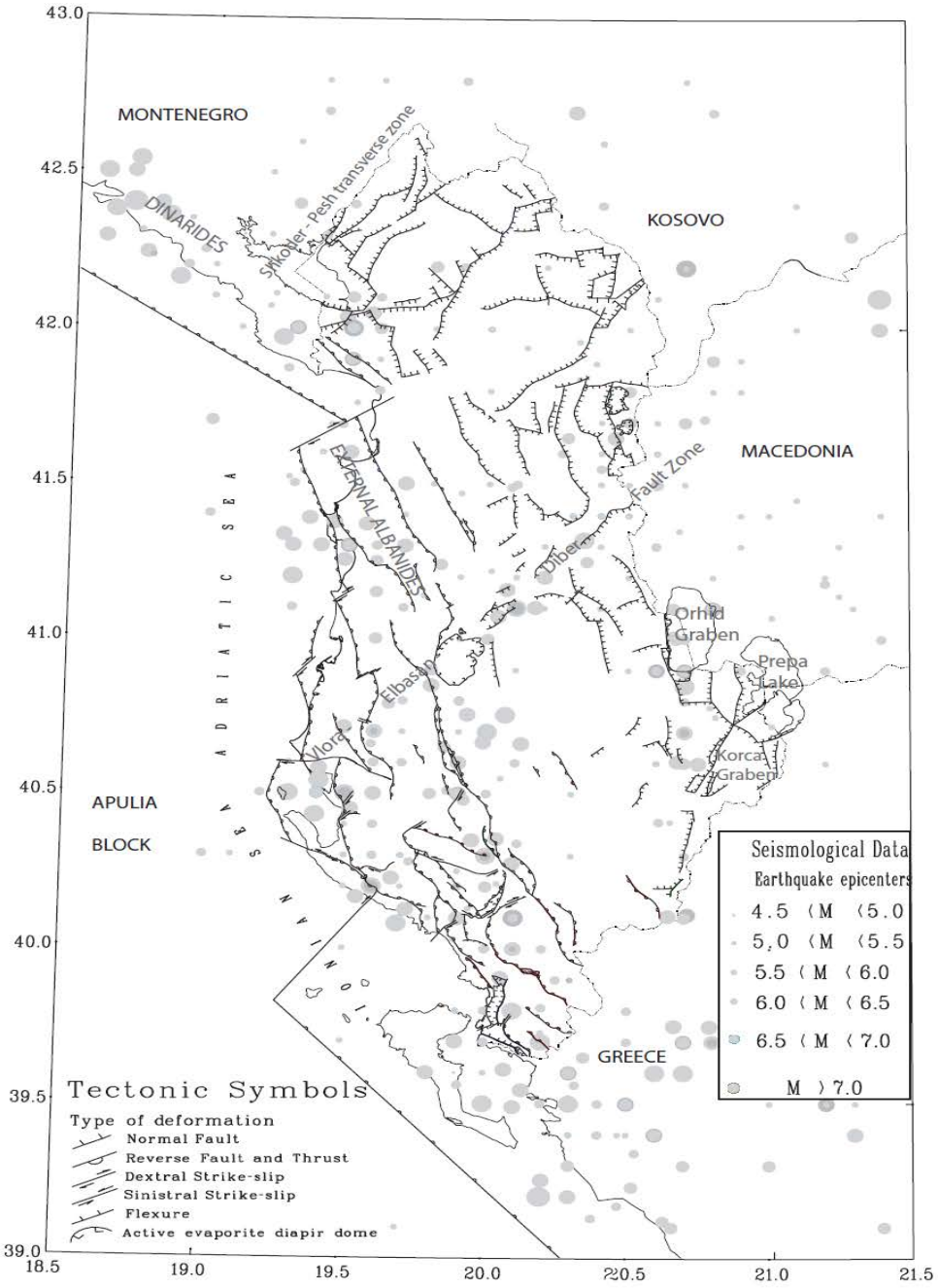

Figure 2.5. *Neotectonics map of Albania, with location of historical seismicity redrawn after Aliaj et al., 2004.*

external Albanides whereas internal Albanides experience an E-W to N-S extension (Tagari et al., 1993). Albanides are crossed by two transversal faults, the Vlora-Elbasani-Dibra fault zone and the Shkodra-Pesh (Scutari-Pesh) one (Roure et al., 2004). This last fault zone seems to be the northern boundary of the Albania – northern Greece zone characterized by NNW-SSE structural direction and by the important post Miocene rotation as shown by Speranza et al., 1995 and van Hinsbergen et al., 2005. North of the Scutari-Pesh or Shkoder – Pesh fault, Dinarides have not experienced such rotation and are characterized by NW-SE structural directions.

2.2.4 Macedonia

Geological investigation published by Burchfiel et al., 2006 presented that the fault pattern shows active N–S extension in eastern Macedonia with associated NNW-striking leftlateral strike-slip faults, a region in central Macedonia characterized by almost no active faults, and a western region dominated by NNW-striking normal faults and associated strike-slip faults with right-lateral displacement. The faults in western Macedonia are responsible for the great local relief along grabens, some of which contain lakes. Faults in northwestern Macedonia curve from their N–S strike to more E–W strike and are strongly influenced by the structural anisotropy of the crust in this region which shows the same change in strike (Dumurdzanov et al., 2005). In this part of Macedonia, the active Skopje graben trends E–W and is the locus of active faults of similar trend. The GPS results (Burchfiel et al., 2006) show an almost uniform southward velocity of 3–4 mm/year relative to stable Europe. The only area where there is a suggestion of velocity differences is within northern Macedonia along a general E–W trend that passes through the Skopje graben, the site of the destructive 1963 magnitude 6.1 earthquake. Here the data suggest, but cannot prove a change in velocity that indicates N–S extension with an associated leftlateral component. The Skopje graben lies along the Kjustindil-Skopje-Debar-Elbasan fault zone of tectonic activity postulated for many decades by Macedonian geologists.

Chapter III

GPS Data

3.1. Introduction

Two different kinds of GPS networks are used to monitor and determine present-day displacements on the territory of Albania, SW Bulgarian, and Northern Greece. Continuous GPS (CGPS) networks of 136 operating stations covering the territory of Italy and Southern Balkans (Figure 3.1, 3.2 and 3.3) and reoccupation geodynamic networks of 94 points in Albania, Macedonia, SW Bulgaria, and Northern Greece (Figure 3.4). The primary goal is to analyse the observation from both continuous and reoccupation networks and to obtain a crustal horizontal velocity and strain rate fields of high resolution. The CGPS networks include observation from IGS and EPN sites, RING, UNAVCO, GeoDAF, HemusNet, NOANet, Corinth, and Albanian permanent stations for the period of 2003 to 2009, which are described details in following sections. The reoccupation networks include data from GPS campaigns (section 3.3) on the territory of four countries (Albania, Macedonia, Bulgaria, and Greece). All used observations in the analyze process are 30 second RINEX format with an elevation cut-off angle of 10 degrees.

3.2. Permanent stations

3.2.1. IGS and EPN

The **I**nternational **G**NSS **S**ervice (IGS, http://igscb.jpl.nasa.gov/), formerly the International GPS Service, is a voluntary federation of more than 200 worldwide agencies that pool resources and permanent GPS & GLONASS station data to generate precise GPS & GLONASS products.

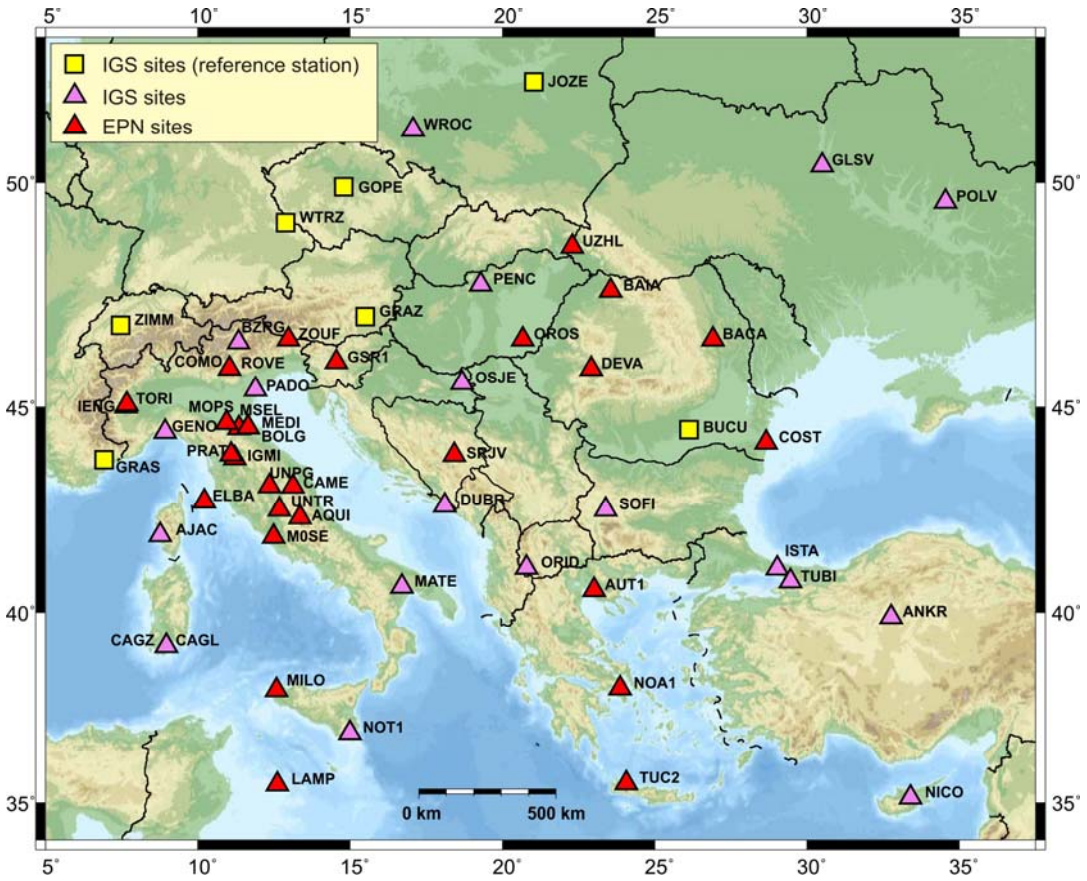

Figure 3.1. *Locations of IGS and EPN sites included in the process. Most of the IGS sites are part of EUREF Permanent Network. In yellow are shown reference stations.*

N°	Site Abbr.	Name	Lon. [°]	Lat. [°]	H [m]	Time span [yr]	Year '03	'04	'05	'06	'07	'08	'09
IGS sites													
1.	**AJAC**	Ajaccio	8.7626	41.9274	99	6.8	x	x	x	x	x	x	x
2.	**ANKR**	Ankara	32.7584	39.8873	974	6.8	x	x	x	x	x	x	x
3.	**BUCU**	Bucuresti	26.1257	44.4639	143	6.8	x	x	x	x	x	x	x
4.	**BZRG**	Bolzano - Bozen	11.3367	46.4990	328	6.8	x	x	x	x	x	x	x
5.	**CAGL**	Cagliari	8.9727	39.1359	238	6.8	x	x	x	x	x	x	x
6.	**CAGZ**	Capoterra	8.9727	39.1358	238	6.8	x	x	x	x	x	x	x
7.	**DUBR**	Dubrovnik	18.1104	42.6499	454	6.8	x	x	x		x	x	x
8.	**GENO**	Genova	8.9211	44.4193	137	6.8	x	x	x	x	x	x	x
9.	**GLSV**	Kiev	30.4967	50.3641	226	6.8	x	x	x	x	x	x	x
10.	**GOPE**	Ondrejov	14.7856	49.9137	592	6.8	x	x	x	x	x	x	x
11.	**GRAS**	Caussols	6.9205	43.7547	1320	6.8	x	x	x	x	x	x	x
12.	**GRAZ**	Graz	15.4934	47.0671	538	6.8	x	x	x	x	x	x	x
13.	**IENG**	Torino	7.6394	45.0151	316	5.9	x	x	x	x	x	x	x
14.	**ISTA**	Istanbul	29.0193	41.1044	147	6.8	x	x	x	x	x	x	x
15.	**JOZE**	Jozefoslaw	21.0315	52.0972	141	6.8	x	x	x	x	x	x	x
16.	**LAMA**	Olsztyn	20.6699	53.8923	187	6.8	x	x	x	x	x	x	x
17.	**MATE**	Matera	16.7044	40.6491	535	6.8	x	x	x	x	x	x	x
18.	**MEDI**	Medicina	11.6468	44.5199	50	6.8	x	x	x	x	x	x	x

N°	Site Abbr.	Name	Lon. [°]	Lat. [°]	H [m]	Time span [yr]	Year '03	'04	'05	'06	'07	'08	'09
19.	**NICO**	Nicosia	33.3964	35.1409	155	6.8	x	x	x	x	x	x	x
20.	**NOT1**	Noto	14.9897	36.8758	126	6.8	x	x	x	x	x	x	x
21.	**ORID**	Ohrid	20.7940	41.1273	773	6.8	x	x	x	x	x	x	x
22.	**OSJE**	Osijek	18.6804	45.5607	153	6.8	x	x	x		x	x	x
23.	**PADO**	Padova	11.8960	45.4111	64	6.8	x	x	x	x	x	x	x
24.	**PENC**	Penc	19.2815	47.7896	291	6.8	x	x	x	x	x	x	x
25.	**POLV**	Poltava	34.5429	49.6026	178	6.8	x	x	x	x	x	x	x
26.	**SOFI**	Sofia	23.3947	42.5560	1119	6.8	x	x	x	x	x	x	x
27.	**TUBI**	Gebze	29.4506	40.7867	221	6.8	x	x	x	x	x	x	x
28.	**WROC**	Wroclaw	17.0620	51.1132	181	6.8	x	x	x	x	x	x	x
29.	**WTRZ**	Bad Koetzting	12.8789	49.1441	666	6.8	x	x	x	x	x	x	x
30.	**ZIMM**	Zimmerwald	7.4652	46.8770	956	6.8	x	x	x	x	x	x	x
EPN sites													
31.	**AQUI**	L'Aquila	13.3502	42.3682	713	6.5	x	x	x	x	x	x	x
32.	**AUT1**	Thessaloniki	23.0037	40.5668	150	4.5			x	x	x	x	x
33.	**BACA**	Bacau	26.9122	46.5620	219	3.8				x	x	x	x
34.	**BAIA**	Baia Mare	23.5577	47.6517	271	3.8				x	x	x	x
35.	**BOLG**	Bologna	11.3567	44.5002	99	4.8		x	x	x	x	x	x
36.	**CAME**	Camerino	13.1239	43.1119	506	6.8	x	x	x		x	x	x
37.	**COMO**	Como	9.0956	45.8021	292	5.8		x	x	x	x	x	x
38.	**COST**	Constanta	28.6575	44.1614	46	3.7				x	x	x	x
39.	**DEVA**	Deva	22.9135	45.8784	246	3.8				x	x	x	x
40.	**ELBA**	Nell'Elba	10.2110	42.7528	269	6.4	x	x	x	x	x	x	x
41.	**GSR1**	Ljubljana	14.5437	46.0481	351	6.8	x	x	x	x	x	x	x
42.	**IGMI**	Firenze	11.2137	43.7956	95	2.9				x	x	x	x
43.	**LAMP**	Lampedusa	12.6056	35.4997	57	6.7	x	x	x	x	x	x	x
44.	**M0SE**	Roma	12.4932	41.8931	120	3.8			x		x	x	x
45.	**MILO**	Trapani - Milo	12.5843	38.0081	92	4.6			x	x	x	x	x
46.	**MOPS**	Modena	10.9491	44.6293	85	2.6					x	x	x
47.	**MSEL**	Medicina	11.6464	44.5200	49	5.1		x	x	x	x	x	x
48.	**NOA1**	Athens	23.8640	38.0470	537	3.6				x	x	x	x
49.	**OROS**	Oroshaza	20.6713	46.5552	134	6.8	x		x	x	x	x	x
50.	**PRAT**	Prato	11.0991	43.8855	119	5.8	x	x	x	x	x	x	x
51.	**ROVE**	Rovereto	11.0420	45.8935	261	3.5				x	x	x	x
52.	**SRJV**	Sarajevo	18.4138	43.8678	645	6.8	x	x	x	x	x	x	x
53.	**TORI**	Torino	7.6612	45.0633	310	6.8	x	x	x	x	x	x	x
54.	**TUC2**	Chania	24.0705	35.5331	161	5.1		x	x	x	x	x	x
55.	**UNPG**	Perugia	12.3556	43.1193	351	6.8	x	x	x	x	x	x	x
56.	**UNTR**	Terni	12.6737	42.5586	219	2.6					x	x	x
57.	**UZHL**	Uzhgorod	22.2976	48.6319	232	6.8	x	x	x	x	x	x	x
58.	**ZOUF**	Cercivento	12.9735	46.5572	1946	6.6	x	x	x	x	x	x	x

Table 3.1. *Site names, approximate coordinates, and time span of occupation of the IGS and EPN permanent stations. Lon.: longitude, Lat.: latitude, H: ellipsoidal height, Time span: occupation between first and last observation in years.*

The IGS is committed to providing the highest quality data and products as the standard for Global Navigation Satellite Systems (GNSS) in support of Earth science research, multidisciplinary applications, and education. Currently the IGS includes two GNSS, GPS and the Russian GLONASS, and intends to incorporate future GNSS.

Figure 3.2. *Sites locations of the RING, UNAVCO, and GEODAF continuous networks on the territory of Italy.*

The **E**UREF (**Eu**ropean **Re**ference **F**rame) **P**ermanent **N**etwork (EPN, http://www.epncb.oma.be/) is a science-driven network of permanent GNSS tracking stations

whose weekly computed positions are used by EUREF to realize the European Terrestrial Reference System supported by EuroGeographics. The EPN is also valuable for scientific applications such as geodynamics, sea level monitoring and weather prediction. More than 200 EPN stations including all European IGS sites, distributed all over Europe, provide in near real-time and real-time high quality GNSS data archived at local and regional data centres.

For present study we include 30 IGS stations for the period 6.8 years from 2003 to 2009, and 28 EPN sites which cover time spans between 2.6 and 6.8 years from 2003 to 2009. The location of the included IGS and EPN sites are shown in Figure 3.1, station name approximate coordinates and time span of occupation are listed in Table 3.1

3.2.2. RING network

The RING (**R**ete **I**ntegrata **N**azionale **G**PS, http://ring.gm.ingv.it/) GPS network is the result of a scientific project started by the Istituto Nazionale di Geofisica e Vulcanologia (INGV) in 2004 with the aim of increasing the number of continuous GPS stations (CGPS) in Italy in order to improve the knowledge of the geodynamics and tectonic processes acting in this area which is characterized by a complex set of independent or partially independent crustal blocks, within the slowly converging African and Eurasian plates.

We use all 35 RING sites in the process beginning from 2003 to 2009 period. The locations of the included RING stations are shown in Figure 3.2, and the names and the time span of the occupation are listed in Table 3.2

N°	Site	Name	Lon. [°]	Lat. [°]	H [m]	Time span [yr]	Year						
							'03	'04	'05	'06	'07	'08	'09
1.	**AMUR**	Altamura	16.6040	40.9073	549	3.2				x	x	x	x
2.	**BRAS**	Brasimone	11.1131	44.1222	901	3.6				x	x	x	x
3.	**BSSO**	Busso	14.5940	41.5460	1007	3.8				x	x	x	x
4.	**CDRU**	Ottati	15.3047	40.4897	1046	3.1				x	x	x	x
5.	**CUCC**	Castrocucco	15.8155	39.9938	669	3.1				x	x	x	x
6.	**EIIV**	Catania-Sede	15.0820	37.5136	89	3.8				x	x	x	x
7.	**ENAV**	Massalubrense	14.3348	40.5823	541	4.8			x	x	x	x	x
8.	**FRES**	Fresagrandinaria	14.6693	41.9735	405	3.1				x	x	x	x
9.	**GROG**	Gorgona island	9.8919	43.4263	241	3.2				x	x	x	x
10.	**GROT**	Grottaminarda	15.0598	41.0728	498	4.4			x	x	x	x	x
11.	**HMDC**	Modica	14.7831	36.9590	587	3.3				x	x	x	x
12.	**INGP**	Preturo	13.3155	42.3824	732	5.1		x	x	x	x	x	x
13.	**INGR**	Roma	12.5148	41.8280	101	6.6	x	x	x	x	x	x	x
14.	**LASP**	La Spezia	9.8396	44.0732	87	3.4				x	x	x	x
15.	**MALT**	Malta	14.5261	35.8379	72	3.4				x	x	x	x

N°	Site	Name	Lon. [°]	Lat. [°]	H [m]	Time span [yr]	Year						
							'03	'04	'05	'06	'07	'08	'09
16.	**MAON**	Monte Argentario	11.1306	42.4281	228	3.5				x	x	x	x
17.	**MOCO**	Biccari	15.1585	41.3711	1073	3.1				x	x	x	x
18.	**MODE**	Modena	10.9487	44.6289	92	2.9				x	x	x	x
19.	**MONC**	Moncucco Torinese	7.9272	45.0739	464	3.5				x	x	x	x
20.	**MRGE**	Morge	7.0610	45.7697	1723	3.2				x	x	x	x
21.	**MRLC**	Muro Lucano	15.4887	40.7564	630	3.9			x	x	x	x	x
22.	**MSRU**	Castanea delle Furie	15.5083	38.2638	397	3.2				x	x	x	x
23.	**MURB**	Monte Urbino	12.5247	43.2631	881	4.1			x	x	x	x	x
24.	**PARM**	Parma	10.3121	44.7645	122	3.1				x	x	x	x
25.	**RSMN**	San Marino	12.4507	43.9334	767	3.8			x	x	x	x	x
26.	**RSTO**	Roseto degli Abruzzi	14.0014	42.6583	103	6.8	x	x	x	x	x	x	x
27.	**SBPO**	San Benedetto Po	10.9197	45.0509	62	3.4				x	x	x	x
28.	**SERS**	Sersale	16.6885	39.0359	1215	3.1				x	x	x	x
29.	**SGIP**	San Giovanni in Persiceto	11.1827	44.6355	63	3.4				x	x	x	x
30.	**STUE**	Madesimo	9.3473	46.4722	1965	3.1				x	x	x	x
31.	**SVIN**	Stromboli-San Vincenzo	15.2341	38.8028	119	3.7				x	x	x	x
32.	**TEOL**	Teolo	11.6772	45.3427	203	4.6			x	x	x	x	x
33.	**TOLF**	Tolfa	11.9999	42.0640	363	4.6			x	x	x	x	x
34.	**USIX**	Ustica	13.1792	38.7078	283	3.0				x	x	x	x
35.	**VAGA**	Valle Agricola	14.2346	41.4154	791	3.6				x	x	x	x

Table 3.2. *Site names, approximate coordinates, and time span of occupation of the RING permanent stations. Lon.: longitude, Lat.: latitude, H: ellipsoidal height, Time span: occupation between first and last observation in years.*

3.2.3. UNAVCO

The UNAVCO Archive (http://facility.unavco.org/data/gnss/perm_sta.php) was created in 1992 as part of the UNAVCO mission to support and promote Earth science by advancing high-precision techniques for the measurement of crustal deformation. The UNAVCO Archive provides secure long-term storage for data and data products from crustal deformation measurements, and holds metadata in a searchable database. Data and data products from the Archive are available to the scientific community and to the public. Today, GNSS (GPS) data from hundreds of campaigns and over 1000 permanent stations make up the largest component of the Archive's holdings. The Archive's GNSS holdings are divided into two categories according to collection style: permanent station and campaign. For our study we include 9 permanent stations located on the territory of Italy. The sites are resented on Figure 3.2. The site names, approximate coordinates, and time span of those stations are listed in Table 3.3.

3.2.4. Geodetic Data Archive Facility – GeoDAF

GeoDAF (http://geodaf.mt.asi.it/html_old/index.html) holds GPS data acquired from ASI Fiducial GPS Network and from other Stations managed by other Institution, mainly in Italy. For our aims in the present investigation we included data from 9 permanent stations. Observation and log files are accessible on ftp server (ftp://geodaf.mt.asi.it/GEOD/GPSD/). Locations of the sites are presented on Figure 3.2. Site names, coordinates, and time span are listed in Table 3.3.

Figure 3.3. *Sites locations of the HemusNet, NOANet, Albania, and Corinth continuous networks on the territory of Balkans.*

3.2.5. HemusNet

HemusNet permanent GPS network (http://www.hemus-net.org/) was established in 2007 under international project "Science for Peace Program", NATO: SFP 981881

(Monitoring Crustal deformation in West Central Bulgaria and Northern Greece using GPS). The aim of the project is to provide basic infrastructure in both Bulgaria and Northern Greece for space-aided navigation, surveying, science, engineering, and atmospheric sensing. The network contains 8 permanent stations that cover West-central Bulgaria and Northern Greece. Locations of the sites are presented on Figure 3.3. Site names, coordinates, and time span are listed in Table 3.3.

3.2.6. NOANet

NOANet (http://www.gein.noa.gr/gps.html) is the new permanent GPS network for geodynamics in Greece. **N**ational **O**bservatory of **A**thens (NOA) has begun installing permanent GPS stations on February 2006 including a EUREF permanent station in Attica, NOA1. Currently the NOANet operate 9 permanent stations including EUREF and NemusNet sites. The monitoring of crustal deformation is one of the new goals of the NOA. For our study we include 6 points which are shown on Figure 3.3. Site names, coordinates, and time span are listed in Table 3.3. The data are available on follow web site: http://www.gein.noa.gr/services/GPS/GPS_DATA/.

N°	Site	Name	Lon. [°]	Lat. [°]	H [m]	Time span [yr]	Year						
							'03	'04	'05	'06	'07	'08	'09
	UNAVCO												
1.	**CAMO**	Camigliatello	16.4491	39.3401	1269	3.0				x	x	x	x
2.	**CCRI**	Caccuri	16.7756	39.226	708	2.7				x	x	x	x
3.	**CETR**	Cetraro	15.9546	39.5287	632	2.6				x	x	x	x
4.	**CRLM**	Carlomagno	16.5473	39.2783	1610	2.6				x	x	x	x
5.	**KROT**	Crotone	17.1250	39.0799	24	3.0				x	x	x	x
6.	**LATT**	Lattarico	16.1377	39.4625	403	3.0				x	x	x	x
7.	**LUZZ**	Luzzi	16.2877	39.4459	436	3.0				x	x	x	x
8.	**STSV**	Santa Severina	16.9151	39.1479	348	3.0				x	x	x	x
9.	**TVRN**	Taverna di Montalto	16.2263	39.4313	197	3.0				x	x	x	x
	GeoDAF												
1.	**BIEL**	Biella	8.0480	45.5607	480	4.2			x	x	x	x	x
2.	**BRIX**	Brescia	10.2325	45.5649	223	4.8			x	x			x
3.	**LEC1**	Lecco	9.4069	45.8572	310	4.8			x	x	x	x	x
4.	**NOVA**	Novara Comune	8.6139	45.4472	218	5.7		x	x	x	x	x	x
5.	**PACA**	Palma Campania	14.5563	40.8704	127	4.8			x		x	x	x
6.	**PAVI**	Pavia	9.1361	45.2029	144	4.7			x	x	x	x	x
7.	**UNFE**	Ferrara	11.5991	44.8329	81	6.8	x		x	x	x	x	x
8.	**VEAR**	Venezia – Arsenale	12.3578	45.4379	47	3.6				x	x	x	x

N°	Site	Name	Lon. [°]	Lat. [°]	H [m]	Time span [yr]	Year '03	'04	'05	'06	'07	'08	'09
9.	**VLUC**	Vallo della Lucania	15.2659	40.2306	445	4.8			x	x	x	x	x
	HemusNet												
1.	**DRAG**	Dragoman	42.9318	22.9335	721	2.5					x	x	x
2.	**KUST**	Kustendil	42.2837	22.7131	516	2.4					x	x	x
3.	**LEMN**	Lemnos	25.1805	39.8972	104	2.3					x	x	x
4.	**NVRK**	Nevrokopion	41.3368	23.8697	579	0.9						x	x
5.	**PAZA**	Pazardjik	42.2310	24.3400	217	2.4					x	x	x
6.	**SAND**	Sandanski	41.5505	23.2678	187	2.5					x	x	x
7.	**SOFA**	Sofia	42.6678	23.2685	661	2.1					x	x	x
8.	**YUND**	Yundola	42.0643	23.8538	1455	2.6					x	x	x
	NOANet												
1.	**KASI**	Kassiopi	19.9355	39.7463	109	2.6					x	x	x
2.	**PONT**	Ponti	20.5851	38.6189	49	2.7					x	x	x
3.	**PRKV**	Lesvos	26.2650	39.2457	169	2.3					x	x	x
4.	**RLSO**	Riolos	21.4647	38.0558	133	3.2				x	x	x	x
5.	**SPAN**	Spanohori	20.6736	38.7812	451	2.4					x	x	x
6.	**VLSM**	Valsamata	20.5886	38.1768	437	3.7				x	x	x	x
	Corinth												
1.	**AKRI**	Arkitsa	23.0336	38.7550	42	2.3		x	x	x			
2.	**DION**	Dionysos	23.9326	38.0785	514	3.6	x	x	x	x			
3.	**EYPA**	Efpalio	21.9283	38.4267	197	5.2	x	x	x	x	x	x	
4.	**KOUN**	Kounina	22.0458	38.2094	594	4.0	x	x	x	x	x		
5.	**LIDO**	Lidoriki	22.2010	38.5289	594	4.8	x	x	x	x	x		
6.	**PSAR**	Psaromita	22.1843	38.3217	89	4.7	x	x	x		x		
7.	**TRIZ**	Trizonia	22.0727	38.3653	56	5.2	x	x	x	x	x	x	
	Albania												
1.	**BERA**	Berati	19.9454	40.7081	269	2.6			x	x	x	x	
2.	**PESH**	Peshkopia	20.4397	41.6847	746	5.1	x	x	x	x	x	x	
3.	**SARA**	Sarande	20.0259	39.8660	294	2.5	x	x	x				
4.	**SHKO**	Shkoder	19.4962	42.0505	67	4.1	x	x	x	x	x		
5.	**TIRA**	Tirane	19.8632	41.3473	237	4.5	x	x	x	x	x	x	

Table 3.3. *Site names, approximate coordinates, and time span of occupation of the UNAVCO, GeoDAF, HemusNet, NOANET, Corinth, and Albanian permanent stations. Lon.: longitude, Lat.: latitude, H: ellipsoidal height, Time span: occupation between first and last observation in years.*

3.2.7. Corinth GPS permanent network

The Corinth GPS permanent stations are located in Greece territory. The data have been downloaded from GPSCOPE web server (https://geodesie.ipgp.jussieu.fr/gpscope/corinth/). The locations of included permanent sites are shown on Figure 3.3. Site names, coordinates, and time span are listed in Table 3.3.

3.2.8. Albania GPS permanent stations

Albanian Permanent GPS stations have been installed to sampled present-day displacements in both sides of the main active structures identified in Albania. Five permanent stations are included in the process. The locations of the sites are presented on Figure 3.3. Site names, coordinates, and time span are listed in Table 3.3.

3.3. Campaigns

3.3.1. Albania

Dense GPS network has been installed to better localize areas undergoing current deformation. Benchmarks allow direct centring of antennas to avoid centrings errors and bad determinations of antenna heights. Measurements of 34 GPS stations were analysed in 4

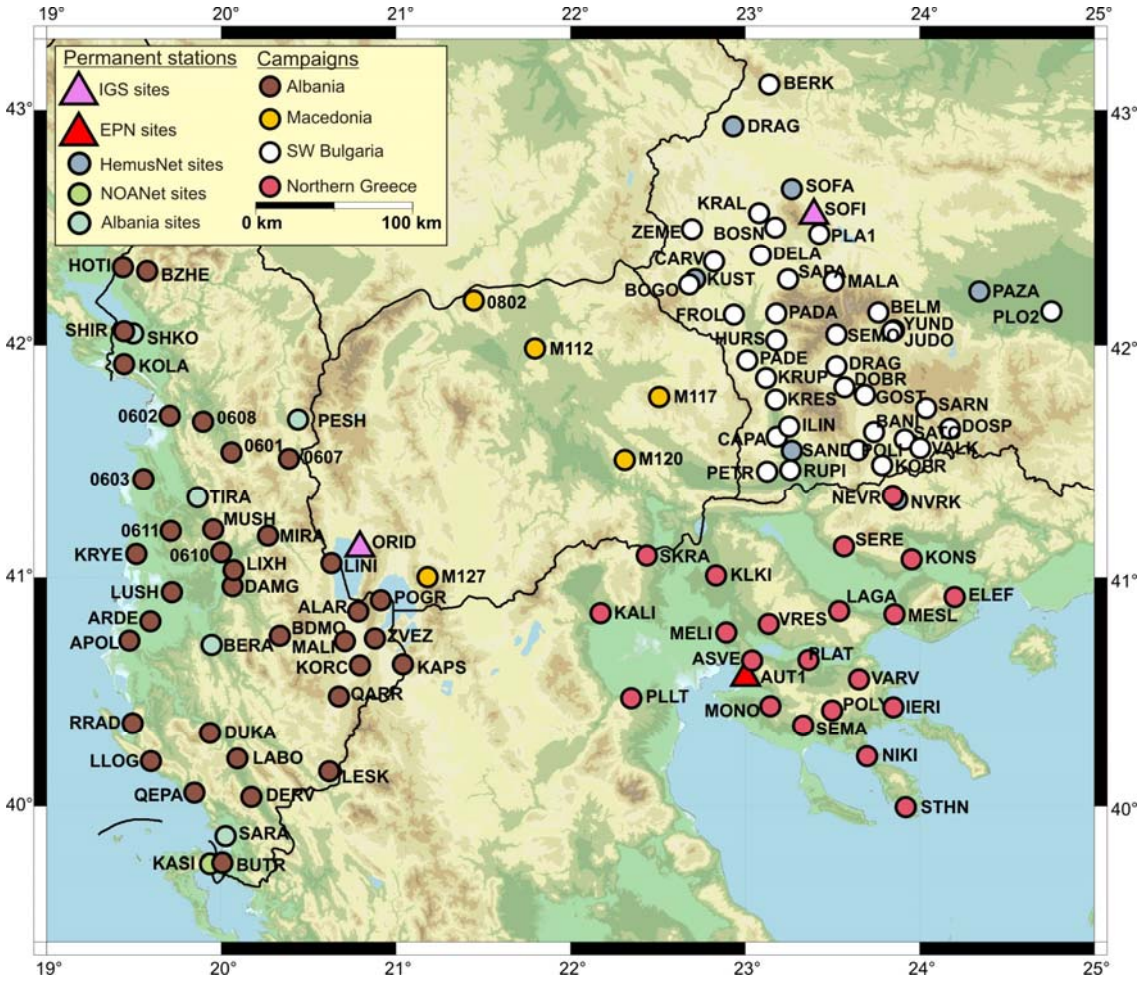

Figure 3.4. *Sites locations of the Albanian, Republic of Macedonian, SW Bulgarian, and Northern Greece campaigns networks cover the territory of Balkans.*

Campaigns in 2003, 2006, 2008, and 2009 (Table 3.4). Observation sessions are between 36 and 72 hours. The sampling rate of the observation was 30 s, with an elevation cut-off angle of 10 degrees.

N°	Site	Year						
		2003	2004	2005	2006	2007	2008	2009
1.	**0601**				x			x
2.	**0602**				x			x
3.	**0603**				x			x
4.	**0607**				x			x
5.	**0608**				x			x
6.	**0611**				x			x
7.	**ALAR**	x			x		x	
8.	**APOL**	x			x		x	
9.	**ARDE**	x			x		x	
10.	**BDMO**				x			x
11.	**BUTR**	x			x		x	
12.	**BZHE**	x			x			
13.	**DAMG**				x			x
14.	**DERV**	x			x		x	
15.	**DUKA**	x			x		x	
16.	**HOTI**	x			x			
17.	**KAPS**	x			x		x	
18.	**KOLA**	x			x			
19.	**KORC**	x			x			
20.	**KRYE**	x			x		x	
21.	**LABO**	x			x		x	
22.	**LESK**	x			x		x	
23.	**LINI**	x			x			
24.	**LIXH**	x			x		x	
25.	**LLOG**	x			x			
26.	**LUSH**	x			x			
27.	**MIRA**	x			x		x	
28.	**MUSH**	x			x		x	
29.	**POGR**	x			x		x	
30.	**QARR**	x			x		x	
31.	**QEPA**	x			x		x	
32.	**RRAD**	x			x		x	
33.	**SHIR**	x			x			
34.	**ZVEZ**	x			x		x	

Table 3.4. *GPS data collected in Albania.*

3.3.2. Southwest Bulgaria

To estimate current displacements in Southwest Bulgaria and Northern Greece, we have used completed existing data of 34 points with new acquisitions performed in 2008. GPS

measurements carried out in 1996, 1997, 1998 and 2000 within the frames of international project with Massachusetts Institute of Technology (MIT) (Geodynamic settings of Bulgaria in the active and young Near East-Balkan geotectonic system) and GPS data of the CLG geodynamic network measured since 2001. The points from the GPS geodynamic network were measured during the period 1996-2008 (Table 3.5). The observation sessions of each campaign were minimum 36 hours.

N°	Site Name	Year												
		1996	1997	1998	1999	2000	2001	2002	2003	2004	2005	2006	2007	2008
South Western Bulgaria														
1.	**BANI**							x	x	x				x
2.	**BELM**		x			x		x	x					x
3.	**BERK**	x	x			x	x							x
4.	**BOGO**	x	x	x		x	x			x				
5.	**BOSN**		x			x				x				
6.	**CAPA**						x	x	x	x				
7.	**CARV**		x			x				x				
8.	**DELA**		x			x				x				
9.	**DOBR**		x			x	x	x	x					x
10.	**DOSP**							x	x	x				
11.	**DRAG**						x	x	x	x				x
12.	**FROL**		x			x		x	x					
13.	**GOST**						x	x	x	x				x
14.	**HURS**							x	x	x				x
15.	**ILIN**						x	x	x	x				x
16.	**JUDO**							x	x	x	x			x
17.	**KOPR**						x	x	x	x				x
18.	**KRAL**		x			x				x				
19.	**KRES**						x	x	x	x				x
20.	**KRUP**						x	x	x	x				
21.	**MALA**		x			x		x	x					
22.	**PADA**		x			x		x	x					x
23.	**PADE**							x	x	x				x
24.	**PETR**	x		x			x	x	x					
25.	**PLA1**	x	x			x	x	x	x	x	x	x		x
26.	**PLO2**	x		x			x							x
27.	**POLI**						x	x	x	x				x
28.	**RUPI**						x	x	x	x				x
29.	**SAPA**		x			x		x	x		x			
30.	**SARN**							x	x	x	x			x
31.	**SATO**		x				x	x	x					x
32.	**SEMO**						x	x	x	x				x
33.	**VALK**							x	x	x	x			x
34.	**ZEME**		x			x					x			
Northern Greece														
1.	**ASVE**				x	x								x
2.	**ELEF**				x	x								x

N°	Site Name	Year												
		1996	1997	1998	1999	2000	2001	2002	2003	2004	2005	2006	2007	2008
3.	**IERI**				x	x								x
4.	**KALI**				x	x								x
5.	**KLKI**				x	x								x
6.	**KONS**				x	x								x
7.	**LAGA**				x	x								x
8.	**MELI**					x								x
9.	**MESL**				x	x								x
10.	**MONO**				x	x								x
11.	**NEVR**				x	x								x
12.	**NIKI**				x	x								x
13.	**PLAT**				x	x								x
14.	**PLLT**				x	x								x
15.	**POLY**				x	x								x
16.	**SEMA**				x	x								x
17.	**SERE**				x	x								x
18.	**SKRA**				x	x								x
19.	**STHN**					x								x
20.	**VARV**				x	x								x
21.	**VRES**				x	x								x
Macedonia														
1.	**0802**	x				x								x
2.	**M112**	x				x								x
3.	**M117**	x				x								x
4.	**M120**	x				x								x
5.	**M127**	x				x								x

Table 3.5. *GPS data collected in South Western Bulgaria, Northern Greece, and Macedonia*

3.3.3. Northern Greece

In Northern Greece we have analysed GPS data of 21 points to determine crustal displacements collected in 1999, 2000 and 2008 with the exception of the points MELI and STHN measured only in 2000 and 2008 (Table 3.5). In 1999 and 2000 only short sessions (3-10 hours) have been performed whereas in 2008, points have been measured between 48 and 72 hours. In 2008 campaign the point ELEF was measured 3h and the point ASVE was measured 6h in two days by 3h.

3.3.4. Macedonia

Measurements of 5 points are analysed from three campaigns in 1996, 2000 and 2008 (Table 3.5). The data for 1996 are courtesy given from Macedonian Agency of Cadastre. For that campaign measurement session for every each GPS station are 72 hours. The data for 2000 campaign were downloaded freely from UNAVCO Archive and observation sessions

are 24 hours. The data from 1996 and 2000 were measured under EUREF project. Observation session for every each GPS station is 24 hours. The 2008 campaign was done with the collaboration of CLG, BAS and Faculty of Civil Engineering, Chair for high geodesy, University “Ss. Cyril and Methodius”, Skopje, Macedonia, with observation session of 8 hours.

Chapter IV

GPS data analysis

4.1. Reference systems

4.1.1. Terrestrial Reference System (TRS)

4.1.1.1. Definition

The Terrestrial Reference System (TRS) is a spatial coordinates system rotating with the Earth during its daily movement in space. In such a reference system the positions of the points experience only small variations with time due to geophysical effects – tectonic movements, tidal changes, post-glacial rebound. The realization of the terrestrial reference system (Terrestrial Reference Frame - TRF) is the set of physical points on the Earth's surface with (precisely) determined coordinates and velocities (and represented in a specific coordinate system – orthogonal, geodetic, spherical, etc.). It is accepted to refer to this set of points as a realization of the Terrestrial Reference System. The three main conceptions of Terrestrial Reference System:

4.1.1.2. Ideal Terrestrial Reference System (iTRS)

An "ideal" TRS is defined as a 3-D spatial geocentric orthogonal coordinate system rotating with the Earth. In the context of Newtonian mechanics the geometry of the physical space is such as that of Euclidian affine space with a dimension of three. The choice of the affine coordinates (O, E) is: O – a point from the space called the origin (the geocentre) and E – the base of the vector space with accepted restrictions for the E coordinate – the basic vectors have to be orthogonal and of equal length. The orientation is set by an additional condition. In contemporary satellite geodesy the geocentric coordinate system with an origin in the geocentre and equatorial orientation (the Z axis points to the pole) is accepted as the "ideal" one.

4.1.1.3. Conventional Terrestrial Reference System (CTRS)

Such a coordinate system is used to designate the set of all conventions – models, algorithms, constants, etc., which determine unambiguously the evaluation of coordinates and velocities of the points (and their covariational matrix) in an ideal TRS.

4.1.1.4. Conventional realization of the Terrestrial Reference System (CTRF)

A conventional realization of the Terrestrial Reference System is defined as a set of physical points with (precisely) determined coordinates and velocities by using the set of conventions for their determination. This coordinate system is called a realization of the "ideal" Terrestrial Reference System (iTRS). Two types of CTRF are distinguished – dynamic and kinematic one, depending on whether a dynamic model is applied for determining the point coordinates or not. CTRF is accessible for user applications.

4.1.2. International Terrestrial Reference System (ITRS)

The International Earth Rotation Service (IERS) and the Terrestrial Reference Frame (TRF) section of the National Geographic Institute (Institut Géographique National), Paris, are international structures, which are responsible for the definition, the realization and the dissemination of the International Terrestrial Reference System (ITRS) according to the resolutions of the International Association of Geodesy (IAG). The International Earth Rotation Service defines the Conventional Terrestrial Reference System (CTRS), which is the basis of the International Terrestrial Reference System (ITRS) and its realization (ITRF).

4.1.2.1. Definition of ITRS

- geocentric;
- length unit – meter, and time coordinate in agreement with a local geocentric system (in the context of relativistic mechanics);
- orientation – initial orientation identical with that of the International Bureau for Time (Bureau International de l'Heure BIH), the predecessor of the IERS;
- the variations in time of the orientation are restricted by the condition that the rotation with respect to the horizontal movements of the Earth's crust on the globe as a whole is minimal (the so-called no-net-rotation).

4.1.2.2. Definition of CTRS

- geocentric, rotating with the Earth;
- identical with the Terrestrial Geocentric System (TGC), defined by the resolutions of the International Association of Geodesy;
- time coordinate - Geocentric Coordinate Time (TGC);
- origin in the geocentre of the Earth, including the oceans and the atmosphere;
- minimal rotation with respect to the horizontal tectonic movements;

4.1.3. Realization of the ITRS reference system – International Terrestrial Reference Frame (ITRF)

The realization of the International Terrestrial Reference System (ITRS) under the name ITRFyy, where yy is the year of publication, is realized by IERS. The present procedure of obtaining the ITRS realizations consists in combining the individual solutions obtained by the analysis centres of space observations of IERS – Very Long Base Interferometry (VLBI), Lunar Laser Ranging (LLR), Satellite Laser Ranging (SLR), GPS and DORIS (Doppler Orbit Determination and Radiopositioning Integrated on Satellite) – coordinates, velocities and covariation matrices. The results obtained using the different observation techniques are independent and also give the possibility to asses the systematic differences between them.

4.1.3.1. ITRF2005

Unlike the past International Terrestrial Reference Frame (ITRF) versions where global long-term solutions were combined, the ITRF2005 uses as input data time series (weekly from satellite techniques and 24-h session-wise from Very Long Baseline Interferometry) of station positions and daily Earth Orientation Parameters (EOPs). The advantage of using time series of station positions is that it allows to monitor station non-linear motion and discontinuities and to examine the temporal behavior of the frame physical parameters, namely the origin and the scale (Altamimi et al., 2007).

4.1.3.2. Origin

The ITRF2005 origin is defined in such a way that it has zero translations at epoch 2000.00 and null translation rates with respect to the Earth center of mass, averaged by the Satellite Laser Ranging (SLR) time series spanning 13 years of observations.

4.1.3.3. Scale

The ITRF2005 scale is defined by nullifying the scale and its rate with respect to the Very Long Baseline Interferometry (VLBI) time series spanning 26 years of observations.

4.1.3.4. Orientation

The ITRF2005 orientation is defined in such a way that there are null rotation parameters at epoch 2000.0 and null rotation rates between the ITRF2005 and ITRF2000 using 70 stations of high geodetic quality. These two conditions are applied over a core network. The estimated level of consistency of the ITRF2005 origin (at epoch 2000.0) and its rate with respect to the ITRF2000 is respectively 0.1, 0.8, 5.8 mm and 0.2, 0.1, 1.8 mm/yr along the X, Y and Z-axis. The estimated formal errors on these components are 0.3 mm and 0.3 mm/yr.

For the first time of the ITRF history, the ITRF2005 rigorous combination provides self-consistent series of EOPs, including Polar Motion from VLBI and satellite techniques and Universal Time and Length of Day from VLBI only (Altamimi et al., 2007).

4.1.4. Geodetic Reference System GRS80

4.1.4.1. Definition

The Geodetic Reference System GRS80 is characterized with the following:

A. It is based on the theory of the geocentric equipotential ellipsoid defined by the following conventional constants:

- equatorial radius of the Earth: a = 6378 137 m,
- geocentric gravitation constant of the Earth (including the atmosphere): GM = 3986 005 x 108 m3 s-2,
- dynamic factor of the Earth (the zonal harmonics J2, with excluded permanent tide: J2 = 108 263 x 10-8,
- angular velocity of the Earth: $\omega = 7292x10^{-11} rad.s^{-1}$

B. The same calculation formulas for the Geodetic Reference System 1967 are used as accepted at the XV General Assembly of IUGG in Moscow, 1971, and published by IAG;

C. An ellipsoid oriented in such a way that the small semi-axis is parallel to the direction defined by the Conventional International Origin (CIO) and the initial meridian is parallel to the accepted by BIH/IERS zero meridians (the longitude origin).

4.1.5. World Geodetic System 84 – WGS84

The global terrestrial reference system WGS84 was introduced (defined and realized) by the National Geospatial Intelligence Agency (NGIA), the former National Imagery and Mapping Agency (NIMA), and the Department of Defence (DoD) of the United States. The initial realization of WGS84 was based only on positions determined by observations of the TRANSIT satellite system and its accuracy was of the order of 1-2 metres. During the next years the accuracy of the subsequent WGS84 realizations was significantly improved. As a first step towards the better conformity between WGS84 and ITRS, the whole network of WGS84 points was recalculated in 1993 with respect to 8 GPS points fixed to their ITRF92 coordinates. This realization is known as WGS84 G730 (730 GPS week). The difference between ITRF92 and WGS84 of the G730 realization is at the level of 10 cm. The further improvement of the coordinates of the observation stations led to the WGS84 – G873 realization in 1996. This realization contains 13 terrestrial stations (of NGIA and the Air Forces of the USA), only one of them being located in Europe. The coordinates of G873 are in agreement with the ITRF94 ones at a level of 2 cm and less. Resolution 4 of the EUREF Symposium in Helsinki, 3-6 May, 1995, recommends the use of ITRS or ETRS89 in their subsequent realizations instead of using WGS84, for all applications requiring sub-metre accuracy.

4.2. Coordinates transformations

4.2.1. Transformation between geocentric Cartesian coordinates to geodetic ellipsoidal coordinates

The most frequency used coordinate transformation during data analyze process is transformation between geocentric Cartesian coordinates to geodetic ellipsoidal coordinates and vice versa. The given geocentric ellipsoidal coordinates φ, λ and H, are calculated to geocentric Cartesian coordinates X, Y, Z as:

$$\begin{aligned} X &= (R_N + H)\cos\varphi\cos\lambda; \\ Y &= (R_N + H)\cos\varphi\sin\gamma; \\ Z &= (R_N(1-e^2) + H)\sin\varphi; \end{aligned} \tag{4.1}$$

where:

φ, λ : geocentric ellipsoidal latitude and longitude

H : ellipsoidal height

R_N : transverse radius of curvature, calculated as:

(4.2)
$$R_N = \frac{a}{\sqrt{1-e^2 \sin^2 \varphi}};$$

a : semi-major axis / equatorial radius of the ellipsoid

e : first numerical eccentricity of the ellipsoid

The inversion of equations 4.1 yield the geodetic ellipsoidal coordinates:

(4.3)
$$\varphi = \arctan\left(\frac{Z}{\sqrt{X^2+Y^2}} \cdot \frac{1}{1-\frac{R_N}{R_N+H} e^2} \right);$$

$$\lambda = \arctan\left(\frac{X}{Y}\right);$$

$$H = \frac{\sqrt{X^2+Y^2}}{\cos\varphi} - R_N;$$

The numerical values of φ, R_N and H can be calculated iteratively. These coordinate transformations depend on the numerical values of the ellipsoid parameters. Relevant for satellite geodesy are those of GRS80 (Geodetic Reference System 1980) and those of WGS84 (World Geodetic System 1984). The semi-major axes and numerical eccentricities of the two ellipsoids are listed in Table 4.1 GRS80 was used as the basis for the WGS84, which is the current reference system for GPS. If geocentric ITRF coordinates have to be transformed to ellipsoidal coordinates, the IERS (International Earth Rotation and Reference Systems Service) recommends to use the GRS80 ellipsoid (IERS Conventions (2003) (McCarthy and Petit, 2004)). However, the difference between the parameters *e* of the two reference ellipsoids is so small that it has no practical consequences on the coordinate transformation (NIMA, 2000). Coordinates on the earth's surface differ by less than 0.1 mm. Therefore, it is irrelevant whether the GRS80 or the WGS84 ellipsoid parameters are used.

Ellipsoid	a	e^2
GRS80	6378137.000	0.00669438002290
WGS84	6378137.000	0.00669437999014

Table 4.1. *Semi-major axis a and square of the first numerical eccentricity e^2 of the GRS80 and the WGS84 ellipsoids (NIMA, 2000)*

4.2.2. Transformation between geocentric Cartesian coordinates to topocentric Cartesian coordinates and vice versa

A vector **ΔX** in a geocentric Cartesian system is transformed into a topocentric Cartesian system by multiplying it with the corresponding rotation matrix **R**:

(4.4) $$x = \mathbf{R} \bullet \mathbf{\Delta X};$$

$$\begin{pmatrix} n \\ e \\ u \end{pmatrix} = \begin{pmatrix} -\sin\Phi\cos\Lambda & -\sin\Phi\sin\Lambda & \cos\Phi \\ -\sin\Lambda & \cos\Lambda & 0 \\ \cos\Phi\cos\Lambda & \cos\Phi\sin\Lambda & \sin\Phi \end{pmatrix} \bullet \begin{pmatrix} \Delta X \\ \Delta Y \\ \Delta Z \end{pmatrix};$$

where

n,e,u	: topocentric vector components: north, east, up
ΔX, ΔY, ΔZ	: geocentric vector components
Λ, Φ	: astronomical longitude and latitude of the topocenter

The rows of the rotation matrix contain the geocentric components of the unity vectors of the topocentric coordinate axes. E.g. in the first row, we have the X-, Y-, and Z- components of the unity vector which is pointing in the direction of the n-axis. Note that the topocentric coordinate system is left-handed system.

As the rotation matrix is orthogonal, in inverse transformation is:

(4.5) $$\mathbf{\Delta X} = \mathbf{R}^T \bullet x;$$

$$\begin{pmatrix} \Delta X \\ \Delta Y \\ \Delta Z \end{pmatrix} = \begin{pmatrix} -\sin\Phi\cos\Lambda & -\sin\Lambda & \cos\Phi\cos\Lambda \\ -\sin\Phi\sin\Lambda & \cos\Lambda & \cos\Phi\sin\Lambda \\ \cos\Phi & 0 & \sin\Phi \end{pmatrix} \bullet \begin{pmatrix} n \\ e \\ u \end{pmatrix};$$

For the case of transforming accuracies of vectors, it is pointed out that possibly existing covariance information is not considered by applying eqns. 4.3 and 4.4, respectively, on 'accuracy vectors'. If covariance information is available, the covariance matrices $\mathbf{K}_{\Delta X \Delta Y}$ and $\mathbf{K}_{xx}$, respectively, must be transformed following the low of error propagation:

(4.6)
$$\mathbf{K}_{xx} = \mathbf{R} \bullet \mathbf{K}_{\Delta X \Delta Y} \bullet \mathbf{R}^{T};$$
$$\mathbf{K}_{\Delta X \Delta Y} = \mathbf{R}^{T} \bullet \mathbf{K}_{xx} \bullet \mathbf{R};$$

In the practical application, the topocentrer is normally located at the "origin" of the vector (e.g. site location for velocity vector). Furthermore, the astronomical longitude and latitude (Λ, Φ) can be replaced by the geodetic longitude and latitude (λ, φ) as log as the vectors to be transformed are too small to be significantly influenced by the deflections of the vertical. This is the case for coordinate differences, eccentricities, velocities and accuracies the vectors transformations.

4.2.3. Transformation between different reference frames (ITRFs)

The basis for transformations between different reference frames is a similarity transformation, a distortion-free coordinatie transformation defined as:

(4.7)
$$\mathbf{X}s = \mathbf{T} + \mu \hat{\mathbf{R}} \mathbf{X};$$

where

X : position vector to be transformed $(X, Y, Z)^T$

Xs : transformed vector $(Xs, Ys, Zs)^T$

T : translation vector (T_1, T_2, T_3)

μ : scale factor

$\hat{\mathbf{R}}$: rotation matrix containing the 3 rotation angles R1, R2, R3 of the rotation around the coordinate axes; $\hat{\mathbf{R}}$ is orthogonal

This transformation is also called 7-parameter transformation or – if μ is not negative (no reflection) – Helmert transformation. Provided thet the scale factor is near to 1 ($\mu = 1+D$, with D very small) and the rotation angles $\mathbf{R_k}$ are very small, the following simplifivcations are possible:

$$\cos R_k \approx 1;$$
$$\sin R_k \approx R_k;$$
$$R_k \bullet R_k \approx 0;$$
$$D \bullet R_k \approx 0;$$

and eqn. 4.5 becomes a lineral system of equations:

$$(4.8)\qquad \begin{pmatrix} Xs \\ Ys \\ Zs \end{pmatrix} = \begin{pmatrix} T_1 \\ T_2 \\ T_3 \end{pmatrix} + (1+D)\bullet \begin{pmatrix} 1 & -R_3 & R_2 \\ R_3 & 1 & -R_1 \\ -R_2 & R_1 & 1 \end{pmatrix} \bullet \begin{pmatrix} X \\ Y \\ Z \end{pmatrix} \approx \begin{pmatrix} T_1 \\ T_2 \\ T_3 \end{pmatrix} + \begin{pmatrix} 1+D & -R_3 & R_2 \\ R_3 & 1+D & -R_1 \\ -R_2 & R_1 & 1+D \end{pmatrix} \bullet \begin{pmatrix} X \\ Y \\ Z \end{pmatrix};$$

The standard model of transformation between two reference frames is described by such a 7-parameter transformation with the parameters T_1, T_2, T_3, D, R_1, R_2, R_3 and their first time derivatives $\dot{T}_1$, $\dot{T}_2$, $\dot{T}_3$, $\dot{D}$, $\dot{R}_1$, $\dot{R}_2$, $\dot{R}_3$. Thus, the coordinate transformation from one reference into another on (s) is given by:

$$(4.9)\qquad \begin{pmatrix} Xs \\ Ys \\ Zs \end{pmatrix} = \begin{pmatrix} T_1 \\ T_2 \\ T_3 \end{pmatrix} + \begin{pmatrix} D & -R_3 & R_2 \\ R_3 & D & -R_1 \\ -R_2 & R_1 & D \end{pmatrix} \bullet \begin{pmatrix} X \\ Y \\ Z \end{pmatrix};$$

or in matrix notation:

$$(4.10)\qquad \mathbf{Xs = X + T + RX};$$

where matrix **R** includes both the scale and rotation parameters.

The equation for the transformation of velocities (**v**) is derived by differentiating eqn. 4.7 with respect to time:

$$(4.11)\qquad \begin{aligned} \dot{\mathbf{X}}s &= \dot{\mathbf{X}} + \dot{\mathbf{T}} + \dot{\mathbf{R}}\mathbf{X} + \mathbf{R}\dot{\mathbf{X}}; \\ \mathbf{v}s &= \mathbf{v} + \dot{\mathbf{T}} + \dot{\mathbf{R}}\mathbf{X} + \mathbf{R}\mathbf{v}; \end{aligned}$$

or

$$(4.12)\qquad \begin{pmatrix} v_{Xs} \\ v_{Ys} \\ v_{Zs} \end{pmatrix} = \begin{pmatrix} v_X \\ v_Y \\ v_Z \end{pmatrix} + \begin{pmatrix} \dot{T}_1 \\ \dot{T}_2 \\ \dot{T}_3 \end{pmatrix} + \begin{pmatrix} \dot{D} & -\dot{R}_3 & \dot{R}_2 \\ \dot{R}_3 & \dot{D} & -\dot{R}_1 \\ -\dot{R}_2 & \dot{R}_1 & \dot{D} \end{pmatrix} \bullet \begin{pmatrix} X \\ Y \\ Z \end{pmatrix} + \begin{pmatrix} D & -R_3 & R_2 \\ R_3 & D & -R_1 \\ -R_2 & R_1 & D \end{pmatrix} \bullet \begin{pmatrix} v_X \\ v_Y \\ v_Z \end{pmatrix};$$

For the transformations between the different ITRFs, the IERS published the corresponding transformation parameters in the IERS Technical Notes and IERS Annual Reports, respectively. A summary is given in the IERS Conventions (2003) (McCarthy and Petit, 2004). The transformation parameters and their rates from ITRF2000 to previous frames are listed in Table 4.2 and 4.3 and a corresponding file can be downloaded from the IERS/ITRF ftp server (ftp://itrf.ensg.ign.fr/pub/itrf/ITRF.TP). They should be used with the

standard model (eqns. 4.9 and 4.13), where the X, Y, Z and Vx, Vy, Vz are coordinates and velocities are in the ITRF2005 and Xs, Ys, Zs and Vx_s, V_{Ys} , Vz_s are the coordinates and velocities in the other frames. The given values for T_1, T_2, T_3, D, R_1, R_2 and R_3 are valid at the indicated epoch. The value of each of these transformation parameters P at any epoch t is obtained by

(4.13) $$P(t) = P(t_{ref}) + \dot{P} \bullet (t - t_{ref});$$

It has to be pointed out that the ITRFs differ by more than a coordinate transformation, because the solutions of each ITRF are based on different observation data and processing strategies. So, if e.g. the solution of ITRF2000 is transformed to ITRF97, not the original ITRF97 solution is obtained but an ITRF2000 solution with respect to the frame ITRF97,

Reference Frame	T_1 [cm] $\dot{T}_1$ [cm/yr]	T_2 [cm] $\dot{T}_2$ [cm/yr]	T_3 [cm] $\dot{T}_3$ [cm/yr]	D [ppb] $\dot{D}$ [ppb/yr]	R_1 [mas] $\dot{R}_1$ [mas/yr]	R_2 [mas] $\dot{R}_2$ [mas/yr]	R_3 [mas] $\dot{R}_3$ [mas/yr]	Epoch [yr]	IERS Tech. Note #
ITRF97	0.67	0.61	-1.85	1.55	0.00	0.00	0.00	1997.0	27
rates	0.00	-0.06	-0.14	0.01	0.00	0.00	0.02		
ITRF96	0.67	0.61	-1.85	1.55	0.00	0.00	0.00	1997.0	24
rates	0.00	-0.06	-0.14	0.01	0.00	0.00	0.02		
ITRF94	0.67	0.61	-1.85	1.55	0.00	0.00	0.00	1997.0	20
rates	0.00	-0.06	-0.14	0.01	0.00	0.00	0.02		
ITRF93	1.27	0.65	-2.09	1.95	-0.39	0.80	-1.14	1988.0	18
rates	-0.29	-0.02	-0.06	0.01	-0.11	-0.19	0.07		
ITRF92	1.47	1.35	-1.39	0.75	0.00	0.00	-0.18	1988.0	15
rates	0.00	-0.06	-0.14	0.01	0.00	0.00	0.02		
ITRF91	2.67	2.75	-1.99	2.15	0.00	0.00	-0.18	1988.0	12
rates	0.00	-0.06	-0.14	0.01	0.00	0.00	0.02		
ITRF90	2.47	2.35	-3.59	2.45	0.00	0.00	-0.18	1988.0	9
rates	0.00	-0.06	-0.14	0.01	0.00	0.00	0.02		
ITRF89	2.97	4.75	-7.39	5.85	0.00	0.00	-0.18	1988.0	6
rates	0.00	-0.06	-0.14	0.01	0.00	0.00	0.02		
ITRF88	2.47	1.15	-9.79	8.95	0.10	0.00	-0.18	1988.0	An.Rep
rates	0.00	-0.06	-0.14	0.01	0.00	0.00	0.02		1988

Table 4.2. *Transforamation parameters and their rates from ITRF2000 to previous frames. They should be used with the standard model (eqns. 4.9). The given values for T_1, T_2, T_3, D, R_1, R_2 and R_3 are valid at the indicated epoch. mas: milliarcseconds. These parameters are derived from those already published in the IERS Technical Notes indicated in the last column.*

which is manifested in slight numerical differences in site coordinates/velocities, especially for newer stations. For best possible a-priori coordinates/velocities, one should always use the newest ITRF solution, which (if necessary) can be transformed back to the frame used in the processing.

Reference Frame	T_1 [mm] $\dot{T}_1$ [mm/yr]	T_2 [mm] $\dot{T}_2$ [mm/yr]	T_3 [mm] $\dot{T}_3$ [mm/yr]	D [10^{-9}] $\dot{D}$ [10^{-9}/yr]	R_1 [mas] $\dot{R}_1$ [mas/yr]	R_2 [mas] $\dot{R}_2$ [mas/yr]	R_3 [mas] $\dot{R}_3$ [mas/yr]	Epoch [yr]
ITRF2000	0.10	-0.80	-5.80	0.40	0.000	0.000	0.000	2000.0
rates	-0.20	0.10	-1.80	0.08	0.000	0.000	0.000	

Table 4.3. *Transformation parameters at epoch 2000.0 and their rates from ITRF2005 to ITRF2000 (ITRF2000 minus ITRF2005. mas: milliarcseconds; These parameters are published by Altamimi et al., 2007.*

As the components of **R** and ***v*** are small ($<10^{-8}$ and < 10 cm/yr, respectively), the product **R*v*** in eqns. 4.11/4.12 is negligible. The transformation of ITRF velocities can therefore be reduced to

(4.14)
$$\dot{\mathbf{X}}s = \dot{\mathbf{X}} + \dot{\mathbf{T}} + \dot{\mathbf{R}}\mathbf{X};$$
$$\mathbf{v}s = \mathbf{v} + \dot{\mathbf{T}} + \dot{\mathbf{R}}\mathbf{X};$$

(4.15)
$$\begin{pmatrix} v_{Xs} \\ v_{Ys} \\ v_{Zs} \end{pmatrix} = \begin{pmatrix} v_X \\ v_Y \\ v_Z \end{pmatrix} + \begin{pmatrix} \dot{T}_1 \\ \dot{T}_2 \\ \dot{T}_3 \end{pmatrix} + \begin{pmatrix} \dot{D} & -\dot{R}_3 & \dot{R}_2 \\ \dot{R}_3 & \dot{D} & -\dot{R}_1 \\ -\dot{R}_2 & \dot{R}_1 & \dot{D} \end{pmatrix} \bullet \begin{pmatrix} X \\ Y \\ Z \end{pmatrix};$$

To transform coordinates from $ITRF_A$, epoch *t* to $ITRF_B$, epoch *t*, the following two strategies yield the same result (higher-order terms are neglected):

a) Calculating the $lTRF_A$ coordinates for the reference epoch t_{ref} using the corresponding velocities, transforming these coordinates using eqn. 4.10 and the transformation parameters valid for the reference epoch, and finally calculating the $lTRF_B$ coordinates for epoch *t* again using the corresponding transformed (eqn. 4.14) velocities:

(4.16)
$$\mathbf{X}_A(t) \xrightarrow{-\mathbf{v}_A(t-t_{ref})} \mathbf{X}_A(t_{ref}) \xrightarrow{\text{eqn 4.10}} \mathbf{X}_B(t_{ref}) \xrightarrow{+\mathbf{v}_B(t-t_{ref})} \mathbf{X}_B(t);$$

b) Transforming the coordinates using eqn. 4.10 where each transformation parameter is calculated according to eqn. 4.13.

Normally, method b) is easier and has the advantage that it is not necessary to know the velocities.

Inverse transformations

If the transformation parameters are small as it is the case for the ITRF transformation parameters (Table 4.2 and 4.3) the following simplifications are possible:

$$\begin{aligned} &(\mathbf{I}+\mathbf{R})^{-1} \approx \mathbf{I}-\mathbf{R} \qquad \text{with } \mathbf{I} = \text{identity matrix} \\ &\mathbf{R}\bullet\mathbf{T} \approx \mathbf{R}\bullet\dot{\mathbf{T}} \approx \mathbf{R}\bullet\dot{\mathbf{R}} \approx 0 \\ &\dot{\mathbf{R}}\bullet\mathbf{X} \approx \dot{\mathbf{R}}\bullet\mathbf{X}s \end{aligned} \tag{4.17}$$

and the inversion of the coordinate and velocity transformations (eqns. 4.10 and 4.11) result in:

$$\begin{aligned} \mathbf{X} &= (\mathbf{I}+\mathbf{R})^{-1}\bullet(\mathbf{X}s-\mathbf{T}) \approx \mathbf{X}s-\mathbf{T}-\mathbf{R}\mathbf{X}s \\ \mathbf{v} &= (\mathbf{I}+\mathbf{R})^{-1}\bullet(\mathbf{v}s-\dot{\mathbf{T}}-\dot{\mathbf{R}}\mathbf{X}) \approx \mathbf{v}s-\dot{\mathbf{T}}-\dot{\mathbf{R}}\mathbf{X}s-\mathbf{R}\mathbf{v}s \end{aligned} \tag{4.18}$$

This means that the parameters of the inverse transformation are obtained by reversing the signs of the original parameters.

4.3. Processing the GPS measurements

One of the important conditions for the acquirement of homogeneous and highly accurate coordinates and velocities in GPS measurements is the use of precise realization of the terrestrial reference system. The measurement processing in the present thesis was performed in ITRF2005. In the process were used IGS precise orbits (Beutler et al. 1999), as recommended by Boucher et al. (2004), as well as IGS Earth rotation parameters. The antenna heights are carefully checked and reduced to the reference point (the so-called Antenna Reference Point – ARP). The satellite orbits and earth rotation parameters (ERP) were transformed using the program `trnfsp3n` (Kouba, 2002). The used transformation parameters are listed in Table 4.4.

ITRF	GPS weeks	(dates)	Transformations performed
ITRF94	860 – 947	30 Jun. 96 – 7 Mar. 98	ITRF94 → ITRF96 → ITRF97 → ITRF2000 → ITRF2005
ITRF96	948 – 1020	8 Mar. 98 – 31 Jul. 99	ITRF96 → ITRF97 → ITRF2000 → ITRF2005
ITRF97	1021 – 1142	1 Aug. 99 – 1 Dec. 01	ITRF97 → ITRF2000 → ITRF2005
IGS00	1143 – 1252	2 Dec. 01 – 10 Jan. 04	ITRF2000 → ITRF2005
IGS00b	1253 – 1399	11 Jan. 04 – 04 Nov. 06	ITRF2000 → ITRF2005
IGS05	1400 –	05 Nov. 06 –	-

Table 4.4. *History of reference frame used for IGS precise orbits and ERP were referred to the specific reference frames (Beutler et al., 2007), and transformations preformed in order to obtain data in ITRF2005.*

The GPS processing of continuous and reoccupation networks was realized using Processing Engine (BPE) of Bernese GPS Software version 5.0. The Bernese software is developed by the Astronomical Institute of the University of Berne (AIUB), Switzerland as a scientific research tool for high performance, high accuracy and highly reference (GPS, GLONASS, SLR) and state-of-art modelling post processing package. Since its appearance in 1993 the software has been developed in seven basic versions, the last one – 5.0, being available since 2004. Its basic characteristics are: high accuracy and reliability of the obtained results; high flexibility; use of the state-of-art scientific and technological achievements; high efficiency. The software is also being constantly developed due to the engagements of the CODE analysis centre in EUREF and IGS. As far as EUREF is concerned, the Bernese software is practically the standard for processing and analysis of the GPS observations (in all the 11 centres for analysis in Europe).

The measurement processing was realized in several major steps:

4.3.1. Data pre-processing

- Transformation of the RINEX files, the precise ephemerides and Earth orientation parameters into BSW format, extraction satellite clock information, and calculation of a-priori coordinates.
- Determining (synchronize) the correction for the GPS receiver clocks. The clock corrections are necessary for making the double differences. The corrections of the clocks of the GPS receivers are calculated for each epoch from the code measurements and are recorded in the file with the phase measurements. The Bernese software used the double differences (DD) as a basic “observed” quantity. The single differences are recorded in a file, while the DD are formed in the course of processing.

- Forming phase single-differences using the maximum observation strategy OBS-MAX (Beutler et al., 2007).
- Detecting and resolving cycle slips in the phase observations. This step consists scanning and correction of the single differences. The main task is to discover intervals in the data, which contain cycle slips, and to correct them, as well as to localize the unusable (short) intervals with measurements and to remove them. The Bernese software uses only phase measurements (combinations of them) for corrections of the single differences and does not depend on code measurements. This means also that the Anti-Spoofing (A/C) does not exert any influence on the processing. The corrected single differences are the input for the basic estimation programme.

4.3.2. Data processing

The calculations are divided in three main steps for each daily solution – check for outliers, obtaining the ambiguities of the phase measurements (phase ambiguity resolution) and obtaining the network solution.

- Checking the observations and removing the outliers.
- Resolving the ambiguities using the QIF (Quasi-Ionosphere-Free) strategy (Beutler et al., 2007) for campaigns data and resolution of the wide-lane ambiguities using the Melbourne–Wubbena linear combination (Melbourne 1985; Wubbena 1985); using DCB files when available,. The European Ionosphere model of CODE (Centre for Orbit Determination in Europe) is used in this step.
- Adjustment of the network and acquiring daily solutions. To eliminate the effect of the tropospheric refraction, every 2h one tropospheric parameter is determined for each station using the tropospheric model of DRY_NIELL mapping function (Niell, 1996). In this step the network is adjusted with minimum constraint. The normal equations being saved for subsequent processing.
- Computation of normal equations, checking the coordinates of fiducial sites and daily repeatability using seven parameters Helmert transformation.
- The velocities are calculated fixing the velocities of 7 reference points – BUCU, GOPE, GRAS, GRAZ, JOZE, WTZR and ZIMM to their ITRF2005 values. In order to obtain the results with respect to the “stable” part of the Eurasian plate, the velocities according to the model of the rigid rotation of the Eurasian plate are subtracted from the obtained absolute values of the points. The

absolute rotation pole of the Eurasian plate is determined by Altamimi et al., 2007 on the basis of 41 points from the Eurasian plate in the ITRF2005 realization. The coordinates of the rotation pole are 56.33°N and 95.979°W and the rotation velocity is 0.261 °/Myr (Altamimi et al., 2007, Figure 4.1).

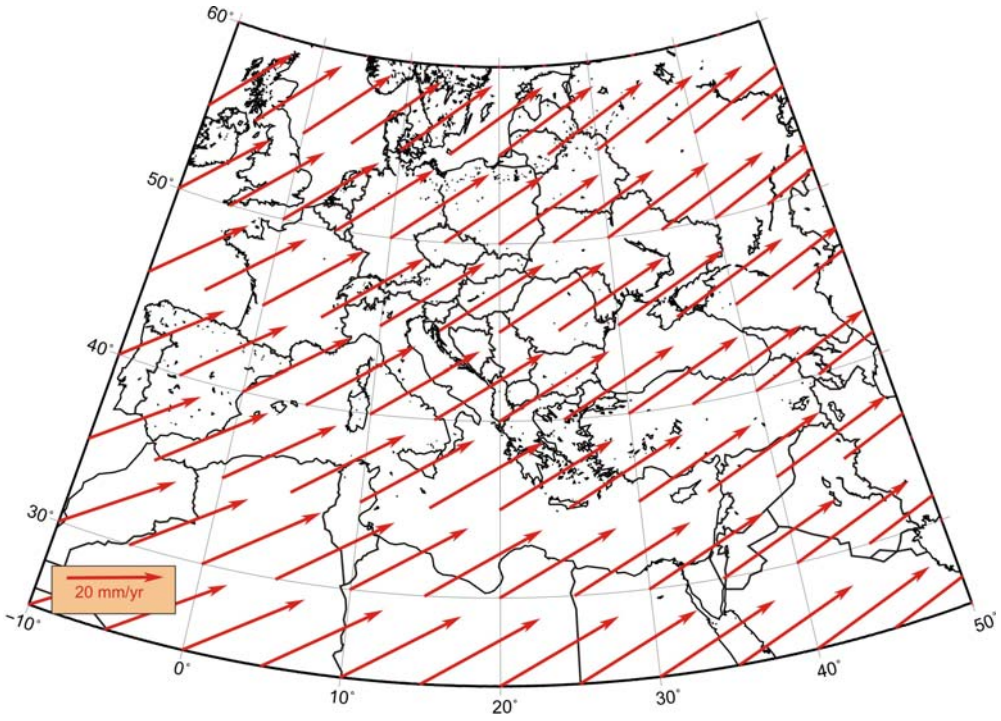

Figure 4.1. *ITRF2005 Absolute Rotation Pole (Altamimi et al,. 2007). The model velocities were estimated using plate motion calculator via Unavco Facility (http://sps.unavco.org/crustal_motion/dxdt/model/). The coordinates of the rotation pole are 56.33°N and 95.979°W and the rotation velocity is 0.261 °/Myr (Altamimi et al., 2007).*

4.4. Strain rate basic theory

4.4.1. The strain tensor

The strain calculations performed base on the fundamental theorem of kinematics, which states that an infinitesimal dislocation **u(x)** in a ductile body can, in a first approximation, be represented as sum of a translation $\mathbf{u}^{[0]}$, a rotation $\mathbf{u}^{[R]}$ and a dilation $\mathbf{u}^{[D]}$:

$$\mathbf{u(x)} = \mathbf{u}^{[0]} + \mathbf{u}^{[R]} + \mathbf{u}^{[D]};$$

or in index notation with summation over *k:*

$$u_i = u_i(0) + \underbrace{\frac{a_{ik} - a_{ki}}{2}}_{antisymmetric} \bullet x_k + \underbrace{\frac{a_{ik} + a_{ki}}{2}}_{symmetric} \bullet x_k ;$$

with the deformation tensor

$$a_{ik} = \frac{\partial u_i}{\partial x_k};$$

which has been divided in an antisymmetric and a symmetric part. u_i is the ith component of u, x_k is the kth component of the coordinate system. The strain tensor ε_{ik} is the symmetric part of the deformation tensor a_{ik}. The antisymmetric part of the deformation tensor can be interpreted as infinitesimal rotation. Detailed description for strain rate thery is described by Peter (2000).

4.4.2. Obtaining strain rates

The QOCA (Quasi-Observation Combination Analysis) software package was used to obtain the strain for the region of Southwest Bulgaria (Dong et al. 1998 and Shen et al. 2000). QOCA is a software package that combines various loosely constrained geodetic site coordinate and velocity solutions (as quasi observations) to obtain crustal deformation information. The software was developed in the Jet Propulsion Laboratory, California Institute of Technology, USA. QOCA accepts also results in SINEX format, obtained with BSW. The strain rates were obtained for triangles using the Delaunay triangles strategy for their formation.

4.5. Time series analysis

The time series analysis have been done using QOQA software package. The advantages of time series analysis are: (1) it is much efficient than the global analysis, (2) it is easy to detect outliers and (3) any misfit of one time series will not affect the estimates of other sites. Although such an analysis neglects the correlations between different sites so that it is not theoretically optimal, however, Zhang (1996) had showed that these correlations are small, such a neglection only imposes very minor impact on the solutions. This time series analysis approach gains great success in the deformation field analysis, in particular for the coseismic field, seasonal deformation field and postseismic deformation field. The The QOCA utility for analyze time series is designed to perform site position time series analysis.

It allows to estimate constant offset, velocity, (also quadratic and cubic terms, if specified), jumps, seasonal variations, non-linear variation (exponential decay and logarithmic decay), and any user defined non-linear periodic variations. This utility considers the correlation between east, north and up components of the station time series.

In our position time series analysis we estimate parameters as jumps, trends, and seasonal variations (annual and semi-annual) of 136 permanent stations. The time series parameters are listed in Appendix A. The north, east and up detrended position time-series, after removing the offsets and constant velocities, with annual and semi-annual signals, for the 136 analyzed stations are shown in Appendix B. In generally we fallowed the distributed processing approach, which is well described by Serpelloni et al. (2006).

The observed motion *f(t)* of each site in each component (east, north and up) can be written as (e.g., Ding et al., 2005):

$$(5.1)\quad f(t_i) = a + bt_i + c\sin(2\pi t_i) + d\cos(2\pi t_i) + e\sin(4\pi t_i) + f\cos(4\pi t_i) + \sum_{j=1}^{n_g} g_j H(t_i - T_{gj}) + \varepsilon_i ,$$

where t_i for i=1,…,N are the daily solution epochs in units of years, and H is the Heaviside step function (Abramowitz and Stegun, 1972). Te first two terms are the constant bias with respect to 2003.00 – *a*, and the linear rate – *b*, respectively. Coefficients *c* and *d* describe the annual periodic motion, while *e* and *f* describe the semi-annual motion. The next term corrects for any number (n_g) of offsets, with magnitudes *g* and epochs *Tg*. In some time-series there are offsets due mainly to antenna or receiver changes, which we model as step functions. Assuming that the offset epochs are known, the model is linear with respect to the coefficients.

Chapter V

Results

5.1. Continuous GPS position time series analysis

The loosely constrained daily solution files in SINEX format from BERNESE have been transformed into so-called QOB (in ASCII format) files as quasi-observations into the Quasi-Observation Combination Analysis (QOCA) software package.

Because of the existence of outliers in daily solutions, the robust-fit algorithm embedded in the QOCA software, which resists outliers better than conventional least squares (Bock et al., 2000), has been employed to estimate simultaneously all the parameters. Appendix A provides the time-series parameters of 136 permanent stations described in Chapter 3 above and derived for the Central and East Mediterranean that observed for more than 2 years. In particular the annual and semi-annual amplitudes (*c*, *d*, *e* and *f*) terms, referred to the 1st January 2003. The Weighted Root Mean Squares (WRMS) of the time-series after removal of constant velocity, and the computed offsets values with 1σ uncertainties, are listed in Appendix A. ITRF2005 horizontal velocities, with 1σ uncertainties, are listed in Table 5.1, as well as horizontal velocities with respect to Eurasia, Nubia, Adria, and Apulia plates using the rotations poles estimated by Altamimi et al., (2007) between ITRF2005 and stable Eurasia (56.33°N, 95.979°W, 0.261°/Myr), and Nubia (49.955°N, 82.501°W, 0.269°/Myr) and by D'Agostino et al., (2008) and Adria microplate (62.466°N, 31.247°W, 0.487°/Myr), and Apulia microplate (4.041°N, 132.659°W, 0.340°/Myr). The north, east and up detrended position time-series for the 136 analyzed stations are shown in Appendix B, after removing the offsets and estimated constant velocities, with theirs annual and semi-annual signals.

The mean value of pos-fit WRMS for the east, north and up components are about 1.4 mm, 1.5 mm, and 4.9 mm, respectively (Appendix A). In particular, the station with the biggest WRMS is VLUC, displaying values of east = 3.6 mm, north = 3.0 mm, and up = 8.4 mm.

The estimated seasonal signals are listed in Appendix A and plotted on Appendix B. The seasonal signals are in general quite small with level below 1 mm. The mean annual sine and cosine amplitudes for the east components are 0.11±0.03 mm and 0.06±0.03 mm, respectively, with the largest value observed at VAGA (Valle Agricola – Italy) -3.49 mm and SOFA (Sofia-Bulgaria) -5.05 mm. The mean annual sine and cosine amplitudes for the north components are 0.14±0.13 mm and 0.86±0.13 mm, respectively, with the largest value observed at SARA (Sarande – Albania) -5.73 mm and BRIX (Brescia) -2.49 mm. The mean annual sine and cosine amplitudes for the up components are 0.33±0.03 mm and 0.47±0.03 mm, respectively, with the largest value observed at VAGA (Valle Agricola-Italy) -5.73 mm and BRIX (Brescia) -2.49 mm.

For the semi-annual seasonal signals, the mean sine and cosine amplitudes for the east components are -0.02±0.03 mm and -0.11±0.03 mm, respectively with the largest value observed at HMDC (Modica – Italy) -1.07±0.03 mm and -0.47±0.04 mm. The mean sine and cosine amplitudes for the north components are -0.13±0.03 mm and -0.08±0.03 mm, respectively with the largest value observed at VAGA (Valle Agricola-Italy) -1.71±0.03 mm and 2.08±0.03 mm. The mean sine and cosine amplitudes for the up components are -0.04±0.12 mm and -0.34±0.12 mm, respectively with the largest value observed at VLUC (Vallo della Lucania – Italy) -3.56±0.21 mm and -2.50±0.21 mm.

The processing procedures (well described by Serpelloni et al. 2006) that have been used to compute and remove the seasonal terms in order to reduce the daily data scatter and look at residual time series, with the aim to improve the determination of the constraint velocity term, which is the main goal of analysis of CGPS. Seasonal variations are generally related to:

- Gravitational excitation. This category includes rotational displacements due to seasonal polar motion (UT1), and loading induced displacement caused by solid Earth, ocean and atmospheric tides, which are modelled in the raw data reduction step. Ocean tide effects should still be present, and are mainly due to the use of global ocean tide models instead of higher quality local tidal models. Pole tide loading also belongs to this first category, with the spectrum of mostly annual and Chandler wobble periods (~465 days).
- Thermal origin coupled with hydrodynamics. In this category belongs the deformation caused by pressure field variation, non-tidal sea surface fluctuation, ground water changes in both liquid and solid form, bedrock expansion beneath the GPS benchmark, and wind shear.

- Sources those are indirect due to geophysical processes, or instrument, or modelling deficiency (Dong et al., 2002). This category contains other error sources, which also generate apparent seasonal variations, such as orbit modelling errors caused by imperfect reference frame, which is defined through a set of stations that are subject to seasonal variation.
- Seasonal hydrological changes, loading/unloading of phreatic napes that induce seasonal changes with low level in summer and higher level in winter.

There are other important phenomena that can affect the position time series with a seasonal signature; these involve tectonic-induced deformation, due to possible seasonal variation in regional fault slip or regional stress (e.g., slow earthquakes; Miller et al. 2002). Dong et al. (2002) provides the magnitudes of some individual source that can potentially affect the GPS time series. These contributions of geophysical sources and model errors to the observed annual and semi-annual variations in site position have a range of effects as follow: Pole tide ~4 mm, Ocean tide ~0.1 mm, Atmospheric mass ~4 mm, Non-tide ocean mass 2-3 mm, Snow mass 3-5 mm, Soil moisture 2-7 mm, Bedrock thermal expansion ~0.5 mm, errors in orbit, phase centre, and troposphere models – no quantitative results yet, Error in network adjustment ~0.7mm, Differences from different software ~2-3 mm at some sites 5-7 mm. There is a set of complex sources that are much more difficult to asses and model such as: neglected seasonal effects in the definition of the ITRF reference frame; imperfect atmospheric modelling (Williams et al., 1998); bedrock thermal expansion, which may affect the site vertical positing of 0.5 mm level (Dong et al., 2002); other environmental factors, including types of domes or monuments (e.g. Meertens et al., 1996; Bock et al., 2000; Hatanaka et al., 2001)

The network of permanent stations that is analyzed is realized through stations characterised by several different monument types such as: pillars steel musts, anchored to stable buildings (e.g. SOFI, SOFA, SAND). Stations realized through pillars founded directly on the bedrock (e.g. AJAC, AQUI, CAGL, CAME, ELBA, GRAS, NOT1) perform very well, with relatively lower amplitudes on both horizontal and vertical components. The stations build on the buildings (e.g. GRAZ, PRAT, SOFI) perform quite well, displaying horizontal seasonal amplitudes significantly bellow the 1 mm level.

The station SOFA, which has built on the high building in urban condition (capital Sofia, Bulgaria), presents large amplitudes on horizontal components. The photos of the monument are presented in Appendix C, however the log file is not available at present time. It is supposed that these large amplitudes are linked with the type of the monument conditions. The other station that presents the large amplitudes on horizontal components is

VAGA, which is stabilized on the sedimentary bedrock and the monument type is steel rods. The log file and photos of the station are presented in Appendix C. It is unclear that large amplitudes have correlation with the monument condition.

Table 5.1. *ITRF 2005 horizontal GPS velocities from permanent stations and their mean square errors with respect to the stable Eurasian, Nubia, Adria, and Apulia plates* Lon.: longitude [°], Lat.: latitude [°], V_N, V_E: north/east component of velocity [mm/yr], S_{V_N}, S_{VE}: 1 sigma uncertainties of corresponding velocity component [mm/yr], ρ_{EN}: correlation coefficient between the eats and north uncertainties.

Site Name	Lon.	Lat.	ITRF2005					Eurasia-fix		Nubia-fix		Adria-fix		Apulia-fix	
			V_N	V_E	S_{V_N}	S_{V_E}	ρ_{EN}	V_N	V_E	V_N	V_E	V_N	V_E	V_N	V_E
AJAC	8.7626	40.9073	16.2	20.8	0.5	0.5	-0.3	0.7	0.1	-3.0	3.5	0.1	-2.2	-7.3	-0.8
AMUR	16.6040	39.8874	19.1	22.9	0.4	0.5	0.0	4.3	0.5	0.1	3.5	0.6	-2.6	-0.2	-0.3
ANKR	32.7585	42.3682	12.0	1.3	0.6	0.6	0.4	-0.6	-23.8	-5.4	-21.6	-10.5	-28.7	2.5	-24.1
AQUI	13.3502	38.7551	17.9	21.8	0.4	0.4	-0.1	2.8	0.4	-1.2	3.5	0.4	-1.8	-3.1	-1.1
ARKI	23.0336	40.5668	-4.6	14.1	0.5	0.5	0.3	-18.7	-9.6	-23.1	-7.0	-24.9	-14.3	-20.1	-9.4
AUT1	23.0037	46.5621	5.8	24.1	0.4	0.5	0.2	-8.3	0.6	-12.7	3.3	-14.5	-3.0	-9.7	-0.2
BACA	26.9122	47.6518	13.8	22.0	0.5	0.4	0.0	0.3	-1.0	-4.3	1.6	-7.4	-1.6	0.6	-5.4
BAIA	23.5577	40.7082	13.4	22.6	0.4	0.4	0.0	-0.6	0.5	-5.1	3.2	-7.0	0.8	-1.8	-4.6
BERA	19.9455	45.5607	14.9	21.4	0.4	0.5	0.1	0.5	-1.5	-3.9	1.3	-4.6	-4.9	-2.4	-2.4
BIEL	8.0481	44.5002	15.7	19.9	0.5	0.4	-0.1	0.1	0.2	-3.5	3.7	-0.2	0.0	-8.2	-2.7
BOLG	11.3568	44.1222	19.3	20.4	0.4	0.4	-0.1	4.0	-0.2	0.2	3.1	2.4	-1.1	-2.8	-2.8
BRAS	11.1131	41.5460	16.8	20.9	0.4	0.4	-0.2	1.4	0.2	-2.4	3.5	-0.1	-0.9	-5.5	-2.2
BRIX	14.5940	44.4639	16.5	20.7	0.4	0.4	-0.1	1.1	0.5	-2.7	3.9	-0.1	0.3	-6.2	-2.6
BSSO	26.1257	46.4990	18.4	22.0	0.5	0.4	0.2	3.4	0.2	-0.7	3.3	0.5	-2.5	-2.0	-0.9
BUCU	11.3368	39.1359	12.5	23.2	0.4	0.4	0.0	-1.2	-0.1	-5.8	2.5	-8.6	-1.8	-1.2	-3.3
BZRG	8.9728	39.1359	16.4	19.7	0.5	0.6	-0.4	1.0	-0.4	-2.8	3.0	-0.6	-0.1	-5.8	-4.1
CAGL	8.9728	43.1120	16.2	21.2	0.5	0.6	-0.4	0.6	-0.2	-3.1	3.0	0.0	-4.2	-7.2	0.5
CAGZ	13.1240	39.3402	16.3	21.1	0.4	0.4	-0.1	0.8	-0.3	-2.9	2.9	0.2	-4.3	-7.1	0.4
CAME	16.4492	39.2262	18.7	22.8	0.4	0.5	0.0	3.5	1.6	-0.4	4.8	1.2	-0.1	-2.5	-0.4
CAMO	16.7756	40.4897	19.0	23.4	0.4	0.5	0.0	4.2	0.8	0.0	3.8	0.5	-3.2	-0.3	0.9
CCRI	15.3047	39.5287	18.6	23.8	0.4	0.5	-0.1	3.8	1.1	-0.4	4.1	0.0	-2.9	-0.5	1.3
CDRU	15.9546	45.8022	17.4	21.0	0.4	0.5	0.0	2.4	-1.2	-1.6	1.9	-0.7	-4.5	-2.6	-1.7
CETR	9.0956	44.1615	18.7	22.2	0.4	0.4	-0.1	3.7	-0.3	-0.4	2.7	0.3	-4.2	-1.0	-0.3
COMO	28.6575	39.2784	15.2	19.9	0.5	0.4	0.2	-0.3	0.1	-4.0	3.6	-1.0	0.0	-8.1	-3.1
COST	16.5473	39.9938	13.0	23.5	0.4	0.5	0.0	-0.3	-0.2	-5.0	2.2	-8.7	-2.3	0.9	-3.2
CRLM	15.8155	45.8784	18.9	23.0	0.4	0.5	0.0	4.0	0.3	-0.1	3.3	0.3	-3.7	-0.4	0.5
CUCC	22.9135	38.0785	19.2	22.0	0.4	0.4	0.1	4.2	-0.4	0.1	2.6	0.8	-4.0	-0.6	-0.6
DEVA	23.9326	42.9318	11.9	20.0	0.5	0.6	0.3	-2.1	-2.4	-6.6	0.4	-8.3	-3.0	-3.6	-6.4
DION	22.9335	42.6500	-11.5	7.4	0.4	0.4	0.2	-25.5	-16.6	-30.0	-14.0	-32.1	-21.7	-26.5	-16.0
DRAG	18.1104	37.5136	12.4	24.8	0.4	0.4	0.0	-1.7	1.8	-6.1	4.5	-7.9	-0.6	-3.2	-0.5
DUBR	15.0821	42.7529	17.4	22.7	0.4	0.6	0.0	2.7	0.4	-1.5	3.4	-1.6	-1.7	-1.0	-1.5
EIIV	10.2111	40.5823	16.5	24.3	0.4	0.4	-0.3	1.5	1.6	-2.6	4.6	-1.6	-3.4	-3.6	2.9
ELBA	14.3349	38.4268	16.3	20.5	0.4	0.5	-0.1	0.9	-0.4	-2.9	3.0	-0.3	-2.2	-6.5	-1.8
ENAV	21.9284	41.9735	18.2	21.1	0.5	0.6	0.2	3.1	-0.9	-0.9	2.2	0.3	-4.1	-2.4	-1.4
EYPA	14.6693	44.4194	1.9	11.4	0.4	0.4	-0.1	-12.3	-12.2	-16.7	-9.5	-18.1	-17.0	-14.3	-11.8

Site Name	Lon.	Lat.	ITRF2005					Eurasia-fix		Nubia-fix		Adria-fix		Apulia-fix	
			V_N	V_E	S_{V_N}	S_{V_E}	ρ_{EN}	V_N	V_E	V_N	V_E	V_N	V_E	V_N	V_E
FRES	8.9211	50.3642	19.0	22.3	0.4	0.4	-0.2	4.0	0.6	0.0	3.7	1.1	-1.8	-1.3	-0.8
GENO	30.4967	49.9137	15.9	20.7	0.5	0.4	-0.2	0.3	0.5	-3.4	4.0	-0.3	-0.3	-7.6	-1.8
GLSV	14.7856	43.7547	13.3	22.4	0.4	0.4	0.0	0.4	-0.4	-4.4	2.0	-8.7	0.8	2.4	-7.0
GOPE	6.9206	47.0671	14.8	20.3	0.5	0.4	-0.3	-0.2	0.3	-4.2	3.6	-3.2	2.5	-5.4	-5.7
GRAS	15.4935	43.4263	16.8	20.1	0.4	0.4	0.0	1.1	0.1	-2.5	3.6	1.3	-1.1	-7.7	-1.6
GRAZ	9.8920	41.0728	15.4	22.1	0.4	0.4	-0.2	0.4	1.3	-3.7	4.5	-2.8	1.8	-4.5	-3.1
GROG	15.0599	46.0481	15.9	20.6	0.4	0.5	-0.1	0.4	0.0	-3.3	3.4	-0.6	-1.4	-7.0	-1.8
GROT	14.5437	36.9590	17.7	21.4	0.4	0.4	0.0	2.7	-0.6	-1.3	2.4	-0.4	-3.6	-2.4	-1.5
GSR1	14.7831	45.0151	17.4	21.0	0.4	0.6	0.0	2.3	0.2	-1.7	3.4	-0.5	0.1	-3.0	-3.5
HMDC	7.6394	43.7956	19.9	20.5	0.5	0.4	-0.2	4.9	-2.3	0.8	0.7	1.9	-7.6	-0.4	-0.7
IENG	11.2138	42.3825	15.7	20.4	0.4	0.4	-0.2	0.1	0.6	-3.5	4.2	0.0	0.1	-8.4	-1.9
IGMI	13.3156	41.8281	17.4	21.1	0.4	0.4	-0.2	2.0	0.4	-1.8	3.7	0.5	-0.9	-4.8	-1.8
INGP	12.5148	41.1044	17.7	21.2	0.4	0.4	-0.2	2.6	-0.3	-1.4	2.9	0.2	-2.4	-3.4	-1.8
INGR	29.0193	52.0973	17.0	20.5	0.5	0.5	0.4	1.8	-0.9	-2.1	2.3	-0.3	-3.4	-4.5	-2.1
ISTA	21.0315	39.7464	11.1	24.7	0.4	0.4	-0.2	-2.1	0.4	-6.8	2.8	-10.6	-3.5	-0.7	-0.8
JOZE	19.9355	38.2095	14.3	20.7	0.4	0.5	0.2	0.0	0.0	-4.4	3.0	-5.4	3.1	-2.4	-7.6
KASI	22.0458	39.0799	15.2	19.5	0.5	0.6	0.2	0.7	-3.6	-3.6	-0.8	-4.3	-7.5	-2.2	-3.9
KOUN	17.1250	42.2837	-11.2	9.8	0.4	0.5	0.0	-25.4	-13.9	-29.8	-11.2	-31.2	-18.8	-27.3	-13.3
KROT	22.7131	53.8924	19.2	28.0	0.4	0.4	0.2	4.4	5.2	0.2	8.1	0.4	1.0	0.2	5.4
KUST	20.6699	35.4998	13.1	24.0	0.4	0.5	-0.2	-1.0	0.9	-5.4	3.7	-7.1	-1.7	-2.6	-0.9
LAMA	12.6057	44.0733	14.1	20.3	0.5	0.7	-0.1	-0.3	0.2	-4.6	3.2	-5.6	4.3	-2.8	-8.4
LAMP	9.8397	39.4626	18.8	19.4	0.4	0.4	-0.2	3.5	-3.3	-0.4	-0.3	1.4	-9.4	-2.7	-0.7
LASP	16.1377	45.8573	15.9	20.8	0.4	0.5	0.0	0.5	0.4	-3.3	3.8	-0.5	-0.7	-7.0	-1.8
LATT	9.4070	39.8972	16.7	26.4	0.4	0.4	-0.1	1.8	3.9	-2.3	6.9	-1.7	0.0	-2.8	4.0
LEC1	25.1806	38.5290	15.8	19.8	0.5	0.5	0.3	0.3	-0.1	-3.4	3.3	-0.5	-0.2	-7.4	-3.3
LEMN	22.2010	39.4460	2.1	7.2	0.5	0.5	0.2	-11.7	-16.7	-16.3	-14.2	-18.8	-20.9	-12.2	-17.2
LIDO	16.2878	41.8931	0.6	13.1	0.4	0.5	0.0	-13.6	-10.6	-18.0	-7.9	-19.5	-15.3	-15.4	-10.2
LUZZ	12.4933	35.8380	20.1	22.3	0.4	0.4	-0.2	5.2	-0.2	1.1	2.8	1.6	-4.1	0.7	-0.2
M0SE	14.5262	42.4282	16.6	19.8	0.5	0.7	0.0	1.3	-1.6	-2.6	1.6	-0.7	-4.0	-4.9	-2.8
MALT	11.1307	40.6491	19.8	21.0	0.4	0.4	-0.2	4.7	-1.9	0.7	1.0	1.8	-7.8	-0.7	0.4
MAON	16.7045	44.5200	16.2	20.3	0.4	0.5	0.0	0.8	-0.8	-3.0	2.5	-0.7	-2.8	-6.1	-2.1
MATE	11.6468	38.0082	18.9	22.9	0.4	0.4	-0.1	4.1	0.5	-0.1	3.5	0.3	-2.7	-0.3	-0.2
MEDI	12.5843	41.3712	17.4	22.3	0.4	0.6	-0.2	2.1	1.6	-1.8	5.0	0.4	0.8	-4.6	-1.0
MILO	15.1586	44.6290	18.3	21.7	0.4	0.5	-0.1	3.1	-0.5	-0.8	2.6	1.0	-5.2	-3.2	0.6
MOCO	10.9487	45.0739	19.3	21.9	0.4	0.4	-0.1	4.3	-0.1	0.2	3.0	1.2	-2.9	-0.8	-1.1
MODE	7.9272	44.6294	19.5	20.5	0.5	0.4	-0.2	4.1	0.0	0.3	3.4	2.7	-0.8	-2.9	-2.6
MONC	10.9492	45.7698	15.5	20.4	0.4	0.4	-0.1	-0.1	0.6	-3.7	4.1	-0.3	0.1	-8.4	-2.0
MOPS	7.0611	40.7564	19.0	20.5	0.5	0.4	-0.1	3.6	0.0	-0.2	3.4	2.2	-0.8	-3.4	-2.6
MRGE	15.4887	44.5200	15.1	20.1	0.4	0.5	-0.1	-0.6	0.6	-4.1	4.2	-0.4	0.5	-9.3	-2.3
MRLC	11.6465	38.2638	18.3	22.1	0.4	0.4	-0.1	3.3	-0.1	-0.8	2.9	0.0	-3.2	-1.6	-0.8
MSEL	15.5083	43.2632	18.0	21.8	0.4	0.6	0.0	2.7	1.1	-1.2	4.4	1.0	0.3	-4.0	-1.5
MSRU	12.5247	35.1410	20.1	22.0	0.4	0.4	-0.2	5.2	-0.6	1.1	2.3	1.9	-5.2	0.3	0.2
MURB	33.3964	38.0471	17.2	22.5	0.7	0.8	0.4	1.9	1.3	-2.0	4.6	-0.1	-0.3	-4.3	-0.6
NICO	23.8640	36.8758	16.3	20.2	0.5	0.6	0.3	3.8	-5.4	-1.1	-3.4	-6.4	-13.0	7.2	-2.9
NOA1	14.9898	45.4472	-11.3	6.9	0.4	0.6	0.0	-25.3	-17.1	-29.8	-14.5	-31.8	-22.2	-26.3	-16.4
NOT1	8.6140	41.1273	19.9	21.0	0.5	0.4	-0.1	4.9	-1.8	0.8	1.1	1.8	-7.2	-0.3	-0.2
NOVA	20.7940	46.5552	15.9	20.2	0.4	0.5	0.2	0.3	0.3	-3.3	3.8	-0.1	0.1	-7.7	-2.5

Site Name	Lon.	Lat.	ITRF2005					Eurasia-fix		Nubia-fix		Adria-fix		Apulia-fix	
			V_N	V_E	S_{V_N}	S_{V_E}	ρ_{EN}	V_N	V_E	V_N	V_E	V_N	V_E	V_N	V_E
ORID	20.6713	45.5608	11.8	23.5	0.4	0.4	0.0	-2.5	0.5	-6.9	3.3	-7.9	-2.7	-5.0	-0.7
OROS	18.6805	40.8705	15.3	21.9	0.4	0.4	0.0	0.9	0.0	-3.4	2.9	-4.4	0.0	-1.6	-4.3
OSJE	14.5564	45.4112	15.9	22.7	0.4	0.5	-0.1	1.3	1.0	-2.9	4.0	-3.2	0.5	-2.1	-2.7
PACA	11.8961	44.7646	17.3	20.6	0.4	0.4	-0.1	2.3	-1.4	-1.8	1.7	-0.6	-4.5	-3.1	-2.1
PADO	10.3122	45.2030	16.9	21.2	0.4	0.4	-0.2	1.6	0.7	-2.2	4.0	-0.2	0.3	-4.9	-2.5
PARM	9.1361	42.2310	17.2	21.2	0.4	0.4	-0.1	1.8	0.8	-2.0	4.2	0.6	0.1	-5.5	-1.8
PAVI	24.3400	47.7896	16.1	20.1	0.4	0.4	0.2	0.6	0.0	-3.1	3.5	-0.1	-0.4	-7.2	-2.8
PAZA	19.2815	41.6848	14.1	22.8	0.4	0.4	0.0	0.2	-0.5	-4.3	2.1	-6.6	-3.3	-0.7	-2.4
PENC	20.4398	49.6026	14.9	22.1	0.4	0.4	0.1	0.4	0.8	-3.9	3.8	-4.4	1.5	-2.8	-4.2
PESH	34.5429	38.6190	12.2	22.5	0.6	0.4	-0.2	-2.2	-0.3	-6.5	2.5	-7.4	-3.2	-4.8	-1.8
POLV	20.5852	43.8856	13.0	22.4	0.4	0.5	0.2	0.8	-1.2	-4.1	0.9	-9.8	-1.0	4.7	-7.2
PONT	11.0991	39.2457	9.4	18.9	0.4	0.4	-0.2	-5.0	-4.4	-9.3	-1.7	-10.2	-9.0	-7.5	-4.1
PRAT	26.2650	38.3217	17.5	21.4	0.5	0.5	0.3	2.1	0.7	-1.7	4.0	0.6	-0.5	-4.8	-1.5
PRKV	22.1843	38.0558	0.6	4.1	0.5	0.6	0.2	-13.0	-20.0	-17.6	-17.6	-20.5	-24.7	-12.9	-20.1
PSAR	21.4647	45.8935	-1.0	8.6	0.5	0.6	0.2	-15.1	-15.1	-19.6	-12.4	-21.1	-19.9	-17.0	-14.5
RLSO	11.0421	43.9335	-8.3	9.8	0.4	0.4	-0.1	-22.6	-13.8	-27.0	-11.1	-28.3	-18.8	-24.8	-13.1
ROVE	12.4507	42.6584	16.3	20.4	0.4	0.4	-0.1	0.9	0.2	-2.9	3.6	-0.6	0.1	-6.0	-3.2
RSMN	14.0015	41.5506	18.5	22.2	0.4	0.4	-0.1	3.2	1.2	-0.7	4.5	1.2	0.0	-3.1	-1.1
RSTO	23.2678	39.8661	18.3	22.8	0.4	0.4	0.2	3.2	1.3	-0.8	4.4	0.5	-0.7	-2.4	-0.4
SAND	20.0259	45.0510	12.4	23.0	0.4	0.5	0.2	-1.6	-0.3	-6.1	2.4	-7.9	-3.4	-2.9	-1.7
SARA	10.9198	39.0359	13.9	20.0	0.4	0.4	-0.1	-0.5	-3.1	-4.8	-0.2	-5.6	-6.9	-3.4	-3.4
SBPO	16.6885	44.6355	16.5	20.1	0.4	0.5	0.0	1.1	-0.3	-2.7	3.1	-0.3	-0.8	-5.9	-3.2
SERS	11.1827	42.0506	18.4	23.8	0.4	0.4	-0.1	3.5	1.1	-0.6	4.1	-0.2	-3.0	-0.9	1.4
SGIP	19.4963	42.6678	16.8	22.2	0.4	0.4	0.1	1.4	1.7	-2.4	5.0	-0.1	0.9	-5.5	-1.0
SHKO	23.2685	42.5561	15.1	22.0	0.4	0.4	0.2	0.6	-0.6	-3.7	2.3	-4.3	-3.2	-2.5	-2.2
SOFA	23.3947	38.7813	13.3	24.6	0.4	0.4	0.2	-0.8	1.5	-5.2	4.2	-7.1	-1.0	-2.1	-0.6
SOFI	20.6736	43.8679	12.1	23.5	0.4	0.5	0.2	-1.9	0.3	-6.4	3.0	-8.3	-2.2	-3.2	-1.7
SPAN	18.4139	39.1478	5.6	19.6	0.4	0.4	0.0	-8.8	-3.7	-13.2	-1.0	-14.1	-8.3	-11.4	-3.5
SRJV	16.9150	46.4722	15.6	23.1	0.4	0.5	0.0	0.9	1.0	-3.3	4.0	-3.5	-0.5	-2.7	-1.6
STSV	9.3473	38.8028	19.0	24.5	0.4	0.4	0.0	4.2	1.8	0.0	4.7	0.3	-2.3	-0.1	2.0
STUE	15.2342	41.0743	20.5	21.8	0.4	0.5	-0.1	5.0	2.0	1.3	5.5	4.2	2.4	-2.7	-1.5
SVIN	23.5514	45.3428	18.6	21.6	0.4	0.5	0.2	3.6	-0.9	-0.5	2.1	0.4	-5.2	-1.5	-0.5
TEOL	11.6773	41.3473	17.3	20.3	0.4	0.4	-0.1	2.0	-0.2	-1.9	3.1	0.3	-0.6	-4.7	-3.3
TIRA	19.8632	42.0640	14.8	21.0	0.4	0.4	0.1	0.3	-1.8	-4.0	1.1	-4.7	-4.8	-2.6	-3.0
TOLF	12.0000	45.0634	17.1	19.7	0.4	0.4	-0.2	1.8	-1.6	-2.1	1.6	-0.1	-3.9	-4.8	-2.8
TORI	7.6613	38.3654	15.9	20.3	0.5	0.4	-0.2	0.3	0.5	-3.3	4.1	0.2	0.0	-8.1	-2.0
TRIZ	22.0727	40.7867	-2.0	8.9	0.5	0.6	0.2	-16.2	-14.7	-20.7	-12.1	-22.1	-19.6	-18.1	-14.2
TUBI	29.4507	35.5332	12.1	21.4	0.6	0.5	0.4	-1.0	-3.0	-5.8	-0.7	-9.7	-7.1	0.5	-4.0
TUC2	24.0706	39.4314	-11.5	7.8	0.5	0.7	0.3	-25.4	-16.6	-30.0	-14.1	-32.1	-23.2	-26.4	-14.5
TVRN	16.2263	44.8329	19.2	22.8	0.4	0.5	0.0	4.3	0.2	0.2	3.2	0.8	-3.7	-0.3	0.3
UNFE	11.5992	43.1194	18.4	21.2	0.4	0.4	-0.1	3.0	0.6	-0.8	3.9	1.3	-0.1	-3.7	-2.2
UNPG	12.3557	42.5587	16.5	21.1	0.4	0.4	-0.2	1.3	0.0	-2.7	3.2	-0.7	-1.7	-5.1	-1.9
UNTR	12.6738	38.7078	17.6	19.4	0.4	0.4	-0.2	2.3	-1.9	-1.6	1.4	0.2	-3.9	-3.9	-3.4
USIX	13.1792	48.6320	18.0	21.6	0.4	0.6	-0.2	2.8	-0.6	-1.1	2.5	0.5	-4.8	-3.1	0.1
UZHL	22.2976	41.4154	13.8	22.0	0.4	0.4	-0.1	-0.4	0.3	-4.8	3.2	-6.3	1.3	-2.2	-5.3
VAGA	14.2343	45.4379	18.0	21.2	0.4	0.5	-0.1	2.9	-0.6	-1.1	2.5	0.2	-3.3	-2.6	-1.6
VEAR	12.3578	38.1768	17.8	20.8	0.4	0.4	-0.1	2.5	0.2	-1.4	3.6	0.5	-0.1	-3.8	-3.0

Site Name	Lon.	Lat.	ITRF2005					Eurasia-fix		Nubia-fix		Adria-fix		Apulia-fix	
			V_N	V_E	S_{V_N}	S_{V_E}	ρ_{EN}	V_N	V_E	V_N	V_E	V_N	V_E	V_N	V_E
VLSM	20.5886	40.2307	3.8	16.9	0.4	0.6	0.2	-10.6	-6.5	-15.0	-3.8	-15.9	-11.4	-13.2	-5.9
VLUC	15.2659	51.1133	16.5	22.3	0.4	0.5	-0.1	1.5	0.0	-2.6	3.1	-1.7	-3.4	-3.6	-0.3
WROC	17.0620	49.1442	13.8	21.0	0.4	0.4	0.0	-1.0	0.9	-5.2	4.1	-4.9	3.7	-5.2	-5.9
WTZR	12.8789	42.0644	15.3	20.2	0.4	0.4	0.1	0.1	0.5	-3.9	3.9	-2.1	2.3	-6.0	-4.9
YUND	23.8538	46.8771	13.2	24.6	0.4	0.4	0.2	-0.7	1.3	-5.2	3.9	-7.3	-1.6	-1.8	-0.5
ZIMM	7.4653	46.5572	16.3	19.8	0.5	0.4	0.0	0.7	0.5	-2.9	4.1	0.7	1.1	-7.8	-3.1
ZOUF	12.9736	40.9073	16.0	20.8	0.4	0.4	0.0	0.8	0.4	-3.2	3.7	-1.5	0.7	-5.3	-3.5

5.1.1. Velocity field

Velocity field of 136 permanent stations are presented on Figure 5.1 (*a*, *b*, *c*, and *d*). The horizontal velocities are given with their 3σ error ellipses to Eurasia-fixed reference (Figure 5.1a.), Nubia-fixed (Figure 5.1b) determined with the rotation pole proposed by Altamimi et al., (2007) and to Adria-fixed (Figure 5.1c) and Apulia-fixed (Figure 5.1d)

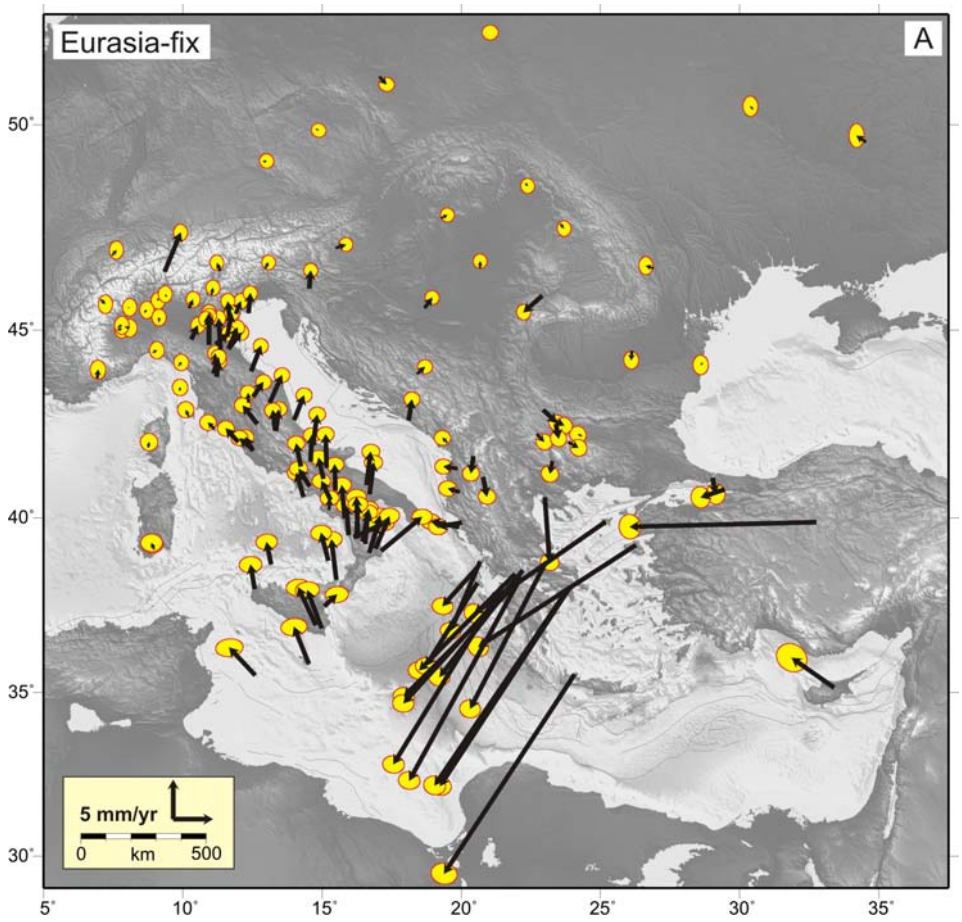

Figure 5.1. *GPS velocities obtained from permanent stations, with their 3σ error ellipses referred to Eurasia plate* ***(a),*** *Nubia plate* ***(b)****, using rotation pole proposed by Altamimi et al., (2007), Adria microplate* ***(c)****, and Apulia micrfopalte* ***(d)*** *using rotation pole published by D'Agostino (2008).*

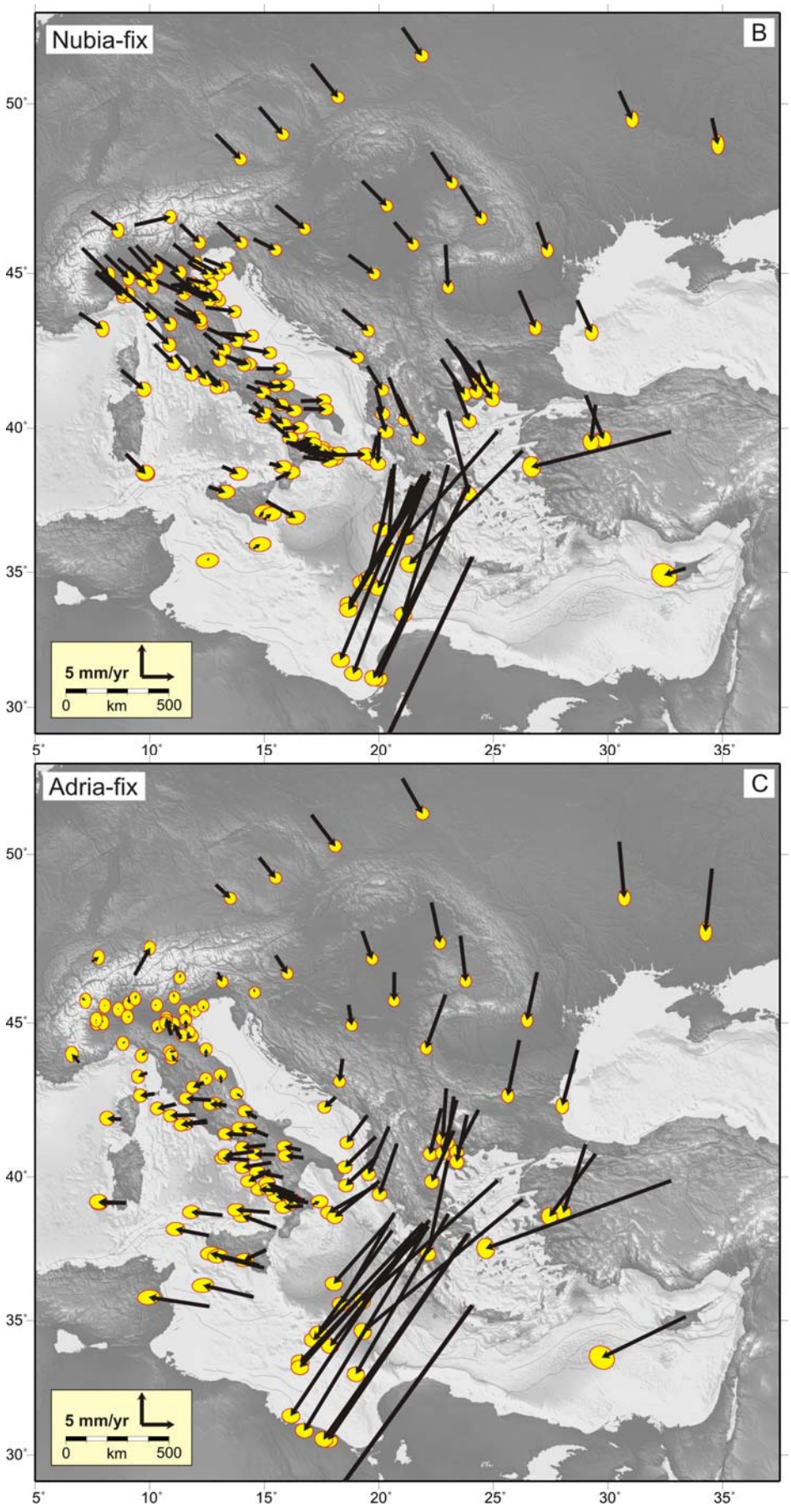

Figure 5.1. *(continued)*

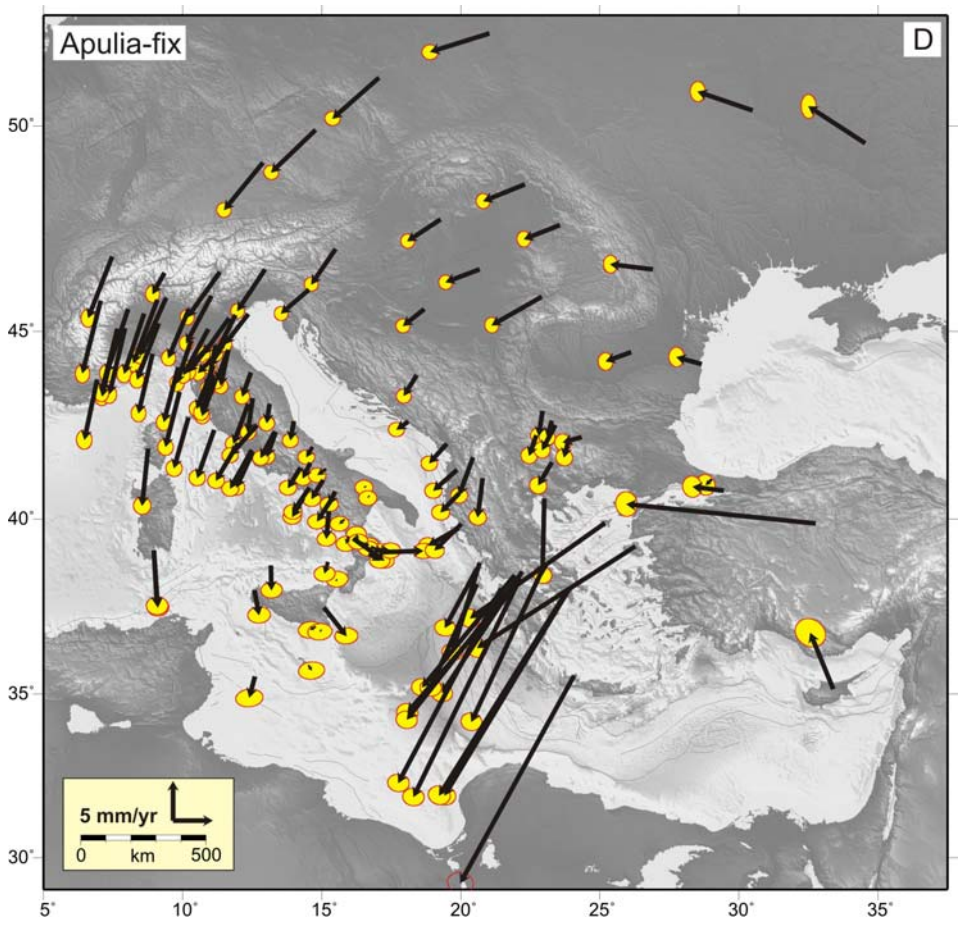

Figure 5.1. *(continued)*

reference using rotation pole published by D'Agostino et al., (2008). The velocity field has esspressed to different fixed references in oreder to illustrate the current displacement based on relative motions of different microplates. In the region of Bulgaria 6 stations from HemuNet permanent network (DRAG, KUST, PAZA, SAND, SOFA and YUND) are showing velocity 0.4 – 2.5mm/yr with overall south direction. IGS site SOFI shows 1.9 mm/yr. The 3 CGPS stations in Albania (SHKO, TIRA, SARA) and one NW Greece KASI are showing motion mainly in west direction and increase of velocity (with value of 0.8, 1.8, 3.1, and 3.7 mm/yr respectively), which might be related to a clockwise rotation. The station PESH in Albania and ORID in Macedonia have a different direction of the motion to south with 2.2 and 2.5 mm/yr expressed in Eurasia-fixed reference frame. Vectors in the territory of Italy are showing various direction and size. The stations which are located on Adria and Apulia microplates present motion overall in NE direction related to Eurasia plate. In the North Italy the velocity are between 0.2 and 2.0 mm/yr (e.g. BIEL, COMO, NOVA, PAVI, SBPO, PARM) and increase their size to south (KROT 6.8 mm/yr). Detail discussion and interpretation of the CGPS result are presented in next chapter in the context of the current tectonic models.

Co-seismic deformations of two large earthquakes have been indicated by 3 CGPS stations. The Mw 6.4 SW-Achaia (Western Greece) earthquake occurred on 8 June 2008 (Ganas et al., 2009). The RLSO permanent station indicates displacements as follow: RLSO East: -4.03±0.10 mm, North: 7.44±0.06 mm, and Up 13.24±0.53 mm (Figure 5.2a). Co-seismic deformations of the destructive April 6, 2009 L'Aquila earthquake with magnitude Mw 6.3 in central Italy (Anzidei et al., 2009.) are indicated by AQUI and INGP permanent station. AQUI East: 7.61±0.05 mm, North: -48.83±0.06 mm, and Up -69.77±0.21 mm (Figure 5.2b). INGP East: 6.15±0.05 mm, North: -31.83±0.06 mm, and Up -23.90±0.21 mm (Figure 5.2c). These values of rupture are quite similar with the calculated one by Anzidei et al., (2009).

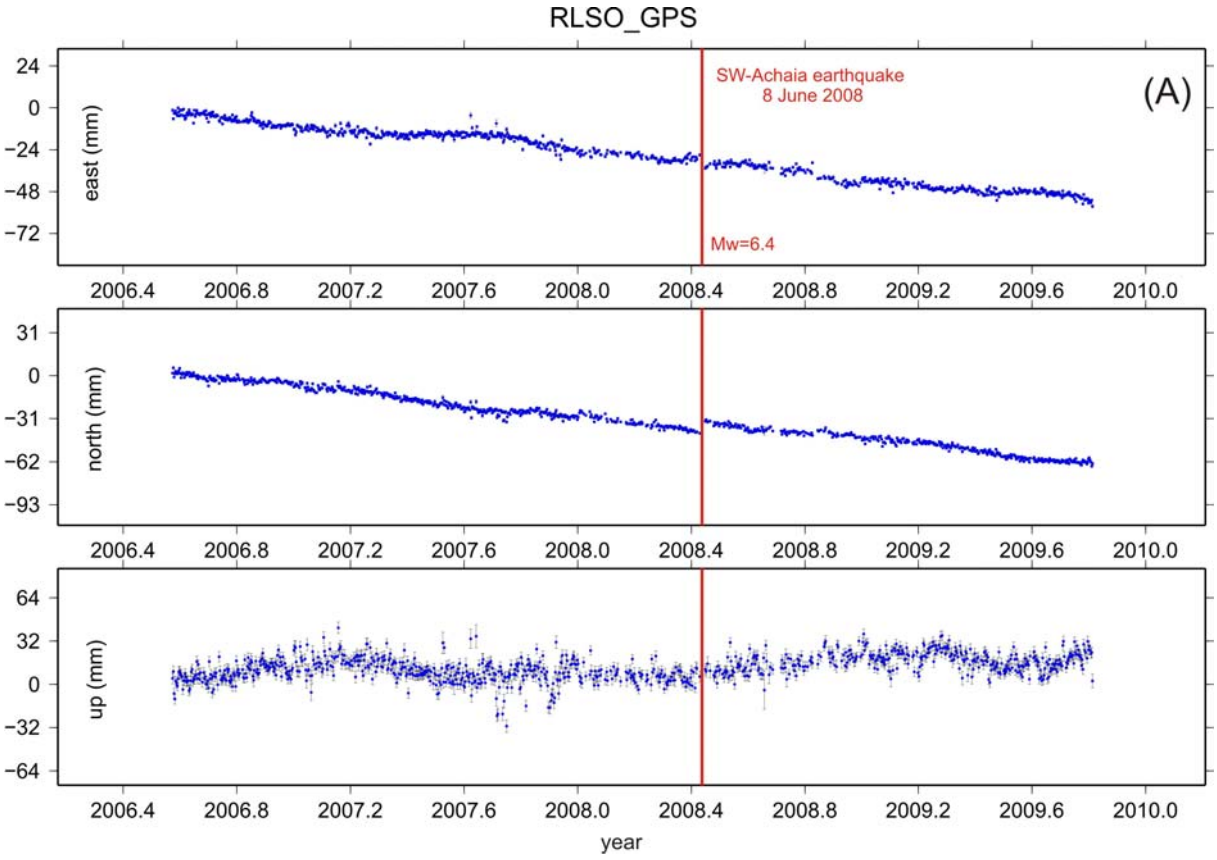

Figure 5.2*. Raw time series of RLSO* ***(a)****, AQUI* ***(b)****, and INGP* ***(c)****, showing coseismic deformation of the Mw 6.4 SW-Achaia (Western Greece) earthquake occurred on 8 June 2008 and the Mw 6.3 L'Aquila earthquake (central Italy) occurred on 6 April 2009.*

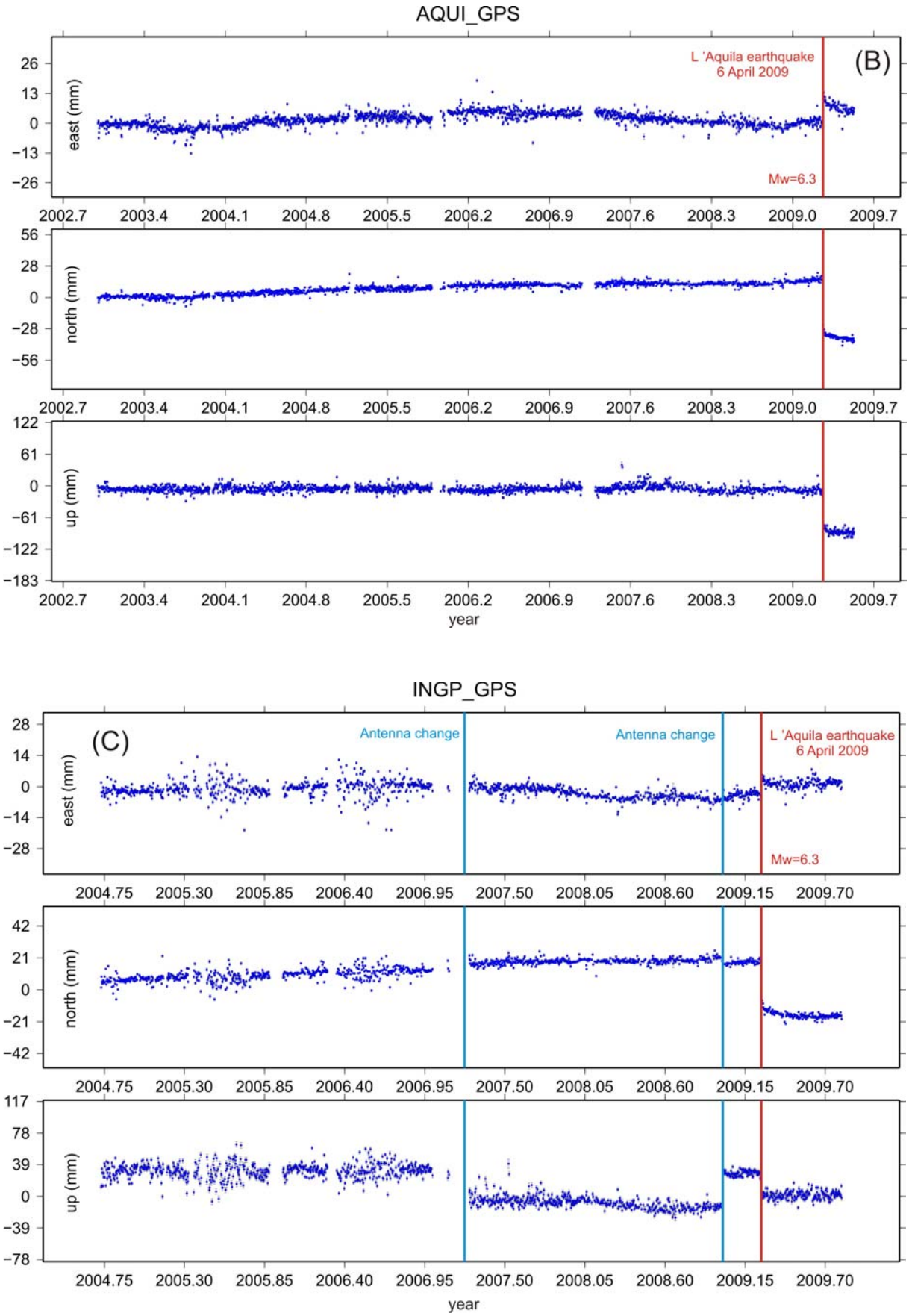

Figure 5.2. *(continued)*

5.2. Horizontal movements and strain rates obtained from GPS campaign-mode observations for the period 1996-2008 in southwest Bulgaria and northern Greece

to be submitted

K. Matev[1 2], I. Georgiev[1], F. Jouanne[2], P. Briole[3], D. Dimitrov[1]

Key words: GPS, geodynamics, horizontal movements, Southwest Bulgaria, Northern Greece

ABSTRACT

The geodynamic processes in the region of Southwest Bulgaria (SWB) and Northern Greece (NG) were investigated by GPS measurements acquired during the 12-year 1996-2008 period. SWB and NG are recent active tectonic and seismotectonic regions. The SWB is the most active seismic region on the Bulgarian territory, in the Krupnik – Kresna region, in 1904, one of the most catastrophic earthquakes in continental Europe during the last two centuries occurred. NG is area with widespread seismic activity ranging from low to high with destructive earthquakes of M≥6.0 in historical to recent times. The obtained velocity field of the Earth's crust is represented by 34 points for SWB and 21 points for NG encompassing the region. The results show southward displacements between 2-10 mm/yr. The strain rates obtained by Global Positioning System (GPS) measurement for the region are presented and discussed together with seismological events. According to the geological and seismotectonic data, the results obtained from the GPS observations confirm the contemporary activity of the fault structures and the dominating extension to the north-south, which is in agreement with the regional tectonic model of the East Mediterranean.

5.2.1. Introduction

Southwest Bulgaria and Northern Greece is a part of most deformational system in the East Mediterranean. Several papers have been published in the last ~30 years using seismological data, active fault distributions, and seafloor bathymetry in order to study better

[1] *Department of Geodesy, National Institute of Geophysics, Geodesy and Geography, Bulgarian Academy of Sciences, Acad. G. Bonchev St., Block 1, 1113 Sofia;*
[2] *ISTerre, Université de Grenoble, Université de Savoie, Chambéry, France;*
[3] *Centre national de la recherche scientifique, Paris, France;*

tectonic evolution in the East Mediterranean region (McKenzie, 1972, 1978; Le Pichon and Angelier, 1979, 1981; McKenzie and Jackson, 1983; DeMets et al., 1990; Taymaz et al., 1991; Jestin et al., 1994; Goldsworthy et al., 2002). The contemporary kinematics of the southern part of Southern Balkan region and Aegean has became better known due to availability of the GPS (Billiris et al., 1991; Le Pichon et al., 1995; Davies et al., 1997: Clarke et al., 1998; Cocard et al., 1999; Briole et al., 2000; McClusky et al., 2000; Kotzev et al., 2001; Ayhan et al., 2002; Meade et al., 2002; Flerit et al., 2003; Le Pichon et al., 2003; Kotzev et al., 2006; Burchfiel et al., 2006; Georgiev et al, 2006). The present paper describes horizontal movements and strain rates in the region of SWB and NG, obtained by GPS observations for the period 1996-2008. The data in SWB come from geodynamic network which was established by Central Laboratory of Geodesy (CLG) for monitoring of present-day crustal motion on the territory of SW Bulgaria. The points of the network cover the main tectonic structures in the region and have been selected after geological investigation of the terrain. The present study gives detail information of displacements in SWB and especially in NG where there is lack of sufficient GPS observations so far.

5.2.2. Tectonic and seismotectonic settings

5.2.2.1. East Mediterranean

The major tectonic regime in the region of the East Mediterranean is determined mainly by the collision of the Arabian and African plates with the Eurasian (McKenzie, 1970; Jackson and McKenzie, 1984; 1988). The earlier tectonic plate models (DeMets et al., 1990; Jestin et al., 1994) based on geological and seismological analyses show that the Arabian plate moves in north-northwest direction with respect to the Eurasian one with a velocity of about 18-25 mm/yr, averaged for a period of 3 million years. These models also show that the African plate moves to the north with respect to the Eurasian with a velocity of about 10 mm/yr. As a result of GPS measurements during the period 1988-1997 McClusky et al. (2000) provided evidence for the existence of an Anatolian plate moves away with ~24 mm/yr in WSW direction from the zone of convergence in eastern Turkey, and an Aegean plate that moves at the different velocity producing extension in the Aegean domain. Central and southern Aegean move as a rigid plate to south-southwest with respect to Eurasia with a velocity of ~35 mm/yr. Nyst and Thatcher (2004) using data of six GPS networks in the Eastern Mediterranean propose that contemporary deformation in Aegean is due to the relative motion of 4 microplates: Anatolian moving WSW at 15-25 mm/yr relative to Eurasia,

South Aegean moving SSW at ~30 mm/yr, Central Greece rotating clockwise at ~4°/Myr around pole in southernmost Albania, and South Marmara moving WSW at 23 mm/yr relative to Eurasia (Figure 5.3). The active faults that have complex influence over the region are: right-lateral strike-slip motion along the North Anatolian fault (NAF) into the North Aegean Trough (NAT); right-lateral strike-slip along the Kefalonia fault zone (KFZ) in the Ionian Sea; and convergence along the Hellenic arc and extension in northern and central Greece as well as on the Peloponnesus (Figure 5.3).

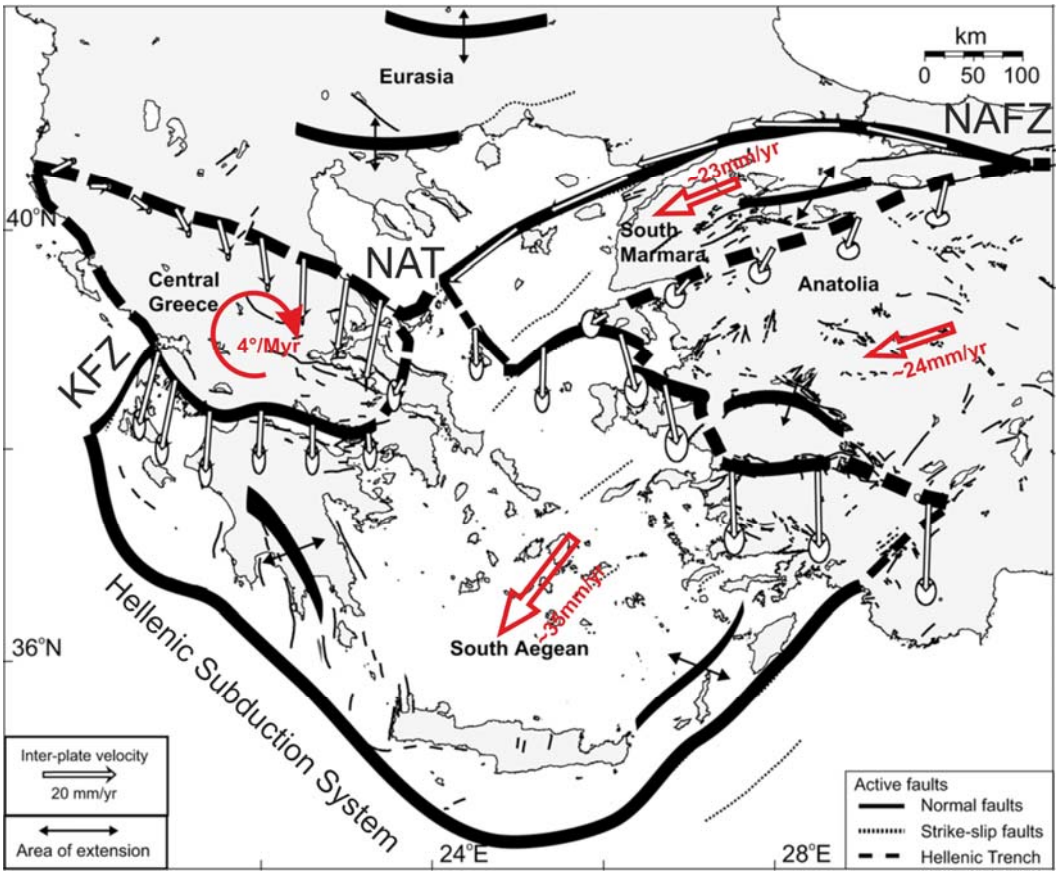

Figure 5.3. *Schematic mapping of stable microplates and their approximate boundaries inferred from GPS results, active fault distribution, and earthquake fault plane solutions. Predicted relative motions across microplate boundaries are shown by arrows that indicate the motion of the south bounding block with respect to the north bounding block. The red arrows show observed direction of motion relative to Eurasia; NAFZ: North Anatolian fault zone, NAT: North Aegean trough; KFZ: Kefalonia fault zone (after Nyst and Thatcher 2004).*

Figure 5.4 shows the seismicity with magnitude larger than 4 in the Mediterranean region during the period 1973-2008. The highest concentration of large (M>6) and very large (M>7) earthquakes is observed along the continuation of the boundary between the Anatolian and Aegean plates and the Hellenic arc (Figure 5.4). The Hellenic arc region exhibits the

biggest tectonic movements related to continental Europe – 30-35 mm/yr (McClusky et al., 2000). The seismic activity in the North Aegean region and East Turkey is associated mainly with the North Aegean trough and the North Anatolian fault.

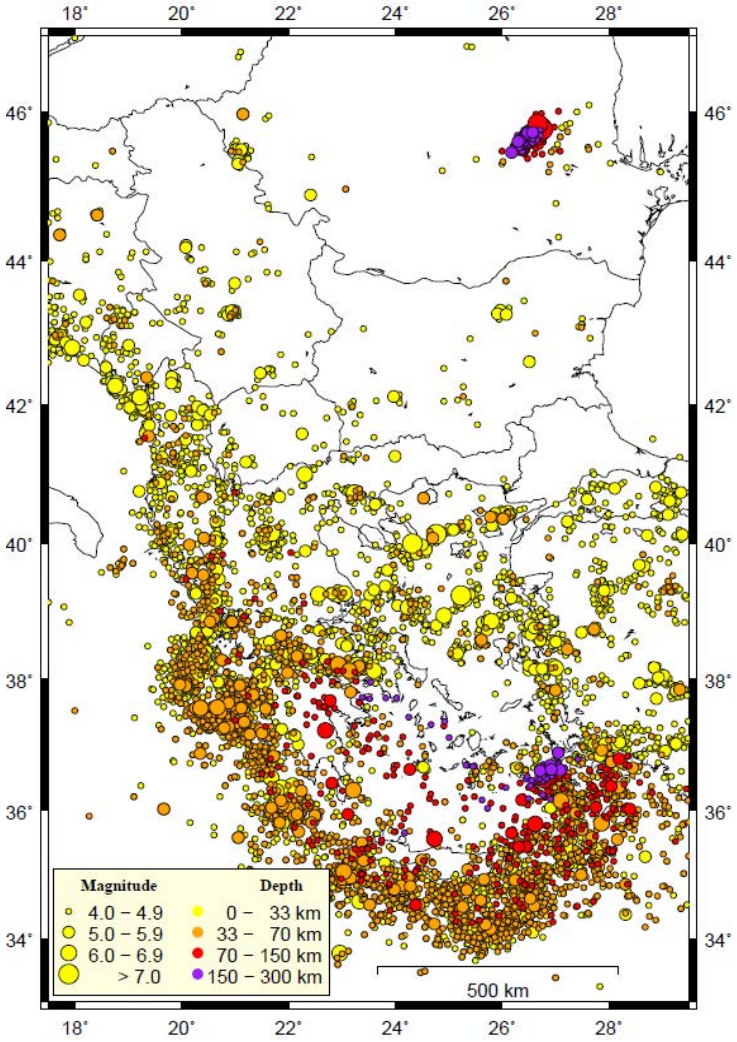

Figure 5.4. *Seismic events in the region of the East Mediterranean for the period 1973-2008 with magnitude M>4 according to USGS-NEIC (National Earthquake Information Center of the U.S. Geological Survey), http://neic.usgs.gov/neis/epic/epic_global.html.*

5.2.2.2 Southwest Bulgaria

The region of Southwest Bulgaria has the most pronounced tectonic and seismotectonic activity on the whole Bulgarian territory (Shanov et al. 2001). The area exhibits diverse relief structures, which are subjected to horizontal and vertical movements of various intensity (Zagorchev, 2001). Southwest Bulgaria falls within a zone of contemporary extension with complex interaction between horizontal and vertical movements of the geological structures (Zagorchev 1992, 2001). The analysis of the geological data provides

evidences for contemporary activity of the fault structures formed during the Late Neogene and the Quaternary (Tzankov et al. 2000). On Figure 5.5 are presented the active faults on the territory of the studied region from geological data and active faults according Geodynamic map of the Mediterranean (Barrier et al., 2004). The contemporary tectonic activity is also closely related with the high seismicity of this area. Results determining the seismic risk for Southwest Bulgaria show potential seismic hazard for the whole region (Bonchev et al. 1982, Papazachos et al. 1996).

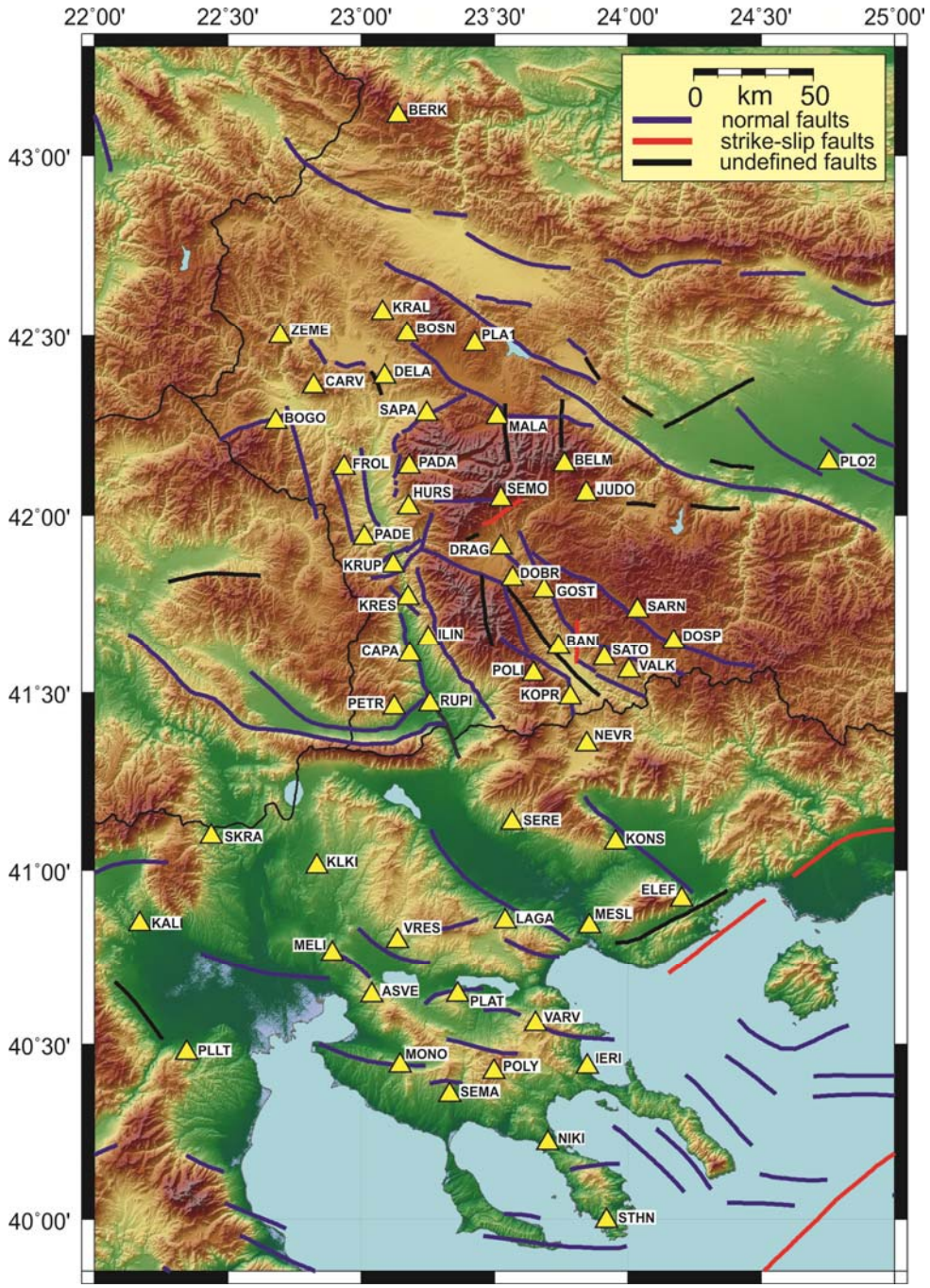

Figure 5.5. *Scheme of the active and potentially active faults in the region of SW Bulgaria and Northern Greece with all points from the campaigns during the period 1996-2008*

5.2.2.3 Northern Greece

Northern Greece is an intracontinental region behind the Hellenic subduction zone with widespread seismic activity ranging from low to high with destructive earthquakes of M≥6.0 in historical to recent times. Geological (Figure 5.5, Barrier et al., 2004) and seismological data indicate that recent seismic activity is mainly localized along, faults zones, which have transected Northern Greece since Oligocene-Miocene times. These data also indicate that seismic activity in Northern Greece is concentrated along normal faults of several kilometres (Mountrakis et al., 2006).

5.2.3. GPS data

To estimate current displacements in Southwest Bulgaria and Northern Greece, we have used completed existing data with new acquisitions performed in 2008. GPS measurements carried out in 1996, 1997, 1998 and 2000 within the frames of international project with Massachusetts Institute of Technology (MIT) (Geodynamic settings of Bulgaria in the active and young Near East-Balkan geotectonic system) and GPS data of the CLG geodynamic network measured since 2001. The points from the GPS geodynamic network were measured during the period 1996-2008 (Table 5.2a). The observation sessions of each campaign were minimum 36 hours. The sampling rate of the observation was 30 s, with an elevation cut-off angle of 10 degrees.

N°	Site Name	Year										
		1996	1997	1998	2000	2001	2002	2003	2004	2005	2006	2008
1.	**BANI**						**X**	**X**	**X**			**X**
2.	**BELM**		**X**		**X**		**X**	**X**				**X**
3.	**BERK**	**X**	**X**		**X**	**X**						**X**
4.	**BOGO**	**X**	**X**	**X**	**X**	**X**			**X**			
5.	**BOSN**		**X**		**X**				**X**			
6.	**CAPA**					**X**	**X**	**X**	**X**			
7.	**CARV**		**X**		**X**				**X**			
8.	**DELA**		**X**		**X**				**X**			
9.	**DOBR**		**X**		**X**	**X**	**X**	**X**				**X**
10.	**DOSP**						**X**	**X**	**X**			
11.	**DRAG**					**X**	**X**	**X**	**X**			**X**
12.	**FROL**		**X**		**X**		**X**	**X**				
13.	**GOST**					**X**	**X**	**X**	**X**			**X**
14.	**HURS**						**X**	**X**	**X**			**X**
15.	**ILIN**					**X**	**X**	**X**	**X**			**X**
16.	**JUDO**						**X**	**X**	**X**	**X**		**X**
17.	**KOPR**					**X**	**X**	**X**	**X**			**X**

N°	Site Name	Year										
		1996	1997	1998	2000	2001	2002	2003	2004	2005	2006	2008
18.	**KRAL**		**X**		**X**				**X**			
19.	**KRES**					**X**	**X**	**X**	**X**			**X**
20.	**KRUP**					**X**	**X**	**X**	**X**			
21.	**MALA**		**X**		**X**		**X**	**X**				
22.	**PADA**		**X**		**X**		**X**	**X**				**X**
23.	**PADE**						**X**	**X**	**X**			**X**
24.	**PETR**	**X**		**X**		**X**	**X**	**X**				
25.	**PLA1**	**X**	**X**		**X**	**X**	**X**	**X**	**X**	**X**	**X**	**X**
26.	**PLO2**	**X**		**X**		**X**						**X**
27.	**POLI**					**X**	**X**	**X**	**X**			**X**
28.	**RUPI**					**X**	**X**	**X**	**X**			**X**
29.	**SAPA**		**X**		**X**		**X**	**X**		**X**		
30.	**SARN**						**X**	**X**	**X**	**X**		**X**
31.	**SATO**		**X**			**X**	**X**	**X**				**X**
32.	**SEMO**					**X**	**X**	**X**	**X**			**X**
33.	**VALK**						**X**	**X**	**X**	**X**		**X**
34.	**ZEME**		**X**		**X**					**X**		

Table 5.2a. *GPS data collected in Southwest Bulgaria* ***(a)****; GPS data collected in Northern Greece* ***(b)***.

N°	Name	Year									
		1999	2000	2001	2002	2003	2004	2005	2006	2007	2008
1.	ASVE	**X**	**X**								**X**
2.	ELEF	**X**	**X**								**X**
3.	IERI	**X**	**X**								**X**
4.	KALI	**X**	**X**								**X**
5.	KLKI	**X**	**X**								**X**
6.	KONS	**X**	**X**								**X**
7.	LAGA	**X**	**X**								**X**
8.	MELI		**X**								**X**
9.	MESL	**X**	**X**								**X**
10.	MONO	**X**	**X**								**X**
11.	NEVR	**X**	**X**								**X**
12.	NIKI	**X**	**X**								**X**
13.	PLAT	**X**	**X**								**X**
14.	PLLT	**X**	**X**								**X**
15.	POLY	**X**	**X**								**X**
16.	SEMA	**X**	**X**								**X**
17.	SERE	**X**	**X**								**X**
18.	SKRA	**X**	**X**								**X**
19.	STHN		**X**								**X**
20.	VARV	**X**	**X**								**X**
21.	VRES	**X**	**X**								**X**

Table 5.2b. *(continued)*

In Northern Greece we have analysed GPS data to determine crustal displacements collected in 1999, 2000 and 2008 with the exception of the points MELI and STHN measured

only in 2000 and 2008 (Table 5.2b). In 1999 and 2000 only short sessions (3-10 hours) have been performed whereas in 2008, points have been measured between 48 and 72 hours. In 2008 campaign the point ELEF was measured 3h and the point ASVE was measured 6h in two days by 3h. The sampling rate of the observation was 30 s, with an elevation cut-off angle of 10 degrees.

5.2.4. Processing and analysis of the GPS measurements

The processing was done with Bernese 5.0 software package in ITRF2005 reference frame and we used the absolute antenna phase centre offsets models. Results were obtained using IGS precise orbits (Beutler et al. 1999), as recommended by Boucher et al. (2004), as well as IGS Earth rotation parameters and data from 32 permanent GPS EPN/IGS stations (Table 5.3). Transformation of the satellite orbits and the Earth orientation parameters from the previous realizations 1996, 1997 and 2000 of ITRF was made by *trnfsp3n* software package (Kouba, 2002). Data have been analyzed using the following strategy: (1) prepare a priori coordinates, constrain orbits, clocks, and Earth Rotation Parameters from IGS products, (2) convert and synchronize observation data, detection and correction of cycle slips in single difference files, (3) initial ionosphere-free analysis with residuals screening, removal outliers (4) estimation of Troposphere-induced propagation delays every 2 h and DRY_NIELL mapping function (Niell, 1999) was used, (5) resolution of the L1 and L2 ambiguities using the Quasi Ionosphere Free strategy of resolution with CODE ionosphere models (Beutler et al., 2007), and (5) computation of normal equations, checking the coordinates of fiducial sites and daily repeatability using seven parameters Helmert transformation. Velocities have been estimated by weighting at 1 mm the coordinates of ITRF2005 values and by fixing the velocities of 10 reference points – BUCU, GLSV, GOPE, GRAS, GRAZ, JOZE, LAMA, PENC, WTZR and ZIMM to their ITRF2005 values. In a second step, velocities have been expressed in the Eurasia fixed reference frame using the rotation pole defined by Altamimi et al., (2007) between ITRF2005 and stable Eurasia (56.33°N, 95.979°W , 0.261 °/Myr).

The QOCA (**Q**uasi-**O**bservation **C**ombination **A**nalysis) software package was used to obtain the strain rates for our region (Dong et al. 1998 and Shen et al. 2000). This software allows combining various loosely constrained geodetic site coordinate and velocity solutions (as quasi observations) to obtain crustal deformation information. As input files for QOCA we use loosely constrained SINEX files obtained from Bernese software packages.

N°	Site Name	Year '96	'97	'98	'00	'01	'02	'03	'04	'05	'06	'08
1.	ANKR 20805M002	X	X	X	X	X	X	X	X	X	X	X
2.	BUCU 11401M001				X	X	X	X	X	X	X	X
3.	CAGZ 12725M004						X	X	X	X	X	X
4.	GENO 12712M002			X	X	X	X	X	X	X	X	
5.	GLSV 12356M001			X	X	X	X	X	X	X	X	X
6.	GOPE 11502M002	X	X	X	X	X	X	X	X	X	X	X
7.	GRAS 10002M006		X	X	X	X	X	X	X	X	X	X
8.	GRAZ 11001M002	X	X	X	X	X	X	X	X	X	X	X
9.	IENG 12724S001								X	X	X	X
10.	ISTA 20807M001				X	X	X	X	X	X	X	X
11.	JOZE 12204M001	X	X	X	X	X	X	X	X	X	X	X
12.	LAMA 12209M001	X	X	X	X	X	X	X	X	X	X	X
13.	LAMP 12706M002				X	X	X	X	X	X	X	X
14.	MATE 12734M008	X	X	X	X	X	X	X	X	X	X	X
15.	MEDI 12711M003	X	X	X	X	X	X	X	X	X	X	X
16.	NICO 14302M001		X	X	X	X	X	X	X	X	X	
17.	NOT1 12717M004					X	X	X	X	X	X	X
18.	PADO 12750S001										X	X
19.	PENC 11206M006	X	X	X	X	X	X	X	X	X	X	X
20.	POLV 12336M001					X	X	X	X	X	X	X
21.	SOFI 11101M002		X	X	X	X	X	X	X	X	X	X
22.	UZHL 12301M001				X	X	X	X	X	X	X	X
23.	WROC 12217M001		X	X	X	X	X	X	X	X	X	X
24.	WTZR 14201M010	X	X	X	X	X	X	X	X	X	X	X
25.	ZIMM 14001M004	X	X	X	X	X	X	X	X	X	X	X
26.	AUT1 12619M002								X	X	X	X
27.	COST 11407M001										X	X
28.	DUBR 11901M001				X	X	X	X	X	X		X
29.	NOA1 12620M001										X	X
30.	ORID 15601M001				X	X	X	X	X	X	X	X
31.	SRJV 11801S001				X	X	X	X		X		X
32.	TUC2 12617M003								X	X	X	X

Table 5.3. *EPN/ IGS permanent stations using in campaign processing.*

5.2.5. Discussion

5.2.5.1 Velocity field and gradient

The obtained horizontal velocities referred to Eurasia and their mean square errors are given in Table 5.4. The values of the velocities are in range from 2 mm/yr for the region of Middle and Central Bulgaria to 10 mm/yr for the region of Chalkidiki. The horizontal velocities with theirs 3σ ellipses are shown in Figure 5.6. The obtained velocities indicate overall motion to the south. In some places the GPS results show local zones of slow internal deformation.

N°	Site Name	Lon.	Lat.	V_N	V_E	$\|V_{hor}\|$	S_{V_N}	S_{V_E}	$S_{\|V_{hor}\|}$	ρ_{EN}
1.	BANI	**23.7391**	**41.6298**	**-3.0**	**0.2**	**3.0**	**0.4**	**0.5**	**0.6**	**0.32**
2.	BELM	**23.7617**	**42.1414**	**-2.6**	**0.4**	**2.6**	**0.4**	**0.5**	**0.6**	**0.32**
3.	BERK	**23.1378**	**43.1095**	**-1.9**	**0.1**	**1.9**	**0.4**	**0.4**	**0.6**	**0.28**
4.	BOGO	**22.6808**	**42.2595**	**-2.3**	**1.3**	**2.7**	**0.4**	**0.5**	**0.6**	**0.27**
5.	BOSN	**23.1728**	**42.5048**	**-2.4**	**1.6**	**2.9**	**0.4**	**0.4**	**0.6**	**0.29**
6.	CAPA	**23.1827**	**41.6088**	**-3.6**	**0.0**	**3.6**	**0.4**	**0.5**	**0.6**	**0.29**
7.	CARV	**22.8214**	**42.3588**	**-2.5**	**1.6**	**3.0**	**0.4**	**0.4**	**0.6**	**0.28**
8.	DELA	**23.0888**	**42.3866**	**-2.5**	**0.8**	**2.6**	**0.4**	**0.4**	**0.6**	**0.29**
9.	DOBR	**23.5686**	**41.8225**	**-3.2**	**1.1**	**3.3**	**0.4**	**0.5**	**0.6**	**0.31**
10.	DOSP	**24.1727**	**41.6453**	**-3.0**	**-0.5**	**3.0**	**0.4**	**0.5**	**0.7**	**0.31**
11.	DRAG	**23.5241**	**41.9106**	**-2.9**	**-1.0**	**3.1**	**0.4**	**0.5**	**0.6**	**0.31**
12.	FROL	**22.9354**	**42.1325**	**-2.5**	**0.4**	**2.5**	**0.4**	**0.5**	**0.6**	**0.28**
13.	GOST	**23.6859**	**41.7899**	**-2.8**	**0.0**	**2.8**	**0.4**	**0.5**	**0.6**	**0.32**
14.	HURS	**23.1772**	**42.0227**	**-2.1**	**1.2**	**2.4**	**0.4**	**0.5**	**0.6**	**0.29**
15.	ILIN	**23.2513**	**41.6540**	**-3.8**	**-0.3**	**3.8**	**0.4**	**0.5**	**0.6**	**0.30**
16.	JUDO	**23.8438**	**42.0609**	**-2.0**	**1.0**	**2.2**	**0.4**	**0.5**	**0.6**	**0.32**
17.	KOPR	**23.7839**	**41.4868**	**-3.3**	**0.5**	**3.3**	**0.4**	**0.5**	**0.6**	**0.32**
18.	KRAL	**23.0801**	**42.5654**	**-2.7**	**0.7**	**2.8**	**0.4**	**0.4**	**0.6**	**0.29**
19.	KRES	**23.1757**	**41.7685**	**-2.9**	**0.7**	**3.0**	**0.4**	**0.5**	**0.6**	**0.30**
20.	KRUP	**23.1201**	**41.8606**	**0.2**	**-0.4**	**0.5**	**0.4**	**0.5**	**0.6**	**0.29**
21.	MALA	**23.5091**	**42.2737**	**-2.9**	**0.4**	**2.9**	**0.4**	**0.5**	**0.6**	**0.30**
22.	PADA	**23.1797**	**42.1355**	**-3.0**	**0.9**	**3.1**	**0.4**	**0.5**	**0.6**	**0.29**
23.	PADE	**23.0112**	**41.9377**	**-2.4**	**0.2**	**2.4**	**0.4**	**0.5**	**0.6**	**0.29**
24.	PETR	**23.1247**	**41.4588**	**-3.7**	**0.6**	**3.7**	**0.4**	**0.5**	**0.6**	**0.30**
25.	PLA1	**23.4253**	**42.4766**	**-1.9**	**0.6**	**2.0**	**0.4**	**0.4**	**0.6**	**0.30**
26.	PLO2	**24.7530**	**42.1464**	**-2.4**	**0.2**	**2.4**	**0.4**	**0.5**	**0.6**	**0.35**
27.	POLI	**23.6451**	**41.5526**	**-3.6**	**1.1**	**3.7**	**0.4**	**0.5**	**0.6**	**0.31**
28.	RUPI	**23.2585**	**41.4672**	**-3.5**	**-0.3**	**3.6**	**0.4**	**0.5**	**0.6**	**0.30**
29.	SAPA	**23.2460**	**42.2817**	**-2.7**	**0.2**	**2.7**	**0.4**	**0.5**	**0.6**	**0.30**
30.	SARN	**24.0362**	**41.7325**	**-2.5**	**0.1**	**2.5**	**0.4**	**0.5**	**0.6**	**0.33**
31.	SATO	**23.9125**	**41.5981**	**-3.0**	**0.4**	**3.0**	**0.4**	**0.5**	**0.6**	**0.33**
32.	SEMO	**23.5241**	**42.0462**	**-2.2**	**0.0**	**2.2**	**0.4**	**0.5**	**0.6**	**0.31**
33.	SOFI	**23.3947**	**42.5561**	**-2.1**	**0.7**	**2.2**	**0.4**	**0.4**	**0.6**	**0.30**
34.	VALK	**24.0043**	**41.5613**	**-2.5**	**0.4**	**2.5**	**0.4**	**0.5**	**0.6**	**0.33**
35.	ZEME	**22.6952**	**42.4982**	**-1.9**	**1.1**	**2.1**	**0.4**	**0.4**	**0.6**	**0.27**

Table 5.4a. *GPS velocities and their mean square errors with respect to the stable Eurasian plate for Southwest Bulgarian and Northern Greece;*

N°	Site Name	Lon.	Lat.	V_N	V_E	$\|V_{hor}\|$	S_{V_N}	S_{VE}	$S_{\|V_{hor}\|}$	ρ_{EN}
1.	AUT1	**23.0037**	**40.5668**	**-8.8**	**0.7**	**8.9**	**0.4**	**0.5**	**0.7**	**0.29**
2.	ASVE	**23.0407**	**40.6402**	**-7.1**	**1.2**	**7.2**	**0.5**	**0.6**	**0.7**	**0.21**
3.	ELEF	**24.2012**	**40.9156**	**-4.4**	**1.3**	**4.6**	**0.5**	**0.5**	**0.7**	**0.30**
4.	IERI	**23.8478**	**40.4362**	**-7.3**	**-0.9**	**7.4**	**0.5**	**0.6**	**0.7**	**0.30**
5.	KALI	**22.1708**	**40.8454**	**-6.8**	**0.8**	**6.8**	**0.4**	**0.5**	**0.7**	**0.25**
6.	KLKI	**22.8334**	**41.0094**	**-5.8**	**-0.2**	**5.8**	**0.4**	**0.5**	**0.7**	**0.27**

N°	Site Name	Lon.	Lat.	V_N	V_E	$\|V_{hor}\|$	S_{V_N}	S_{VE}	$S_{\|V_{hor}\|}$	ρ_{EN}
7.	KONS	**23.9538**	**41.0778**	**-4.6**	**-0.7**	**4.7**	**0.4**	**0.5**	**0.7**	**0.31**
8.	LAGA	**23.5398**	**40.8545**	**-6.0**	**0.2**	**6.0**	**0.4**	**0.5**	**0.7**	**0.29**
9.	MELI	**22.8929**	**40.7609**	**-7.2**	**-0.1**	**7.2**	**0.4**	**0.5**	**0.7**	**0.27**
10.	MESL	**23.8561**	**40.8403**	**-4.1**	**0.5**	**4.2**	**0.4**	**0.5**	**0.7**	**0.30**
11.	MONO	**23.1451**	**40.4398**	**-8.3**	**-0.5**	**8.3**	**0.4**	**0.6**	**0.7**	**0.28**
12.	NEVR	**23.8461**	**41.3548**	**-4.3**	**0.3**	**4.3**	**0.4**	**0.5**	**0.7**	**0.31**
13.	NIKI	**23.6998**	**40.2186**	**-8.9**	**-1.4**	**9.0**	**0.5**	**0.6**	**0.7**	**0.29**
14.	PLAT	**23.3618**	**40.6422**	**-7.5**	**-0.4**	**7.5**	**0.4**	**0.5**	**0.7**	**0.29**
15.	PLLT	**22.3466**	**40.4761**	**-8.3**	**0.2**	**8.3**	**0.4**	**0.5**	**0.7**	**0.25**
16.	POLY	**23.4981**	**40.4204**	**-10.3**	**-4.4**	**11.2**	**0.5**	**0.6**	**0.7**	**0.29**
17.	SEMA	**23.3315**	**40.3556**	**-9.4**	**-0.5**	**9.4**	**0.5**	**0.6**	**0.7**	**0.28**
18.	SERE	**23.5669**	**41.1336**	**-4.0**	**-0.2**	**4.0**	**0.4**	**0.5**	**0.7**	**0.30**
19.	SKRA	**22.4375**	**41.0955**	**-6.0**	**0.2**	**6.1**	**0.4**	**0.5**	**0.7**	**0.26**
20.	STHN	**23.9192**	**39.9942**	**-8.1**	**-1.5**	**8.3**	**0.5**	**0.6**	**0.7**	**0.29**
21.	VARV	**23.6537**	**40.5582**	**-7.0**	**-0.9**	**7.0**	**0.5**	**0.6**	**0.7**	**0.29**
22.	VRES	**23.1363**	**40.7981**	**-7.3**	**-0.1**	**7.3**	**0.4**	**0.5**	**0.7**	**0.28**

Table 5.4b. *GPS velocities and their mean square errors with respect to the stable Eurasian plate for Southwest Bulgarian Lon.: longitude [°], Lat.: latitude [°],* V_N, V_E *: north/east component of velocity [mm/yr],* $|V_{hor}|$*: magnitude of horizontal component [mm/yr],* S_{V_N}, S_{VE}, $S_{|V_{hor}|}$*: 1 sigma uncertainties of corresponding velocity component [mm/yr],* ρ_{EN} *: correlation coefficient between the eats and north uncertainties.*

The point KRUP, stabilized on the northern side of the Krupnik fault (Figure 5.6), is not in correspondence with the basic trend of the movement. Its velocity is under 1mm/yr with north direction. The strongest earthquake during the last two centuries in Europe occurred in 1904 in the region of Krupnik-Kresna with magnitude Mw = 6.8 and MS = 7.2 (Dineva et al., 2002). Based on geological and seismological data, Krupnik fault is the most active fault in the whole territory of Bulgaria (Meyer et al. 2002, 2007). The results, shown by GPS monitoring (Georgiev et al., 2006) and extensiometric monitoring (Dobrev et al., 2006) indicate an extensional regime with NNW-SSE orientation, perpendicular to the Krupnik fault. These studies indicate and confirm the activity of Krupnik faults as well.

Velocity gradient for the studied area is presented on Figure 5.7, where we plot the north component of velocities as a function of UTM Y coordinates in south direction. It is clearly seen that size of velocities increase from north to south.

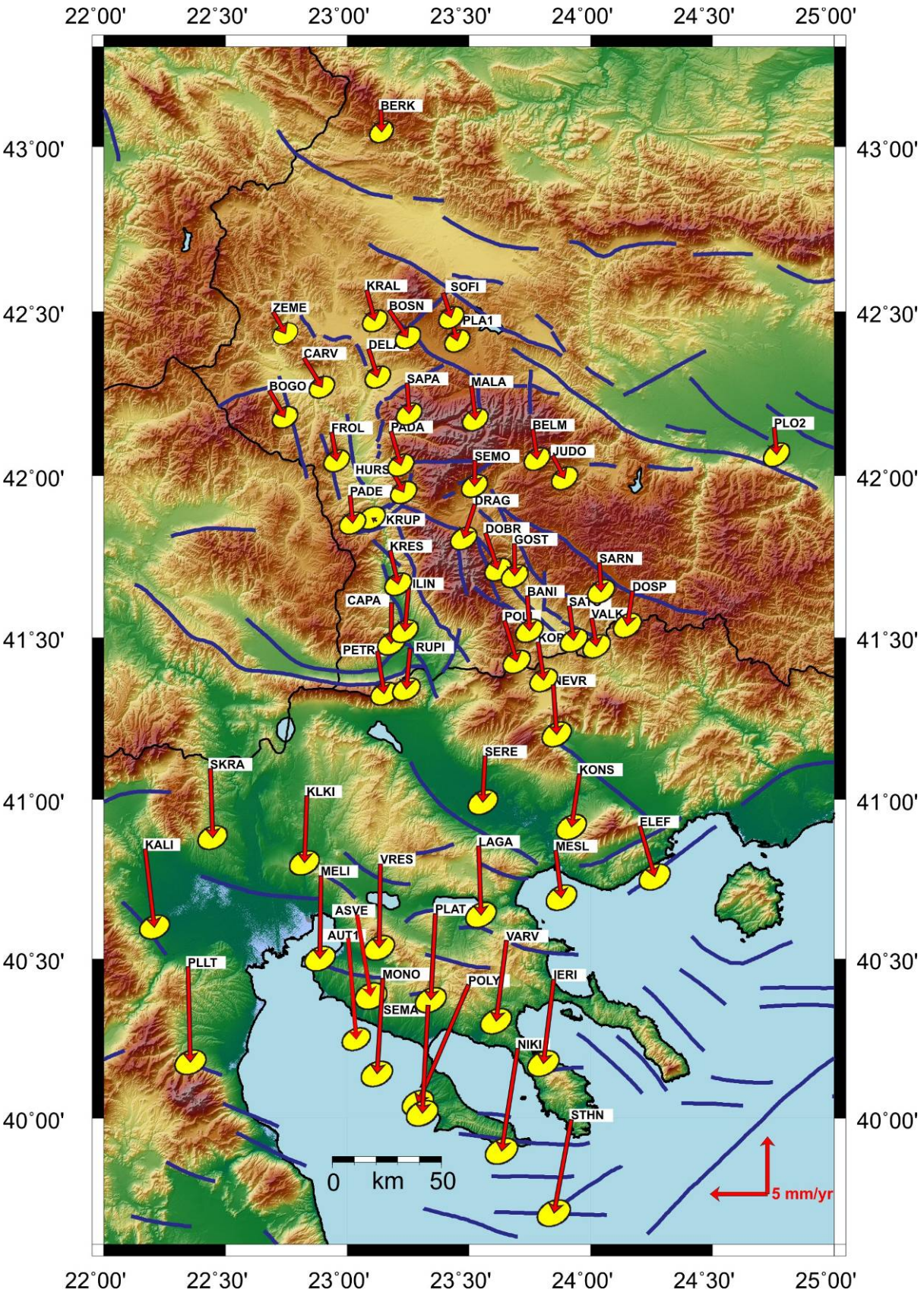

Figure 5.6. *GPS velocities referred to stable Eurasia with their 3σ error ellipses for SWB and NG region.*

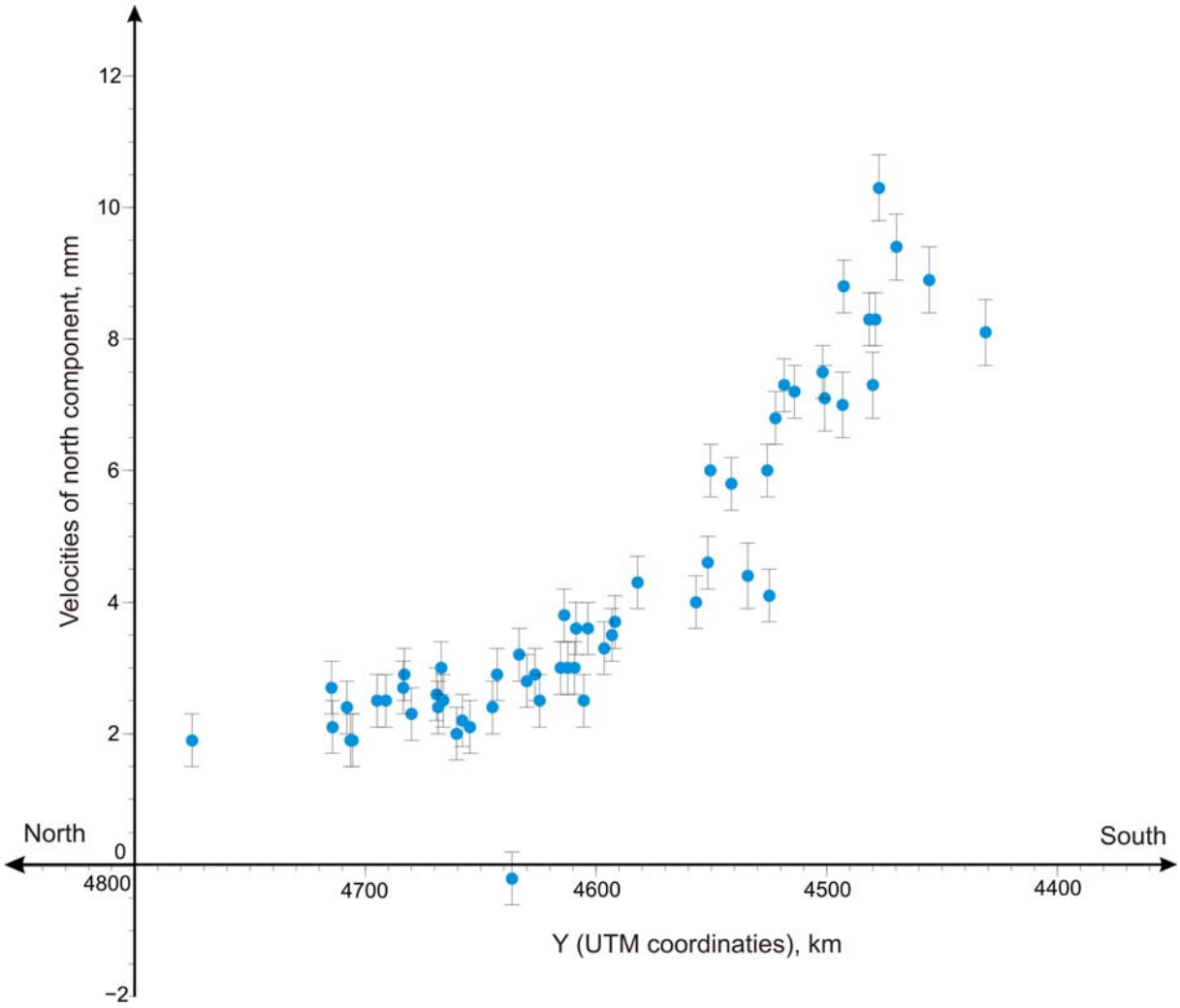

Figure 5.7. *Velocity gradient of Southwest Bulgaria and Northern Greece*

Date and Time	Location		Depth		Nodal plane I			Nodal plane II			P axis		T axis	
	Latitude	Longitude	(km)	M_w	Strike	Dip	Rake	Strike	Dip	Rake	Azimuth	Plunge	Azimuth	Plunge
Global CMT Catalog, http://www.globalcmt.org/CMTsearch.html														
7711030222	41.46	23.85	15	5.5	104	35	-94	289	55	-87	210	80	17	10
7805232334	39.85	23.19	10	5.8	74	36	-96	262	54	-85	191	80	349	9
7806191031	40.73	23.13	15	5.3	281	44	-66	69	50	-111	274	73	174	3
7806202003	39.60	23.58	10	6.2	286	43	-88	104	47	-92	344	87	195	2
8201181927	39.56	24.47	10	6.6	241	57	-176	148	87	-33	100	25	199	20
8308061543	39.89	24.66	10	6.6	229	81	-174	138	84	-9	93	10	184	2
8308261252	40.11	24.04	15	5.1	72	73	-168	338	78	-17	294	20	26	4
8407091857	41.05	22.55	10	5.2	212	38	-105	51	54	-79	2	78	133	8
8509281450	41.22	22.18	20	5.2	209	70	-158	111	70	-22	70	29	160	0
8511092330	41.24	24.12	21	5.2	256	33	-85	70	57	-93	329	78	162	12
9012210657	40.27	22.28	15	6.1	249	41	-72	45	52	-105	260	77	146	5
9207232012	39.88	24.68	15	5.4	267	41	-160	161	77	-50	110	44	222	22
9505040034	40.30	23.60	15	5.3	260	42	-132	131	60	-59	91	61	199	10
0306090706	39.77	22.23	15	5.2	110	36	-107	310	56	-78	254	76	32	10
0808030039	39.54	23.76	12	5.3	267	52	-143	152	61	-44	115	50	211	5
0905241617	41.22	22.72	12	5.3	62	45	-123	285	54	-61	254	67	355	5
Vannucci-Gasperini, (2003); European-Mediterranean Seismological Centre (EMSC), http://www.emsc-csem.org/index.php?page=euromed-sub=emt														
8808211951	39.93	23.90	18	3.9	132	49	-55	265	50	-124	119	56	17	2
8808162134	39.92	23.94	17	4.5	145	35	-80	314	54	-96	198	75	48	5
8511092330	41.24	23.93	20	5.2	256	33	-85	70	57	-93	327	72	162	6
8509281450	41.59	22.22	20	5.2	111	70	-21	208	70	-158	69	18	159	2
8308261252	40.51	23.92	15	5.1	72	73	-168	338	78	-17	294	12	25	2
8308061543	40.18	24.73	10	6.6	229	81	-174	138	84	-9	93	5	183	1
8201181927	40.00	24.32	10	6.5	241	57	-176	148	86	-33	99	16	198	11
8201180000	39.96	24.39	0	6.8	233	62	-173	139	83	-28	92	16	189	8
7806202003	40.74	23.25	3	6.1	278	46	-70	69	49	-109	268	69	174	1
7806191031	40.75	23.22	15	5.3	280	44	-67	69	50	-110	274	68	173	2
7805232334	40.76	23.30	8	5.7	277	49	-60	55	49	-119	255	60	346	2
5408031818	40.20	24.40	0	5.5	292	33	149	48	73	60	160	14	284	41
4706040029	40.00	24.00	80	5.5	154	72	106	290	24	48	230	16	86	49
4103010000	39.70	22.40	0	6.1	58	41	-128	284	58	-61	243	55	354	5
3209290000	40.50	23.70	0	6.1	72	73	-168	338	78	-17	294	12	25	1
3209260000	40.50	23.90	0	6.8	72	73	-168	338	78	-17	294	12	25	1
3103080000	41.30	22.50	0	6.6	271	42	-74	69	50	-103	278	73	169	2
3003010000	39.60	23.20	0	6.0	310	45	-70	102	48	-108	302	70	205	2
2804180000	42.00	24.70	0	6.8	125	45	-90	305	45	-90	0	90	214	2
2312050000	39.90	23.20	0	6.3	315	45	-45	80	60	-125	298	49	194	4
Adapted from Kiratzi and Louvari (2003)														
9207232012	39.81	24.40	8	5.3	272	51	-148	161	66	-43	120	47	220	9
9505040034	40.54	23.63	12	5.2	84	66	-103	294	27	-63	330	66	184	20
7805232334	40.70	23.30	8	5.8	265	40	-82	75	50	-96	305	83	170	5
7806202003	40.73	23.25	7	6.3	257	41	-96	85	49	-85	36	84	171	4
8308061543	40.05	24.70	9	6.7	50	76	177	141	87	14	275	8	6	12
9012210657	40.91	22.36	16	6.1	54	47	-103	253	45	-76	249	80	153	1
6404111600	40.30	24.80	33	5.5	310	89	1	220	89	179	265	0	175	1
6512200008	40.20	24.80	33	5.6	132	32	-90	312	58	-90	222	77	42	13
7806191031	40.71	23.26	12	5.3	283	56	-60	57	44	-127	248	65	352	7

Table 5.5. *(continued on next page)*

Date and Time	Location		Depth		Nodal plane I			Nodal plane II			P axis		T axis	
	Latitude	Longitude	(km)	M_w	Strike	Dip	Rake	Strike	Dip	Rake	Azimuth	Plunge	Azimuth	Plunge
Adapted from Kotzev et al., (2006)														
7205080920	41.69	23.60	12	4.9	144	59	17	45	75	148	97	10	359	32
7711030222	42.20	24.20	15	5.3	306	28	-67	100	65	-102	347	68	199	18
7812311626	41.97	23.17	10	4.4	28	50	171	124	83	41	248	21	354	32
7812311556	41.99	23.22	15	4.6	7	40	139	130	65	58	243	14	355	57
8003091652	42.95	23.35	25	4.4	142	42	113	293	52	71	36	5	144	74
8105060441	41.88	23.99	10	3.6	291	23	-43	61	74	-108	307	57	165	27
8107171917	41.92	23.00	10	3.0	49	36	-78	214	55	-99	93	77	30	9
8108261942	41.96	23.12	15	3.6	131	39	-39	253	67	-122	121	55	5	15
8202200445	41.82	24.34	12	3.4	237	36	-71	35	56	-103	265	75	134	10
8204270351	41.89	23.35	12	3.1	291	40	-52	66	60	-117	288	63	174	10
8303112306	41.83	23.07	15	3.1	87	31	-103	283	60	-82	212	73	7	14
8308130208	41.81	23.18	16	3.3	54	40	119	199	56	68	304	8	57	70
8309101840	42.17	23.73	11	3.4	298	36	-72	96	56	-103	327	75	195	10
8312221456	42.64	23.27	15	3.6	320	45	54	186	55	120	255	5	152	64
8401100929	41.92	23.39	13	4.4	119	41	-100	312	50	-81	270	81	36	4
8401231026	41.94	23.39	12	4.8	306	40	-90	126	50	-90	36	85	216	5
8502160633	42.05	23.64	10	3.8	101	50	-145	347	64	-46	307	50	46	8
8605151645	41.99	23.16	19	4.2	323	40	52	188	60	117	259	10	145	63
8705020905	41.90	24.65	10	3.5	236	40	44	110	63	121	177	13	65	59
8710231825	41.78	23.74	10	3.0	332	45	14	232	80	135	289	22	181	38
8901160836	42.31	24.81	10	3.2	291	28	-90	111	62	-90	21	73	201	17
8901180714	41.47	24.64	10	3.0	278	41	-96	106	49	-85	57	84	191	4
8911281230	41.95	23.00	15	3.0	105	50	-51	233	54	-127	81	61	348	2
8912061305	42.07	24.83	15	3.2	200	57	169	296	81	34	63	15	163	29
9003111754	41.85	23.27	13	3.2	198	48	131	325	56	53	80	4	177	60
9007280928	41.97	23.18	10	3.2	359	29	165	102	83	62	215	32	343	45
9101161445	41.32	23.25	14	3.9	182	44	56	46	55	119	115	6	12	66
9102090856	42.34	23.64	10	3.5	333	45	116	119	51	67	224	2	324	71
9103080525	41.91	24.27	3	2.8	352	45	110	145	48	71	247	1	344	75
9106171446	43.01	22.89	16	3.3	11	36	-60	156	59	-110	23	69	260	12
9203071248	42.03	24.67	14	3.1	230	30	129	7	67	70	111	19	245	62
9208242143	42.51	24.91	20	4.2	320	30	-90	140	60	-90	50	75	230	15
9312160922	41.47	23.08	10	4.5	248	49	-52	18	53	-126	226	62	132	2
9401110159	41.68	24.24	10	3.7	240	50	-136	119	58	-49	83	55	181	4
9408030352	41.97	23.07	17	3.6	103	36	-67	256	57	-106	124	72	356	10
9512141625	42.61	23.37	10	3.2	128	27	-85	303	63	-92	208	71	34	17
9604201956	42.70	23.58	8	3.6	270	43	-101	105	48	-80	78	81	188	2
9604202002	42.72	23.56	3	3.3	87	35	-103	283	56	-81	223	76	6	10
9710030020	42.05	23.47	10	3.1	215	44	-125	79	55	-61	45	65	149	5
9711260846	42.04	23.46	6	3.4	67	33	-106	266	59	-80	203	74	348	13

Table 5.5. *Fault plane solutions of earthquakes with M>3 adapted from Global CMT catalogue 1976–2009 http://www.globalcmt.org, European-Mediterranean Seismological Centre (EMSC) 1923-1995 http://www.emsc-csem.org/index.php?page=euromed&sub=emt, Kotzev et al., (2006) 1956-1998, and Kiratzi and Louvari (2003) 1964-1995.*

LON (deg)	LAT (deg)	EPS1 (1/yr)	EPS1SIG (1/yr)	EPS2 (1/yr)	EPS2SIG (1/yr)	THETA (deg)	THETASIG (deg)	TRIANGLE corners
23.1672	40.6691	5.50E-08	3.59E-09	-4.02E-08	3.40E-09	95.3732	1.43E+00	AUT1-PLAT-VRES
23.7098	42.0829	4.66E-08	2.29E-09	-5.89E-08	7.05E-09	7.9864	2.27E+00	BELM-JUDO-SEMO
24.3196	41.8419	2.73E-08	8.28E-08	-2.46E-08	4.67E-08	97.9219	5.99E+01	DOSP-PLO2-SARN
23.8554	41.8612	3.69E-08	7.24E-09	-3.77E-09	2.40E-09	128.4357	4.12E+00	GOST-JUDO-SARN
24.1194	42.1171	1.68E-08	5.11E-08	-8.05E-08	1.90E-07	24.0707	5.13E+01	BELM-JUDO-PLO2
23.9347	41.3313	5.73E-08	1.93E-08	-5.68E-08	4.48E-08	117.6898	1.20E+01	KONS-NEVR-VALK
23.9843	41.6307	1.59E-08	4.05E-09	-2.83E-08	3.17E-09	-38.1918	2.87E+00	SARN-SATO-VALK
22.9705	42.7245	2.80E-08	6.56E-08	-1.97E-08	6.04E-09	58.9104	4.64E+01	BERK-KRAL-ZEME
22.8760	42.1100	-5.99E-09	1.33E-08	-4.37E-08	4.29E-08	75.2889	3.57E+01	BOGO-FROL-PADE
22.8566	41.4977	2.97E-08	3.96E-08	9.96E-09	4.04E-07	106.9033	5.05E+02	PADE-PETR-SKRA
23.2814	42.4211	3.47E-08	2.34E-09	-5.80E-08	1.90E-09	115.0838	9.35E-01	BOSN-PLA1-SAPA
23.1693	42.3910	3.44E-08	7.26E-09	-1.46E-08	4.22E-09	-44.6686	4.80E+00	BOSN-DELA-SAPA
23.2937	42.0682	-3.29E-08	5.12E-09	-7.03E-08	4.48E-09	19.2930	4.54E+00	HURS-PADA-SEMO
23.2044	42.7438	1.29E-08	3.78E-08	-1.60E-09	4.35E-09	110.0727	7.91E+01	BERK-KRAL-SOFI
22.9485	42.2927	5.02E-09	2.82E-09	-4.36E-08	4.04E-09	108.9833	3.02E+00	CARV-DELA-FROL
22.8126	42.2503	1.90E-09	2.55E-09	-2.25E-08	3.88E-09	124.9800	6.27E+00	BOGO-CARV-FROL
24.0710	41.6464	1.07E-08	5.23E-09	-6.74E-08	7.69E-09	71.0627	3.75E+00	DOSP-SARN-VALK
23.6646	41.7474	2.57E-08	8.75E-09	-1.21E-07	1.07E-08	90.6380	3.00E+00	BANI-DOBR-GOST
23.4883	41.6765	5.11E-08	2.41E-09	1.34E-08	2.12E-09	-15.0256	2.48E+00	DOBR-ILIN-POLI
23.1214	41.9097	6.03E-08	5.98E-09	2.66E-08	3.47E-09	-11.4157	5.37E+00	HURS-KRES-PADE
23.3309	42.5126	-1.61E-08	3.13E-09	-5.06E-08	2.70E-09	101.1535	3.59E+00	BOSN-PLA1-SOFI
23.6510	41.6683	2.28E-08	2.39E-09	-9.13E-08	1.03E-08	94.5511	2.25E+00	BANI-DOBR-POLI
23.0413	42.0310	5.96E-08	2.68E-09	-6.21E-09	3.09E-09	-19.2991	1.77E+00	FROL-HURS-PADE
23.3318	41.7485	6.98E-08	6.26E-09	-1.21E-08	4.54E-09	112.4191	2.33E+00	DOBR-ILIN-KRES
23.4227	41.8340	1.38E-07	3.99E-09	-7.13E-08	7.82E-09	40.4841	1.05E+00	DOBR-DRAG-KRES
23.4085	41.9933	5.37E-08	4.29E-09	-5.11E-08	5.22E-09	104.4583	1.65E+00	DRAG-HURS-SEMO
23.6845	41.9205	7.95E-08	5.87E-09	1.33E-08	2.82E-09	-10.7309	2.96E+00	DRAG-GOST-JUDO
23.8780	41.4677	6.71E-08	3.08E-09	-5.49E-09	6.91E-09	98.1197	2.46E+00	KOPR-NEVR-VALK
23.3850	41.5581	4.54E-08	6.62E-09	-1.01E-08	2.23E-09	-0.3665	3.25E+00	ILIN-POLI-RUPI
23.1139	42.4856	1.25E-07	6.89E-09	-1.15E-08	2.52E-09	-5.6628	1.65E+00	BOSN-DELA-KRAL
22.9967	42.4370	-1.09E-08	5.11E-09	-3.37E-08	6.40E-09	86.1588	8.90E+00	CARV-DELA-KRAL
23.2033	41.6771	3.64E-08	4.15E-09	-7.96E-08	9.14E-09	83.1686	2.58E+00	CAPA-ILIN-KRES
23.2923	41.9007	2.80E-08	2.55E-09	-6.44E-08	2.73E-09	88.9776	1.01E+00	DRAG-HURS-KRES
23.0975	42.0969	2.90E-08	3.44E-09	-7.19E-08	4.37E-09	14.2891	1.47E+00	FROL-HURS-PADA
23.0679	42.2182	3.05E-08	3.29E-09	3.94E-09	3.34E-09	33.5204	5.68E+00	DELA-FROL-PADA
23.5983	42.1538	1.54E-08	1.24E-09	-2.74E-08	2.26E-09	-6.9942	1.60E+00	BELM-MALA-SEMO
23.3935	42.3440	4.32E-08	1.91E-09	1.16E-08	1.90E-09	88.5734	2.50E+00	MALA-PLA1-SAPA
23.1701	40.5497	1.47E-08	6.87E-09	-7.67E-08	2.55E-09	121.3471	1.91E+00	AUT1-MONO-PLAT
23.6859	41.3471	1.00E-08	2.59E-09	-2.97E-09	1.86E-08	94.5122	3.48E+01	NEVR-POLI-SERE
23.5656	42.2973	8.26E-08	4.36E-08	-5.91E-09	1.98E-08	116.3744	1.27E+01	BELM-MALA-PLA1
23.9810	42.2562	2.08E-08	5.90E-07	-1.29E-10	4.35E-07	93.1921	1.19E+03	BELM-PLA1-PLO2
23.2159	42.5422	5.18E-08	6.06E-09	-7.60E-08	1.14E-08	41.9123	2.59E+00	BOSN-KRAL-SOFI
23.2308	41.5767	-5.01E-09	5.52E-09	-4.71E-08	1.06E-08	68.0455	8.48E+00	CAPA-ILIN-RUPI
23.7227	41.5564	2.50E-08	2.58E-09	-7.22E-08	3.55E-09	89.4054	1.26E+00	BANI-KOPR-POLI
23.0109	40.7086	9.25E-08	4.14E-09	2.49E-11	3.55E-09	68.2229	1.67E+00	AUT1-MELI-VRES
23.1886	41.5116	4.10E-09	4.90E-09	-8.11E-08	2.70E-09	87.1904	1.77E+00	CAPA-PETR-RUPI
23.1716	42.2679	2.00E-08	1.86E-09	-6.46E-08	1.20E-08	81.6150	4.13E+00	DELA-PADA-SAPA
23.3115	42.2304	4.60E-08	8.88E-09	-1.48E-08	1.38E-09	50.9794	5.23E+00	MALA-PADA-SAPA
24.2105	41.9806	1.30E-08	4.56E-08	-1.20E-08	6.34E-08	100.5222	8.76E+01	JUDO-PLO2-SARN
23.8204	41.7175	1.76E-08	3.73E-09	3.80E-09	4.18E-09	93.5716	1.19E+01	BANI-GOST-SARN
23.8118	41.5716	2.13E-08	2.55E-09	9.41E-09	1.52E-09	59.8680	6.85E+00	BANI-KOPR-SATO
23.8959	41.6536	2.76E-08	8.38E-09	6.89E-09	1.83E-09	64.6264	1.22E+01	BANI-SARN-SATO

LON (deg)	LAT (deg)	EPS1 (1/yr)	EPS1SIG (1/yr)	EPS2 (1/yr)	EPS2SIG (1/yr)	THETA (deg)	THETASIG (deg)	TRIANGLE corners
23.6306	42.0060	7.60E-08	2.28E-09	9.46E-09	6.74E-09	131.1528	3.87E+00	DRAG-JUDO-SEMO
23.4043	42.1519	-1.15E-08	2.42E-09	-3.87E-08	2.28E-09	-43.3668	3.94E+00	MALA-PADA-SEMO
23.7659	42.6062	7.93E-09	2.91E-07	-1.19E-08	1.07E-06	59.7791	1.36E+03	BERK-PLO2-SOFI
23.8594	42.3948	2.54E-09	3.92E-07	-2.76E-08	3.11E-07	6.7130	5.06E+02	PLA1-PLO2-SOFI
23.3459	40.7650	6.41E-08	6.85E-09	-1.19E-08	3.47E-09	116.0233	3.21E+00	LAGA-PLAT-VRES
23.9002	41.5488	1.59E-08	3.19E-09	-3.51E-08	5.52E-09	-30.3301	3.35E+00	KOPR-SATO-VALK
22.8655	42.4742	4.74E-08	2.41E-09	-2.59E-08	6.03E-09	54.2889	2.20E+00	CARV-KRAL-ZEME
22.7325	42.3722	5.30E-08	5.69E-09	-5.15E-10	4.19E-09	37.0365	4.05E+00	BOGO-CARV-ZEME
24.3740	41.5694	4.94E-08	1.29E-06	8.89E-09	1.57E-07	24.5728	9.27E+02	DOSP-ELEF-PLO2
24.1091	41.2130	8.43E-08	1.23E-07	1.68E-08	6.54E-08	-1.2308	6.25E+01	DOSP-ELEF-KONS
22.4279	41.4003	2.88E-08	4.35E-07	-4.53E-08	2.78E-06	94.2501	8.21E+02	BOGO-KALI-SKRA
22.7087	41.7645	3.02E-08	2.85E-07	-2.97E-08	5.45E-07	109.1941	2.46E+02	BOGO-PADE-SKRA
24.0433	41.4282	4.68E-08	4.99E-08	-8.55E-08	6.30E-08	81.0438	1.47E+01	DOSP-KONS-VALK
23.4902	41.3846	4.11E-08	2.53E-09	4.23E-09	7.92E-09	-15.1278	6.10E+00	POLI-RUPI-SERE
23.1749	41.2010	3.71E-08	1.63E-08	-1.23E-08	6.04E-09	115.7508	1.03E+01	KLKI-PETR-SERE
24.0037	40.9447	6.44E-08	5.82E-09	-2.96E-08	3.07E-09	21.3947	2.03E+00	ELEF-KONS-MESL
23.3171	41.3533	2.21E-08	2.56E-08	-8.37E-08	2.18E-08	76.1438	1.01E+01	PETR-RUPI-SERE
23.7585	41.4648	9.38E-08	1.85E-08	-6.29E-08	1.52E-08	101.7073	4.43E+00	KOPR-NEVR-POLI
22.4700	40.6945	3.48E-08	1.36E-08	-1.52E-08	1.69E-08	94.9483	1.31E+01	KALI-MELI-PLLT
22.7979	41.1882	3.73E-08	4.61E-08	-1.53E-08	2.70E-08	112.5857	3.34E+01	KLKI-PETR-SKRA
23.9681	40.7308	7.16E-08	2.66E-08	2.68E-08	3.21E-08	88.5789	2.21E+01	ELEF-IERI-MESL
23.4489	40.5188	6.33E-08	5.57E-09	-1.34E-08	3.79E-09	103.8781	2.78E+00	PLAT-SEMA-VARV
22.7474	40.6016	9.25E-08	4.62E-09	1.56E-09	3.12E-08	66.7253	9.93E+00	AUT1-MELI-PLLT
23.9888	40.4488	7.27E-08	6.09E-07	-7.67E-09	4.29E-07	-37.2034	3.10E+02	ELEF-IERI-STHN
23.6544	40.9429	6.88E-08	1.10E-08	1.38E-09	4.39E-09	114.8800	4.48E+00	LAGA-MESL-SERE
23.7924	41.0174	1.70E-08	3.17E-09	-4.57E-08	9.80E-09	48.2019	4.33E+00	KONS-MESL-SERE
23.5184	40.6850	6.35E-08	5.98E-09	-1.38E-08	4.34E-09	118.5472	2.42E+00	LAGA-PLAT-VARV
23.2794	40.4792	7.17E-08	3.79E-09	-1.64E-08	7.45E-09	74.5522	2.90E+00	MONO-PLAT-SEMA
23.6832	40.7511	8.94E-08	4.76E-09	-1.82E-08	5.17E-09	124.4194	1.83E+00	LAGA-MESL-VARV
23.7858	40.6116	8.83E-08	1.45E-08	1.07E-08	1.16E-08	118.5865	5.52E+00	IERI-MESL-VARV
23.8224	40.2164	6.96E-08	2.54E-08	-2.74E-08	1.86E-08	132.9180	9.81E+00	IERI-NIKI-STHN
22.9543	40.8562	4.73E-08	6.07E-09	2.92E-09	6.51E-09	75.7412	6.24E+00	KLKI-MELI-VRES
23.7889	41.1889	6.96E-09	2.33E-09	-6.47E-09	1.74E-09	110.4012	5.94E+00	KONS-NEVR-SERE
22.5006	40.9010	2.74E-08	2.21E-08	-1.80E-08	1.29E-08	83.9974	1.55E+01	KALI-MELI-SKRA
22.7216	40.9554	5.36E-08	2.42E-08	-1.62E-08	2.44E-08	97.4290	1.47E+01	KLKI-MELI-SKRA
23.7338	40.4044	6.30E-08	9.69E-09	9.49E-09	1.07E-08	113.5657	6.40E+00	IERI-NIKI-VARV
23.5617	40.3776	6.43E-08	3.12E-09	-2.87E-08	3.24E-09	107.0460	1.33E+00	NIKI-SEMA-VARV
23.1786	40.9808	7.60E-08	2.82E-08	2.22E-09	9.62E-09	91.6509	1.48E+01	KLKI-SERE-VRES
23.4140	40.9289	6.07E-08	1.30E-08	1.04E-08	2.26E-08	97.0324	1.29E+01	LAGA-SERE-VRES

Table 5.6. *Strain rates for every each triangle obtain from QOCA software package.* ***LON****: Longitude [°],* ***LAT****: Latitude [°],* ***EPS1****: value of the maximum principal axis of the tensor of deformation rate,* ***EPS1SIG****: 1 sigma uncertainties of EPS1,* ***EPS2****: value of the minimum principal axis,* ***EPS2SIG****: 1 sigma uncertainties of EPS2,* ***THETA****: orientation of the axis of maximum deformation rate,* ***THETASIG****: 1 sigma uncertainties of THETASIG. If EPS1 or EPS2 are positive it is an extension, otherwise it is a compression.*

5.2.5.2 Comparison between strain and stress

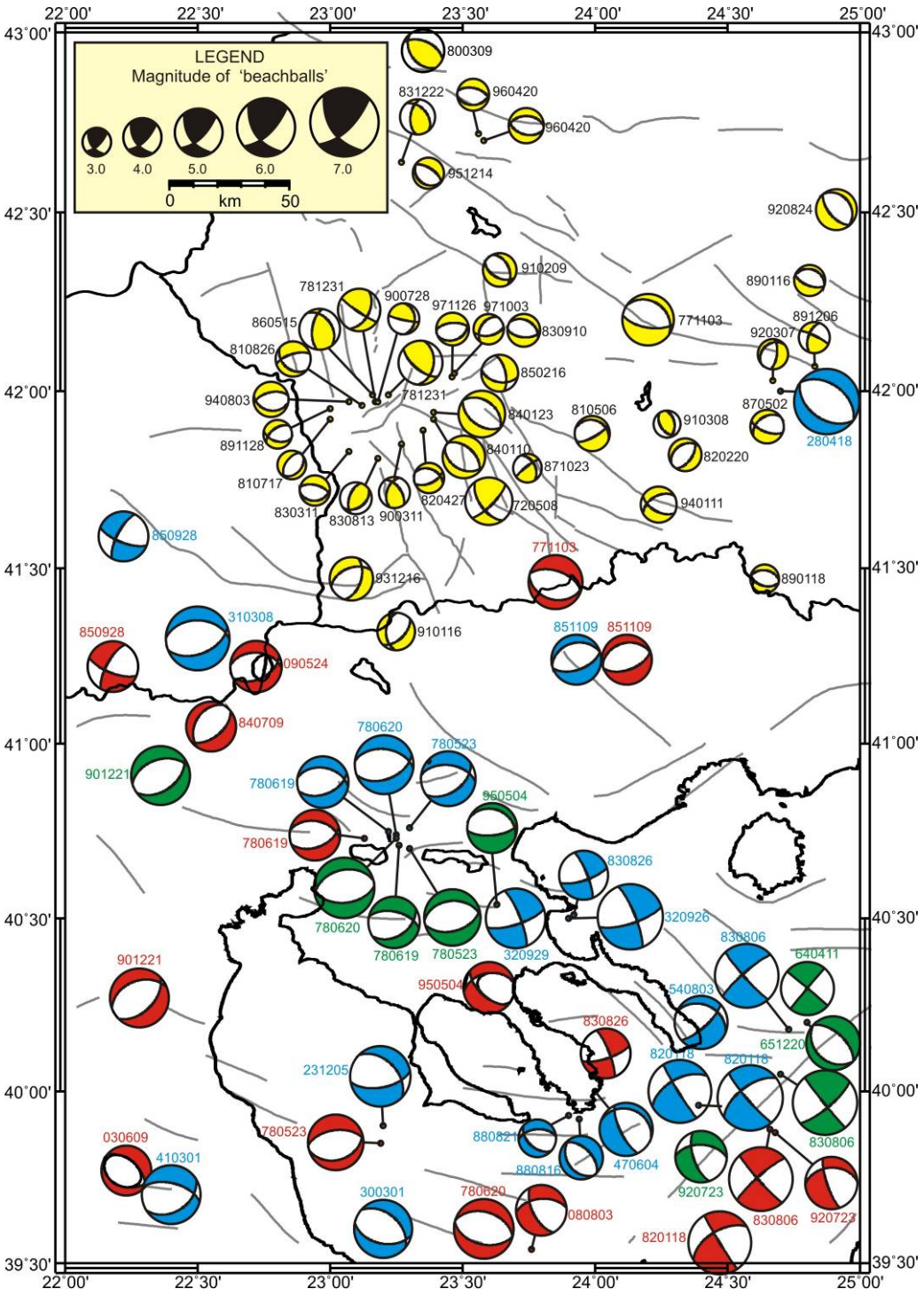

Figure. 5.8. *Focal mechanisms available for the northern Greece south-west Bulgaria region. The focal mechanisms are taken from four sources. Red colour – CMT Harvard solution http://www.globalcmt.org/CMTsearch.html; blue colour – Vannucci-Gasperini (2003); European-Mediterranean Seismological Centre (EMSC), http://www.emsc-csem.org/index.php?page=euromed-sub=emt; yellow colour - Kotzev et al., (2006); green colour – Kiratzi and Louvari (2003);*

The obtained geodetic strain from QOCA software packages (Table 5.6) is presented on Figure 5.9a,c. The seismic data that we collected consist of fault plane solutions for 85 earthquakes with a range of magnitude of 3.0 to 6.8 spanning the period 1928 to 2009 from four different sources (Global CMT catalog http://www.globalcmt.org, European-Mediterranean Seismological Centre (EMSC) http://www.emsc-csem.org/index.php?page=euromed&sub=emt, Kotzev et al., 2006 and Kiratzi and Louvari 2003). The fault plane solutions are plotted with different colour in Figure 5.8 and the solutions are given in Table 5.5.

In order to compare obtained geodetic strain with seismic stress we plotted the principal stress P and T axes on Figure 5.9b. The scale factor of the arrows is a function of the plunge. The orientation of these principal stress axes allows only qualitative comparison with geodetic results.

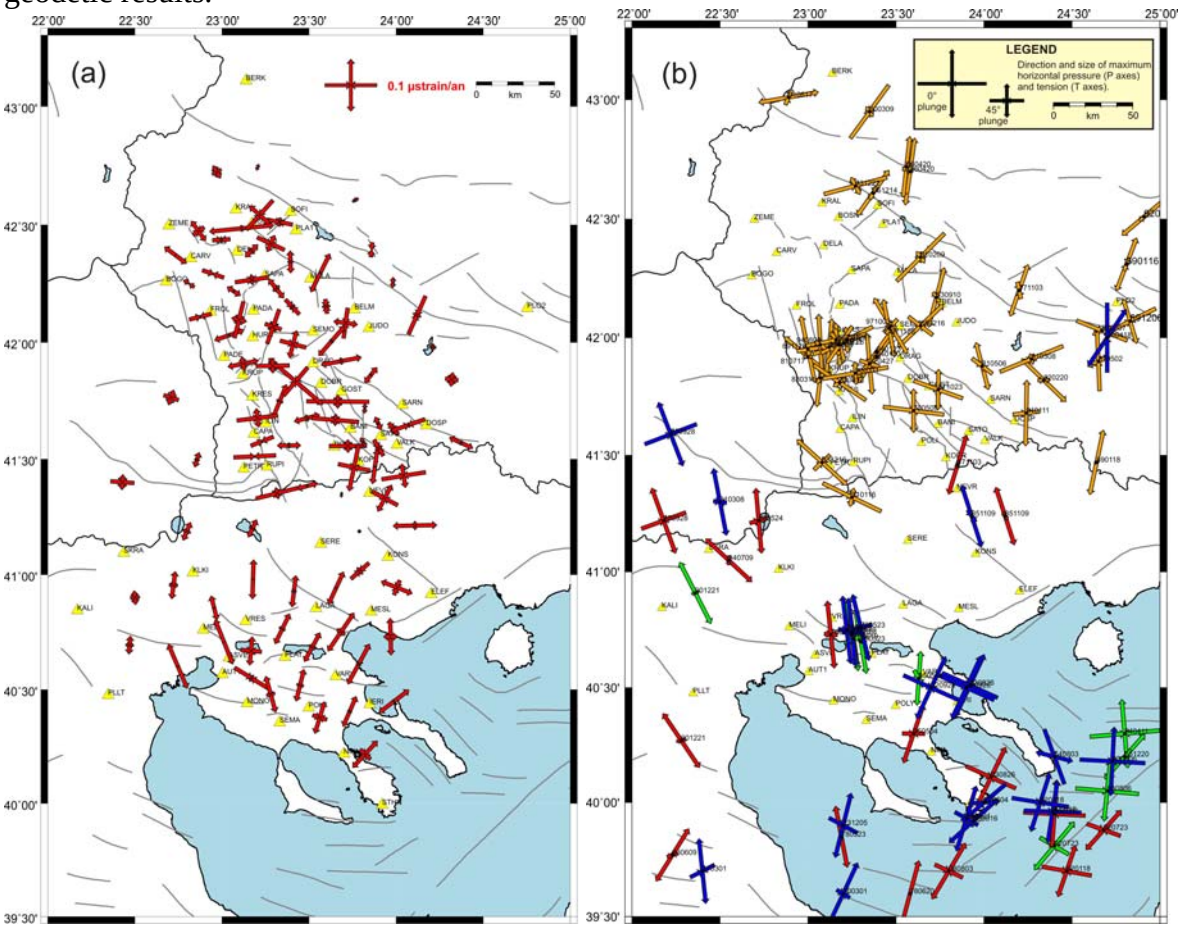

Figure 5.9. (a) *Strain rates in the Southwest Bulgaria and Northern Greece.* ***(b)*** *Orientation of principal stress P (pressure) and T (tension) axes.* ***(c)*** *Strain rates in the most active region of Bulgaria around Krupnik fault.* ***(d)*** *Orientation of principal stress P (pressure) and T (tension) axes in the most active region of Bulgaria around Krupnik fault*

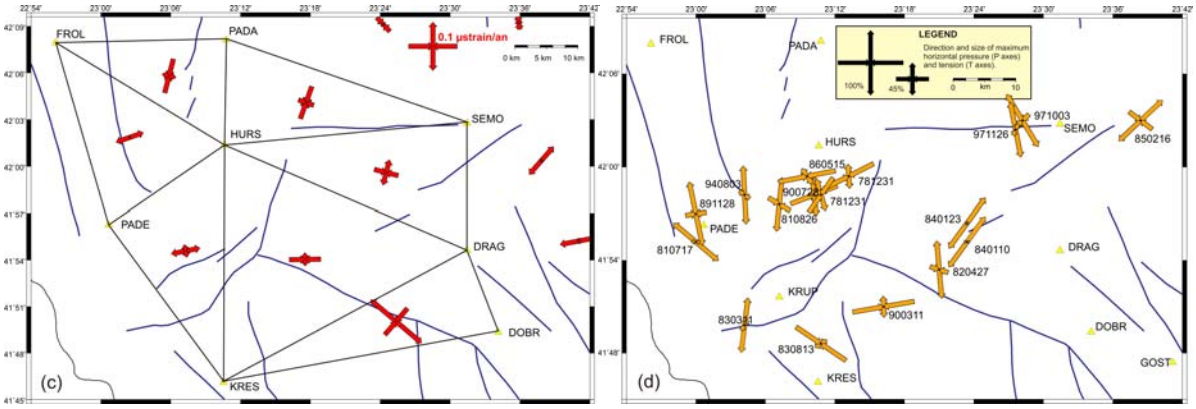

Figure 5.9. *(continued)*

The strain rate tensors show us complex behaviour with both compression and extension. In the region of Northern Greece is clearly seen the major extensional regime which is in good agreement with the principle stress axes from seismic events. In region of Southwest Bulgaria the strain rates field is more complex and that is well supported by seismological evidences (Figure 5.9b). We can see both extension and compression which covers SWB region. To focus on the most active region in SWB we plotted Figure 5.9c and 5.9d in different scale. On Figure 5.9c we can see that major stress axes are with extension character with various directions. The stresses near to point HURS have pressure axes.

5.2.5.3. Hypothesis of the existence of a stable block

Based on velocity gradient (Figure 5.7) we can see area with homogenous displacements. We assume for existence of a stable block in this region of the central west Bulgaria. The results of strain and stresses presented on Figure 5.9 show low rate of strain

Vector of rotation

determined parameters by minimizing error	Lat	Long	Angle	Ωx	Ωy	Ωz
	(°)	(°)	(°/Ma)	(°/Ma)	(°/Ma)	(°/Ma)
	43,20	26,16	0,5183	0,3391	0,1666	0,3548

			Data						Model						
	Lat	Long	V-east	errors	V-north	errors	V	Azimuth	V-east	residuals (obs-calc)	V-north	residuals (obs-calc)	V	Azimuth	(errors)²
	(°)	(°)	(mm/yr)		(mm/yr)		(mm/yr)	(°)	(mm/yr)		(mm/yr)		(mm/yr)	(°)	
KRAL	42,57	23,08	0,7	0,4	-2,7	0,4	2,79	165,47	0,67	0,03	-2,26	-0,44	2,36	163,4	1,22
SOFI	42,56	23,39	0,7	0,4	-2,1	0,4	2,21	161,57	0,68	0,02	-2,03	-0,07	2,14	161,6	0,04
PLA1	42,48	23,43	0,6	0,4	-1,9	0,4	1,99	162,47	0,76	-0,16	-2,01	0,11	2,14	159,4	0,22
DELA	42,39	23,09	0,8	0,4	-2,5	0,4	2,62	162,26	0,85	-0,05	-2,25	-0,25	2,41	159,2	0,40
BOGO	42,26	22,68	1,3	0,5	-2,3	0,4	2,64	150,52	0,99	0,31	-2,55	0,25	2,74	158,7	0,77
BERK	43,11	23,14	0,1	0,4	-1,9	0,4	1,90	176,99	0,13	-0,03	-2,22	0,32	2,22	176,7	0,63
HURS	42,02	23,18	1,2	0,5	-2,1	0,4	2,42	150,26	1,22	-0,02	-2,19	0,09	2,50	150,9	0,05
														Σ=	0,30

Table. 5.7. *Determined parameters of rotation by minimizing error for local block.*

accumulation in the alleged stable block, which are in good agreement with our hypothesis. In order to support the hypothesis of stable block we estimate parameters of rotation pole for the set of points (KRAL, SOFI, PLA1, DELA, BOGO, BERK, and HURS) by minimizing errors, which define this block (Table 5.7). On Figure 5.10 are plotted residuals between observation and model vectors and results show quite good coincidence.

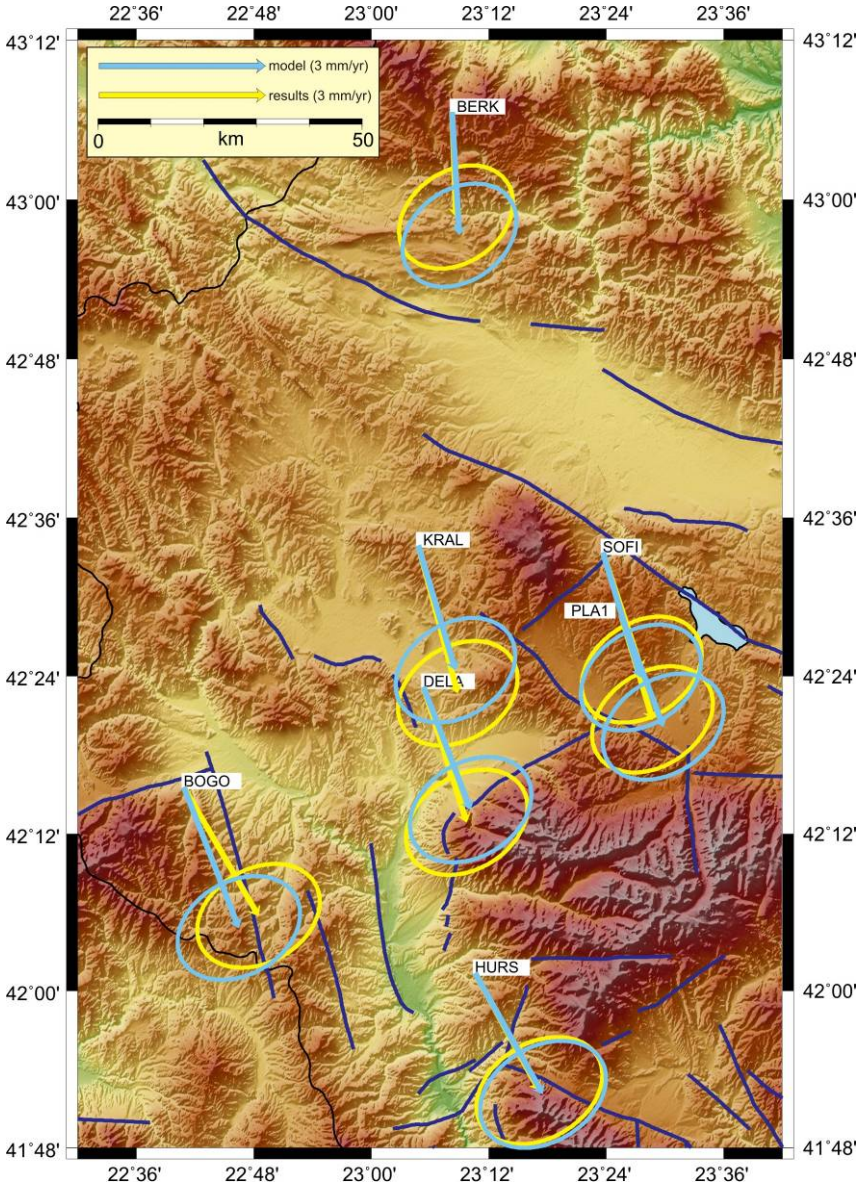

Figure 5.10. *Residuals between observation and model vectors.*

5.2.5.4 Results in the contest of East Mediterranean

The active deformation in extensional region in South Balkan has been separated from the main Aegean regime since ~6-10Ma by the propagation of the North Anatolian fault zone into the northern Aegean Sea (Armino et al., 1996; Sengor et al., 2004). After that

deformational event, the Aegean region to south of the North Anatolian fault zone began to move SSW as a single plate and the extension within the South Balkan region became more N-S oriented and with a lower rate than southward movement of the Aegean plate. Geological investigations (Burchfiel et al., 2000, 2003; Nakov et al, 2001) suggest that the northern boundary of the Aegean extensional regime passes through north central Bulgaria.

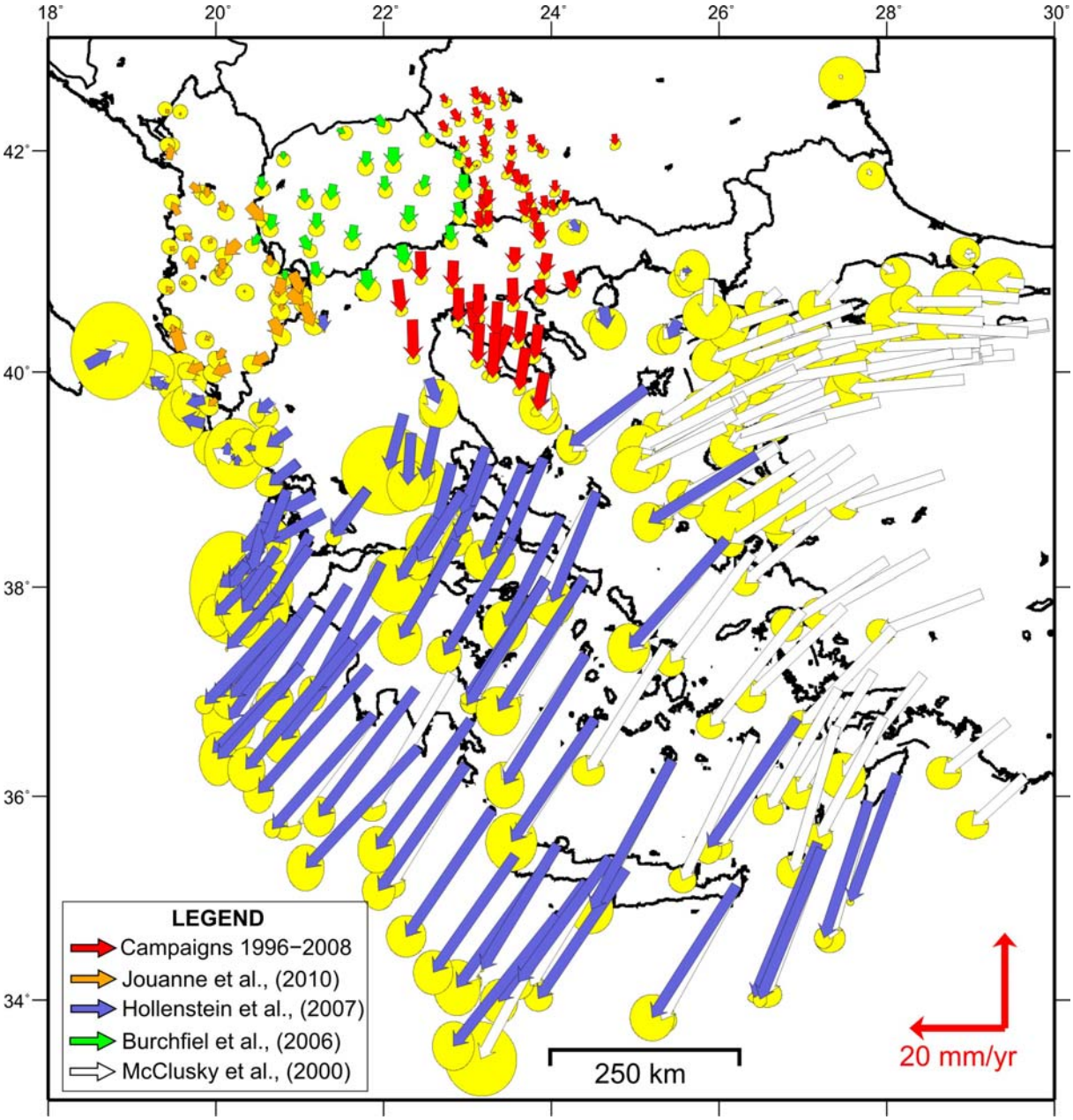

Figure 5.11. *GPS velocities obtained for the region of the East Mediterranean according to McClusky et al., (2000) – white vectors; Burchfiel et al., (2006) – green vectors; Hollenstein et al., (2007) – black vectors; Jouanne et al., (2011) – orange vectors. The red vectors are the obtained velocities in the present work.*

Their analysis of young and active faulting indicates that much of the Balkan Peninsula is characterized by extensional tectonics which refers to the southern Balkan extensional regime. GPS results from 25 stations in Macedonia measured in 1996 and 2000 (Burchfiel et al., 2006), and GPS results between 1996 and 2004 in western Bulgaria define an approximately ESE-trending extensional boundary that marks the northernmost extent of Aegean extensional domain. Another GPS study of 89 point in the whole territory of Bulgaria for the period 1993 to 2007 by Georgiev (2009) suggests that limit of Aegean extension domain is going from central west Bulgaria along Maritza lineament passing to E-SE.

We use combined GPS results from (McClusky et al., 2000, Burchfiel et al., 2006, Hollenstein et al., 2007, and Jouanne et al., 2010) as a background to show gradual increase in velocity from north to south to ~35 mm/year toward the Aegean See (Figure 5.11). Our results cover a part of Aegean region and they are not enough to determinate northernmost limit of Aegean extensional domain, however the results are in good agreement it previous studies (Burchfiel et al., 2006, Georgiev, 2009)

5.2.6. Conclusion

The results of GPS measurements in SWB and NG give details information of the displacements. In agreement with geological and seismological data, the results confirm the contemporary activity in the region. The presented velocity gradient (Figure 5.7) clearly indicates the increase of the motion from north to south direction and reaches the Hellenic arc with values of up to 30-35 mm/yr (Hollenstein et al., 2007, McClusky et al., 2000) (Figure 5.11). The obtained strain rate field shows overall north-south extension regime. In region of SWB the strain rate tensors present more complex behaviour with both compression and extension. Comparing with principal stress axes obtained from seismological events, extension regime is in quite good agreement in NG area. The anomaly of point KRUP which is stabilized on the north part of Krupnik fault confirms activity of that fault. Based on our geodetic results presented velocity gradient, strain rate tensors and geological and seismological data from previous studies we assume for existence of small homogeneous stable block in the region of west part of central Bulgaria. Pole rotation parameters were determined to confirm our hypothesis. Our GPS results confirm the studies (Burchfiel et al., 2006, Georgiev, 2009) for northernmost limit of Aegean extension domain. The GPS results confirm contemporary activity of the region of SWB and NG and they are in good agreement with velocity field in Aegean (Figure 5.11).

5.3. GPS constrains on current tectonics of Albania

F. Jouanne (1), J. L. Mugnier (1), R. Koci (3), S. Bushati (2) , K. Matev (1, 5), N. Kuka (3), I. Shinko (3), M. Pasha (4), S Kociu

(1) Institut des Sciences de la Terre, Université de Savoie

(2) Academy of Sciences of Albania

(3) Institute of Seismology of the Academy of Sciences of Albania

(4) Military Geographical Institute of Albania

(5) Department of Geodesy, National Institute of Geophysics, Geodesy and Geography, Bulgarian Academy of Sciences.

submitted in

Geophysical Journal International

ABSTRACT

Current Tectonics of Albania is documented by neotectonics indices and by a large number of medium size earthquakes. Focal mechanisms suggest the existence of current shortening across the external Albanides whereas internal Albanides are affected by E-W to N-S extension. To investigate the kinematics of Albanides, we integrate continuous and episodic GPS measurements with focal mechanisms of the Regional Centroid Moment Tensor catalogue. This study has allowed distinguishing a western Albania affected by westward motions relative to Apulia microplate, illustrating the ongoing collision of external Albanides, whereas inner Albanides present southward motion relative to both Apulia and stable Eurasia. The Skutar-Pesh Fault Zone, between Dinarides and Albanides, is identified as the probable northern limit of an area including Albania and western Greece, affected by a clockwise rotation relative to Apulia and also the northern limit of the Balkan (inner Albanides, Macedonia, Bulgaria) affected by southward motion relative to Apulia and stable Eurasia. The other transverse fault zone of Albanides, the Diber-Elbasani fault, appears to be mainly affected by a moderate extension. Compilation of published GPS data with our data set allow to identify the external-inner Albanides limit as the western border of the domain (inner Albania,

northern Greece, Macedonia, Bulgaria) affected by southward displacements relative to stable Eurasia, whereas Skutar-Pesh fault form probably also its northern limit.

5.3.1. Introduction

Current tectonics of Albania (Figure 5.12) is characterized by an important microseismicity, small and medium size earthquake and a few large events as shown by the occurrence of 6 earthquakes with Ms magnitudes exceeding 6 during the last century (1905, Shkodra earthquakes Ms 6.6, 1911 Ohrid lake earthquake Ms 6.7, 1920 Tepelena Ms 6.4, 1926 Durres earthquake Ms 6.2, 1967 Dibra earthquake Ms 6.6 and 1979 Montenegro earthquake Ms 6.9). Focal Mechanisms (Sulstarova et al., 1980, Louvari et al. 2001, Pondrelli et al., 2002, 2004, 2006 and 2007), as well as neotectonics investigations (Figure 5.12) (Aliaj et al, 2000; Carcaillet et al, 2009) underline the existence of a current E-W shortening across external Albanides whereas internal Albanides experience an E-W to N-S extension (Tagari et al., 1993). Albanides are crossed by two transversal faults, the Vlora-Elbasani-Dibra fault zone and the Shkodra-Pesh (Scutari-Pesh) one (Roure et al., 2004). This last fault zone seems to be the northern boundary of the Albania – northern Greece zone characterized by NNW-SSE structural direction and by the important post Miocene rotation as shown by Speranza et al., (1995) and van Hinsbergen et al., (2005). North of the Scutari-Pesh or Shkoder – Pesh fault, Dinarides have not experienced such rotation and are characterized by NW-SE structural directions.

5.3.2. Data collection and processing

To quantify current displacements, we have installed since 2003 a network of five permanent GPS stations designed to record present-day displacement across the main active tectonic zones of Albania completed with a dense episodic GPS network measured four times allowing the localization of the boundaries between external Albanides affected by current shortening and inner Albanides affected by extension.

5.3.2.1. Permanent GPS network.

Permanent GPS stations have been installed in 2003 in Albania to sample present-day displacements in both sides of the main active structures identified in Albania (Figure 5.12). SARA, SHKO and TIRA permanent stations allow estimating the shortening across external Albanides and Adriatic Sea by comparison with the Matera IGS station installed on the

Adriatic platform. The Peshkopia station (PESH), the Berati (BERA) and the ORID station in Macedonia allow the quantification of current deformation in internal Albania by comparison with the SHKO, TIRA and SARA stations.

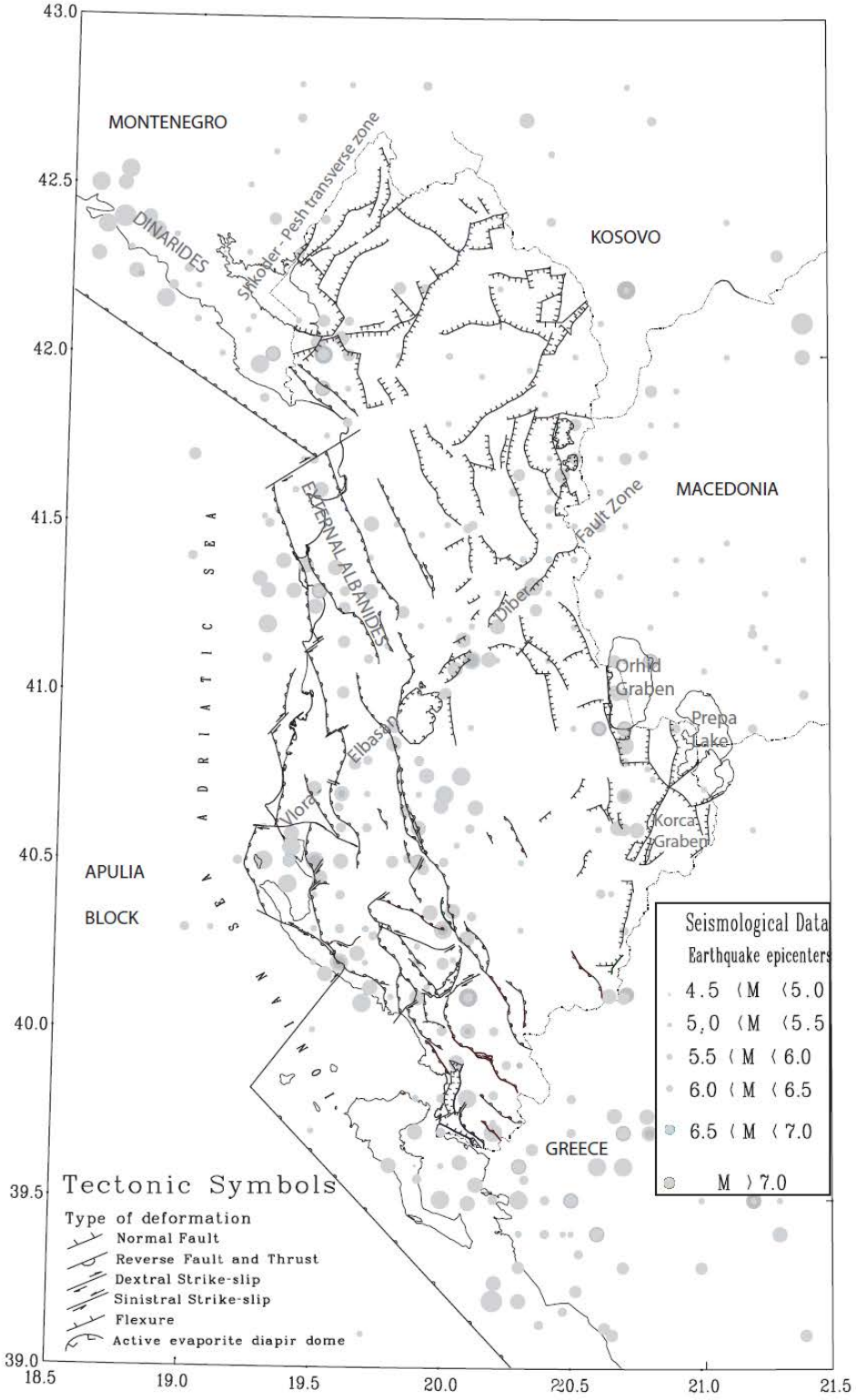

Figure 5.12. *Neotectonics map of Albania, with location of historical seismicity redrawn after Aliaj et al., (2004).*

Albanian permanent GPS data are analyzed together with GPS data from IGS, EUREF network, RING network (**R**ete **I**ntegrata **N**azionale **G**PS, http://ring.gm.ingv.it/), Geodaf network, HemusNet permanent GPS network (http://www.hemus-net.org/), NOANet (http://www.gein.noa.gr/gps.html) and Corinth GPS permanent network (https://geodesie.ipgp.jussieu.fr/gpscope/corinth/) and data from Unavco web site collected in southern Italia.

	latitude	longitude	july 2003	may 2006	october 2008	november 2009
601	41.542867	20.059746		3		3
602	41.700657	19.705671		3		3
603	41.428186	19.553470		3		3
605	40.464793	20.264570		3		3
606	40.908277	20.646068		3	3	3
607	41.515326	20.387959		3		3
608	41.675032	19.896559		3		3
609	41.265541	19.668844		3		3
611	41.202650	19.709713		3		3
ALAR	40.661691	20.783624	3	3	3	
APOL	40.725704	19.474820	4	3	3	
ARDE	40.811245	19.594071	4	2	4	
BDM0	40.747853	20.335471		3		3
BUTR	39.749802	20.005527	3	5	4	
DAMG	40.962322	20.063150		3		3
DERV	40.039073	20.171019	3	3	4	
DUKA	40.322349	19.936268	3	3	4	
KAPS	40.62257	21.040371	3	3	3	
KORC	40.619116	20.793464	3	3		
KRYE	41.101478	19.514794	4	3	4	
LABO	40.209427	20.092219		3	4	
LESK	40.153191	20.619866	2	3	3	
LINI	41.062599	20.631250	3	3		
LIXH	41.032869	20.072279	4	3	3	
LLOG	40.196656	19.595466	2	3		
LUSH	40.936663	19.717865	1	3		
MALI	40.725058	20.707164	3	3		
MIRA	41.181072	20.268220	4	3	4	
MUSH	41.209662	19.953588	1	2	5	
POGR	40.900928	20.914627	3	3	3	
QARR	40.482218	20.674689	3	3	3	
QEPA	40.058058	19.847192	3	2	3	
RRAD	40.36541	19.493794	4	3	3	
ZVEZ	40.735823	20.879393	2	3	3	

Table 5.8. *Occupation of the geodetic points of the dense episodic network with 12-24 hours sessions.*

5.3.2.2. Episodic dense GPS network.

Dense GPS network has been installed in 2003 and in 2006 to better localize areas undergoing current deformation. Benchmarks allow direct centering of antennas to avoid

centrings errors and bad determinations of antenna heights. The measurements performed are summarized in Table 5.8, points have been observed with three sessions of 12-24 hours in 2003, 2006, 2008 and 2009.

5.3.3. Data analysis.

Permanent and dense GPS data (2003 – 2009) have been analyzed using absolute phase center determination. Results were obtained using IGS final precise orbits, IGS Earth rotation parameters and data from nearby permanent GPS stations (ANKR, BUCU, CAGZ, GENO, GLSV, GOPE, GRAS, GRAZ, ISTA, JOZE, LAMA, LAMP, MATE, MEDI, NICO, NOT1, PADO, PENC, POLV, SOFI, UZH, WROC, WTZR and ZIMM).

site	lon	lat	Ve	Vn	σe	sn	Ren
601	20.0598	41.5429	22.949	12.407	1.147	1.149	-0.0003
602	19.7057	41.7007	23.867	12.789	1.138	1.140	-0.0001
603	19.5535	41.4282	20.233	16.580	1.253	1.254	-0.0004
607	20.3880	41.5153	25.190	10.964	1.128	1.130	-0.0021
608	19.8966	41.6750	22.074	12.351	1.126	1.128	-0.0011
611	19.7097	41.2026	22.053	15.932	1.171	1.173	0.0000
ALAR	20.7836	40.8520	22.497	11.037	0.980	0.983	-0.0011
APOL	19.4748	40.7257	21.597	16.866	0.972	0.973	0.0007
ARDE	19.5941	40.8112	24.162	15.326	0.980	0.983	-0.0003
BDMO	20.3355	40.7479	23.375	14.035	1.299	1.297	0.0032
BUTR	20.0055	39.7498	21.464	13.430	0.972	0.975	0.0010
BZHE	19.5757	42.3168	23.246	14.540	1.199	1.206	-0.0078
DAMG	20.0631	40.9623	22.284	12.382	1.284	1.286	-0.0003
DERV	20.1710	40.0391	20.027	13.736	0.946	0.950	-0.0006
DUBR	18.1104	42.6500	25.345	19.153	0.828	0.828	0.0002
DUKA	19.9363	40.3224	21.090	15.329	0.946	0.950	0.0002
HOTI	19.4367	42.3329	21.727	15.482	1.229	1.235	-0.0013
KAPS	21.0404	40.6226	25.005	10.365	0.936	0.936	-0.0018
KOLA	19.4440	41.9206	23.728	17.741	1.196	1.202	-0.0016
KORC	20.7935	40.6191	22.907	12.556	1.241	1.246	-0.0020
KRYE	19.5148	41.1015	21.814	16.546	0.907	0.911	0.0000
LABO	20.0922	40.2094	20.235	13.395	0.961	0.966	0.0008
LESK	20.6199	40.1532	19.810	13.393	0.941	0.944	-0.0031
LINI	20.6313	41.0626	23.915	12.767	1.295	1.299	-0.0019
LIXH	20.0723	41.0329	22.929	12.074	0.884	0.889	-0.0008
LLOG	19.5955	40.1967	20.943	19.452	1.324	1.329	0.0017
LUSH	19.7179	40.9367	23.222	18.554	1.208	1.228	0.0052
MALI	20.7072	40.7251	24.332	14.231	1.297	1.301	-0.0026
MIRA	20.2682	41.1811	19.822	11.921	0.927	0.930	-0.0011
MUSH	19.9536	41.2097	21.819	13.548	0.938	0.943	-0.0017
POGR	20.9146	40.9009	25.598	9.882	0.963	0.966	-0.0011
POLV	34.5429	49.6026	22.600	12.600	0.010	0.010	0.0000
QARR	20.6747	40.4822	24.667	11.723	0.960	0.963	-0.0013
QEPA	19.8472	40.0581	19.336	13.423	0.973	0.975	-0.0023
RRAD	19.4938	40.3654	23.748	17.168	0.978	0.977	0.0008
SHIR	19.4442	42.0611	22.880	14.677	1.251	1.260	-0.0009
ZVEZ	20.8794	40.7358	25.040	11.621	0.956	0.959	-0.0016

Table 5.9. *Velocities of dense GPS network determined in the ITRF2005 reference frame (Altamimi et al., 2007).*

Data have been analyzed with the Bernese 5.0 software using the following strategy: (1) initial ionosphere-free analysis with residuals computation, (2) residuals analysis; (3) resolution of ambiguities using the Quasi Ionosphere Free strategy using CODE ionosphere models and (4) computation of normal equations. Troposphere-induced propagation delays were estimated from the observations every 2 h. Each daily solution has been transformed in the ITRF2005 reference frame with a six parameters Helmert solution. Each discontinuities introduced in the ITRF2005 solutions (changes of materiel of the permanent station by example) has been introduced. Outliers detection has been performed using the Bernese 5.0

software using ITRF2005 sites coordinates and velocities constrained at theirs ITRF2005 values for points defined in the ITF2005.

Finally, we computed a free network solution with the Quasi-Observation Combination Analysis software (Dong et al. 1998 and Shen et al. 2000), assigning the following degrees of freedom to the ITRF2005 sites: N = 0.02 m; E = 0.02 m; Up = 1.0 m, Vn = 0.002 m.yr^{-1}; Ve = 0.002 m.yr^{-1}; Vup = 0.050 m.yr^{-1}.

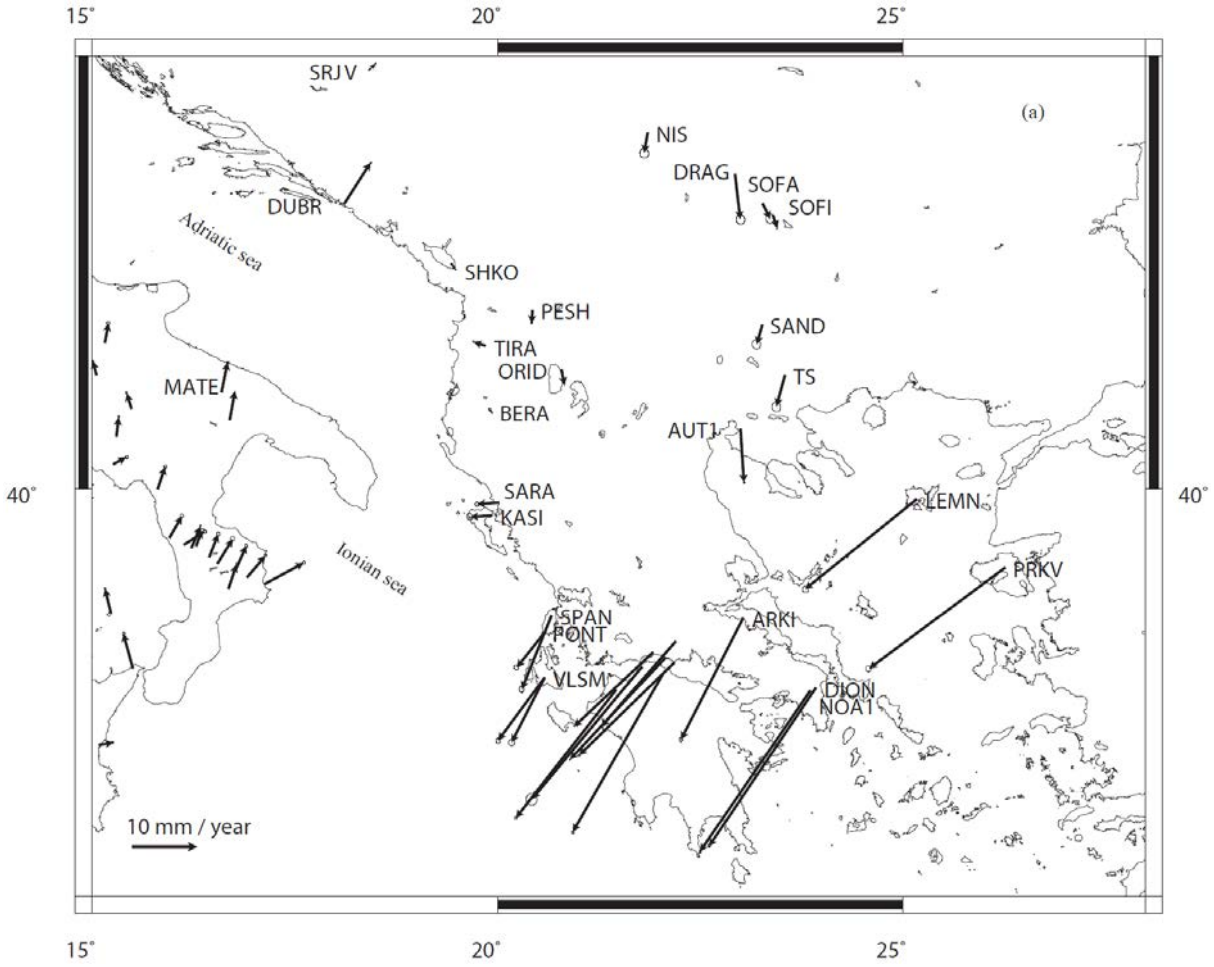

Figure 5.13. *Displacements rates determined from permanent GPS stations expressed in the Eurasia fixed reference frame (a) and Apulia fixed reference frame (b).*

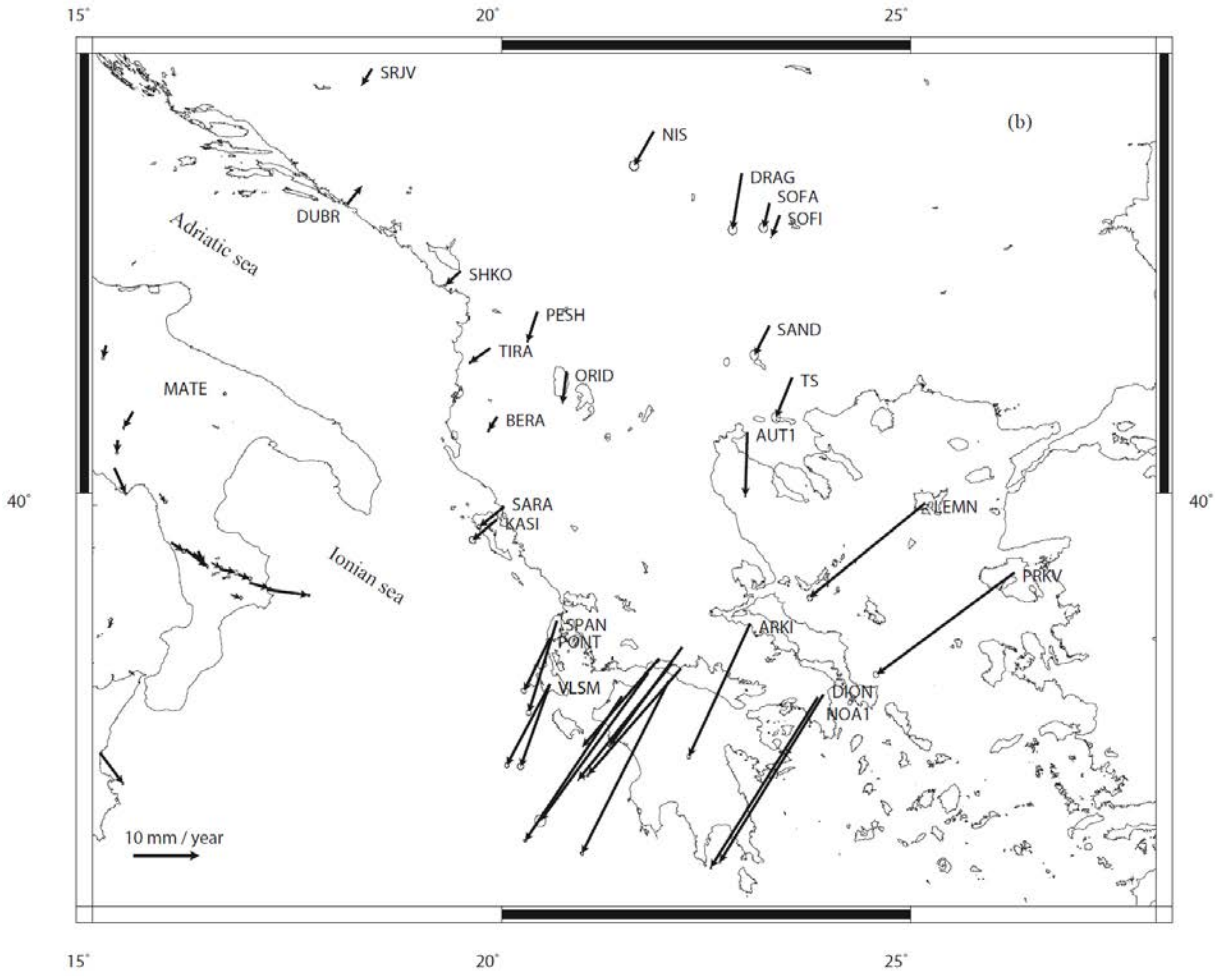

Figure 5.13. (continued)

Site velocities were estimated from the daily solutions (Table 5.8.). The Qoca modeling of the time-series data was done through sequential Kalman filtering, allowing adjustment for global translation and rotation of each daily solution. Strain rates tensors with theirs uncertainties have been estimated with the Qoca software to better visualize the current deformation and the geographical evolution of strain rates axes.

Displacements have been expressed in the Eurasia fixed reference frame (Figure 13a) using the rotation pole proposed by Altamimi et al. (2007) (56.330°N +/- 0.261, 95.979°E ± 0.549 and an angular rotation of 0.969°/Ma +/- 0.003). We have also expressed displacements relative to Adriatic plate, this microplate being the foreland of Albanides. In the North Adria reference frame, the Matera station located in southern Adria presents a residual reaching 1.1 mm/year which suggested the segmentation of the Adria microplate in two parts, a northern the Adria block, and a southern one, the Apulia block formed by the calabrian platform as already suggested (Calais et al., 2002; Oldow et al. 2002, Nocquet et Calais, 2003; Babucci et al., 2004; Battaglia et al., 2004; D'Agostino et al., 2008).

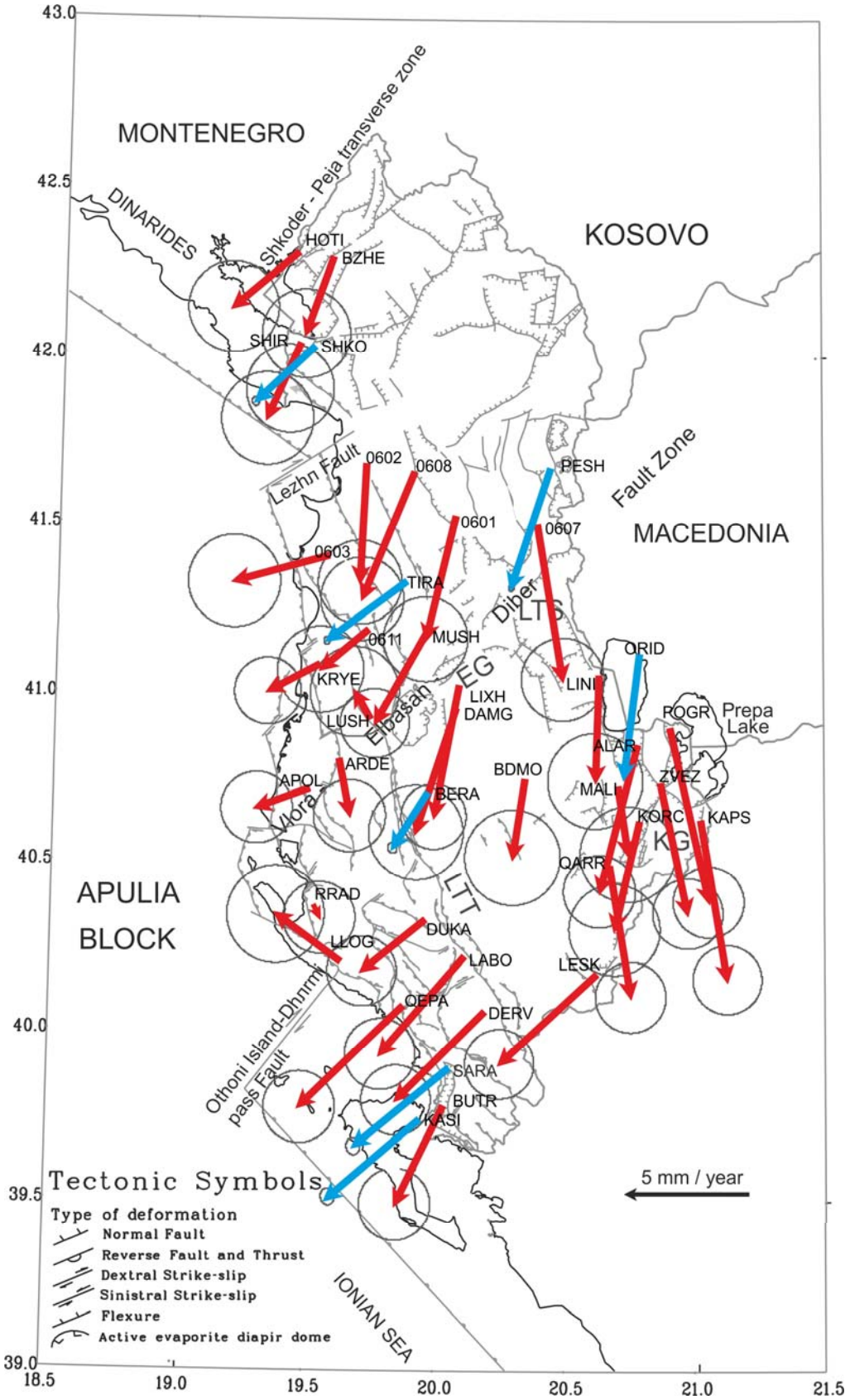

Figure 5.14. *Displacement rates expressed relative to Apulia (rotation pole proposed by D'Agostino et al.,(2008). Red arrows represent displacement rates of points of the episodic network, blue arrows represent displacement rates of permanent stations.*

The boundary between these two microplates would be the Gargano-Dubrovnik fault zone (Calais et al., 2002, Oldow et al. 2002, D'Agostino et al., 2008). The motion of Apulia microplate would be characterized by a rotation pole relative to ITRF2005 (longitude -132.659 ± 0.3, latitude 4.041° ± 16.8, rotation rate 0.340° / Ma ± 0.054) (D'Agostino et al., 2008). We have then expressed displacements field relative to stable Apulia, to illustrate the current displacements in both sides of the southern Adriatic Sea, south of the Gargano-Dubrovnik fault zone.

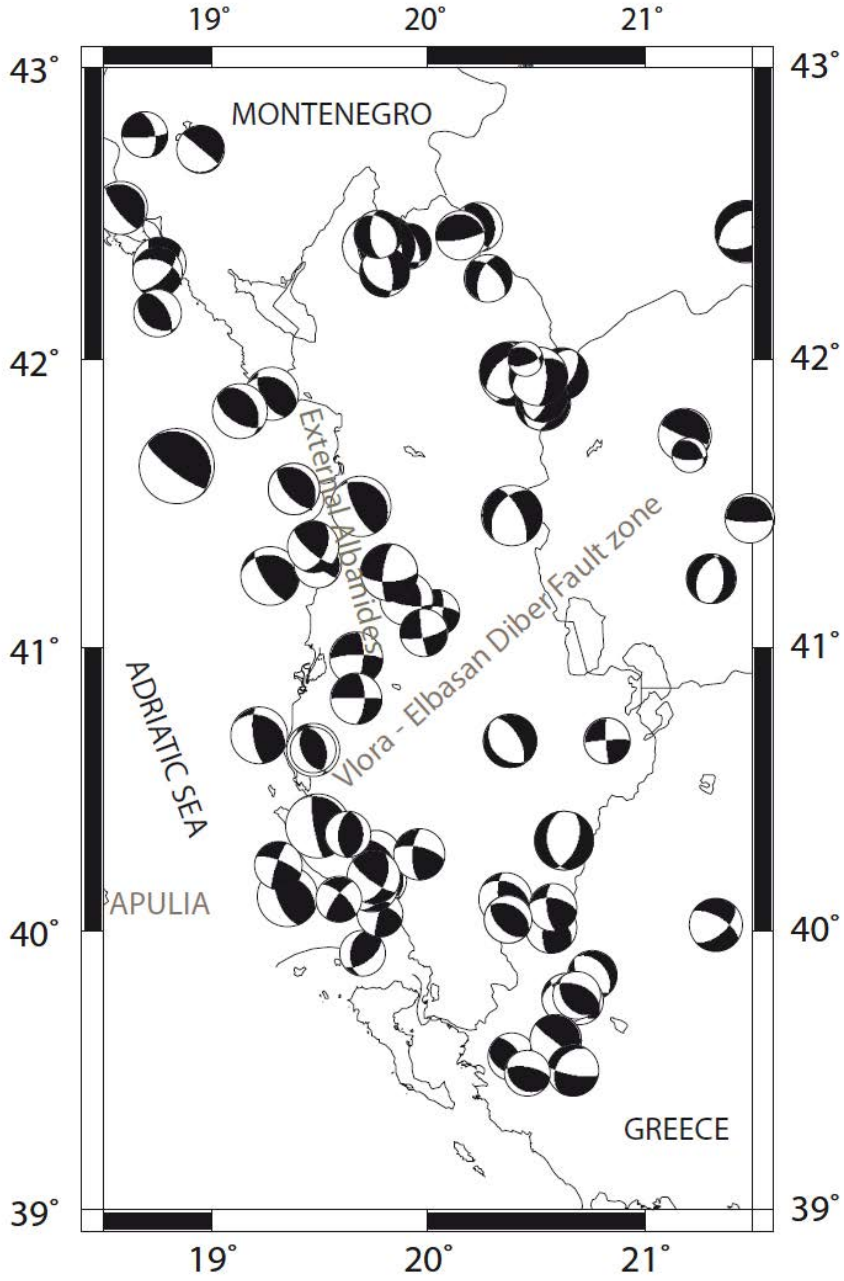

Figure 5.15. *CMT Focal mechanisms for Adriatic, Dinarides, Albanides and Helenides (http://www.bo.ingv.it/RCMT) with catalogs for Italia (1976 – present) Pondrelli et al., 2002; 2004; 2006 and 2007 and Europe (1997-present).*

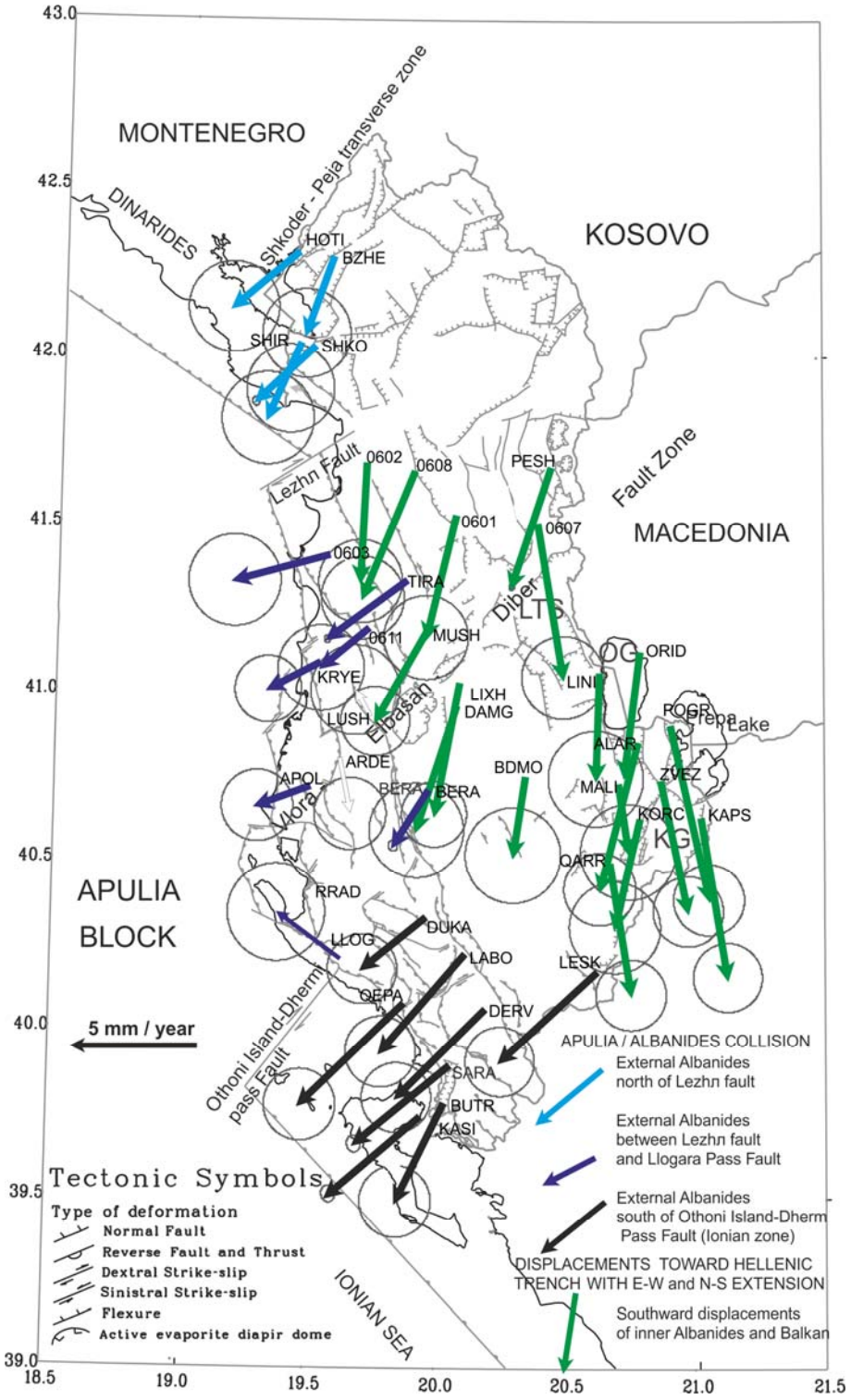

Figure 5.16. *Displacement rates expressed in the Apulia fixed reference frame, with interpretation of the main tendencies of the displacement rates field. The displacement rates field is the expression of the competition between ongoing compression between Apulia microplate and Balkan, southward motion toward Hellenic trench and perhaps E-W extension induced by the relief contrast between external and inner Albanides. OG: Orhid lake Graben; KG: Korca Graben.*

5.3.4. Results

5.3.4.1. Dinarides

The anticlockwise rotation of northern Adria microplate (Calais et al. 2002; Oldow et al. 2002, Nocquet et Calais, 2003; Babucci et al., 2004; Battaglia et al., 2004; Grenerczy et al., 2005; D'Agostino et al. 2005; Serpelloni et al. 2005, D 'Agostino et al., 2008); induced N-S shortening in the Friuli area with an evolution to a NW-SE shortening along the Dinarides coast north of Dubrovnik (Grenerczy et al.. 2005).

A major change occurs between the Dinarides and the northern Albanides (Figure 16): the Dubrovnik station is affected by a northward movement in the Eurasia reference frame whereas stations in external Albanides are affected by westward or southwestward displacements.

Dubrovnik station is affected by a displacement with a 1.25 mm/year eastward component and a 2.78 mm/year northward component by comparison with the Shkodra station. ln this hypothesis, this fault would be affected by a 3 mm/year dextral strike-slip displacement. If the relative displacement between these two permanent stations is accommodated along a single fault, the most probable structure is the Shkodra – Pesh (or Scutari-Pesh) fault that limits Dinarides and Albanides. This fault has been during Neogen a major limit between Dinarides affected by a moderated rotation and Albanides, north-western Greece and Eubean affected by two successive rotations: a fist one 40° clockwise between 15-13 Ma and 8 and a second one, 10° clockwise during the last 4 Ma years (van Hinsbergen et al.. 2005).

5.3.4.2. External Albanides.

External Albanides formed by Kruja, Ionian and Sazani zones have been affected by an important pre-Pliocene compression and also by a significant post-Pliocene shortening in the Periadriatic foredeep. External Albanides are structured by NNW-SSE to NW-SE thrusts, backthrusts and folds and by transverses faults with an orientation NE-SW to nearly E-W. Numerous focal mechanism solutions of shallow earthquakes demonstrate an ongoing horizontal compression (thrust faulting) dominating along the Adriatic collision. This tectonics is expressed by important magnitude historical earthquakes as shown by the repeated historic destructions of Durres (177 B.C, 334 or 345 A.C., 506, 1273, 1279, 1869, 1870, 1926 Ms 6.2), Apolonia (II-III BC, 217 AD), the 1920 Tepelena Ms 6.4 earthquake, the 1962 Ms 6.0 Fieri earthquake and the 1979 Montenegro earthquake (M 6.9) (Figure 5.13).

GPS results demonstrate the occurrence of south-westward motion of points located in External Albanides relative to Apulia (Figure 5.16). It is possible to distinguish a moderate deformation across the inland part of the periadriatic foredeep (2 mm/year at the latitude of Tirana between TIRA and KRYE) and an important shortening across Adriatic sea increasing from north to south Albania. This shortening is expressed by offshore active thrusts and back-thrusts and also by numerous focal mechanism (Figure 5.15) mainly located along the off-shore active thrusts.

From north to south, displacements rates of points located in the external Albanides present changes in directions and norms.

In northern Albanides, between the Shkoder-Pest fault zone and the Lezhë fault, displacements are perpendicular to fold axis, the observed rapid change between the western GPS point and the others points of this area suggests an ongoing shortening of 3 +/- 1.7 mm/year perpendicular to the fold axis with a direction compatible with focal mechanisms.

In both sides of the transfer Lezhë fault, plio-quaternary fold axis change from N 125° to N160° south of the fault. This rapid change is also shown by a rapid change in displacement rates direction from N205° north of the fault to 235° south of the fault, the orientation of motions measured by GPS followed the change of fold axis directions.

In central external Albanides, between the Lezhë fault and the Vlora Bay, displacements rates illustrate the occurrence of an ongoing shortening, partly offshore (2.3 +/- 1.3 mm/year) and partly onshore (1.7 +/- 1.3 mm/year).

Between central and southern Albanides a major change occur in displacement direction and also in norm of displacements, this major change occurred near the Vlora town affected by earthquakes in 1601, 1833, 1862, 1865 and 1866 in an area characterized by an intense seismicity with focal mechanisms showing the occurrence of both thrust and dextral strike-slip events if the direction parallel to the Llogara Pass Fault is preferred. GPS points suggest the existence of a 4.5 mm/year dextral strike-slip displacement rate along this major fault that allows the tectonic contact between the Apulian plateforme and Albanides.

In southern external Albanides, the ongoing deformation occurred off-shore (4.9 mm/year +/- 0.3 for the SARA permanent station in the Apulia fixed reference frame). Displacement rates do not allow identifying an E-W extension component that could be related to the quaternary graben system south of Saranda.

The North-East – South-West Vlora-Elbasani-Dibra transversal fault zone crosses all the Albanides (Roure et al., 2004). It is underlined from south-west to north-east by the Lushnja flexure, the Dumrea diapire, the depression of Elbasani marked by important quaternary infills (Melo. 1961) and the transversal structure of Labinoti. Furthermore this

structure continues in Macedonia (Dumurdzanov et al., 2005). Current tectonics along this structure is expressed by an alignment of important historical seismicity with 15 historical and instrumental earthquakes with Ms> 6.

This active faults zone is also underlined by the NEE-SW alignment of the clusters of the after-shocks consecutive to the 1 September 1959 and 30 November 1967 earthquakes respectively located at the south-western end at the north-eastern end of the fault zone (Louvari et al., 2001) .

The current tectonics of this fault zone is expressed by the extension measured in both sides of the Elbasani graben, whereas no relative displacements are recorded in both sides of the fault zone in its southwestern end (Figure 5.16). It is then highly probable that this fault is mainly active in the Elbasani area and in its eastern end as shown by the 1967 Diber earthquake (Sulstarova and Koçiaj, 1980). Relative displacements across the fault zone indicate that this fault is almost purely normal which is in good accordance with the Diber earthquake focal mechanism (Sulstarova and Koçiaj, 1980) and surface displacement. The continuation of the fault zone in Macedonia is also marked by a noticeable increase of southward displacements (Burchfiel et al. 2006). Therefore it is suggested that this fault is a major limit in the current deformation of Balkan. Nevertheless, this fault is not the northern boundary of the area affected by a southward displacement relative to Eurasia as underlined by the displacement of the Peshkopia permanent station in Albania and by stations in northern Macedonia. The northern boundary of this tectonics (Figure 5.13) is localized between Peshkopia and Sarajevo station that shows a northward displacement component. The previous discussion of the Dinarides-Albanides transition suggests that the Scutari-Pesh crustal fault is a good candidate for this northern boundary.

5.3.4.3. Inner Albanides

In the Apulia and Eurasia fixed reference frame, inner Albanides points present south-westward displacements reaching 2 mm / year north of the Elbasani-Diber fault (Peshkopia permanent station) and up to 4 mm/year for points located south of the fault zone. External – Inner Albanides boundary (Figure 5.16) appears to be the western boundary of the active tectonics, expressed by E-W extension and N-S extension in Bulgaria (Kotzev et al.. 2006), Macedonia (Burchfiel et al.. 2006), Albania and northern Greece and the Corinth Gul (Briole. et al., 2000; Goldsworthy et al.. 2002; Avallone et al., 2004; Bernard et al., 2006; Hollenstein et al., 2006; Carcaillet et al.. 2009).

In the Orhid – Korca graben system, current displacements (Figure 5.16) are indicating a moderate E-W extension across the Orhid graben that change to a N-S or multidirectional extension in the Korca graben. This highlights that the rapid change between early quaternary E-W extension and late quaternary N-S extension as described by Tagari et al. (1993) may also be explained by a current multidirectional extension identical to the present-day one. Historical seismicity (Figure 5.12) clearly indicates that this deformation is released during earthquakes with magnitudes exceeding 6.

5.3.5. Discussion

Current displacements of external Albanides are the expression of the ongoing collision between Apulia microplate and the deformed Balkan area. The increase of shortening rate across Adriatic between north-western Albania and southwestern Albania (SHKO 3.2 mm/year of southwestward motion, TIRA 3.9 mm/year, SARA 4.9 mm/year) could be the expression of an anticlockwise rotation of Apulia block and of a possible clockwise rotation of external Albanides and north-western Greece. Major changes occurred in the displacements field reflecting the occurrence of major transverse zones: the Shkoder-Pesh fault zone between Dinarides and Albanides, the Lezhë fault, the Llogara Pass Fault between the Ionian zone and the Sasani zone that may be the south-western part of the Vlora-Elbasan-Diber fault zone. A major change in velocity field occurs in both side of the Llogara Pass Fault along which a 4.5 mm/year dextral strike-slip may be estimated. This structure can be clearly identified as a major seismogenic source for Albania as also underlined by the repeated destruction of the Vlora town.

East of the area undergoing deformation linked with the ongoing collision, southwestward or southeastward displacements are probably induced by the roll back of the Hellenic subducted slab. The limit of respective influence of collision and southward displacements appears to be the western limit of the area including internal Albanides, Macedonia, Bulgaria and Greece, the Aegean extensional region, affected by southward displacements and N-S extension relative to stable Eurasia (Figure 5.13).

Collision and slab roll back seem to not be able to explain alone the recorded displacement rates field, they cannot, by example, explain the E-W extension in both sides of the Korca graben shown by the divergence of displacement rates vectors. This E-W extension may be related to gravitational potential energy contrasts between the lowlying Adriatic Sea and the elevated mountainous areas inland as proposed by Copley et al, (2009). But in any case, this last source of deformation is not the main one, as underlined by the small E-W

component between vectors in both sides of the active grabens of inner Albanides (maximum 2 mm/year).

5.3.6. Conclusions

This study has allowed to characterize a complex current tectonics pattern in Albania: (1) western Albania is affected by westward motions relative to Eurasia and Apulia microplate, the main part of this deformation is probably absorbed off shore along N-S to NNW-SSE active thrusts, our results illustrated the importance of transverse faults (Lezhë Fault and Llogara Pass Fault) restricted to external Albanides in the current deformation (2) two major NE-SW transverse active faults affected the collision belt, the Skutar-Pesh fault between Dinarides and Albanides and the Diber-Elabasani-Vlora fault zone mainly affected by an extensional displacement; (3) external/inner Albanides boundary and the Scutari-Pesh fault form respectively the western and the northern limit of the domain inner Albania. Northern Greece, Macedonia. Bulgaria) affected by southward displacements relative to stable Eurasia; (4) local multidirectional extension affected the Korca and the Orid active grabens at the boundary between Albania-Macedonia and Greece as also suggested by neotectonics investigations.

5.4 Macedonia

In this section is presented result of 5 GPS stations measurement in three epochs (1996, 2000, and 2008). The size of the vectors ar listed in Table 5.10 and plotted on Figure 5.17 with combination of results in southwest Bulgaria, Northern Greece and Albania. The blue vectors indicate the displacements obtained from permanent GPS stations. The vectors are showing small displacemant in the teritory of Macedonia. It is seen a small increasment from nort to south directions (2.1 mm/yr ÷ 4.3 mm/yr)

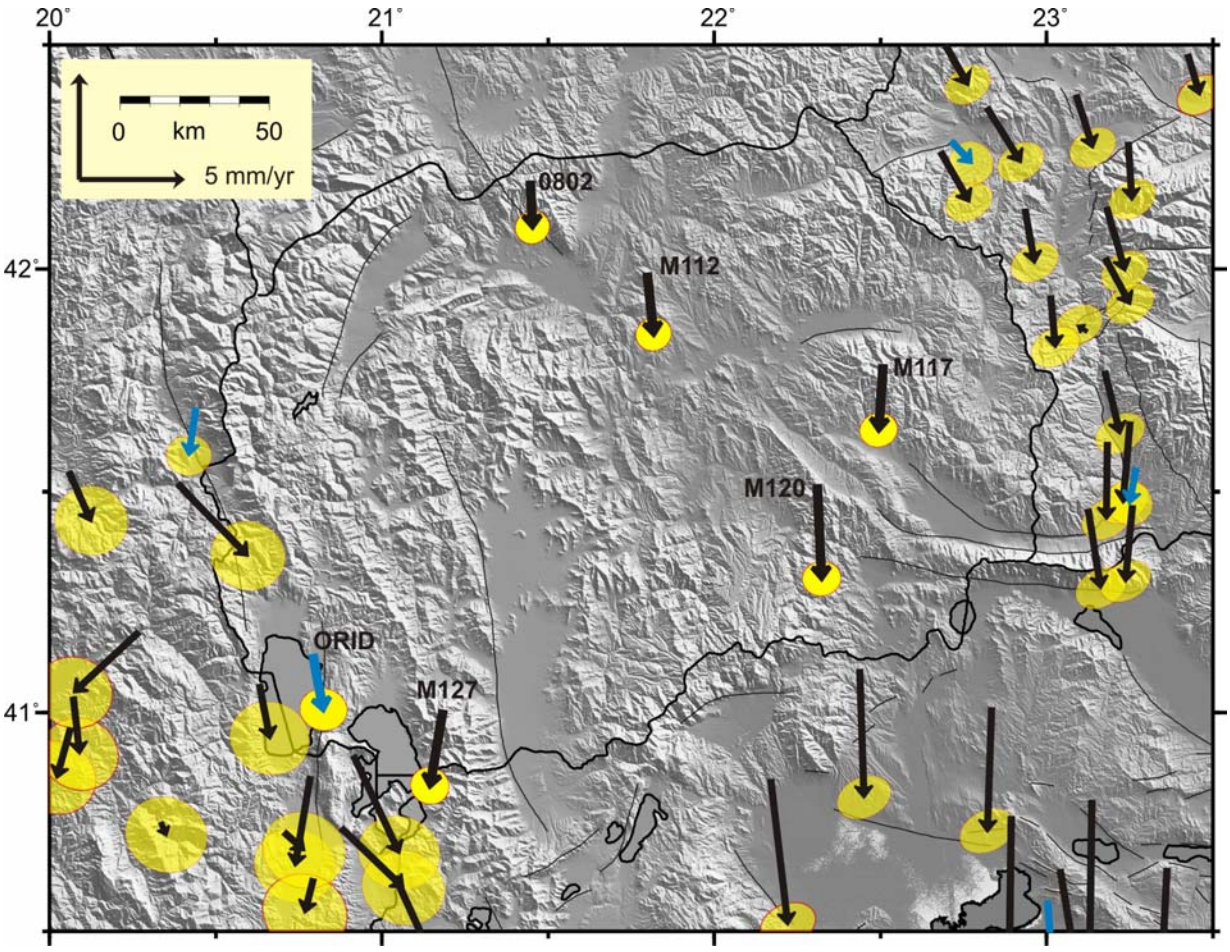

Figure 5.17. *GPS velocities referred to Eurasia with their 3σ error ellipses for Republic of Macedonia region. The blue arrows present results of permanet stations.*

N°	Site Name	Lon.	Lat.	V_N	V_E	$\|V_{hor}\|$	S_{V_N}	S_{V_E}	$S_{\|V_{hor}\|}$	ρ_{EN}
1.	0802	21.4464	42.1922	-2.1	0.1	2.1	0.3	0.3	0.05	0.0
2.	M112	21.7982	41.9862	-2.8	0.3	2.8	0.3	0.3	0.05	0.1
3.	M117	22.5069	41.7806	-3.0	-0.2	3.0	0.4	0.3	0.05	0.1
4.	M120	22.3102	41.5096	-4.3	0.2	4.3	0.4	0.3	0.05	0.0
5.	M127	21.1823	41.0015	-3.5	0.6	3.6	0.4	0.4	0.05	-0.1

Table. 5.10. *GPS velocities and their mean square errors with respect to Eurasian plate for Republic of Macedonia. Lon.: longitude [°], Lat.: latitude [°],* V_N , V_E *: north/east component of velocity [mm/yr],* $|V_{hor}|$ *: magnitude of horizontal component [mm/yr],* S_{V_N} , S_{VE} , $S_{|V_{hor}|}$ *: 1 sigma uncertainties of corresponding velocity component [mm/yr],* ρ_{EN} *: correlation coefficient between the eats and north uncertainties.*

Chapter VI

Comparison, discussion and overall conclusion

In this Chapter we discuss the GPS results from 230 GPS stations of campaign mode and the continuous observations on the territory of Central and East Mediterranean. Analysis and interpretation of the obtained results are considered in the context of contemporary

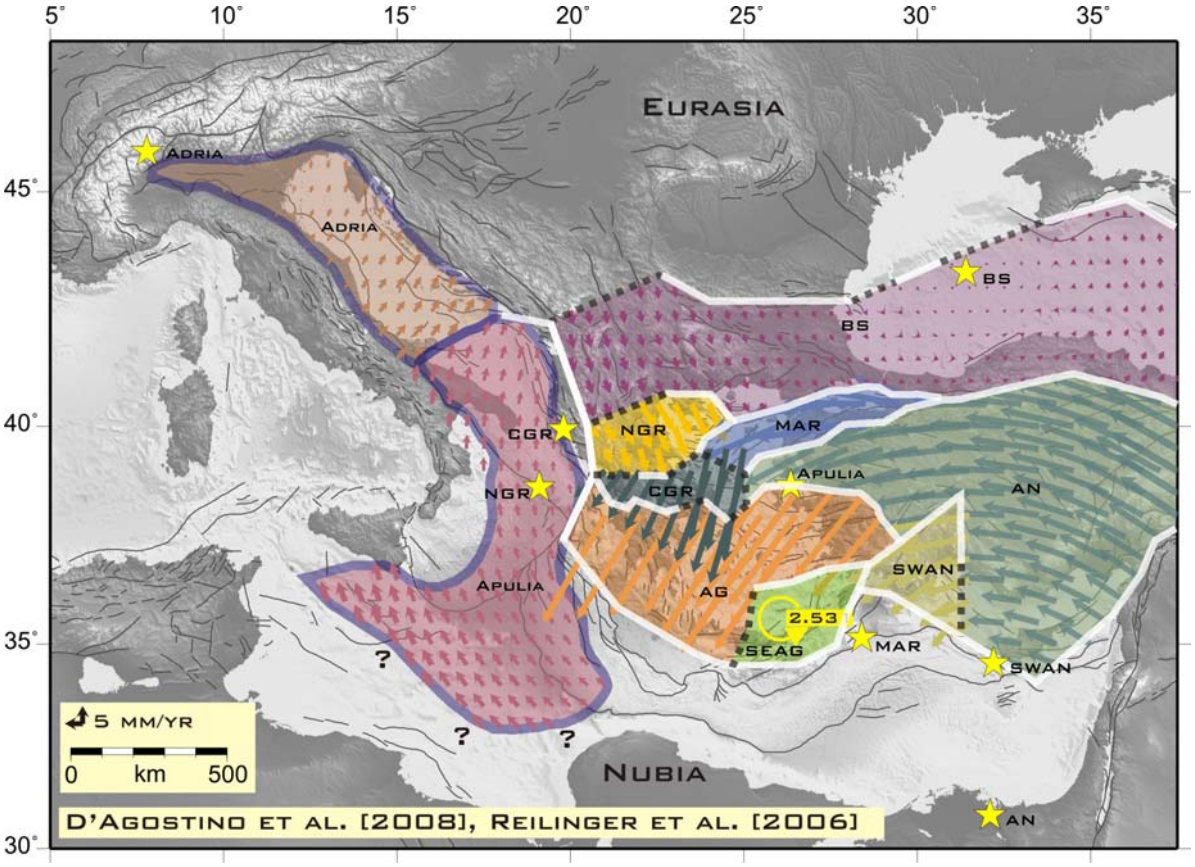

Figure 6.1. *Schematic illustration of present-day East and Central Mediterranean tectonics. White lines show well-defined boundaries that follow known, active faults. Black dotted lines show less well defined boundaries.* ***AG****: Aegean;* ***AN****: Anatolian;* ***BS****: Black Sea;* ***SEAG****: southeast Aegean;* ***SWAN****: southwest Anatolian;* ***CGR****: central Greece,* ***NGR****: northern Greece;* ***MAR****: Marmara (Reilinger et al., 2006). The Apulia and Adria microplates are proposed by D'Agostino et al., (2008). The yellow stars are the Eulerian poles of proposed blocks by Reilinger et al., (2006) and D'Agostino et al., (2008) relative to Eurasian plate.*

tectonic models proposed by different authors in the past few decades. Comparisons with previous studies have been done in next sections. Figure 6.1 is presents a schematic illustration of present-day East and Central Mediterranean tectonics. The block structures on Figure 6.1 are proposed and discussed by Reilinger et al. (2006) and D'Agostino et al. (2008).

6.1. Discussion results with previous studies

6.1.1. Adriatic region

Figure 6.2 (a-f) summarizes the kinematic patterns of deformation proposed in each of the six major studies that have notably advanced understanding of Adria tectonics during the last 30 years. Based on geological, seismological, and geodetic studies, many hypotheses have been developed about the past and current tectonic features of Adria and its surroundings.

Several models have been successively proposed:

Argand (1924) suggested that Adria moved into Europe as a promontory of the African continent, and the collision formed the Alpine mountain chain (Figure 6.2a). McKenzei (1972) first proposed the existence of an Adriatic microplate that moves independently of both Africa (Nubia) and Eurasia in the Mediterranean.

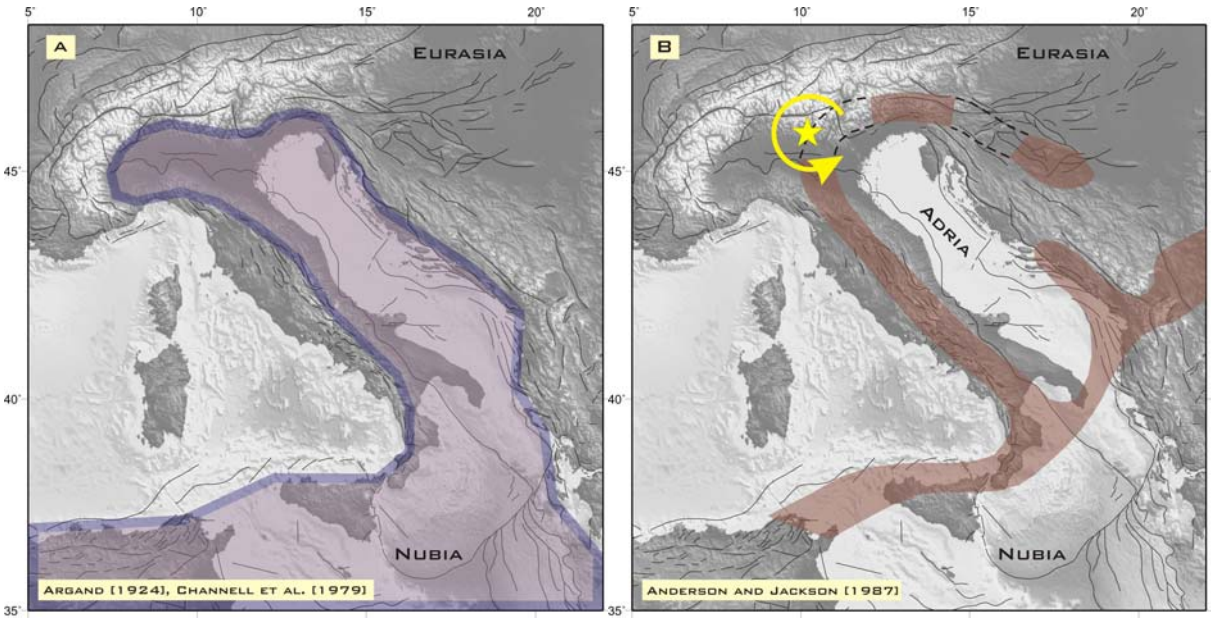

Figure 6.2. *Schematic illustration of kinematic models of Adria tectonics (a–f) proposed in previous studies,* ***(a):*** *Argand (1924),* *Channell et al., (1979),* ***(b):*** *Anderson and Jackson (1987),* ***(c):*** *Calais et al., (2002),* ***(d):*** *Oldow et al. (2002),* ***(e):*** *Battaglia et al. (2004),* ***(f):*** *Serpelloni et al., (2005).*

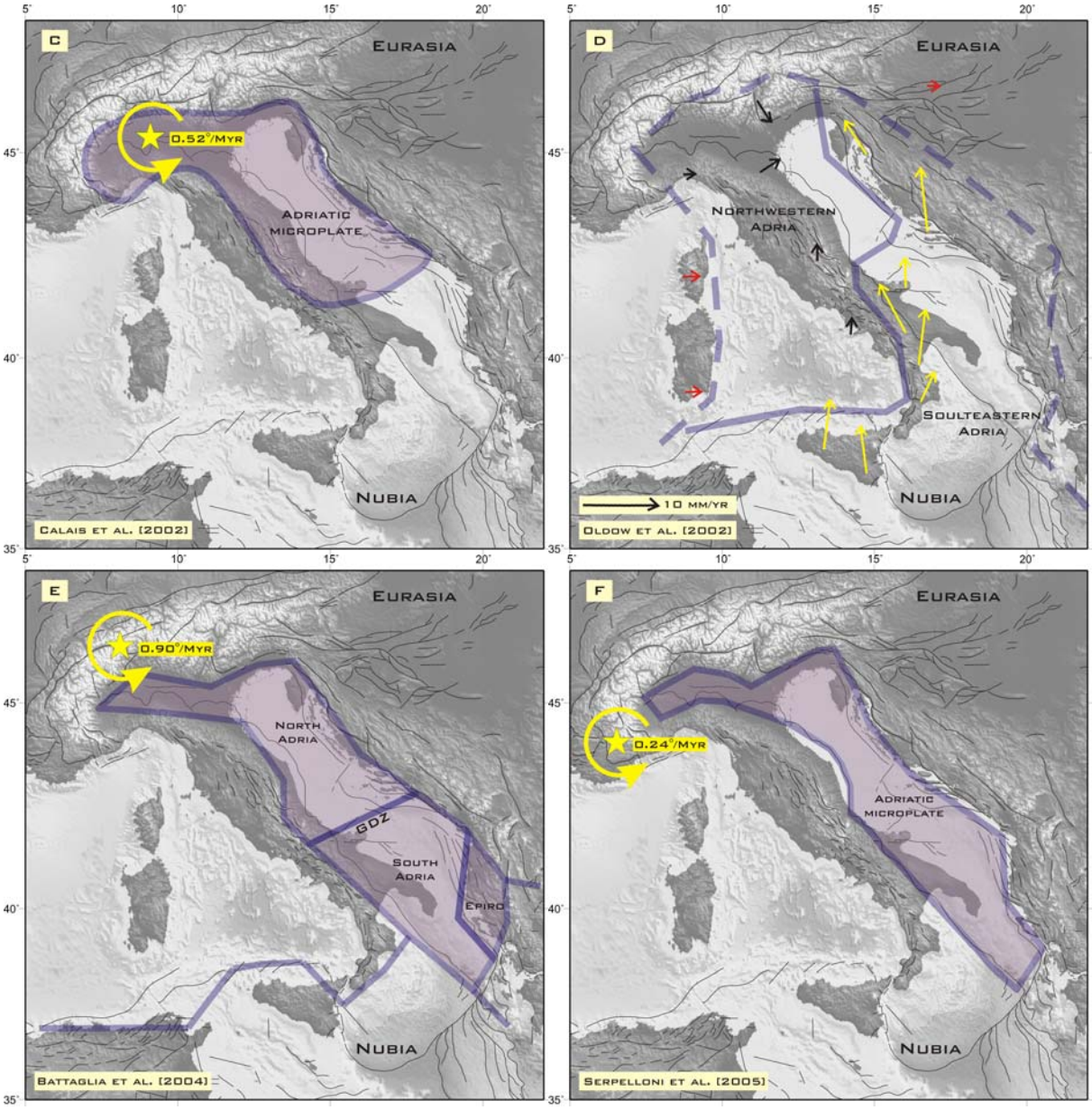

Figure 6.2. *(continued)*

Anderson and Jackson (1987) analysis of earthquake slip-vectors determined for the large (mb>5.5) earthquakes that rimmed the deforming edges of the aseismic Adriatic core showed consistent NE–SW extension in the Apennines, N–S shortening in northern Italy, and NE–SW shortening in Croatia and Albania, suggesting the presence of a microplate rotating counter-clockwise with respect to stable Europe around a pole located at 45.8°N/10.2°E (Figure 6.2b). Jackson and McKenzie (1988) suggested that Adria is not a promontory of the Africa plate now, but may have been in the past. Westaway (1990) used tectonic information and earthquake focal mechanisms to infer a rotation of the Adriatic microplate at 0.3°/Ma around a pole at 44.5°N/9.5°E and assumed that Adria is an independent rigid block and that a SW-NE oriented decoupled zone existed between the Africa plate and Adria, linking the area from the northern Gargano zone to the central Dinarides. Whereas Favali et al. (1993)

identified the fact that seismicity crosses the central Adriatic from the Gargano zone to the central Dinarides as evidence for a tectonic boundary separating Adria into north and south blocks. Geomagnetic data averaged over several Myr and Sn shear wave propagation observations (Mantovani et al., 1990, Channell, 1996; Mele, 2001) suggest that Nubia extends as a promontory into the Adriatic region. Kuk et al. (2000) and Markusic et al. (1998) proposed that Adria is divided into three seismic zones (northern, central, and southern), giving as a physical reason for the zonation the differential movement of the zones due to resistance of the Dinarides to the pressure force of the Africa plate and the existence of the active faults along the Adriatic margin.

Previous geodetic investigations of crustal motion in the central Mediterranean have shown significant deviations from the direction of relative motion between the Eurasia and Nubia plate (Ward, 1994, Calais et al., 2002, Oldow et al., 2002, Caporali et al., 2003, Battaglia et al., 2004, Nocquet and Calais, 2003, D'Agostino and Selvaggi, 2004, D'Agostino et al., 2005, Grenerczy et al., 2005, Serpelloni et al., 2005, 2007, Devoti et al., 2008).

Ward (1994), using VLBI data at MATE and MEDI, published the first space geodetic study of the Adria microplate and proposed a rotation pole located at 46.8°N/6.3°E and an angular rate of 0.30±0.06°/Ma. Calais et al. (2002) simultaneously inverted GPS velocities from only two continuous GPS sites in the Po Plain (Figure 6.2c), UPAD and TORI, together with Anderson and Jackson's (1987) slip vector data set, deriving an Adria–Eurasia angular velocity vector similar in position to Anderson and Jackson's (1987) pole of rotation. They find a rotation pole at 45.36°N/9.10°E and an angular rate of 0.52°/Ma (Figure 6.2c); Calais et al. (2002) used this constraint, together with the inferred curved western Adria–Eurasia boundary, to explain the unexpected dextral shear and extension that they observed geodetically in the western Alps, where clearly collision and thrusting seem to have ceased. We use the proposed kinematic model and the rotation pole by Calais et al (2002) to compare our velocities with the predicted model velocities (Figure 6.3a). 37 points which cover block model have been used to calculate misfits of between our results and the models velocities. The range of obtained misfits is 0.04÷4.41 mm/yr. It is seen from the Figure 6.3a that the value of misfits increase from SW to NS, where the stations with the biggest are UNPG, DUBR, MOCO, VAGA, and BSSO. Based on GPS site velocities and seismicity Oldow et al. (2002), propose that Adria is divided by the Gargano-Dubrovnik fault into two blocks. North-western and South-eastern tectonic blocks separated by a boundary extending around the southern Tyrrhenian Sea, across central Italy, and along the coast of the eastern Adriatic. Oldow et al. (2002) suggested that sites in northwestern Adria exhibit little or no motion relative to the Eurasian plate, whereas those in southeastern Adria are moving together with

the Africa plate and exhibit a spatially heterogeneous velocity field, with northward velocities of ~10 mm/yr. Battaglia et al. (2004) using a block model, brought support to the idea that the Adriatic block is part of neither the Eurasian plate nor the Africa plate, giving the Apulia escarpment as a possible location of the southern Adriatic–African boundary. Their results show that independent microplate models of Adria offer a better fit to GPS velocities than models considering Adria as continuous with the Nubia or Eurasian plate. Battaglia et al. (2004) proposed following rotation pole relative to Eurasia 46.3°N/8.1°E and an angular rate of 0.90°/Ma for North Adria and 46.0N°/-2.0°E and an angular rate of 0.20°/Ma for South Adria. We use these rotation poles to plot model vectors and compare them with our observed velocities (Figure 6.3b). Misfits are between 1.31÷8.57 mm/yr for North Adria and 2.14÷3.39 for South Adria. Proposed rotation poles by Battaglia et al. (2004) do not fit well our results in Adria microplate.

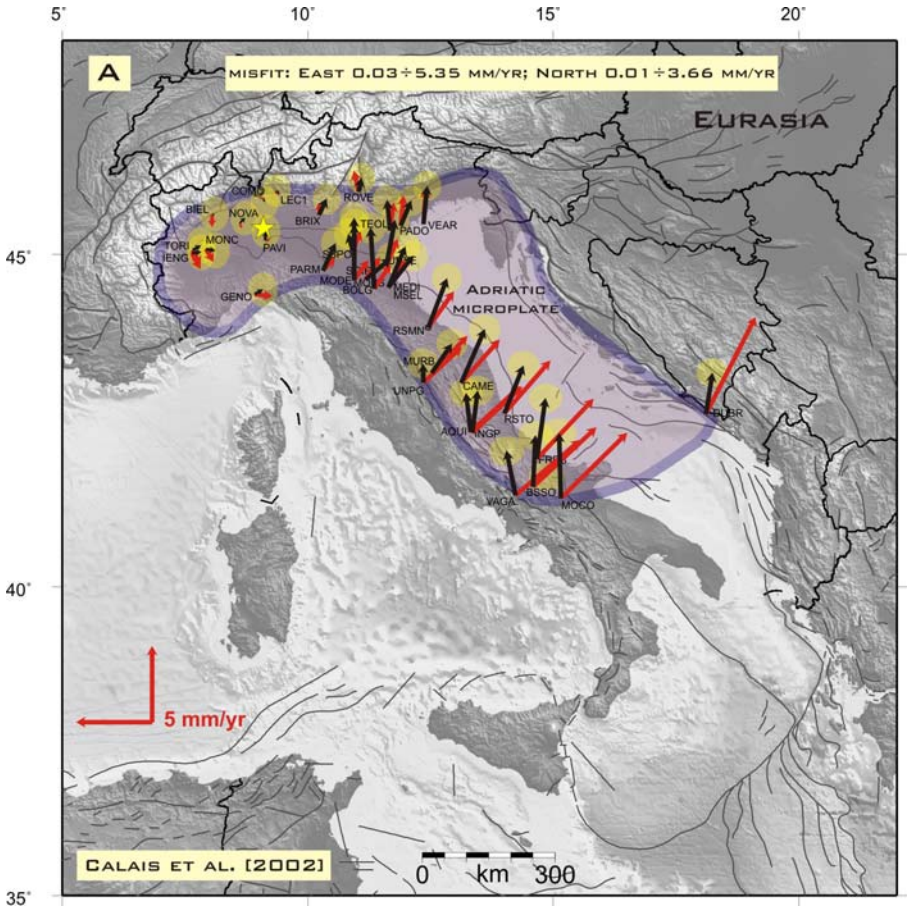

Figure 6.3. *Kinematics of the Adriatic microplate (a-f). Red arrows show the velocities predicted by six different models with respect to Eurasia. Black arrows show observed velocities from continuous GPS stations.*

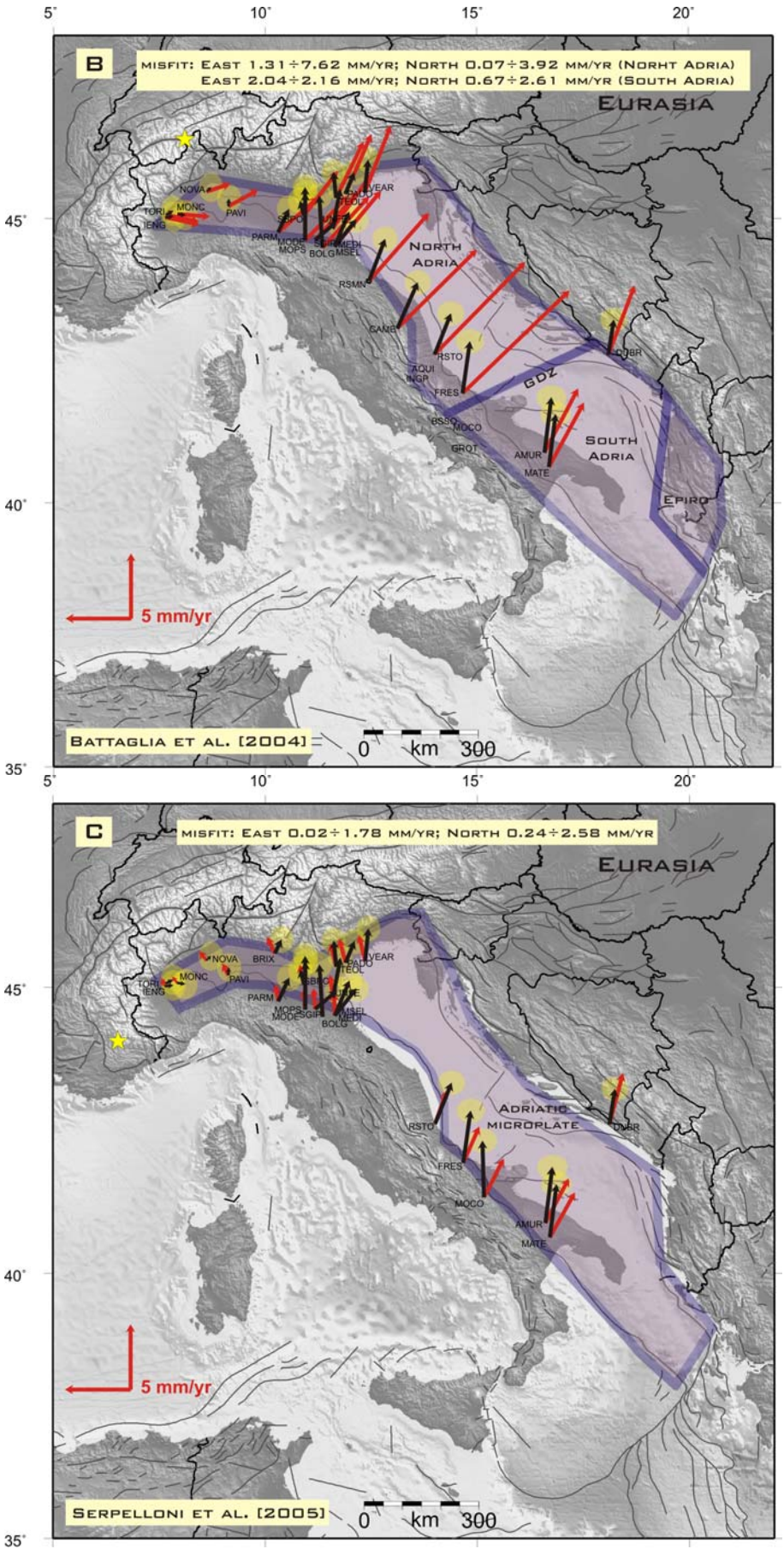

Figure 6.3. (continued)

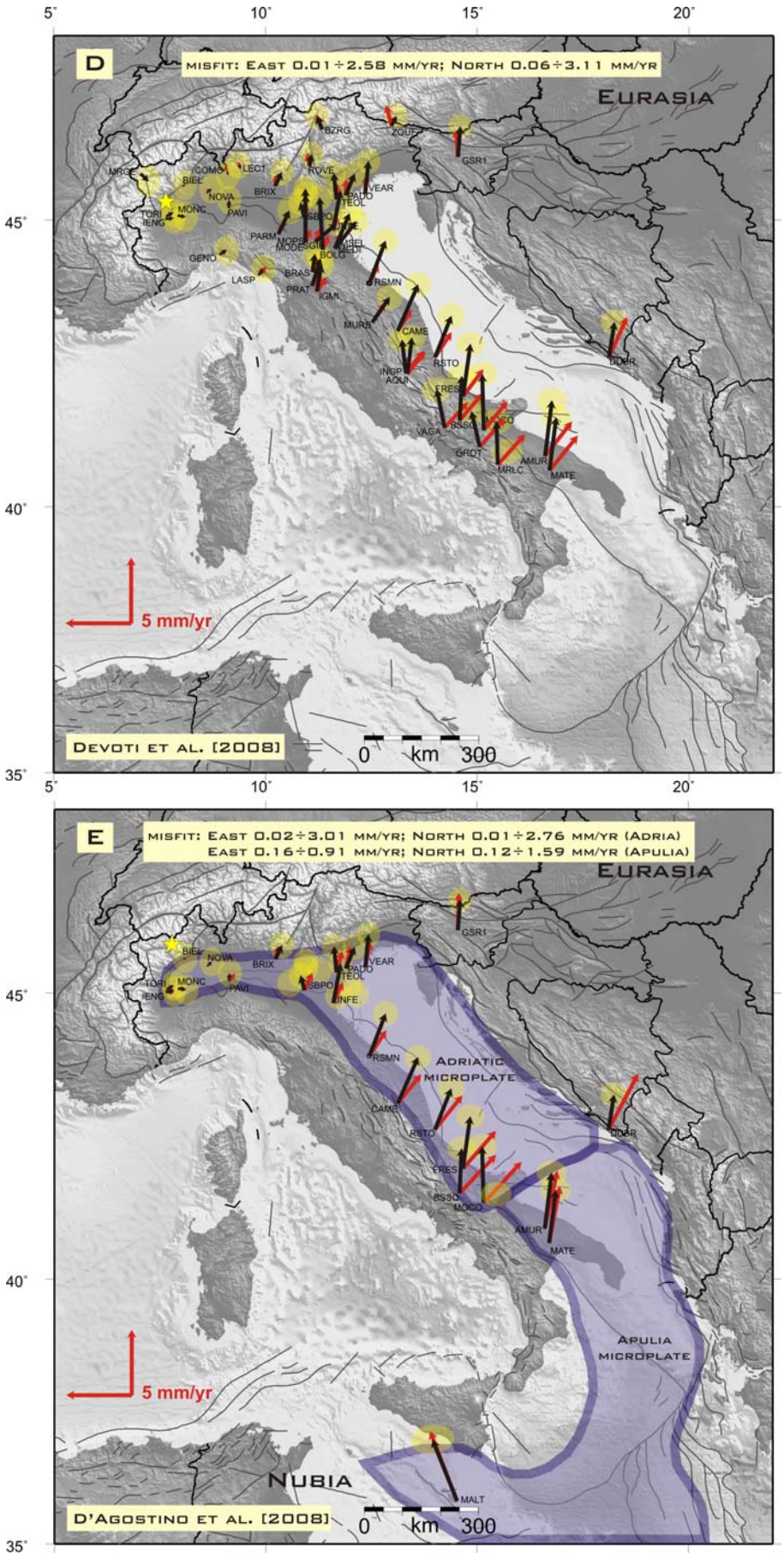

Figure 6.3. (continued)

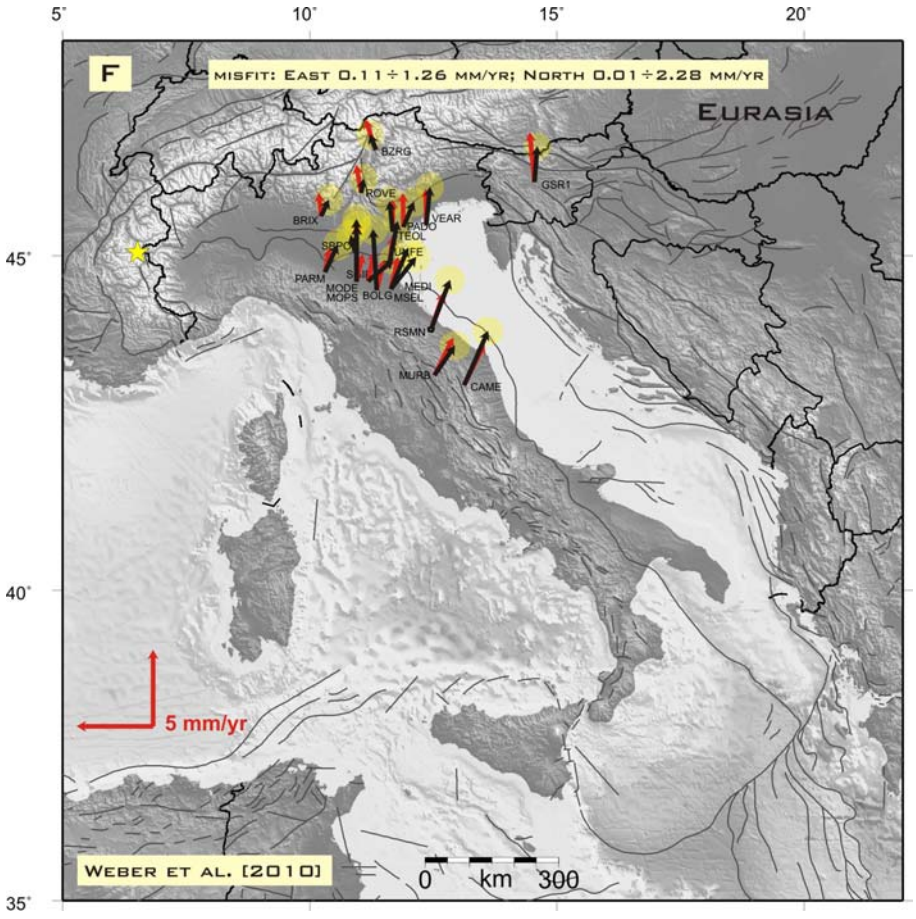

Figure 6.3. (continued)

Mantovani et al. (2005) suggested that the Gargano structural high and the adjacent off-shore area are an active tectonic zone including faults with limited seaward extension, but there is no clear evidence in favour of central Adriatic decoupling zones. Weber et al. (2005) inverted GPS velocities from sites on the Istria Peninsula for an Adria-Eurasia Euler pole and obtained a slow counter-clockwise rotation and a pole position very close to that of Anderson and Jackson (1987), consistent with the rigid microplate model. Altiner et al (2006) suggest that Adria exists as an independent microplate. North-eastern Adria moves very slowly and produces almost no surface deformation (Oldow et al., 2002). The direction of movement of stations as well as the results of principal strain rate estimates suggests that Adria is divided into northern, central, and southern deformation zones. Serpelloni et al., 2005 present velocities solution for Italy and surrounding area, obtained from an analysis of continuous and survey-mode GPS observations collected between 1991 and 2002. The kinematics observed in the Adriatic domain are mainly governed by the counter-clockwise rotation of the Adriatic microplate, with respect to Eurasia, around a pole in the western Apls located on 44.07°N/6.53°E and an angular rate of 0.244°/Ma. Space geodetic results by Serpelloni et al.,

2005 support the hypothesis that Adriatic microplate is moving independently from African plate. On Figure 6.3c we compare our results of 24 stations that are located on the proposed Adria block. The comparison shows good agreement with proposed predicted vectors. The misfits are between 0.24÷3.13 mm/yr. Devoti et al., 2008 presented recent robust kinematics analyses using data from a large number of GPS sites. The authors estimated Euler pole of the Adriatic microplate located on 45.29°N/7.65°E and an angular rate of 0.216°/Ma. Comparing our results with the predicted model vectors (Figure 6.3d) it is seen we have good agreement from the region of Alps to central Italy. The misfits are between 0.06÷4.04 which are increasing from NW to SE direction. From central Italy in direction to south it is not visible good coincidence. D'Agostino et al., 2008 investigate the kinematics of the Adriatic region integrated continuous and episodic GPS measurements with earthquake slip vectors. They compared the predictions of the GPS-inferred angular velocities with the earthquake slip vectors, showing that the seismically expressed deformation at the microplate boundaries is consistent with the observed geodetic motion. The remarkable consistency between geodetic, seismological, and geological evidence of active tectonics suggests that active deformation in the central Adriatic is controlled by the relative motion between the Adria and Apulia microplates (Figure 6.1). The angular rotation rates of the microplates are compared with the rotation rates calculated with a simple block model supporting the hypotheses that Apulia forms a single microplate with the Ionian Sea and possibly with the Hyblean region and that Adria and Apulia rotate in such a way as to accommodate the Eurasia-Nubia relative motion. D'Agostino et al., 2008 suggest that the present-day microplate configuration follows a recent fragmentation of the Adriatic promontory that during the Neogene rigidly transferred the Africa motion to the orogenic belts that now surround the Adriatic region. Using two relative rotarion pole respect to Eurasian plate located on 45.79°N/7.78°E and an angular rate of 0.309°/Ma for Adria and 38.642°N/26.350°E and an angular rate of -0.299°/Ma for Apulia, we plotted predicted vectors for these two defined microplates on Figure 6.3e. Comparing our results with proposed models we have a good agreement especially the three stations located on proposed Apulian block. Misfits are between 0.02÷4.08 mm/yr for Adria microplate and 0.20÷1.83 mm/yr for Apulian microplate. Weber et al., 2010 treat only the northern segment of Adriatic lithosphere north of the Gargano–Dubrovnik zone and proposed best-fitting GPS Adria–Eurasia angular velocity vector comes from 7 Istria Peninsula (Slovenia, Croatia) and 10 Po Plain (Italy) sites, it locates at 45.03°N, 6.52°E, with a 0.297±0.116°/Myr counter-clockwise rotation rate. Figure 6.3f shows a good agreement between 19 station that are located on north of the Gargano-Dubrovnik zone and predicted model vectors. The misfits between are in the range of 0.11 and 2.60 mm/yr.

The consideration of the previous studies in this section and comparison of our estimated velocity field with proposed kinematics models of Adriatic region the results generally show good agreement with the kinematics models. Our results support the hypothesis of existence of independent Adria microplate. This microplate is limited to the south by a region of diffuse deformation in the central Adriatic which separates the Adria microplate from a newly defined microplate including the Apulian promontory, the Ionian Sea and, possibly, the Hyblean region in southern Sicily (D'Agostino et al., 2008). We estimated our own rotation pole using 12 GPS station located on Po Plain which parameters are 45.51°N, 7.82°E, and 0.336±0.052°/Myr. Detail output file for estimating rotation pole is given in Table 6.1. Our proposed pole is very close to the rotation pole proposed by D'Agostino et al., 2008. For Apulia microplate we have only 2 GPS stations which are not enough to calculate good parameters of rotation pole. The comparison with the six kinematics models shown on Figure 6.3 it is visible that sets of station in central Adriatic have a large misfits comparing with others

Table 6.1. *Determined parameters of rotation pole for Adria microplate expressed in Eurasia-fixed reference frame.*

Rotation pole:					Lat (°)	Long (°)		Angle (°/Ma)			
					45.51	7.82		0.336			
Name	Ve	Vn	σ(Vn)	σ(Vn)	corre	dVe	dVn	dV	dVaz	lon	lat
BIEL	0.16	0.09	0.37	0.46	0.0021	0.07	-0.01	0.07	98.732	8.048	45.561
BRIX	0.50	1.07	0.37	0.42	0.0087	0.39	-0.03	0.39	93.826	10.233	45.565
IENG	0.63	0.07	0.38	0.47	0.0067	0.18	0.15	0.24	49.487	7.639	45.015
LEC1	-0.13	0.28	0.37	0.43	-0.0077	-0.04	-0.45	0.45	184.650	9.407	45.857
MONC	0.61	-0.09	0.38	0.47	-0.0006	0.20	-0.14	0.24	124.812	7.927	45.074
NOVA	0.34	0.34	0.37	0.45	0.0032	0.17	-0.03	0.17	98.682	8.614	45.447
PADO	0.68	1.64	0.37	0.39	-0.0065	0.45	-0.22	0.50	116.318	11.896	45.411
PAVI	0.04	0.60	0.37	0.44	0.0000	-0.29	0.00	0.29	270.185	9.136	45.203
SBPO	-0.31	1.13	0.37	0.41	-0.0035	-0.76	-0.28	0.81	249.464	10.920	45.051
TEOL	-0.20	1.99	0.37	0.40	-0.0074	-0.48	0.23	0.53	295.669	11.677	45.343
TORI	0.53	0.30	0.38	0.47	0.0060	0.11	0.37	0.39	16.954	7.661	45.063
VEAR	0.25	2.50	0.37	0.39	0.0098	0.01	0.43	0.43	1.758	12.358	45.438
								∑= 0.38			

6.1.2. Aegean region

Recent studies of the kinematics of the region, particularly those using the GPS to measure crustal velocities, have interpreted the tectonics in terms of the relative motions of rigid microplates or blocks (e.g., McClusky et al., 2000; Nyst and Thatcher, 2004 ; Reilinger et al., 2006; Floyd et al., 2010, Figure 6.1 and Figure 6.4). Geodetic determinations of

velocities in the Aegean region have been interpreted in terms of between two (Le Pichon et al., 1995) and six (Reilinger et al., 2006) blocks. Figure 6.4 summarizes previous block models.

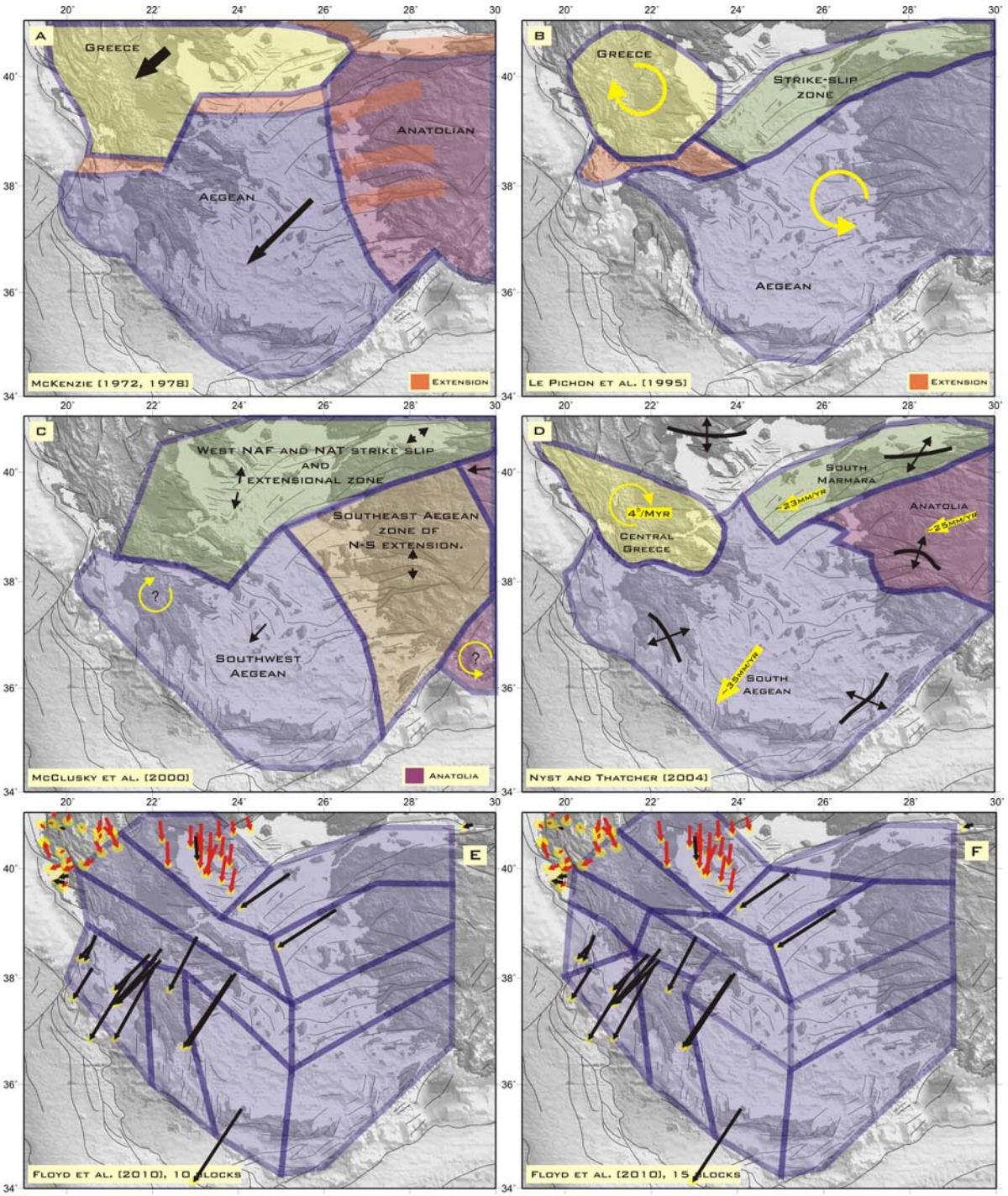

Figure 6.4. *Kinematic models of Aegean tectonics (a–f) proposed in previous studies. Vectors show velocity field in Aegean from this study (e, f). Black vectors present velocities of permanent stations. Blue vectors present velocities of campaigns stations.*

McKenzie (1972, 1978) was the first to use plate tectonic principles, seismicity, fault plane solutions and active fault distributions to define the Aegean's major tectonic elements and suggest a plate-like model for the kinematics. This model is shown on Figure 6.4a has three rigid elements and also includes several zones of intraplate deformation in western Anatolia. This model is close to the model proposed by Nyst and Thacher (2004). McKenzie and Jackson (1983, 1986) were the first to suggest that clockwise rotation of crustal blocks in central Greece was required to explain the absence of strike-slip faulting and predominance of normal faulting observed there. They reasoned that the N-S orientation of earthquake slip vectors in central Greece could be reconciled with expected SSW motion relative to Eurasia if the normal faults and intervening blocks of crust in central Greece were rotating clockwise with respect to Eurasia. Results of Nyst and Thacher (2004) define only one largely undeformed microplate in central Greece where McKenzie and Jackson (1983, 1986) predict several rotating slats, but one expected effect of their predicted block rotation is nicely confirmed by the GPS data itself. Taymaz et al. (1991) noted the preponderance of strike-slip faulting in the northern Aegean and extension in central Greece and proposed a quantitative, nine microplate, ''broken slats'' model to account for these features. Le Pichon et al. (1995) presciently used early GPS measurements to quantify clockwise rotation of central Greece and westward increasing extension across the Gulf of Corinth. Although primarily focused on motions in central Greece, they suggested a two-block model of Aegean deformation with clockwise rotation of central Greece, counter-clockwise rotation of the South Aegean and Anatolia, extension across the Gulf of Corinth, and a wide zone of distributed strike-slip deformation in the northern Aegean (Figure 6.4b). Their central Greece/Eurasia Euler vector (41°N, 18°E, 2.8°/Myr) is similar to ours (39.8°N, 20.0°E, 4.3°/Myr). Armijo et al. (1996) proposed a model emphasizing the necessary extensional end effects of right-lateral strike-slip fault termination in the NW Aegean and central Greece. They suggested that present day extension is localized in the northern Aegean and central Greece near the ends and at offsets across the northern and southern branches of the North Anatolian fault. They proposed that lower rates of extension occur across several discrete arcuate zones in the central Aegean and SW Anatolia. McClusky et al. (2000) carried out a careful analysis and synthesis of a large set of high quality GPS data from western Greece to the South Aegean and western Turkey and used their results to define rigid blocks in central Anatolia and the southern Aegean (Figure 6.4c). In particular, they were the first to identify the South Aegean microplate and quantify its motion from the eastern Aegean to the SW Peloponnese. McClusky et al.'s (2000) network contains few sites in mainland Greece and they did not consider its motion relative to the rest of the Aegean. They suggested that much of the Aegean region is deforming by distributed

extension that is widespread in Greece and within their study area in the northern Aegean Sea and western Anatolia. Goldsworthy et al. (2002) use tectonic geomorphology integrated with seismic, geologic and GPS data to support a model for central and northern Greece that includes three clockwise-rotating blocks with localized extension between them. They further observe that extension in the Gulf of Corinth decreases to the east, while extension in the Gulf of Evia and grabens in Thessaly and Greek Macedonia decreases to the west. Block rigidity then requires Corinth opening be balanced by the summed extension across Evia, Locris and Thessaly. Goldsworthy et al. (2002) caution that their model is semi-quantitative and should not be viewed too literally. Although GPS nets in northern Greece are sparse the available data do not support this three-block model. Bulgaria, Thrace and Greek Macedonia are moving south at 5–10 mm/yr with no evidence for the comparable strike-slip motion on the Kavali-Xanthi fault system (the northernmost block boundary) the model requires. They define a block boundary across central Evia that extends west into central Greece, while Nyst and Thacher (2004) provide no evidence for relative motion across this zone. The Gulf of Corinth is a major block boundary in both models. The Goldsworthy et al. model specifies three rotating blocks in central and northern Greece. Nyst and Thacher (2004) have used the GPS velocity field from 374 stations to identify deforming regions, rigid elements, and potential microplate boundaries. They have proposed a quantitative four-microplate model (Central Greece, South Aegean, Anatolia, and South Marmara) to explain first-order features of present day deformation of the entire Aegean region (Figure 6.4d). Their analysis also suggests the existence of isolated zones of deformation within the nominally rigid microplates and an indication of low rate internal straining within the Anatolia microplate. Comparable deformation may occur in zones lying outside current GPS networks, particularly in the NW Peloponnese and adjacent Ionian Sea and near the west coast of Anatolia. It is also possible that the apparently isolated zones are the boundaries of even smaller microplates. Reilinger et al., (2006) have developed an elastic block model to constrain present-day plate motions (relative Euler vectors), regional deformation within the interpolate zone, and slip rates for major faults. As part of a wider study of the entire collision zone between Africa, Arabia, and Eurasia, they divided the Aegean region into six blocks (Aegean, Anatolian, Southeast Aegean, Central Greece, Northern Greece, and Marmara), basing the choice of block boundaries on the observed major faults of the region (Figure 6.1).

The most recent study is presented by Floyd et al., (2010), using a new set of geodetic velocities for Greece and the Aegean derived from 254 survey-mode and continuous GPS sites to test models for the deformation based on the relative motion of between 4 and 15 rigid blocks (Figure 6.6e,f), and upon a smoothly varying field of strain rate. To investigate the

influence of using a finer scale of block, they adopt the suggestion of Taymaz et al. (1991) that the northern and central Aegean may be treated as a set of parallel slats that are aligned with the major fault systems of the region. The authors found out that rigid blocks with linear dimension ~400 km or greater misfit the observed velocities by up to 15 mm/yr (4–5 mm/yr RMS), and the distributions of active faults and large earthquakes show that deformation is required in the interiors of such blocks. Decreasing the size of the blocks, and thereby increasing their number, improves the fit of block models to the observations. The velocities they reported can be fit to within about 2–3 mm yr−1 RMS by the relative motions of 10 or more rigid blocks that are of scale ~1–200 km on a side. These velocities are fit equally well by a field of velocity gradients that is locally uniform on the scale of 100–200 km but varies smoothly on larger scales, though such a field underestimates the strain rates in the western Gulf of Corinth. Continuous and block models fit the GPS velocities comparably well, the continuously varying field of velocity gradients offers the advantage of explaining the locations of, and sense of slip on, the major faults and earthquakes of the region. Floyd et al., (2010) concluded the velocities field that they report are inconsistent with models for the tectonics of Greece and the Aegean that divide the region up into a small number of microplates for instance Nyst and Thatcher (2004) four block and Reilinger et al., (2006) six blocks.

Our results are insufficient for detailed comparison of the newly proposed kinematic block models with 10 and 15 blocks (Figure 6.4 e, f) in Aegean. The stations which are located in the region of Aegean are in concordance with the velocity field, presented by Floyd et al., (2010). This could be seen well on Figure 6.7.

6.1.3. South Balkan Extension Region (SBER)

The Southern Balkan extensional system is not well known concerning the active deformation. Most of the studies in the Eastern Mediterranean are concentrated on the south of the North Anatolian fault and its westward continuation to one of the most rapidly deforming Aegean region (20-35 mm/yr). The Southern Balkan extensional system is north of the western part of the North Anatolian fault zone and south of a poorly defined boundary that extends through northern Bulgaria west to the Adriatic coast (McKenzie, l972; Burchfiel et al., 2006, 2008; Kotzev et al., 2006, 2008). The SBER has been separated from the main Aegean regime since ~6-10 Ma by the propagation of the North Anatolian fault into the northern Aegean Sea (Armino et al., 1996; Sengor et al., 2004). After that deformational event, the Aegean region to south of the North Anatolian fault zone began to move SSW as a

single plate and the extension within the South Balkan region became more N-S oriented and with a lower rate than southward movement of the Aegean plate. Geological investigations (Burchfiel et al., 2000, 2003; Nakov et al, 2001) suggest that the northern boundary of the Aegean extensional regime passes through north central Bulgaria whereas Jouanne et al., (2011), proposes that the north-western boundary probably coincides with the Scutari-Pesh Fault that forms the boundary between Albanides and Dinarides. Figure 6.5 presents the previous study on the SBER by Burchfiel et al., (2006, 2008), Reilinger et al., (2006) and Kotzev et al., (2006).

Burchfiel et al., (2006) analysed 25 GPS stations in Macedonia measured in two epochs 1996 and 2000 and suggested that Macedonia moves SSE relative to Eurasia essentially as a single crustal piece with velocity of 3–4 mm/yr along parts of westernmost Bulgaria.

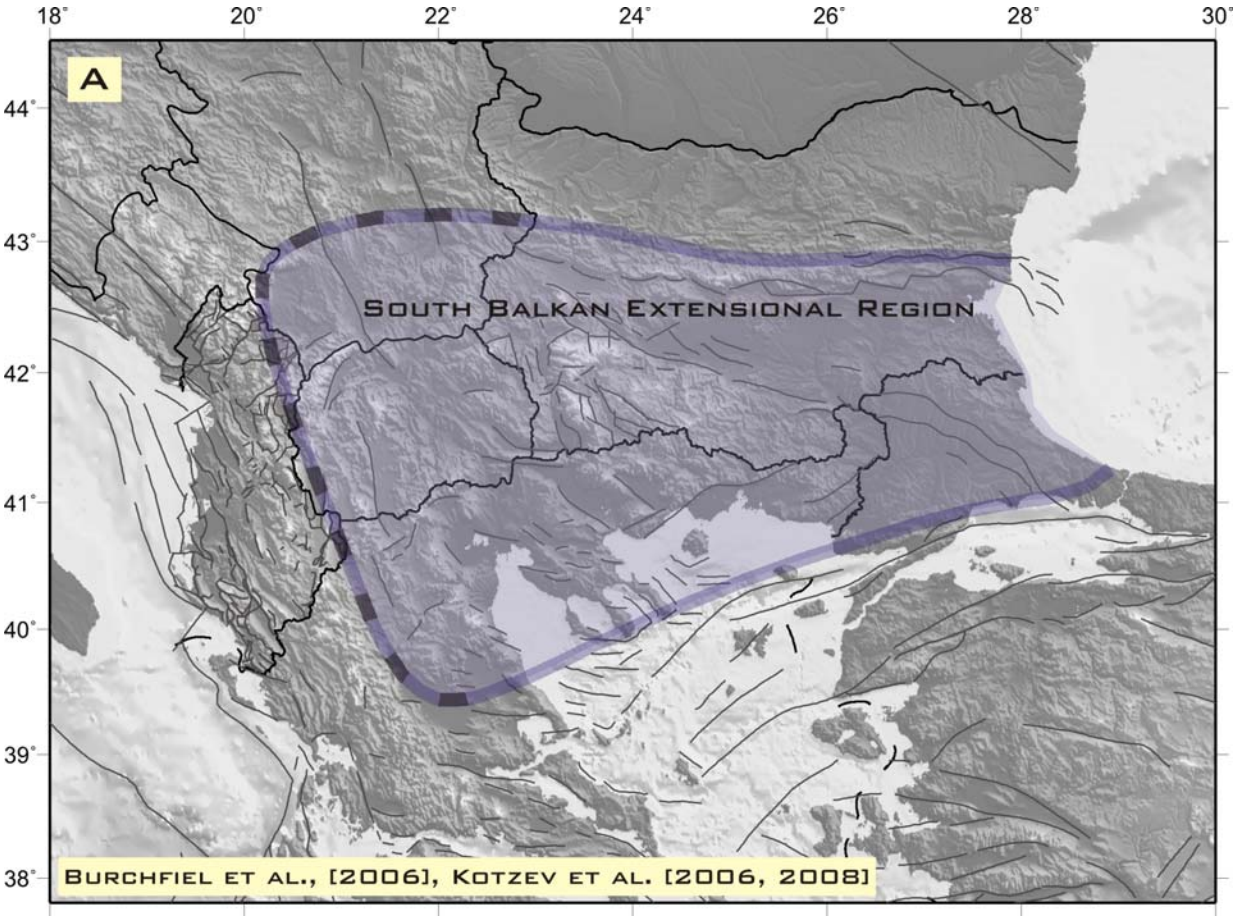

Figure 6.5. *Previous study (a-c) on the South Balkan extensional region.* ***BZ:*** *boundary zone where there is an abrupt change from shortening structures to the west and north-south–trending extensional structures to the east.;* ***EDSK:*** *Regional Elbasan-Debar-Skopje-Kjustendil fault zone;* ***ML:*** *Maritza lineament;* ***SBGS:*** *South Balkan graben system; The arrows indicate direction of extension relative to European plate to the north.*

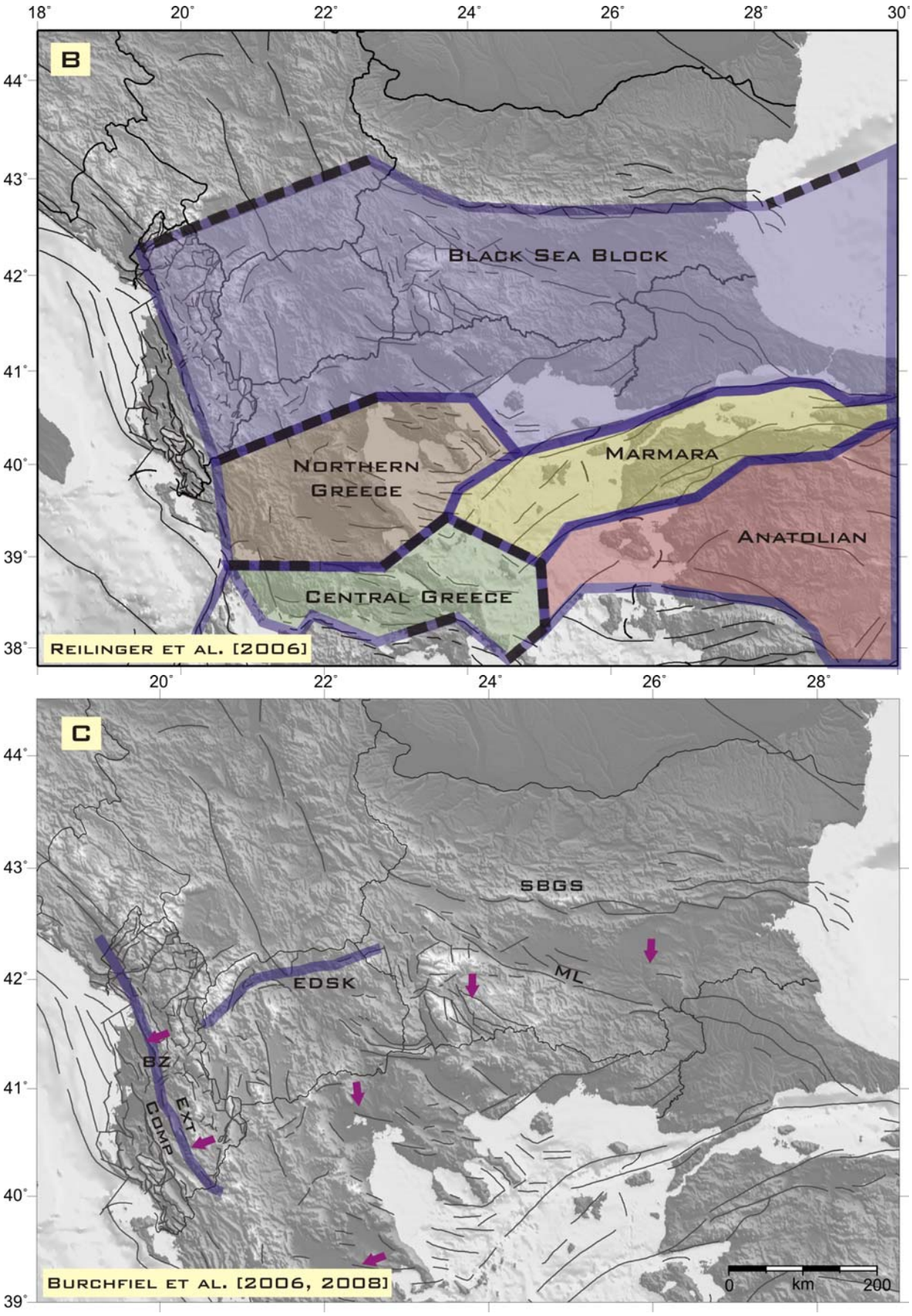

Figure 6.5. *(continued)*

The authors proposed that the GPS velocities and focal mechanisms can be interpreted and to suggest that the Aegean plate is now moving south–southwest and pulling the South Balkan lithosphere away from the region north of the South Balkan extensional regime. On the territory of Macedonia we have results of points that does not allow to confirm the of the unit peace. The velocity show small incensement from north to south (0802 - 2.1 mm/yr, M112 - 2.8mm/yr, M117 - 3.0mm/yr, M120 - 4.3 mm/yr) probably marks extensional regime. On the Figure 6.6a is plotted the velocity field of this study and its is combined with others authors (Reilinger et al., 2006, Holenstain et al., 2008, Georgiev 2009, Floyd et al., 2010) Reilinger et al., (2006) developed elastic block model to constrain present-day plate motion. Using 57 GPS points the authors suggest a Black Sea block which reaches the 45° east. On Figure 6.5b is shown proposed Black Sea block defined with Euler pole of rotation around 43.3°N/31.4°E with angular rate of 0.231°/Ma. Comparing this block model with vectors of this study with combination with others authors it is obviously that this block does not have behave as a single block. Kotzev et al., (2008) presented results from GPS observations in Bulgaria, Macedonia, and Albania which delineate a clear extensional zone that probably marks the northern limit of the South Balkan extensional terrain and the Aegean extensional province. The extensional zone passes through central Bulgaria along an approximately east-west trend separating a northern region with insignificant motion relative to Eurasia from south-western region characterized by E-W extensional grabens and increasing southward velocities between 2 and 4 mm/yr. The zone of extension passes obliquely trough the east-west trending Stara Planina Mountains of central Bulgaria. A more recent paper of geological investigation by Burchfiel et al., (2008) suggests that the South Balkan extensional system consists of normal faults and associated sedimentary basins within southern Bulgaria, Macedonia, eastern Albania, northern Greece, and north-western Turkey. With the formation of the western part of the North Anatolian fault zone, extension within the South Balkan extensional system became largely decoupled from the main Aegean extension south of the fault zone in late Miocene time. During late Cenozoic time, rapid south-southwest movement of the Aegean area was bounded by the North Anatolian fault zone on the north, and its rapid movement was caused by rollback at the Hellenic subduction zone that pulled the southern Balkan lithosphere more slowly to the south, causing the north-south extension and possible counter-clockwise rotation of the western part of the North Anatolian fault zone. The progressive development of the Hellenic subduction zone into an increasingly more arcuate shape and formation of the North Anatolian fault zone caused the north-south extension to migrate westward in tandem with westward migration of the east-west extension in the western part of the South Balkan extensional system. Active extension within the South Balkan extensional

system consists of two parts: (1) a eastern part, where east-west extension in eastern Albania and western Macedonia is related to slab rollback along the northern Hellenic subduction zone marked by a narrow belt of shortening, and (2) an eastern part, consisting of north-south extension in central and southern Bulgaria, eastern Macedonia, and northern Greece related to the slow southward movement of the South Balkan extensional system lithosphere, pulled southward by rapid south-southwest movement of the Aegean Sea lithosphere, which is mostly decoupled from the South Balkan extensional system across the North Anatolian fault zone. The two regions of extension overlap within Macedonia and north-western Greece and eastern Albania with the coexistence of both E-W (Ohrid graben) and NE-SW extension (Elbasani-Diber fault zone). Trench rollback was the dominant dynamic process, but during late Miocene time it was modified by the formation of the western part of the North Anatolian fault zone that partially decoupled the South Balkan extensional system from the Aegean extensional region. Georgiev (2009) has analyzed 89 campaign-mode and continuous GPS points covering whole territory of Bulgaria for the period 1996-2007, presented with red arrows on Figure 6.6. The author discussed new limit SBER and suggest that it passes through Maritza lineament passing to E-SE (Figure 6.6c).

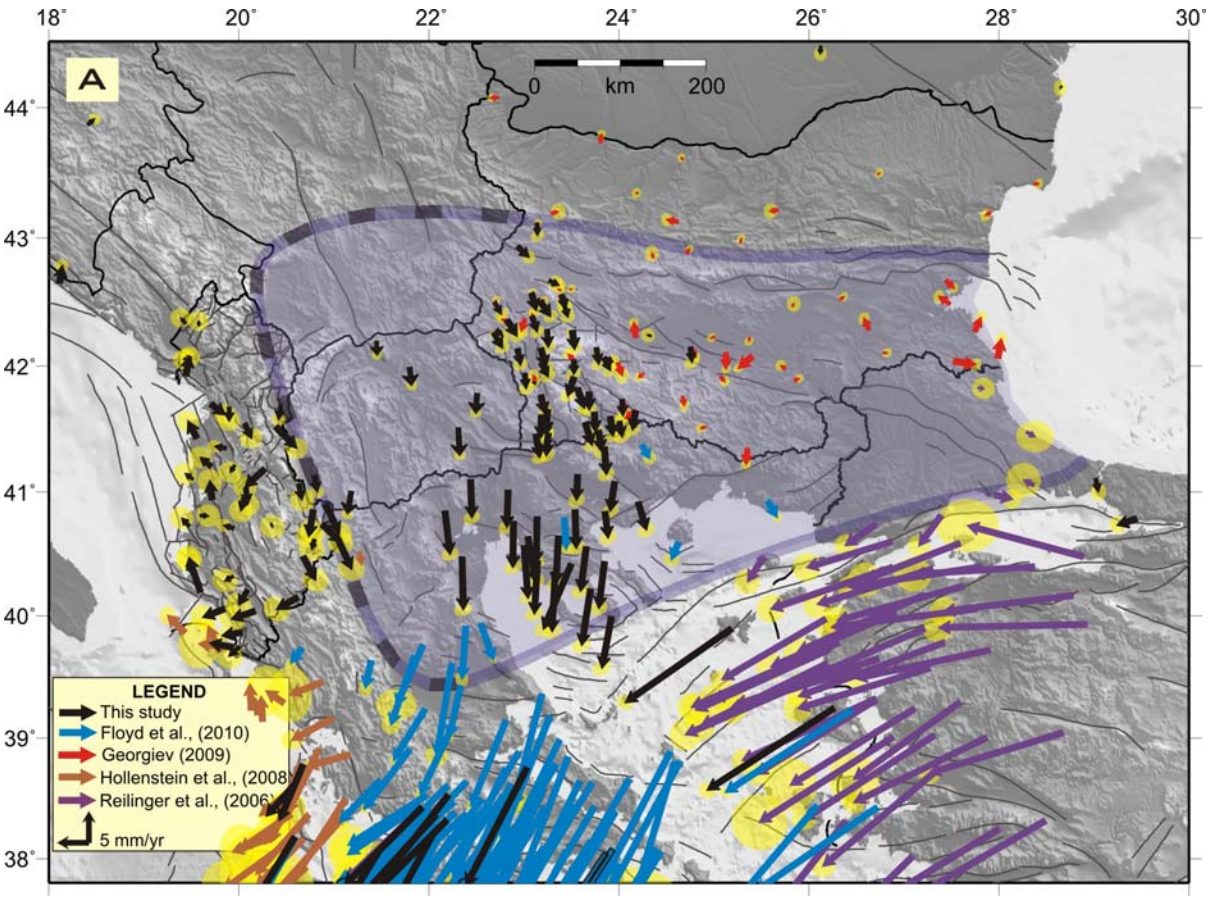

Figure 6.6. *Velocity field in South Balkan extension region (a-c) in the context of previous studies.*

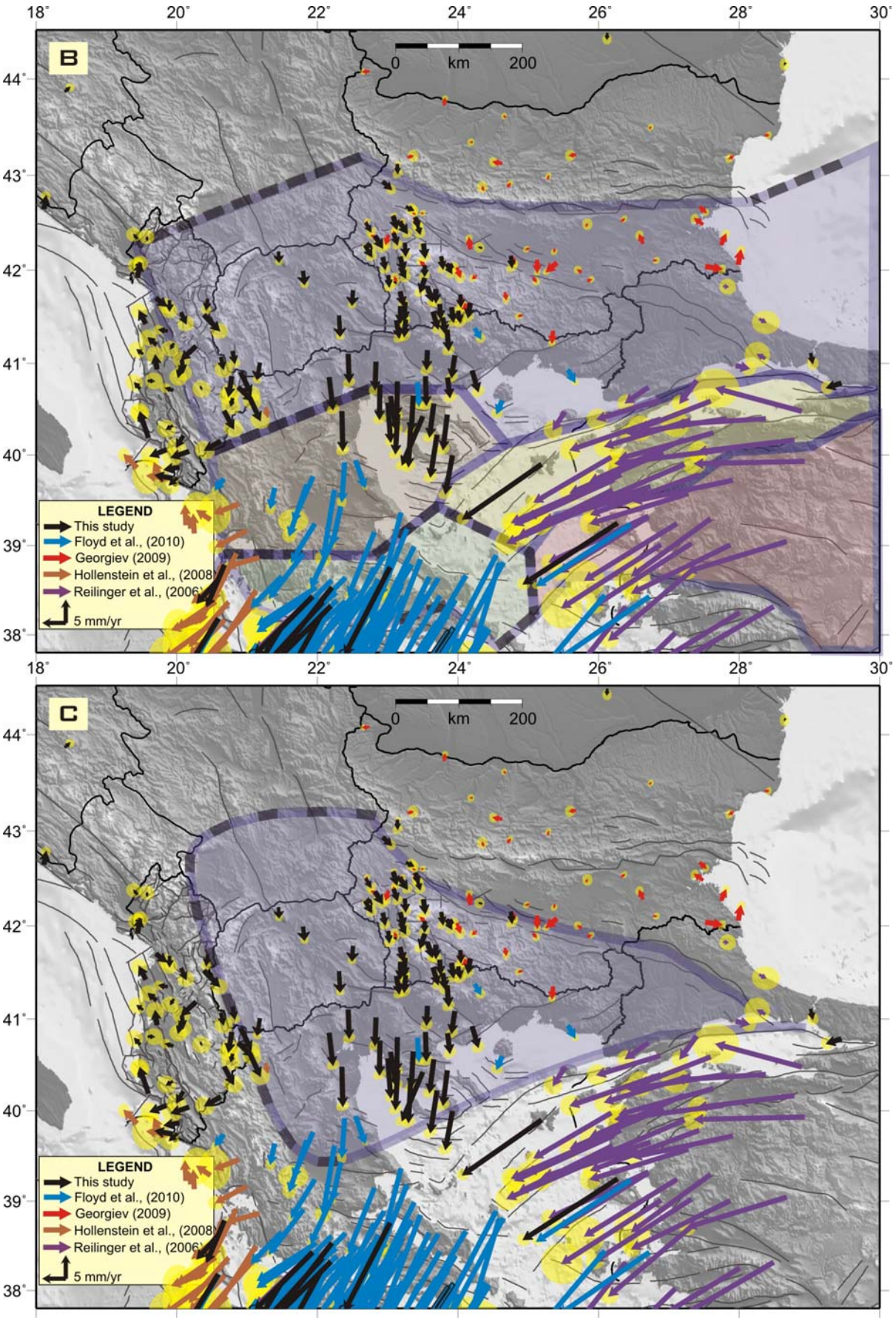

Figure 6.6. *(continued)*

A new set of geodetic velocities for the region of South Balkan extension obtained from campaign-mode and continuous GPS data in SWB, NG, Albania and 5 stations in Macedonia is used to test the block models, proposed by Reilinger et al., (2006) (Black Sea and North Greece blocks Figure 6.5b) and Nyst and Thacher, (2004) (Central Greece block Figure 6.4d). For this purpose different rotation poles are estimated taking into account the Eurasian plate (using EST_POLE tool from QOCA software package http://gipsy.jpl.nasa.gov/qoca/) which provided misfit vectors between observed velocities and the best fitting model vectors.

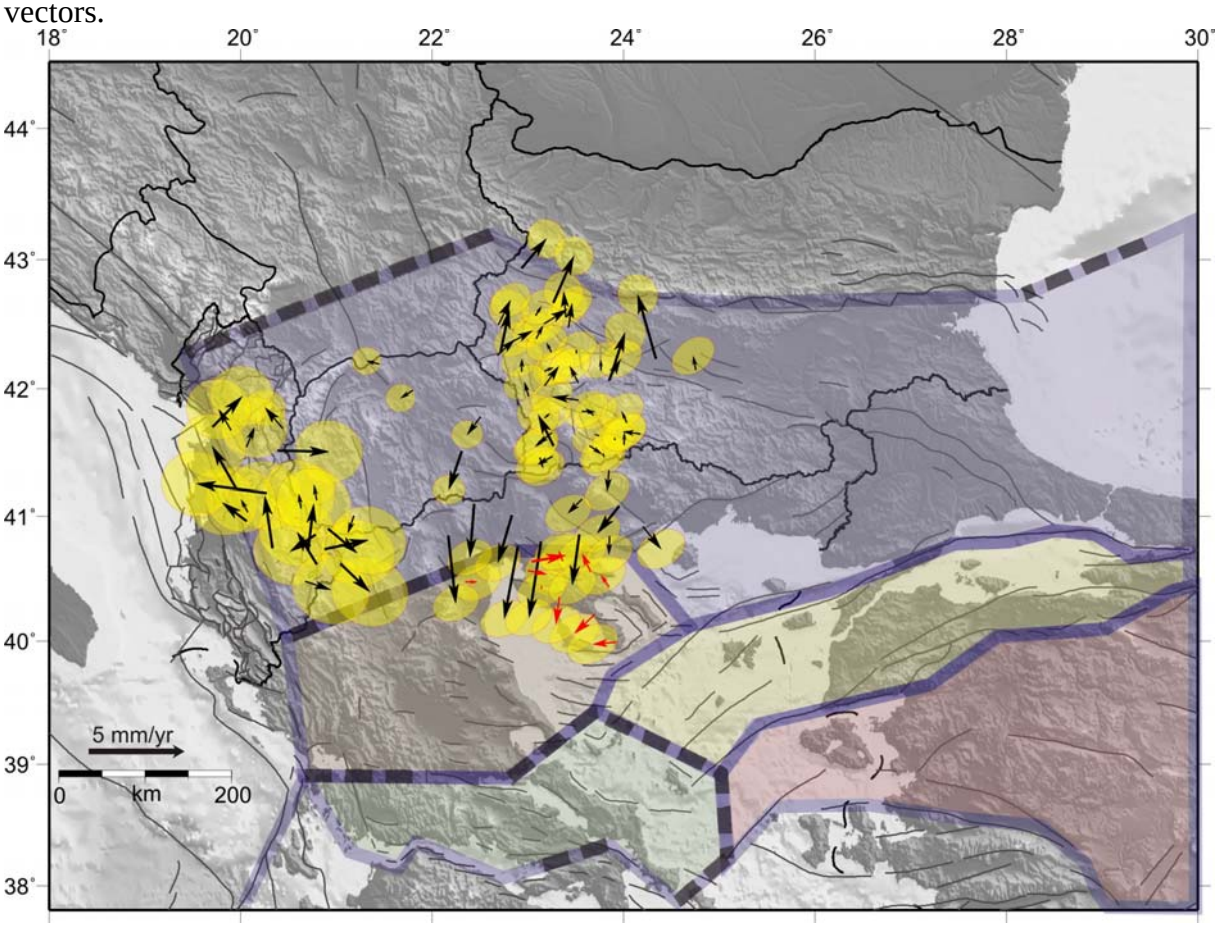

Figure 6.7. *Misfits between the observed velocities and best fitting angular velocities for the block models relative to Eurasian plate. Black arrows show the misfits for Black Sea block, and red arrows show misfits for Northern Greece block, both are proposed by Reiliger et al., (2006).*

Rotation pole relative to Eurasia is estimated from 74 GPS station which are located on the proposed Black Sea block by Reilinger et al., (2006) in order to test the existence of rigid block on the territory of SBER. The authors have estimated rotation pole located on 43.3°N, 31.4°E angular rate 0.231°/Ma. We obtained the following rotation pole parameters: 23.30°N, 89.95°E, and 0.036°/Ma, and this pole is not close to the proposed one. The misfits values are between 0.12 mm/yr and 4.03 mm/yr. The misfits are plotted on Figure 6.7 with

black vectors. The presented by the misfits results are not consistent with the proposed Black Sea block and clearly show that there is no rigid block which can perform the current displacement shown through our study as single stable block within such large area.

With 10 GPS stations located in the North Greece block proposed by Reilinger et al., (2006) rotation pole (30.67°N, 64.62°E, and 0.127°/Ma) relative to Eurasia is obtained. It presents misfits in the range of 0.15÷1.82 mm/yr., plotted on Figure 6.7 with red vectors. The smaller NG block size gives better fitting between observed and model velocities.

The Central Greece block proposed by Nyst and Thacher, (2004) includes the territory of South Albania. In that area are located 9 GPS stations that have been chosen to estimate a new rotation pole (-40.25°N, -160.06°E, and 2.941°/Ma) to test the rigid block existence model. The obtained misfits are between 0.23 mm/yr and 3.87 mm/yr. These geodetic results clearly show that there is inconsistency confirmed by Floyd et al., (2010) study as well.

On the territory of North Greece there are 16 GPS stations included in our study that cover the proposed model block Floyd et al., (2010) as it is shown on Figure 6.4e,f . We use the velocities of this area to calculate a rotation pole (-37.55°N, -173.66, and 0.299°/Ma). The estimated misfits on that area are in the range of 0.21÷1.99 mm/yr which is quite similar to those, obtained by Reilinger et al.'s proposed North Greece block.

Several different rotation poles covering different scale of areas have been tested to fit better with the observed velocities. First we tried to find a large single block in SWB and NG calculating rotation pole using 61 GPS stations and the following parameters have been estimated: 41.93°N, 35.56°E, and 0.222°/Ma. The obtained misfits between the observed and model velocities (not plotted) are between 0.20 mm/yr and 5.80 mm/yr. Using 40 GPS stations on smaller areas in SWB and 21 GPS stations on NG territory we estimated rotation pole -35.77°N, -176.76°E, and 0.082°/Ma and 40.17°N, 31.28°E, and 0.565°/Ma, respectively. With those areas the obtained misfits are between 0.09 mm/yr and 3.07 mm/yr and 0.07 mm/yr and 3.26 mm/yr, respectively. These results still do not provide good fitting. The misfits decrease with the decreasing the scale of blocks area. We indicated 5 blocks that present better fitting between observed and model vectors - plotted on Figure 6.8. The estimated parameters of the rotation pole and the misfits are listed in Table 6.2. A set of 7 points (BERK, BOGO, DELA, HURS, KRAL, PLA1, SOFI) are used to define a block corresponding to the observed velocities (Fig. 5.10.). This block with homogenous displacement is the possible north limit of extension which is discussed in section 5.2.5.3.

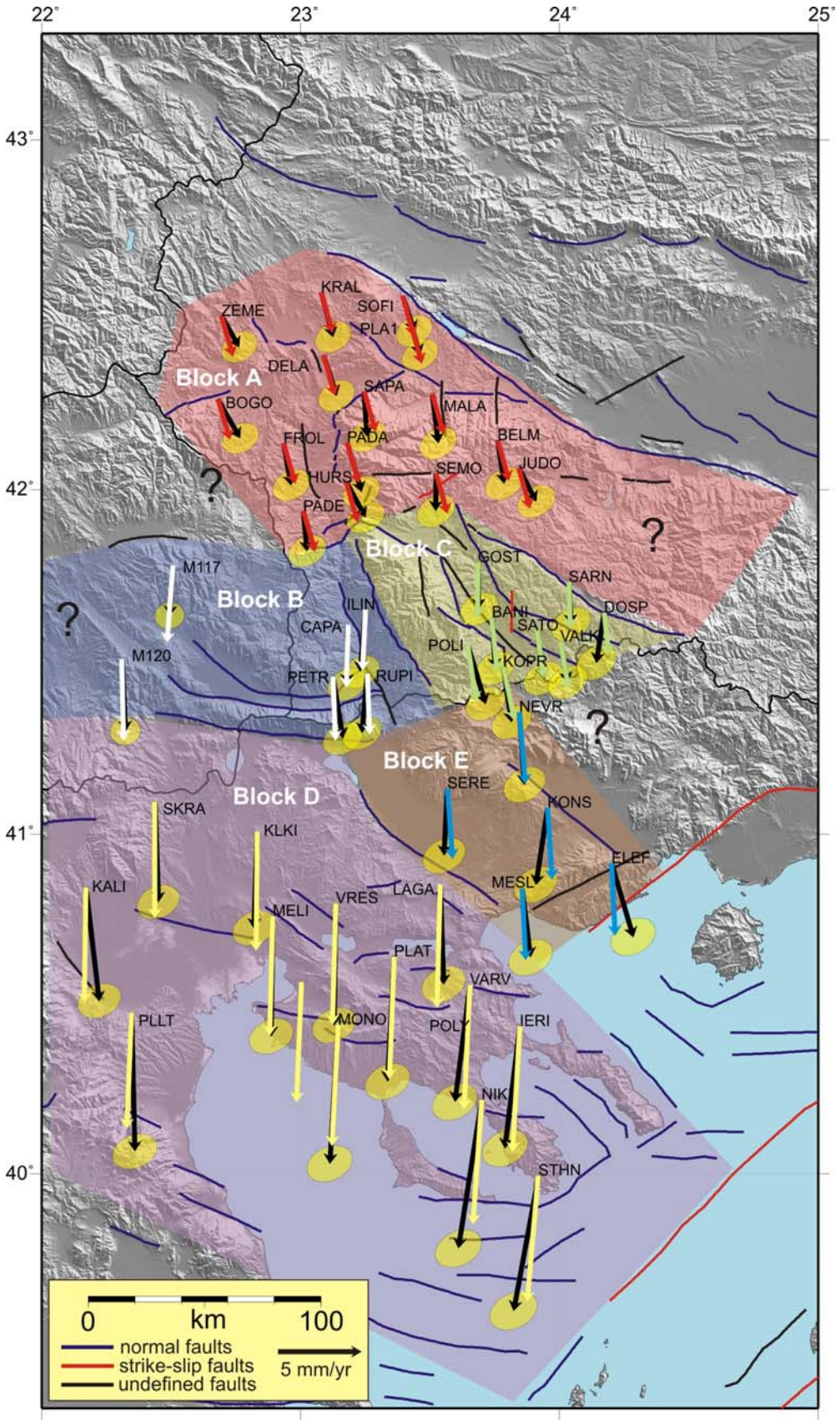

Figure 6.8. *Schematic mapping of block structure and their approximate boundaries inferred from GPS results. Black arrows show observed velocities, The red, white, green, yellow, and blue arrows present the predicted model velocities for Block A, Block B, Block C, Block D, and Block E, respectively.*

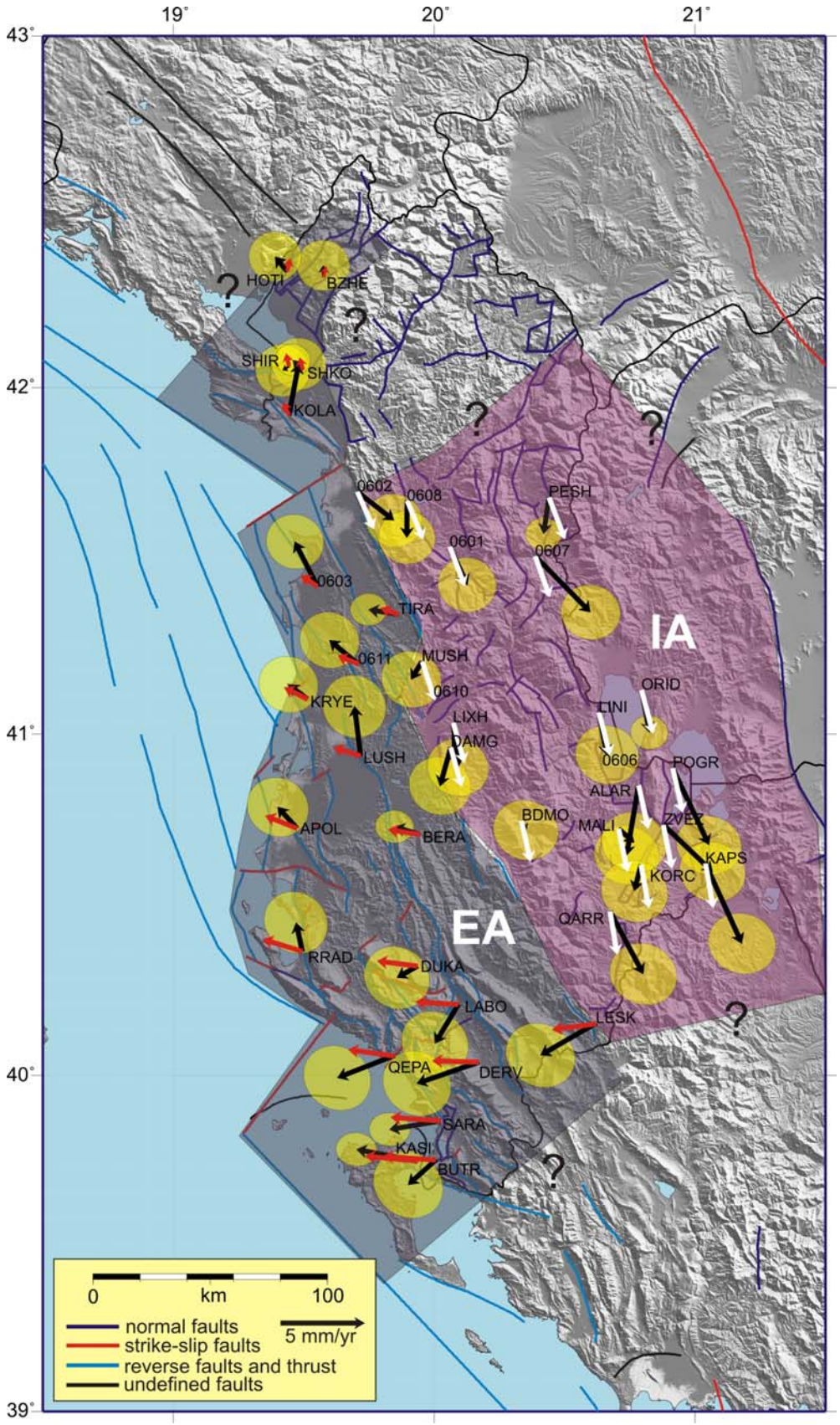

Figure 6.9. *Schematic mapping of block structure and their approximate boundaries inferred from GPS results. Black arrows show observed velocities, the red and white arrows present the predicted model velocities for* ***EA:*** *External Albanides block and* ***IA:*** *Inner Albanides block, respectively.*

In the Albanian territory we tested 36 GPS stations to calculate a rotation pole (-40.96°N, -160.62, and 0.943°/Ma not plotted) and the obtained misfits are between 0.29 mm/yr and 5.65 mm/yr. These results do not confirm the existence of single rigid block. We indicated two blocks External and Inner Albanides, which provide better fitting of observed and model vectors. Schematic illustration for these two blocks is shown on Figure 6.9. The rotation pole parameters are listed in Table 6.2. The misfits for these two blocks are between 0.04 mm/yr and 2.73 mm/yr for External Albanides and between 0.23 mm/yr and 2.59 mm/yr for Inner Albanides. These two blocks show better fitting between observed and model vectors, however the results do not determine rigid blocks yet. The geodetic data which we provided do not show existence of stable block in Albania. The rotation poles calculation in the SBER corresponds better to the decreasing of the block scale.

Table 6.2. *Determined parameters of rotation pole for blocks in SWB and NG expressed in Eurasia-fixed reference frame.*

Rotation pole:					Lat (°)	Long (°)		Angle (°/Ma)			
					30.76	98.85		0.026			
Name	Ve	Vn	σ(Vn)	σ(Vn)	corre	dVe	dVn	dV	dVaz	lon	lat
SOFI	0.34	-1.88	0.42	0.42	-0.0467	-0.34	0.57	0.66	329.100	23.395	42.556
BELM	0.46	-2.67	0.45	0.39	0.3082	-0.23	-0.22	0.32	225.333	23.762	42.141
BOGO	1.40	-2.40	0.44	0.37	0.2655	0.69	0.06	0.69	85.403	22.681	42.260
DELA	0.83	-2.53	0.43	0.38	0.2801	0.13	-0.08	0.15	119.409	23.089	42.387
FROL	0.51	-2.57	0.44	0.38	0.2773	-0.20	-0.12	0.23	238.867	22.935	42.132
HURS	1.21	-2.21	0.45	0.39	0.2868	0.51	0.24	0.56	64.584	23.177	42.023
JUDO	1.10	-2.07	0.45	0.40	0.3121	0.41	0.37	0.56	47.879	23.844	42.061
KRAL	0.76	-2.75	0.43	0.38	0.2769	0.07	-0.30	0.31	167.497	23.080	42.565
MALA	0.43	-3.00	0.44	0.39	0.2972	-0.26	-0.56	0.61	204.688	23.509	42.274
PADA	0.93	-3.04	0.44	0.38	0.2875	0.23	-0.59	0.63	159.085	23.180	42.135
PADE	0.27	-2.48	0.45	0.38	0.2808	-0.44	-0.02	0.44	266.848	23.011	41.938
PLA1	0.64	-1.96	0.43	0.38	0.2925	-0.05	0.49	0.49	354.007	23.425	42.477
SAPA	0.23	-2.75	0.44	0.38	0.2884	-0.46	-0.29	0.55	237.418	23.246	42.282
SEMO	0.03	-2.33	0.45	0.39	0.3001	-0.66	0.12	0.67	280.047	23.524	42.046
ZEME	1.12	-1.94	0.43	0.37	0.2629	0.41	0.51	0.66	38.657	22.695	42.498
Block A in SWB.							∑= 0.50				

Rotation pole:					Lat (°)	Long (°)		Angle (°/Ma)			
					41.32	26.11		0.879			
Name	Ve	Vn	σ(Vn)	σ(Vn)	corre	dVe	dVn	dV	dVaz	lon	lat
CAPA	-0.02	-3.65	0.47	0.39	0.2869	0.08	0.09	0.13	42.109	23.183	41.609
ILIN	-0.27	-3.85	0.46	0.39	0.2944	-0.09	-0.19	0.21	204.808	23.251	41.654
PETR	0.66	-3.78	0.47	0.39	0.2900	0.51	0.04	0.51	85.080	23.125	41.459
RUPI	-0.28	-3.64	0.47	0.39	0.2961	-0.41	0.01	0.41	271.519	23.258	41.467
M117	-0.18	-4.18	0.34	0.30	0.0136	0.19	0.44	0.47	23.106	22.507	41.781
M120	-0.14	-5.26	0.35	0.31	-0.0148	-0.25	-0.40	0.47	212.109	22.310	41.510
Block B in SWB							∑= 0.37				

Table 6.2. *(continued)*

Rotation pole:					Lat (°)	Long (°)	Angle (°/Ma)				
					41.57	25.64	1.186				
Name	Ve	Vn	σ(Vn)	σ(Vn)	corre	dVe	dVn	dV	dVaz	lon	lat
BANI	0.25	-3.15	0.47	0.40	0.3129	-0.09	0.13	0.16	325.514	23.739	41.630
DOSP	-0.43	-3.08	0.48	0.42	0.3058	-0.72	-0.54	0.90	232.784	24.173	41.645
GOST	0.09	-2.89	0.46	0.40	0.3097	0.12	0.48	0.49	14.256	23.686	41.790
KOPR	0.54	-3.40	0.47	0.40	0.3157	-0.13	-0.20	0.24	211.711	23.784	41.487
POLI	1.14	-3.65	0.47	0.40	0.3084	0.62	-0.21	0.65	108.924	23.645	41.553
SARN	0.20	-2.62	0.46	0.40	0.3223	0.11	0.15	0.18	37.023	24.036	41.733
SATO	0.46	-3.08	0.47	0.40	0.3203	0.05	-0.10	0.11	153.985	23.912	41.598
VALK	0.49	-2.57	0.47	0.40	0.3228	0.01	0.25	0.25	1.680	24.004	41.561
Block C in SWB							∑= 0.37				

Rotation pole:					Lat (°)	Long (°)	Angle (°/Ma)				
					-39.50	-175.37	0.266				
Name	Ve	Vn	σ(Vn)	σ(Vn)	corre	dVe	dVn	dV	dVaz	lon	lat
AUT1	0.61	-8.27	0.48	0.44	-0.0609	0.91	-1.07	1.41	139.699	23.004	40.567
IERI	-0.86	-7.35	0.52	0.42	0.3163	-0.42	0.17	0.45	292.274	23.848	40.436
KALI	0.95	-6.80	0.49	0.39	0.2494	1.05	0.08	1.05	85.400	22.171	40.845
KLKI	-0.19	-5.71	0.49	0.40	0.2782	-0.13	1.43	1.43	354.896	22.833	41.009
LAGA	0.15	-5.87	0.50	0.41	0.2985	0.35	1.53	1.57	12.842	23.540	40.854
MELI	-0.16	-7.03	0.50	0.40	0.2773	0.03	0.13	0.14	13.385	22.893	40.761
MONO	-0.39	-8.21	0.52	0.41	0.2892	-0.01	-0.96	0.96	180.718	23.145	40.440
NIKI	-1.46	-8.99	0.53	0.42	0.3093	-0.93	-1.52	1.78	211.330	23.700	40.219
PLAT	-0.65	-7.49	0.51	0.41	0.3000	-0.35	-0.15	0.38	246.612	23.362	40.642
PLLT	0.29	-8.19	0.51	0.40	0.2532	0.58	-1.24	1.37	154.764	22.347	40.476
SKRA	0.33	-6.04	0.48	0.39	0.2600	0.32	0.94	0.99	18.918	22.437	41.095
STHN	-1.58	-8.05	0.54	0.43	0.3143	-0.92	-0.50	1.05	241.383	23.919	39.994
VARV	-0.90	-7.03	0.51	0.41	0.3096	-0.54	0.41	0.68	307.376	23.654	40.558
VRES	-0.09	-7.20	0.50	0.40	0.2911	0.11	0.05	0.12	65.423	23.136	40.798
Block D in NG							∑= 0.96				

Rotation pole:					Lat (°)	Long (°)	Angle (°/Ma)				
					-39.50	-175.37	0.266				
Name	Ve	Vn	σ(Vn)	σ(Vn)	corre	dVe	dVn	dV	dVaz	lon	lat
ELEF	1.44	-4.38	0.51	0.43	0.3146	1.23	-0.03	1.23	91.516	24.201	40.916
KONS	-0.64	-4.63	0.49	0.41	0.3232	-0.91	-0.34	0.98	249.715	23.954	41.078
MESL	0.47	-4.16	0.50	0.41	0.3170	0.26	0.11	0.29	66.817	23.856	40.840
NEVR	0.40	-4.28	0.48	0.41	0.3164	0.04	-0.02	0.04	114.068	23.846	41.355
SERE	-0.23	-3.95	0.49	0.40	0.3087	-0.53	0.25	0.59	295.527	23.567	41.134
Block E in NG							∑= 0.63				

Rotation pole:					Lat (°)	Long (°)	Angle (°/Ma)				
					-42.00	-159.75	0.661				
Name	Ve	Vn	σ(Vn)	σ(Vn)	corre	dVe	dVn	dV	dVaz	lon	lat
BERA	-1.52	0.46	0.47	0.40	-0.0285	0.38	0.18	0.42	65.355	19.945	40.708
KASI	-3.62	0.69	0.50	0.41	-0.0491	-0.49	0.40	0.63	309.096	19.936	39.746
SARA	-3.05	-0.52	0.50	0.41	-0.0220	-0.07	-0.73	0.73	185.813	20.026	39.866
SHKO	-0.60	0.61	0.43	0.38	-0.0281	-0.42	-0.11	0.43	255.408	19.496	42.051
TIRA	-1.77	0.28	0.45	0.39	0.0035	-0.69	-0.08	0.70	263.009	19.863	41.347

Rotation pole:					Lat (°)	Long (°)		Angle (°/Ma)			
					-42.00	-159.75		0.661			
Name	Ve	Vn	σ(Vn)	σ(Vn)	corre	dVe	dVn	dV	dVaz	lon	lat
0603	-1.35	2.65	0.70	0.67	-0.0440	-0.36	1.99	2.02	349.614	19.553	41.428
0611	-1.72	1.43	0.72	0.69	-0.0546	-0.45	0.92	1.02	333.747	19.710	41.203
APOL	-1.16	1.26	0.75	0.72	-0.0769	0.72	0.53	0.90	54.069	19.475	40.726
BUTR	-1.63	-1.47	0.85	0.82	-0.1299	1.50	-1.70	2.27	138.446	20.006	39.750
BZHE	-0.01	0.68	0.64	0.62	-0.0185	-0.17	0.04	0.17	281.798	19.576	42.317
DERV	-3.68	-1.27	0.83	0.79	-0.1177	-0.93	-1.34	1.63	214.582	20.171	40.039
DUKA	-1.24	-0.69	0.80	0.76	-0.1019	1.16	-0.99	1.52	130.495	19.936	40.322
HOTI	-0.73	0.88	0.64	0.61	-0.0039	-0.90	0.10	0.91	276.514	19.437	42.333
KOLA	0.57	3.08	0.66	0.63	-0.0206	0.92	2.31	2.49	21.679	19.444	41.921
KRYE	-1.14	0.86	0.72	0.69	-0.0596	0.26	0.16	0.31	57.648	19.515	41.101
LABO	-1.38	-2.31	0.81	0.78	-0.1071	1.16	-2.46	2.72	154.855	20.092	40.209
LESK	-3.29	-1.89	0.84	0.78	-0.1178	-0.68	-1.53	1.68	203.871	20.620	40.153
LUSH	-0.36	2.93	0.77	0.76	-0.0528	1.25	2.42	2.73	27.218	19.718	40.937
QEPA	-3.40	-1.33	0.82	0.79	-0.1146	-0.66	-1.71	1.83	201.176	19.847	40.058
RRAD	-0.37	1.72	0.77	0.76	-0.0945	1.97	1.00	2.21	63.087	19.494	40.365
SHIR	-0.39	-0.24	0.66	0.64	-0.0113	-0.21	-1.01	1.03	191.969	19.444	42.061
External Albanides block							∑= 1.35				

Rotation pole:					Lat (°)	Long (°)		Angle (°/Ma)			
					-39.34	-166.48		0.254			
Name	Ve	Vn	σ(Vn)	σ(Vn)	corre	dVe	dVn	dV	dVaz	lon	lat
ORID	0.47	-2.51	0.46	0.40	-0.0361	-0.20	0.25	0.32	321.682	20.794	41.127
PESH	-0.32	-2.18	0.44	0.39	0.0008	-1.28	0.45	1.35	289.238	20.440	41.685
0601	1.03	-2.28	0.71	0.66	-0.0362	0.14	0.21	0.25	33.552	20.060	41.543
0602	2.18	-1.70	0.68	0.65	-0.0299	1.19	0.66	1.36	61.201	19.706	41.701
0607	3.29	-3.35	0.72	0.67	-0.0386	2.41	-0.74	2.52	106.972	20.388	41.515
0608	-0.02	-2.20	0.69	0.65	-0.0321	-0.98	0.23	1.01	282.918	19.897	41.675
ALAR	-0.71	-4.17	0.79	0.72	-0.0735	-1.25	-1.41	1.88	221.446	20.784	40.852
DAMG	-0.64	-2.31	0.75	0.71	-0.0673	-1.25	0.18	1.27	278.114	20.063	40.962
KAPS	2.17	-4.76	0.82	0.74	-0.0853	1.75	-1.91	2.59	137.378	21.040	40.623
KORC	-0.40	-1.57	0.82	0.75	-0.0877	-0.82	1.19	1.44	325.448	20.793	40.619
LINI	0.50	-2.52	0.77	0.71	-0.0620	-0.15	0.18	0.23	320.647	20.631	41.063
LIXH	0.30	-2.65	0.75	0.70	-0.0633	-0.34	-0.16	0.38	245.248	20.072	41.033
MUSH	-0.63	-1.05	0.73	0.69	-0.0565	-1.37	1.39	1.95	315.509	19.954	41.210
POGR	2.15	-4.57	0.79	0.72	-0.0684	1.60	-1.76	2.37	137.694	20.915	40.901
QARR	1.98	-3.72	0.82	0.75	-0.0976	1.62	-1.00	1.90	121.753	20.675	40.482
ZVEZ	2.92	-2.80	0.80	0.73	-0.0804	2.44	0.00	2.44	90.015	20.879	40.736
Inner Albanides block							∑= 1.45				

Table 6.2. *(continued)*

6.2. Overall Conclusion

This study presents the contemporary tectonics in the south Balkans region. The results were interpreted and discussed in the context of the current tectonic models proposed in the past few decades in geodetic, geological and seismological aspects.

For better understanding of the regional tectonics in South Balkans GPS permanent stations from Adria, Apulia, and Aegean regions have been included in the process.

GPS results of 134 permanent stations have been computed. Most of the permanent points are located in the region of Italy and the obtained vectors have been considered in the context of Adria and Apulia microplates. Compared with the results of other proposed models, the results we obtained confirm the existence of Adria and Apulia microplates. We also estimated our own rotation pole parameters using 12 GPS stations in Po Plain. The obtained pole is located on 45.51°N and 7.82°E with angular rate 0.336±0.052°/Myr, which is very similar to the rotation pole, proposed by D'Agostino et al., (2008). We do not calculate the rotation pole for Apulia microplate because the data is insufficient.

The GPS results in Aegean region are insufficient to confirm the recently proposed kinematic models; however the results are in concordance with the velocity field, published by different authors (Figure 6.10).

Several different rotation poles have been estimated in order to test the proposed kinematics model for SBER. The obtained misfits do not confirm the existence of rigid block, which is in agreement with the geological aspect that the SBER consists mainly of active normal faults (Burchfiel et al., 2008).

Campaign-mode GPS results in Albania has allowed characterizing a complex current tectonics pattern in Albania. West Albania is affected by westward motions related with Eurasia and Apulia microplate, the main part of this deformation is probably absorbed off shore along N-S to NNW-SSE active thrusts. Our results illustrated the importance of transverse faults (Lezhë Fault and Llogara Pass Fault) restricted to external Albanides in the current deformation. Two major NE-SW transverse active faults affected the collision belt, the Skutar-Pesh fault between Dinarides and Albanides and the Diber-Elabasani-Vlora fault zone mainly affected by an extensional displacement. External/Inner Albanides boundary and the Scutari-Pesh fault form respectively the western and the northern border of the domain (Inner Albania, North Greece, Macedonia and Bulgaria) affected by southward displacements related to stable Eurasia. A new modification is proposed changing the western boundary of SBER (Figure 6.11). Local multidirectional extension affected the Korca and the Orid active grabens at the boundary between Albania-Macedonia and Greece as suggested by neotectonic studies as well.

Episodic GPS results in South-west Bulgaria and North Greece give detailed information on the displacements. In concordance with the geological and seismological data, the results confirm the contemporary activity in the region. The presented velocity gradient (Figure 5.5) clearly indicates the increase of the motion from north to south and

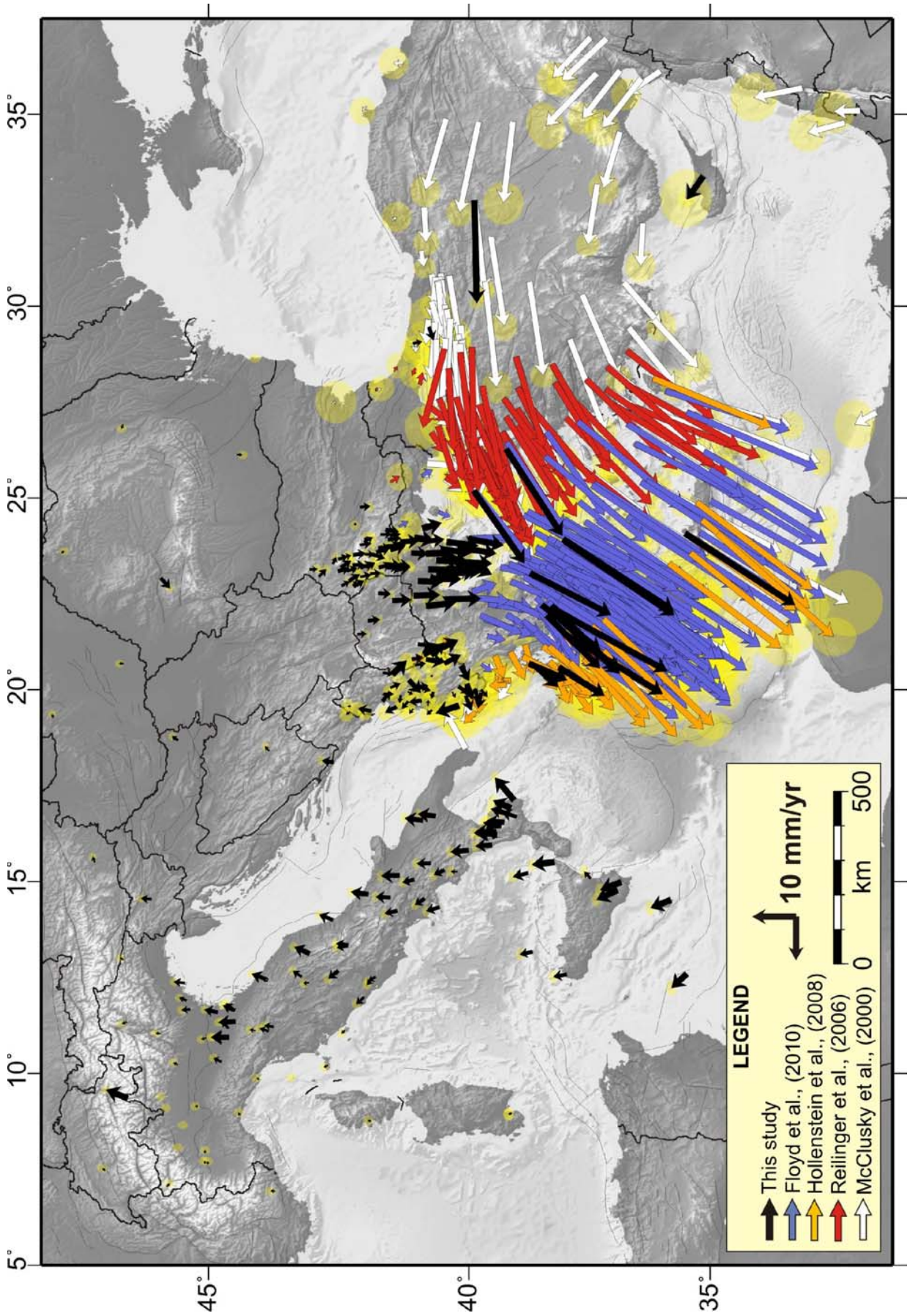

Figure 6.10. *Velocity field in Central and East Mediterranean expressed in the Eurasia fixed reference frame.*

reaches the Hellenic arc with values of up to 30-35 mm/yr. (Figure 6.10).The obtained strain rate field shows overall north-south extension regime. Compared to the main stress axes obtained from seismological events, extension regime is in quite good agreement in NG area. The GPS results confirm contemporary activity of the region of SWB and NG and they are in concordance with the velocity field in Aegean (Figure 5.9).

The proposed SBER by Kotzev et al., (2006), (2008), Burchfil et al., (2006), (2008) is modified by changing the western boundary (External/Inner Albanides). The new modification is shown on Figure 6.11.

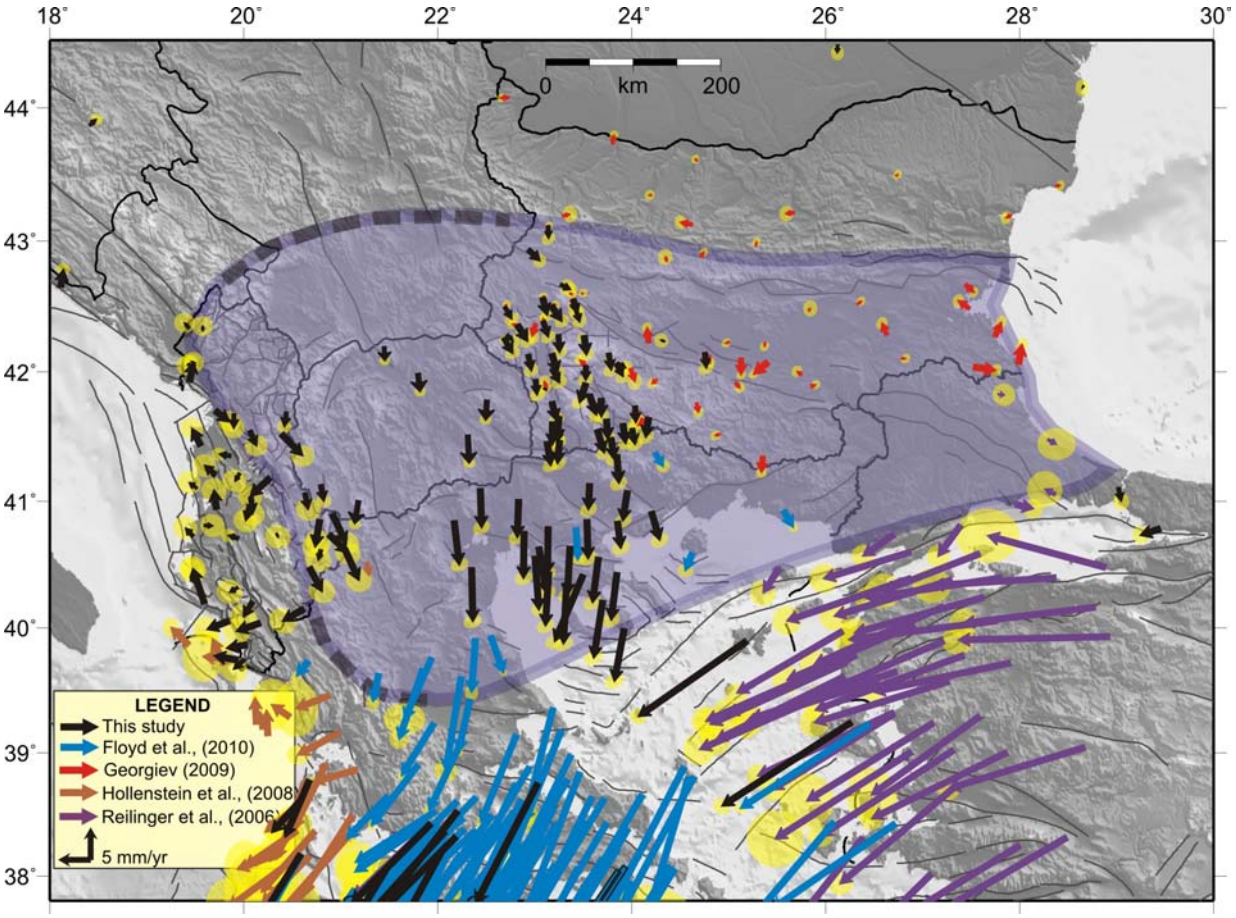

Figure 6.11. *Modified west boundary of South Balkan extension region. Velocities expressed in Eurasia fixed reference frame using the rotation pole proposed by Altamimi et al., (2007).*

Bibliography

Abramowitz, M. and I.A. Stegun (Editors) (1972), Handbook of Mathematical Functions with Formulas, Graphs, and Mathematical Tables (Dover, New York), 9th printing.

Aliaj S., Sulstarova. E.. Muço. B.. Koçiu. S., (2000), "Seismotectonic Map of Albania in scale 1:500.000". Seismological Institute Tirana.

Aliaj S., Adams J., Halchuk S., Sulstarova E., Peci V., Muco B., (2004), Probalistic seismic hazard maps for Albania, 13th World Conference on Earthquake Engineering Vancouver, B.C., Canada, August 1-6, 2004 Paper No. 2469.

Altamimi Z., Collilieux X.. Legrand J.. Garayt B.. Boucher C., (2007), ITRF2005: A new release of the International Terrestrial Reference Frame based on time series of station positions and Earth Orientation Parameters. Journal of Geophysical Research. VOL. 112, B09401, doi:10.1029/2007JB004949/.

Altiner, Y., (2001). The contribution of GPS to the detection of the Earth's crust deformations illustrated by GPS campaigns in the Adria region. Geophys. J. Int. 145, 550–559.

Ambraseys, N., and J. Jackson (1990), Seismicity and associated strain of central Greece between 1890 and 1988, Geophys. J. Int., 101(3), 663–708, doi:10.1111/j.1365-246X.1990.tb05577.x.

Anderson, H., Jackson, J., (1987). Active tectonics of the Adriatic region. Geophys. J. R. Astron. Soc. 91, 937–983.

Angelier, J., N. Lyberis, X. Le Pichon, E. Barrier, and P. Huchon (1982), The tectonic development of the Hellenic arc and the Sea of Crete: A synthesis, Tectonophysics, 86, 159– 196.

Anzidei, M., et al. (2009), Coseismic deformation of the destructive April 6, 2009 L'Aquila earthquake (central Italy) from GPS data, Geophys. Res. Lett., 36, L17307, doi:10.1029/2009GL039145.

Argand, E. (1924), La tectonique de L'Asie, paper presented at the 13th Congress, Geol. Int., Brussels.

Armijo, R., B. Meyer, G. King, A. Rigo, and D. Papanastassiou (1996), Quaternary evolution of the Corinth rift and its implications for Late Cenozoic evolution of the Aegean, Geophys. J. Int., 126, 11–53.

Avallone A.. Briole P.. Agatza-Balodimou A. M.. Billiris H.. Charade O.. Mitsakaki C.. Nercessian A.. Papazissi K.. Paradissis D.. Veis G.. (2004). Analysis of eleven years of deformation measured by GPS in the Corinth Rift Laboratory area. C. R. Geoscience 336 301–311.

Ayhan, M. E., et al. (2002), Interseismic strain accumulation in the Marmara Sea region, Bull. Seismol. Soc. Am., 92, 216– 229.

Babucci D.. Tamburelli C. Viti M.. Mantovani E.. Albarello D.. d'Onza F.. Cenni N. and Mugnaioli E., (2004), Relative motion of the Adriatic with respect to the confining plates: seismlogical and geodetic constrains. Geophys. J. .Int. 159. 765-775.

Barrier, E., N. Chamot-Rooke, G. Giordano, (2004), "Geodynamic map of the Mediterranean", Sheet 1- Tectonics and Kinematics. CGMW, France.

Battaglia M.. Murray M.H.. Serpelloni E. Bürgmann R., (2004), The Adriatic region: An independent microplate within the Africa- Eurasia collision zone. G.R.L., Vol. 31. L09605. doi:10.1029/2004GL019723.

Belyashky T., I. Georgiev, D. Dimitrov, L. Pashova, G. Nicolov (2006), Recent vertical crustal movements in South-western Bulgaria. Geodesy 17, Bulgarian Academy of Sciences.

Bernard P., Lyon-Caen H.. Briole P.. Deschamps A.. Boudin F.. Makropoulos K.. Papadimitriou P.. Lemeille F.. Patau G.. Billiris H.. Paradissis D.. Papazissi K.. Castarède H.. Charade O.. Nercessian A.. Avallone A.. Pacchiani F.. Zahradnik J.. Sacks S.. Linde A.. (2006) Seismicity. deformation and seismic hazard in the western rift of Corinth: New insights from the Corinth Rift Laboratory (CRL). Tectonophysics.

Beutler, G., M. Rothacher, S. Schaer, T.A. Springer, J. Kouba, and R.E. Neilan (1999), The International GPS Service (IGS): An Interdisciplinary Service in Support of Earth Sciences, Advances in Space Research, 23(4), pp. 631–653.

Beutler G., H. Bock, R. Dach, P. Fridez, A. Gade, U. Hugentobler, A. J¨aggi, M. Meindl, L. Mervart, L. Prange, S. Schaer, T. Springer, C. Urschl, P. Walser (2007), Bernese GPS Software Version 5.0. Astronomical Institute, University of Bern.

Billiris, H., et al. (1991), Geodetic determination of tectonic deformation in central Greece from 1900 to 1988, Nature, 350, 124– 129.

Bock, Y., R.M. Nikolaidis, P.J. de Jonge and M. Bevis (2000), Instantaneous geodetic positioning at medium distances with the Global Positioning System, J. Geophys. Res., 105 (B12), 28223-28254, doi: 10.1029/2000JB900268.

Boncev, E., V. Bune, L. Christoskov, J. Karagjuleva, V. Kostadinov, G. Reisner, S. Rizhikova, N. Shebalin, V. Sholpo, D. Sokerova (1982), A method for compilation of seismic zoning prognostic maps for the territory of Bulgaria. Geologica Balcanica, 12, 2, pp. 3-48.

Botev E., I. Georgiev, D. Dimitrov (2006), Recent seismicity, stress and strain in South-western Bulgaria. Geodesy 17, Bulgarian Academy of Sciences.

Briole, P., et al. (2000), Active deformation of the Corinth rift, Greece: Results from repeated Global Positioning System surveys between 1990 and 1995, J. Geophys. Res., 105, 25,605– 25,625.

Burchfiel, B.C., Nakov, R., Tzankov, Tz., Royden, L.H., (2000). Cenozoic extension in Bulgaria and northern Greece: the northern part of the Aegean extensional regime. In: Bozkurt, E., Winchester, J.A., Piper, J.D.A. (Eds.), Tectonics and Magmatism in Turkey and the Surrounding Area, Spec. Publ.-Geol. Soc. Lond, vol. 173, pp. 325–352.

Burchfiel, B.C., Nakov, R., Tzankov, T., (2003), Evidence from the Mesta half-graben, SW Bulgaria, for the late Eocene beginning of Aegean extension in the Central Balkan Peninsula. Tectonophysics 375, 61– 76.

Burchfiel, B.C., King, R.W., Todosov, A., Kotzev, V., Durmurdzanov, N., Serafimovski, T., Nurce, B., (2005), GPS results for Macedonia and its importance for the tectonics of the Southern Balkan extensional regime. Tectonophys 413, 239–248.

Burchfiel B. C.. King R. W. . Todosov A.. Kotzev V.. Durmurdzanov N.. Serafimovski T.. Nurce B.. (2006), GPS results for Macedonia and its importance for the tectonics of the Southern Balkan extensional regime. Tectonophysics 413 239–248.

Burchfiel B.C., R. Nakov, N. Dumurdzanov, D. Papanikolaou, T. Tzankov, T. Serafi movski , R.W. King, V. Kotzev, A. Todosov, B. Nurce (2008), Evolution and dynamics of the Cenozoic tectonics of the South Balkan extensional system, Geosphere; December 2008; v. 4; no. 6; p. 919–938; doi: 10.1130/GES00169.1.

Calais, E., J. M. Nocquet, F. Jouanne, and M. Tardy (2002), Current strain regime in the western Alps from continuous Global Positioning System measurements, 1996– 2001, Geology, 7, 651– 654.

Caporali, A., S. Martin, and M. Massironi (2003), Average strain rate in the Italian crust inferred from a permanent GPS network - II. Strain rate versus seismicity and

structural geology, Geophys. J. Int., 155, 254-268, doi:10.1046/j.1365-246X.2003.02035.x.

Carcaillet, J., Mugnier J.L. , Koçi R., Jouanne F., (2009) Uplift and active tectonics of southern Albania inferred from incision of alluvial terraces, Quaternary Research), doi:10.1016/j.yqres.2009.01.002

Channell, J. E. T., B. D'Argenio, and F. Horvath (1979), Adria, the African promontory in Mesozoic Mediterranean paleogeography, Earth Sci. Rev., 15, 213–292.

Channell, J. E. T. (1996), Palaeomagnetism and palaeogeography of Adria, in Palaeomagnetism and Tectonics of the Mediterranean Region, edited by A. Morris and D. H. Tarling, Geol. Soc. Spec. Publ., 105, 119–132.

Christoskov, L., Grigorova, E., (1968), On the relationship between earthquake energy and magnitude for Bulgaria. C. R. Acad. Bulg. Sci. 21 (2), 127–129.

Clarke, P. J., et al. (1998), Crustal strain in central Greece from repeated GPS measurements in the interval 1989–1997, Geophys. J. Int., 135, 195– 214.

Cocard, M., et al. (1999), New constraints on the rapid crustal motion of the Aegean region: Recent results inferred from GPS measurements (1993–1998) across the West Hellenic Arc, Greece, Earth Planet. Sci. Lett., 172, 39– 47.

Copley, A., F. Boait, J. Hollingsworth, J. Jackson, and D. McKenzie (2009), Subparallel thrust and normal faulting in Albania and the roles of gravitational potential energy and rheology contrasts in mountain belts, J. Geophys. Res., 114, B05407, doi:10.1029/2008JB005931.

D'Agostino, N., R. Giuliani, M. Mattone, and L. Bonci (2001), Active crustal extension in the central Apennines (Italy) inferred from GPS measurements in the interval 1994-1999, Geophys. Res. Lett., 28, 2121–2124.

D'Agostino, N., and G. Selvaggi (2004), Crustal motion along the Eurasia-Nubia plate boundary in the Calabrian Arc and Sicily and active extension in the Messina Straits from GPS measurements, J. Geophys. Res., 109, B11402, doi:10.1029/2004JB002998.

D'Agostino, N., D. Cheloni, S. Mantenuto, G. Selvaggi, A. Michelini, and D. Zuliani (2005), Strain accumulation in the southern Alps (NE Italy) and deformation at the northeastern boundary of Adria observed by CGPS measurements, Geophys. Res. Lett., 32, L19306, doi:10.1029/2005GL024266.

D'Agostino, N., A. Avallone, D. Cheloni, E. D'Anastasio, S. Mantenuto, and G. Selvaggi (2008), Active tectonics of the Adriatic region from GPS and earthquake slip vectors, J. Geophys. Res., 113, B12413, doi:10.1029/2008JB005860.

Davies, R., P. England, B. Parsons, H. Billiris, D. Paradissis, and G. Veis (1997), Geodetic strain of Greece in the interval 1892– 1992, J. Geophys. Res., 102, 24,571– 24,588.

Delacou, B., C. Sue, J. D. Champagnac, and M. Burkhard (2004), Presentday geodynamics in the bend of the western and central Alps as constrained by earthquake analysis, Geophys. J. Int., 158, 753 – 774, doi:10.1111/j.1365-246X.2004.02320.x.

DeMets C., R. Gordon, D. Argus, S. Stein (1990), Current plate motions. Geophys. J. Int., 101, 425–478, 1990.

DeMets C., R. Gordon, D. Argus, S. Stein (1994), Effects of recent revisions to the geomagnetic reversal time scale on estimates of current plate motions. Geophys. Res. Lett., 21, 2191–2194.

Devoti, R., F. Riguzzi, M. Cuffaro, and C. Doglioni (2008), New GPS constraints on the kinematics of the Apennines subduction, Earth Planet. Sci. Lett., 273, 163– 174, doi:10.1016/j.epsl.2008.06.031.

Dewey, J. F., M. L. Helman, E. Turco, D. H. W. Hutton, and S. D. Knott (1989), Kinematics of the western Mediterranean, in Alpine Tectonics, edited by M. P. Coward, D. Dietrich, and R. G. Park, Geol. Soc. Spec. Publ., 45, 265–283.

Dineva S., Batllo J., Mihaylov D. & van Eck T (2002), Source parameters of four strong earthquakes in Bulgaria and Portugal at the beginning of the 20th century Journal of Seismology 6: 99–123.

Dobrev N., I. Georgiev, B. Košták (2006), Extensometric and GPS monitoring of tectonic movements in the Simitli graben, SW Bulgaria. Geodesy 17, Bulgarian Academy of Sciences.

Dong D. Herring TA. King RW, (1998), Estimating regional deformation from a combination of space and terrestrial geodetic data. J Geod 72(4):200–214.

Dong, D., P. Fang,Y. Bock, M.K. Cheng and S. Miyazaki (2002), Anatomy of apparent seasonal variation from GPS-derived site position, J. Geophys. Res., 107, doi: 10.1029/2001JB000573.

Dumurdzanov N.. T. Serafimovski. C. Burchfiel, (2005), Cenozoic tectonics of Macedonia and its relation to the South Balkan extensional regime. Geosphere; v. 1; No.1; p.1-22.

Favali, P., R. Funiciello, and P. Pieri (1993), An active margine across the Adriatic Sea (central Mediterranean Sea), Tectonophysics, 219, 109–117.

Flerit, F., R. Armijo, G. C. P. King, B. Meyer, and A. Barka (2003), Slip partitioning in the Sea of Marmara pull-apart determined from GPS velocity vectors, Geophys. J. Int., 154, 1–7.

Floyd, M. A., et al. (2010), A new velocity field for Greece: Implications for the kinematics and dynamics of the Aegean, J. Geophys. Res., 115, B10403, doi:10.1029/2009JB007040.

Ganas, A., Serpelloni, E., Drakatos, G., Kolligri, M., Adamis, I., Tsimi, Ch. and Batsi, E. (2009), "The Mw 6.4 SWAchaia (Western Greece) Earthquake of 8 June 2008: Seismological, Field, GPS Observations, and Stress Modeling", Journal of Earthquake Engineering, 13:8,1101-1124.

Georgiev I. and D. Dimitrov (2006), Assessment of horizontal velocities at South-western Bulgaria by GPS. Geodesy 17, Bulgarian Academy of Sciences.

Georgiev I., D. Dimitrov, L. Pashova, E. Botev, S. Shanov, G. Nikolov (2006), Kinematics and geodynamics of the Krupnik-Kresna seismogenic zone. Geodesy 17, Bulgarian Academy of Sciences.

Georgiev I., (2009). National and Permanent GPS networks of Bulgaria – processing of the observation, analysis and application in Geodynamic – dissertation for doctor of science.

Goldsworthy, M., and J. A. Jackson (2000), Active normal fault evolution and interaction in Greece revealed by geomorphology and drainage patterns, J. Geol. Soc., 157, 967–981, doi:10.1144/jgs.157.5.967.

Goldsworthy, M., and J. Jackson (2001), Migration of activity within normal fault systems: Examples from the Quaternary of mainland Greece, J. Struct. Geol., 23(2–3), 489–506, doi:10.1016/S0191-8141(00)00121-8.

Goldsworthy. M.. J. Jackson. and J. Haines (2002). The continuity of active faults in Greece. Geophys. J. Int.. 148. 596– 618.

Grenerczy G.. Sella G. and Stein S., Kenyeres A.. (2005) Tectonic implications of the GPS velocity field in the northern Adriatic region. G.R.L.. VOL.32. L16311. doi:10.1029/2005GL022947.

Gutenberg, B., Richter, C.F., (1954). Seismicity of the Earth and Associated Phenomena. Princeton University Press, Princeton. 310 pp.

Hatanaka, Y., M. Sawada, A. Horita, M. Kusaka, J. Johnson and C. Rocken (2001), Calibration of antenna-radome and monument-multipath effect on GEONET, Part 2. Evaluation of the phase map by GEONET data, Earth Planets Space, 53, 23-30.

Hatzfeld, D., J. Martinod, G. Bastet, and P. Gautier (1997), An analog experiment for the Aegean to describe the contribution of gravitational potential energy, J. Geophys. Res., 102(B1), 649–659, doi:10.1029/96JB02594.

Hollenstein, Ch., H.-G. Kahle, A. Geiger, S. Jenny, S. Goes, and D. Giardini (2003), New GPS constraints on the Africa-Eurasia plate boundary zone in southern Italy, Geophys. Res. Lett., 30(18), 1935, doi:10.1029/2003GL017554.

Hollenstein Ch.. Geiger A... Kahle H.-G and Veis G.. CGPS time-series and trajectories of crustal motion along theWest Hellenic Arc. Geophys. J. Int. (2006) 164. 182–191 doi: 10.1111/j.1365-246X.2005.02804.x.

Hollenstein, C., M. D. Müller, A. Geiger, and H.-G. Kahle (2008), Crustal motion and deformation in Greece from a decade of GPS measurements, 1993–2003, Tectonophysics, 449(1–4), 17–40, doi:10.1016/j.tecto.2007.12.006.

Hunstad, I., G. Selvaggi, N. D'Agostino, P. England, P. Clarke, and M. Pierozzi (2003), Geodetic strain in peninsular Italy between 1875 and 2001, Geophys. Res. Lett., 30(4), 1181, doi:10.1029/2002GL016447.

Italiano, F., Martelli, M., Martelli, G., Nuccio, P.M., (2000). Geochemical evidence of melt intrusions along lithospheric faults of the Southern Apennines, Italy: geodynamic and seismogenic implications. J. Geophys. Res. 105, 13,569–13,578.

Jackson J., D. McKenzie (1984), Active tectonics of the Alpine-Himalayan Belt between western Turkey and Pakistan. Geophys. J.R. Astr. Soc., 77, 185–246.

Jackson J., D. McKenzie (1988), The relationship between plate motions and seismic tremors, and the rates of active deformation in the Mediterranean and Middle East. Geophys. J. R. Astr. Soc., 93, 45–73.

Jackson J. (1992), Partitioning of strike-slip and convergent motion between Eurasia and Arabia in eastern Turkey. J. Geophys. Res., 97, 12471–12479.

Jackson, J., A. Haines, and W. Holt (1995), The accommodation of Arabia-Eurasia plate convergence in Iran, J. Geophys. Res., 100, 15,205–15,220, doi:10.1029/95JB01294.

Jestin F., P. Huchon, J.M. Gaulier (1994), The Somalia Plate and the East African rift system; present-day kinematics. Geophys J. Int., 116, 637–654.

Kahle, H.-G., Cocard, M., Peter, Y., Geiger, A., Reilinger, R., Barka, A., Veis, G., (2000), GPS-derived strain rate field within the boundary zones of the Eurasian, African and Arabian Plates. J. Geophys. Res. 105 (B10), 23353–23370.

Kiratzi, A., E. Louvari (2003), Focal mechanisms of shallow earthquakes in the Aegean Sea and the surrounding lands determined by waveform modelling: a new database, Journal of Geodynamics 36 (2003) 251–274.

Kotzev, V., R. Nakov, B. C. Burchfiel, R. King, and R. Reilinger (2001a), GPS study of active tectonics in Bulgaria: Results from 1996 to 1998, J. Geodyn., 31, 189–200.

Kotzev, V., Nakov, R., Burchfiel, B.C., King, R.W., (2001b). GPS constraints on the kinematics of southwestern Bulgaria. C. R. Acad. Bulg. Sci. 54 (7), 51–54.

Kotzev, V., Nakov, R., Georgiev, Tz., Burchfiel, B.C., King, R.W., (2006). Crustal motion and strain accumulation in western Bulgaria. Tectonophysics 413, 127–145. doi:10.1016/j.tecto.2005.10.040.

Kotzev, V., King, R.W., Burchfi el, B.C., Todosov, A., Nurce, B., and Nakov, R., (2008), Crustal motion and strain accumulation in the South Balkan region inferred from GPS measurements, in Husebye, E., ed., Earthquake monitoring and seismic hazard mitigation in Balkan countries: Proceedings of the NATO Advanced Research Workshop on Earthquake Monitoring and Seismic Hazard Mitigation in Balkan Countries, Borovetz, Bulgaria, 11–18 September 2005: NATO Science Series IV: Earth and Environmental Sciences Volume 81, p. 19–43.

Kouba, J., (2002), The GPS Toolbox ITRF transformations, GPS Solutions, Vol. 5, No. 3, pp. 88-90.

Kuk, V., Prelogovic, E., and Dragicevic, I., (2000), Seismotectonically active zones in the Dinarides: Geological Journal of Croatia, v. 53, p. 295–303.

Le Pichon, X., and J. Angelier (1979), The Hellenic Arc and trench system: A key to the neotectonic evolution of the eastern Mediterranean area, Tectonophysics, 60, 1 –42.

Le Pichon, X., and J. Angelier (1981), The Aegean Sea, Philos. Trans. R. Soc. London, Ser. A, 300, 357– 372.

Le Pichon, X., N. Chamot-Rooke, S. Lallemant, R. Noomen, and G. Veis (1995), Geodetic determination of the kinematics of central Greece with respect to Europe, J. Geophys. Res., 100, 12,675– 12, 690.

Le Pichon, X., N. Chamot-Rooke, C. Rangin, and A. M. C. Sengor (2003), The North Anatolian fault in the Sea of Marmara, J. Geophys. Res., 108(B4), 2179, doi:10.1029/2002JB001862.

Louvari E.. Kiratzi A.. Papazachos B.. Hatzidimitriou (2001). Fault-plane solutions determined by waveform modelling confirm tectonic collision in the eastern Adriatic. Pure appl. Geophys.. 158 1313-1637.

Mantovani, E., D. Babbucci, D. Arbarello, and M. Mucciarelli (1990), Deformation pattern in the central Mediterranean and behavior of the African/Adriatic promontory, Tectonophysics, 179, 63– 79.

Mantovani, E., Albarello, D., Babbucci, D. & Tamburelli, C., (1997), Recent/ Present tectonic processes in the Italian region and their relation with seismic and volcanic activity, Ann. Tecton., 11, 27–57.

Markusic, S., Herak, D., Ivancic, I., Sovic, I., Herak, M., and Prelogovic, E., (1998), Seismicity of Croatia in the period 1993–1996 and the Stone-Slano earthquake of 1996: Geofizika, v. 15, p. 83–101.

Mazzoli, S., and M. Helman (1994), Neogene patterns of relative plate motion of Africa-Europe: Some implications for recent central Mediterranean tectonics, Geol. Rundsch., 83, 464– 468.

McCarthy, D.D., and G. Petit (2004), IERS Conventions (2003), IERS Technical Note 32, Bundesamt fur Kartographie und Geodasie, Franfkurt am Main.

McClusky S., S. Balassanian, A. Barka, C. Demir, S. Ergintav, I. Georgiev, O. Gurcan, O. Hamburger, K. Hurst, H. Kahle, K. Kastens, G. Kekelidze, R. King, V. Kotzev, O. Lenk, S. Mahmoud, A. Mishin, M. Nadariya, A. Ouzounis, D. Paradissis, Y. Peter, M. Prilepin, R. Reilnger, I. Sanli, H. Seeger, A. Tealeb, M. Toksoz, G. Veis. Global (2000), Positioning System Constraints on Plate Kinematics and Dynamics in the Eastern Mediterranean and Caucasus. Journal of Geophysical Research – Solid Earth – Vol. 105, No.B3.

McKenzie D (1970), Plate tectonics of the Mediterranean region, Nature, 226, 239–243.

McKenzie, D (1972), Active tectonics of the Mediterranean region, Geophys. J.R. Astr. Soc., 30(2), 109–185.

McKenzie, D. (1978a), Some remarks on the development of sedimentary basins, Earth Planet. Sci. Lett., 40(1), 25–32, doi:10.1016/0012-821X (78)90071-7.

McKenzie D. (1978b), Active tectonics of the Alpine-Himalayan belt: the Aegean Sea and surrounding regions (tectonics of Aegean region). Geophys. J.R. Astr. Soc., 55, 217–254.

McKenzie, D. P., and J. A. Jackson (1983), The relationship between strain rates, crustal thickening, paleomagnetism, finite strain and fault movements within a deforming zone, Earth Planet. Sci. Lett., 65, 182–202.

McKenzie, D., and J. Jackson (1986), A block model of distributed deformation by faulting, J. Geol. Soc., 143, 349–353, doi:10.1144/gsjgs.143.2.0349.

Melbourne, W. G. (1985), The Case for Ranging in GPS Based Geodetic Systems, in Proceedings of the 1st International Symposium on Precise Positioning with the Global Positioning System, edited by Clyde Goad, pp. 373–386, US Department of Commerce, Rockville, Maryland.

Meade, B. J., B. H. Hager, S. C. McClusky, R. Reilinger, S. Ergintav, O. Lenk, A. Barka, and H. Ozener (2002), Estimates of seismic potential in the Marmara Sea region from

block models of secular deformation constrained by Global Positioning System measurements, Bull. Seismol. Soc. Am., 92, 208–215.

Meertens, C., C. Alber, J. Braun, C. Rocken, B. Stephens, R. Ware, M. Exner and P. Kolesnikoff (1996), Field and anechoic chamber tests of GPS antennas, in Proceedings of IGS Analysis Center Workshop, June 1996, Silver Springs, MD, U.S.A., 107-118.

Mele, G. (2001), The Adriatic lithosphere is a promontory of the Africa Plate; Evidence of a continuous mantle lid in the Ionian Sea from efficient Sn propagation, Geophys. Res. Lett., 28, 431–434.

Melo. V. (1961) Reflet des mouvements neotectoniques dans la construction des terrasses du fleuve Shkumbin sur son trajet Elbasan-Pequin. in Albanian Language. Bul. i USHT. ser. shkenc. nat.. 2. 135-148.

Meyer B., R. Armijo1, D. Dimitrov. Active faulting in SW Bulgaria: possible surface rupture of the 1904 Struma earthquakes. Geophys. J. Int. (2002) 148, 246–255, 2001.

Miller, M.M., T. Melbourne, D.J. Johnson and W.Q. Sumner (2002), Periodic slow earthquakes from the Cascadia subduction zone, Science, 295 (5564), 2423.

Mountrakis D., M. Tranos, C. Papazachos, E. Thomaidou, E. Karagianni and D. Vamvakaris (2006), Neotectonic and seismological data concerning major active faults, and the stress regimes of Northern Greece, Geological Society, London, Special Publications, v. 260; p. 649-670.

Nakov, R., Kotzev, V., Burchfiel, B.C., King, R.W., (2001). GPS data on the active tectonics of the Bulgarian Rhodopes. Geologica Balkanica 31 (1–2), 123– 125.

Niell, A. E. (1996), Global Mapping Functions for the Atmosphere Delay at Radio Wavelengths, Journal of Geophysical Research, 101(B2), pp. 3227–3246.

Nocquet, J. M., and E. Calais (2003), Crustal velocity field of western Europe from permanent GPS array solutions, 1996–2001, Geophys. J. Int., 154, 72– 88, doi:10.1046/j.1365-246X.2003.01935.x.

Nyst, M., Thatcher, W., (2004). New constraints on the active tectonic deformation of the Aegean. JGR 109 (B11), B11406.

Oldow. J. S.. et al. (2002), Active fragmentation of Adria. the north Africa promontory. central Mediterranean orogen, Geology. 30. 779– 782.

Papazachos, C.C., Kiratzi, A.A., (1996). A detailed study of the active crustal deformation in the Aegean and surrounding area. Tectonophysics 253 (1–2), 129–153.

Peter, Y., Kahle, H.-G., Cocard, M., Veis, G., Felekis, S., Paradissis, D., (1998), Establishment of a continuous GPS network across the Kephalonia Fault Zone, Ionian Islands, Greece. Tectonophysics 294, 253–260.

Peter, Y., (2000). Present-day crustal dynamics in the Adriatic–Aegean plate boundary zone inferred from continuous GPS-measurements. PhD thesis, no. 13700, Eidgenössische Technische Hochschule ETH Zürich. http://e-collection.ethbib.ethz.ch/show?type=diss&nr=13700.

Plag et al., (1998), Scientific objectives of current and future WEGENER activities, Tectonophysics 294 (1998) 177–223.

Platt, J., Behrmann, J., Cunningham, P., Dewey, J., Helman, M., Parish, M., Shepley, M., Wallis, S., Weston, P., (1989). Kinematics of the Alpine arc and motion history of Adria. Nature 337, 158–161.

Pondrelli, S., A. Morelli, G. Ekström, S. Mazza, E. Boschi, and A. M. Dziewonski, (2002), European-Mediterranean regional centroid-moment tensors: 1997-2000, Phys. Earth Planet. Int., 130, 71-101.

Pondrelli S., A. Morelli, and G. Ekström, (2004), European-Mediterranean Regional Centroid Moment Tensor catalog: solutions for years 2001 and 2002, Phys. Earth Planet. Int., 145, 1-4, 127-147.

Pondrelli, S., S. Salimbeni, G. Ekström, A. Morelli, P. Gasperini and G. Vannucci, (2006) The Italian CMT dataset from 1977 to the present, Phys. Earth Planet. Int. doi:10.1016/j.pepi.2006.07.008, 159/3-4, pp. 286-303.

Pondrelli S., Salimbeni S., A. Morelli, G. Ekström and Boschi E., (2007), European-Mediterranean Regional Centroid Moment Tensor catalog: Solutions for years 2003 and 2004, Phys. Earth Planet. Int., 164, 1-2, 90-112.

Reilinger, R., et al. (2006), GPS constraints on continental deformation in the Africa-Arabia-Eurasia continental collision zone and implications for the dynamics of plate interactions, J. Geophys. Res., 111, B05411, doi:10.1029/2005JB004051.

Rosenbaum, G., G. S. Lister, and C. Duboz (2004), The Mesozoic and Cenozoic motion of Adria (central Mediterranean): A review of constraints and limitations, Geodin. Acta, 17, 125– 139.

Roure F.. S. Nazaj. I. Fili. J.P. Cadet. K. Mushka. M. Bonneau. (2004) Kinematic evolution and Petroleum systems-an appraisal of the Outer Albanides. AAPG memoir 82. 474-493.

Selvaggi, G., and A. Amato (1992), Subcrustal earthquakes in the northern Apennines (Italy): Evidence for a still active subduction?, Geophys. Res. Lett., 19, 2127–2130.

Serpelloni. E.. Anzidei. M.. Baldi. P.. Casula. G. & Galvani. A., (2005) Crustal velocity and strain-rate fields in Italy and surrounding regions: new results from the analysis of permanent and non-permanent GPS networks. Geophysical Journal International 161 (3). 861-880. doi: 10.1111/j.1365-246X.2005.02618.x.

Serpelloni, E., G. Casula, A. Galvani, M. Anzidei, and P. Baldi, (2006), Data analysis of permanent GPS networks in Italy and surrounding regions: application of a distributed processing approach, Annals of Geophysics, Vol. 49, N. 4/5, August/October 2006.

Sengor, A.M.C., Tuysuz, O., Imren, C., Sakinc, M., Eyidogan, H., Gorur, N., Le Pichon, X., Claude Rangin, C., (2004), The North Anatolian Fault. A new look, Ann. Rev. Earth Planet. Sci. 33, 1-75.

Shanov, S., K. Kourtev, G. Nikolov, A. Boykova, B. Rangelov (2001), Seismotectonic characteristics of the western periphery of the Rhodope Mountain region. Geologica Balcanica, 31, 1/2, pp.53-66.

Shaw, B., and J. Jackson (2010), Earthquake mechanisms and active tectonics of the Hellenic subduction zone, Geophys. J. Int., 181(2), 966–984, doi:10.1111/j.1365-246X.2010.04551.x.

Sledzinski J. (Ed.). Reports on Geodesy, 4(49) (2000), Warsaw University of Technology, Warsaw, Poland, 256 p.

Smith, D., R. Kolenkiewicz, J. Robbins, P. Dunn, and M. Torrence (1994), Horizontal crustal motion in the central and eastern Mediterranean inferred from satellite laser ranging measurements, Geophys. Res. Lett., 21, 1979– 1982.

Sonder, L. J., and P. C. England (1989), Effects of a temperature–dependent rheology on large-scale continental extension, J. Geophys. Res., 94(B6), 7603–7619, doi:10.1029/JB094iB06p07603.

Speranza, F., Islami, I., Kissel, C., Hyseni, A., (1995). Palaeomagnetic evidence for Cenozoic clockwise rotation of the external Albanides. Earth Planet. Sci. Lett. 129, 121–134.

Sue, C., F. Thouvenot, J. Fre´chet, and P. Tricart (1999), Widespread extension in the core of the western Alps revealed by earthquake analysis, J. Geophys. Res., 104, 25,611 – 25,622, doi:10.1029/1999JB900249.

Sulstarova. E.. Koçiaj. S. and Aliaj. Sh.., (1980). Seismic regionalization of Albania (in Albanian and in English). Published by Kombinati Poligrafik. Shtypshkronja "Mihal Duri" Tirana.

Sulstarova. E.. Koçiaj. S., (1980). The Dibra (Albania) earthquake of November 30, 1967. Tectonophysics, Vol. 67, issue 3, p 333-343.

Tagari D.. Vergely P.. and Aliaj S. (1993) . Tectonique polyphasee plio-quaternaire en Albanie orientale (region de Korca-Pogradeci). Bulletin de la Société Géologique de France; September 1993; v. 164; no. 5; p. 727-737, 1993.

Taymaz, T., J. A. Jackson, and D. McKenzie (1991), Active tectonics of the north and central Aegean Sea, Geophys. J. Int., 106, 433–490.

Thouvenot, F., and J. Fre´chet (2005), Seismicity at the North-Western Edge of Adria, NATO Science Series, vol. 4, edited by N. Pinter et al., pp. 335–350, Springer, New York.

Tzankov Tz., N. Spassov, G. Nikolov (2000). On the character of the late Paleogene and Neogene relief and landscape building in South West Bulgaria. Reports in Geodesy, Warsaw University Technology, v. 4 (49), p. 137–143.

Vamvakaris, D.A., Papazachos, C.B., Savvaidis, P.D., Tziavos, I.N., Karagianni, E.E., Scordilis, E.M., Hatzidimitriou, P.M., (2003), Stress-field and time-variation of active crustal deformation in the Mygdonia basin based on the joined interpretation of seismological, neotectonic and geodetic data, Geophys. Res. Abstr. 5, 08794.

Vamvakaris, D.A., C.B. Papazachos, E.E. Karagianni, E.M. Scordilis, and P.M. Hatzidimitriou (2006), Small-scale spatial variation of the stress field in the back-arc Aegean area: Results from the seismotectonic study of the broader area of Mygdonia basin (N. Greece), Tectonophysics 417 (2006) 249–267.

Van der Voo, R. (1993), Paleomagnetism of the Atlantic, Tethys and Iapetus Oceans, 44 pp., Cambridge Univ. Press, New York.

Van Hinsbergen D.J.J.. Langereis C.G.. Meulenkamp J.E.. (2005) Revision of the timing. magnitude and distribution of Neogene rotations in the western Aegean region. Tectonophysics 396. 1 –34.

Vatsov, S., (1905). Earthquakes in Bulgaria in 1904 (in Bulgarian). Central Meteorological Survey, Sofia.

Veis, G., H. Billiris, B. Nakos, and D. Paradissis (1992), Tectonic strain in Greece from geodetic measurements, C. R. Acad. Sci. Athens, 67, 129–166.

Ward, S., (1994). Constraints on the seismotectonics of the central Mediterranean from Very Long Baseline Interferometry. Geophys. J. Int. 117, 441–452.

Weber J., M. Vrabec, P. Pavlovčič-Prešeren, T. Dixon, Y. Jiang, B. Stopar (2010), GPS-derived motion of the Adriatic microplate from Istria Peninsula and Po Plain sites, and geodynamic implications, Tectonophysics 483 (2010) 214–222

Williams, S.,Y. Bock and P. Fang (1998), Integrated satellite interferometry: tropospheric noise, GPS estimates and implications for interferometric synthetic aperture radar products, J. Geophys. Res., 103 (B11), 27051-27068, doi: 10.1029/98JB02794.

Wortmann, U.G., Weissert, H., Funk, H. & Hauck, J., (2001). Alpine plate kinematics revisited: the Adria problem, Tectonics, 20, 134–147.

Wortel, M., Spakman, W., (2000). Subduction and slab detachment in the Mediterranean–Carpathian region. Science 290, 1910–1917.

Wubbena, G. (1985), Software Developments for Geodetic Positioning with GPS Using TI 4100 Code and Carrier Measurements, in Proceedings First International Symposium on Precise Positioning with the Global Positioning System, edited by Clyde Goad, pp. 403–412, US Department of Commerce, Rockville, Maryland.

Zagorchev I. (1990), Neotectonic crustal extension in SW Bulgaria. Geologica Balc., 20, 6; 14.

Zagorchev I. (1992a), Neotectonic development of the Struma (Kraistid) Lineament, southwest Bulgaria and Northern Greece. - Geological Magazine, 129, 2; 197-222.

Zagorchev I. (1992b), Neotectonics of the central parts of the Balkan Peninsula: basic features and concepts. - Geologische Rundschau, 81, 3; 635-654.

Zagorchev I. (2001), Southwest Bulgaria, Geological Guidebook, Bulg. Acad. Sci.

Zhang, J., Y. Bock, H. Johnson, P. Fang, S. Williams, J. Genrich, S. Wdowinski and J. Behr (1997), Southern California permanent GPS geodetic array: error analysis of daily position estimates and site velocities, J. Geophys. Res., 102, 18.035-18.055.

Appendix A

Time series parameters

Amplitudes of the annual, semi-annual signals and offsets detected from the analysis of position time-series. For each station (ID code), the annual and semi-annual cosine and sine amplitudes (in mm), the weighted RMS, the epochs of jumps in the time-series and the related offsets are listed for the north, east and vertical components.

Station name	Component	Annual		Semi-annual		WRMS	Offsets		
		SIN [mm]	COS [mm]	SIN [mm]	COS [mm]	[mm]	yyyy/mm/dd [mm]	yyyy/mm/dd [mm]	yyyy/mm/dd [mm]
AJAC	East	-0.080±0.021	-0.029±0.024	0.031±0.022	0.068±0.022	1.365	2008/11/26 -7.62±0.06		
	North	0.582±0.022	0.258±0.024	-0.107±0.023	0.229±0.023	1.142	2008/11/26 1.33±0.06		
	Up	1.524±0.073	0.668±0.081	0.459±0.077	0.244±0.076	4.048	2008/11/26 3.99±0.21		
AMUR	East	-0.150±0.027	0.204±0.027	-0.187±0.027	-0.020±0.027	0.931			
	North	0.378±0.029	0.328±0.030	-0.278±0.029	-0.420±0.029	0.948			
	Up	-0.644±0.120	0.514±0.123	-0.304±0.120	-0.691±0.119	3.026			
ANKR	East	-0.382±0.033	-0.566±0.036	0.022±0.035	-0.076±0.035	1.896	2008/05/06 3.09±0.10		
	North	1.385±0.031	0.775±0.034	-0.110±0.032	-0.205±0.033	1.651	2008/05/06 3.68±0.09		
	Up	0.864±0.137	2.395±0.150	-1.016±0.143	-1.255±0.145	5.628	2008/05/06 -19.48±0.40		
AQUI	East	0.528±0.018	-0.049±0.018	-0.304±0.017	-0.024±0.018	2.275	2009/04/06 7.61±0.05		
	North	0.248±0.019	0.143±0.019	-0.113±0.018	-0.106±0.019	1.983	2009/04/06 -48.83±0.06		
	Up	-1.806±0.067	1.148±0.068	0.664±0.067	0.108±0.067	4.754	2009/04/06 -69.78±0.21		
ARKI	East	0.351±0.052	0.635±0.070	-0.473±0.050	-0.050±0.054	1.315			
	North	1.883±0.057	1.194±0.078	-0.276±0.055	-0.043±0.060	2.029			
	Up	2.470±0.261	1.928±0.349	0.001±0.248	1.506±0.268	6.313			
AUT1	East	-0.246±0.025	-1.553±0.026	0.203±0.025	-0.129±0.025	1.068			
	North	1.266±0.027	0.723±0.028	-0.196±0.027	-0.244±0.027	1.177			
	Up	0.938±0.119	1.252±0.126	-0.091±0.122	-0.377±0.122	4.113			
BACA	East	0.331±0.023	-0.248±0.024	0.050±0.023	-0.167±0.024	1.091			
	North	0.255±0.025	0.477±0.025	0.191±0.025	0.341±0.025	0.912			
	Up	0.188±0.083	-0.249±0.086	-0.505±0.083	0.185±0.084	3.362			
BAIA	East	-0.151±0.021	-0.282±0.022	-0.345±0.021	-0.140±0.021	1.211			
	North	-0.245±0.023	-0.243±0.024	-0.256±0.023	-0.204±0.023	1.209			
	Up	0.436±0.072	-1.171±0.075	-0.660±0.073	0.021±0.073	3.798			
BERA	East	0.564±0.039	-0.599±0.034	0.543±0.034	-0.243±0.039	1.801			
	North	1.204±0.042	1.554±0.037	-0.244±0.037	0.075±0.042	1.593			
	Up	0.901±0.181	2.946±0.158	-0.843±0.160	0.719±0.182	5.512			
BIEL	East	0.398±0.028	0.736±0.029	-0.386±0.028	-0.121±0.028	1.215			
	North	0.227±0.030	-0.049±0.031	0.290±0.030	0.050±0.030	1.241			
	Up	-0.462±0.096	0.432±0.100	0.215±0.097	-0.691±0.096	4.846			
BOLG	East	0.590±0.022	1.349±0.023	-0.381±0.022	-0.906±0.022	3.028	2009/05/15 7.65±0.05		
	North	-0.522±0.024	0.172±0.025	-0.479±0.024	0.211±0.024	2.036			
	Up	2.510±0.079	-1.496±0.082	1.608±0.077	-0.731±0.078	6.973	2009/05/15 -50.67±0.18		

Station name	Component	Annual		Semi-annual		WRMS	Offsets		
		SIN [mm]	COS [mm]	SIN [mm]	COS [mm]	[mm]	yyyy/mm/dd [mm]	yyyy/mm/dd [mm]	yyyy/mm/dd [mm]
BRAS	East	-0.138±0.023	0.413±0.024	0.026±0.024	0.189±0.023	1.302			
	North	-0.255±0.025	0.419±0.026	-0.045±0.025	0.092±0.025	1.769			
	Up	-1.216±0.080	-0.836±0.085	0.995±0.083	-1.195±0.081	3.952			
BRIX	East	-0.045±0.028	0.507±0.032	0.198±0.028	-0.105±0.028	1.210	2009/04/24 -0.74±0.13		
	North	-0.305±0.031	-2.506±0.034	0.736±0.030	0.075±0.030	1.226	2009/04/24 -0.66±0.14		
	Up	0.568±0.099	-1.161±0.110	1.349±0.098	0.007±0.097	4.288	2009/04/24 114.91±0.46		
BSSO	East	0.114±0.024	-0.435±0.025	0.014±0.024	-0.179±0.024	1.467			
	North	0.637±0.026	-0.106±0.027	-0.083±0.026	-0.291±0.026	1.286			
	Up	-0.230±0.100	1.829±0.103	0.070±0.101	-0.760±0.101	4.552			
BUCU	East	0.250±0.017	0.079±0.017	0.114±0.017	0.079±0.017	0.974			
	North	-0.519±0.017	-0.356±0.018	-0.062±0.017	-0.109±0.017	0.927			
	Up	-0.222±0.062	-0.380±0.064	0.082±0.063	0.171±0.063	2.688			
BZRG	East	-0.045±0.016	0.669±0.016	-0.100±0.016	0.005±0.016	1.189	2007/12/12 -1.30±0.04	2009/01/01 -5.01±0.04	
	North	0.445±0.018	1.244±0.018	0.187±0.018	0.088±0.017	1.306	2007/12/12 3.64±0.05	2009/01/01 4.87±0.05	
	Up	-0.695±0.057	-1.247±0.058	0.299±0.058	-0.283±0.057	4.090	2007/12/12 -1.11±0.15	2009/01/01 7.57±0.15	
CAGL	East	-0.446±0.021	-0.411±0.022	-0.105±0.022	0.031±0.021	1.134			
	North	-0.218±0.020	-0.265±0.022	0.010±0.021	-0.017±0.021	0.906			
	Up	1.355±0.073	1.093±0.078	0.086±0.075	0.446±0.075	2.495			
CAGZ	East	-0.308±0.024	-0.085±0.025	-0.352±0.024	0.068±0.024	1.355			
	North	0.033±0.024	-0.217±0.025	-0.032±0.024	0.074±0.024	1.331			
	Up	1.147±0.090	0.446±0.094	-0.014±0.091	0.762±0.091	4.146			
CAME	East	-0.228±0.022	-0.180±0.022	-0.202±0.021	0.219±0.022	1.618			
	North	-0.160±0.023	-0.155±0.024	-0.285±0.023	0.231±0.023	1.513			
	Up	-0.425±0.083	2.352±0.085	0.919±0.082	-0.134±0.083	5.432			
CAMO	East	0.759±0.032	1.131±0.032	0.039±0.032	-0.611±0.032	1.635			
	North	0.098±0.035	1.205±0.036	-0.268±0.036	-0.478±0.036	1.895			
	Up	-0.911±0.151	1.599±0.152	0.940±0.152	-0.912±0.152	7.324			
CCRI	East	0.003±0.036	-0.267±0.033	0.243±0.034	-0.227±0.034	1.417			
	North	0.723±0.038	1.013±0.035	-0.968±0.036	-0.253±0.036	1.704			
	Up	-1.208±0.170	2.825±0.155	0.077±0.162	-0.933±0.160	6.567			
CDRU	East	0.469±0.028	0.965±0.029	-0.148±0.029	0.023±0.028	1.651			
	North	0.867±0.030	1.137±0.031	-0.090±0.031	-0.382±0.030	1.635			
	Up	-1.047±0.123	0.682±0.128	-0.709±0.128	0.087±0.122	4.366			
CETR	East	0.646±0.049	0.156±0.038	0.094±0.040	0.001±0.043	1.202			
	North	0.396±0.053	0.757±0.040	-0.244±0.043	-0.022±0.046	1.522			
	Up	1.198±0.225	2.362±0.172	-0.169±0.186	-0.635±0.198	6.287			

Station name	Component	Annual		Semi-annual		WRMS	Offsets		
		SIN [mm]	COS [mm]	SIN [mm]	COS [mm]	[mm]	yyyy/mm/dd [mm]	yyyy/mm/dd [mm]	yyyy/mm/dd [mm]
COMO	East	-0.799±0.020	-1.727±0.020	0.231±0.020	0.041±0.020	1.128			
	North	-0.090±0.021	-0.914±0.021	0.345±0.021	0.013±0.021	1.427	2005/12/15 -3.70±0.05		
	Up	-0.334±0.069	-1.406±0.068	0.680±0.068	-0.683±0.068	3.761	2005/12/15 -5.61±0.18		
COST	East	0.513±0.027	-0.663±0.029	-0.089±0.028	-0.121±0.028	1.318			
	North	1.296±0.028	0.987±0.030	-0.137±0.028	-0.176±0.029	0.894			
	Up	-0.610±0.108	1.457±0.115	-0.609±0.110	-0.633±0.112	3.488			
CRLM	East	-0.132±0.045	-1.291±0.038	0.097±0.038	0.040±0.040	1.316			
	North	1.086±0.049	-0.861±0.041	-0.635±0.041	-0.278±0.043	1.952			
	Up	0.874±0.213	0.332±0.180	-0.024±0.181	-0.815±0.189	6.766			
CUCC	East	0.210±0.032	1.332±0.036	-0.044±0.034	0.192±0.033	1.606			
	North	-0.263±0.034	0.365±0.039	-0.281±0.037	-0.210±0.036	1.666			
	Up	-0.363±0.146	-0.109±0.165	-0.870±0.159	0.102±0.153	6.655			
DEVA	East	0.167±0.021	-0.886±0.022	0.029±0.021	-0.278±0.021	1.140			
	North	0.253±0.023	-0.172±0.024	0.034±0.023	0.058±0.023	0.987			
	Up	-0.121±0.078	-0.135±0.080	-0.455±0.078	0.085±0.079	3.921			
DION	East	-0.097±0.048	-0.731±0.050	-0.186±0.047	0.219±0.048	1.899			
	North	0.488±0.052	1.277±0.055	-0.194±0.051	0.562±0.053	2.140			
	Up	0.735±0.238	2.757±0.261	1.529±0.236	0.704±0.246	7.142			
DRAG	East	-1.842±0.033	-2.123±0.034	0.082±0.034	-0.324±0.034	2.925			
	North	1.529±0.036	1.957±0.036	-0.765±0.036	-0.357±0.036	1.916			
	Up	2.281±0.146	1.038±0.146	-1.663±0.147	-0.025±0.148	5.972			
DUBR	East	0.985±0.023	0.529±0.023	-0.539±0.023	-0.258±0.022	2.149	2006/01/01 13.38±0.09		
	North	-1.630±0.025	0.065±0.025	-0.306±0.026	-0.796±0.024	1.909	2006/01/01 13.38±0.10		
	Up	0.807±0.098	0.331±0.099	-0.301±0.102	0.114±0.093	4.055	2006/01/01 12.35±0.40		
EIIV	East	-0.500±0.032	0.658±0.033	-0.540±0.032	-0.330±0.033	1.963			
	North	2.047±0.034	1.206±0.035	0.410±0.033	-0.336±0.034	2.172			
	Up	-0.163±0.148	3.244±0.154	-0.606±0.148	0.417±0.152	4.366			
ELBA	East	-0.012±0.019	0.394±0.020	-0.286±0.020	-0.003±0.019	1.624			
	North	0.430±0.020	-0.068±0.021	-0.036±0.020	0.034±0.020	1.467			
	Up	-0.710±0.068	-0.153±0.072	0.210±0.071	0.043±0.069	5.047			
ENAV	East	0.225±0.024	0.354±0.024	-0.021±0.024	-0.069±0.024	1.007			
	North	0.744±0.026	0.697±0.026	-0.054±0.026	-0.162±0.026	1.277	2006/01/01 1.70±0.04	2007/04/30 -2.70±0.07	
	Up	2.150±0.103	1.905±0.106	1.037±0.104	0.266±0.103	4.697	2006/01/01 11.00±0.17	2007/04/30 -8.63±0.28	
EYPA	East	0.555±0.036	-0.354±0.039	-0.015±0.037	-0.243±0.035	1.654			
	North	0.581±0.039	1.834±0.043	-0.397±0.041	-0.186±0.039	2.029			
	Up	0.193±0.179	2.953±0.198	1.055±0.185	-0.075±0.176	7.322			

Station name	Component	Annual		Semi-annual		WRMS	Offsets		
		SIN [mm]	COS [mm]	SIN [mm]	COS [mm]	[mm]	yyyy/mm/dd [mm]	yyyy/mm/dd [mm]	yyyy/mm/dd [mm]
FRES	East	-0.596±0.027	-0.128±0.028	0.083±0.029	-0.130±0.026	1.044			
	North	0.285±0.029	0.445±0.031	-0.376±0.032	-0.104±0.029	1.413			
	Up	-0.729±0.111	1.057±0.116	-0.104±0.120	-0.712±0.109	6.001			
GENO	East	0.166±0.017	0.492±0.017	-0.002±0.017	-0.027±0.017	0.968			
	North	0.445±0.017	-0.048±0.018	0.046±0.018	0.110±0.018	0.903			
	Up	-0.782±0.055	-0.025±0.057	0.408±0.056	-0.219±0.056	2.904			
GLSV	East	-0.463±0.020	-0.750±0.021	0.103±0.021	0.178±0.021	1.495	2007/11/13 3.58±0.06		
	North	-0.004±0.021	-1.128±0.022	0.042±0.021	0.272±0.021	1.406	2007/11/13 -7.11±0.06		
	Up	-0.616±0.065	-2.237±0.067	-0.510±0.065	-0.200±0.066	3.961	2007/11/13 -9.15±0.18		
GOPE	East	-0.574±0.016	-0.141±0.016	-0.040±0.016	0.105±0.016	0.991	2006/07/14 -2.65±0.05		
	North	0.102±0.018	0.264±0.018	0.102±0.018	0.037±0.018	1.195	2006/07/14 5.93±0.05		
	Up	0.231±0.064	-1.762±0.065	-0.033±0.063	-0.083±0.064	4.158	2006/07/14 -2.56±0.18		
GRAS	East	0.362±0.020	0.492±0.021	-0.124±0.020	0.075±0.020	1.227	2003/04/22 5.86±0.05		
	North	0.700±0.021	0.038±0.022	0.046±0.021	0.093±0.021	1.611	2003/04/22 1.73±0.06		
	Up	0.145±0.065	0.410±0.069	0.236±0.067	-0.364±0.066	3.860	2003/04/22 -2.75±0.18		
GRAZ	East	0.192±0.014	0.178±0.014	-0.178±0.014	0.054±0.014	1.106	2005/03/22 9.28±0.03	2005/11/02 3.16±0.04	
	North	0.094±0.015	0.041±0.016	0.083±0.015	0.052±0.016	1.052	2005/03/22 -1.17±0.03	2005/11/02 3.06±0.04	
	Up	-0.059±0.047	-0.624±0.049	-0.331±0.048	0.034±0.048	3.153	2005/03/22 5.54±0.09	2005/11/02 1.17±0.13	
GROG	East	0.465±0.028	0.407±0.027	-0.095±0.027	0.052±0.027	1.039			
	North	0.571±0.030	-0.019±0.029	-0.133±0.029	-0.022±0.029	1.006			
	Up	0.615±0.099	1.068±0.097	0.605±0.096	-0.391±0.098	3.590			
GROT	East	0.182±0.023	0.028±0.023	-0.190±0.023	-0.068±0.023	1.199			
	North	0.462±0.025	0.223±0.025	-0.169±0.025	-0.358±0.025	1.146			
	Up	-1.224±0.098	0.674±0.100	-0.060±0.099	-0.410±0.098	3.800			
GSR1	East	-0.008±0.014	-0.325±0.015	-0.281±0.015	-0.238±0.015	1.255	2008/09/19-2008/12/30 7.63±0.04		
	North	0.426±0.016	-0.135±0.016	0.041±0.016	-0.089±0.016	1.033	2008/09/19-2008/12/30 -1.83±0.04		
	Up	0.267±0.050	-1.292±0.052	-0.057±0.051	-0.455±0.051	3.938	2008/09/19-2008/12/30 -2.29±0.13		
HMDC	East	0.048±0.036	0.901±0.037	-1.103±0.037	-0.395±0.036	1.900			
	North	-0.268±0.039	0.282±0.039	-0.010±0.039	-0.401±0.038	1.321			
	Up	2.315±0.171	1.793±0.171	-0.220±0.172	-0.019±0.168	5.094			
IENG	East	0.351±0.020	1.220±0.020	-0.232±0.020	-0.396±0.020	1.283			
	North	-0.573±0.021	0.233±0.022	0.449±0.021	0.096±0.021	1.566			
	Up	-0.903±0.068	-1.301±0.069	0.834±0.068	-0.351±0.068	3.922			
IGMI	East	0.258±0.030	0.364±0.029	-0.163±0.029	-0.089±0.028	0.987	2008/12/03 -4.43±0.09		
	North	0.472±0.032	1.698±0.031	-0.376±0.031	-0.219±0.030	1.175	2008/12/03 6.90±0.09		
	Up	-1.287±0.108	0.831±0.104	0.208±0.104	0.018±0.102	5.344	2008/12/03 -3.09±0.30		

Station name	Component	Annual		Semi-annual		WRMS	Offsets		
		SIN [mm]	COS [mm]	SIN [mm]	COS [mm]	[mm]	yyyy/mm/dd [mm]	yyyy/mm/dd [mm]	yyyy/mm/dd [mm]
INGP	East	-0.034±0.022	-0.165±0.024	-0.113±0.023	-0.186±0.022	1.951	2007/03/16 -1.05±0.07	2008/12/30 -0.18±0.05	2009/04/06 6.15±0.05
	North	0.904±0.024	0.622±0.026	0.080±0.024	-0.185±0.023	1.983	2007/03/16 4.35±0.07	2008/12/30 -5.22±0.06	2009/04/06 -31.83±0.06
	Up	0.475±0.087	1.111±0.094	0.798±0.088	0.582±0.085	5.342	2007/03/16 -36.10±0.26	2008/12/30 38.19±0.21	2009/04/06 -23.90±0.21
INGR	East	1.524±0.018	2.761±0.019	-0.205±0.018	-0.233±0.018	1.114	2007/03/16-2009/01/01 8.43±0.03		
	North	0.460±0.019	0.906±0.020	0.047±0.019	-0.035±0.019	1.187	2007/03/16-2009/01/01 -2.70±0.04		
	Up	0.102±0.068	2.097±0.074	0.963±0.071	-0.246±0.071	3.682	2007/03/16-2009/01/01 -61.71±0.14		
ISTA	East	0.481±0.025	0.009±0.026	-0.113±0.026	-0.137±0.026	1.394			
	North	0.987±0.025	1.456±0.026	-0.251±0.025	-0.223±0.025	1.309			
	Up	-0.583±0.109	0.399±0.114	0.092±0.112	-0.822±0.111	4.838			
JOZE	East	0.023±0.016	0.063±0.017	0.026±0.016	-0.187±0.016	1.222			
	North	-0.039±0.017	0.049±0.018	-0.043±0.017	-0.108±0.017	0.944			
	Up	-0.346±0.061	0.570±0.063	-0.171±0.062	0.369±0.061	3.042			
KASI	East	0.963±0.038	1.895±0.045	-0.893±0.044	-0.017±0.040	1.331			
	North	0.787±0.042	1.267±0.049	-0.550±0.048	-0.308±0.044	1.693			
	Up	-2.316±0.187	0.739±0.218	-1.797±0.215	-0.884±0.194	6.260			
KOUN	East	-0.016±0.064	0.566±0.052	-0.207±0.050	0.136±0.057	1.834			
	North	0.405±0.071	1.260±0.058	-0.635±0.056	0.646±0.063	1.994			
	Up	2.789±0.319	6.553±0.261	1.951±0.254	0.660±0.289	7.784			
KROT	East	-0.006±0.031	-0.128±0.032	0.068±0.032	-0.267±0.032	0.942			
	North	0.695±0.034	1.881±0.035	-0.736±0.034	-0.348±0.035	1.552			
	Up	-1.116±0.150	0.531±0.154	-0.410±0.152	-1.134±0.152	6.132			
KUST	East	1.149±0.051	0.582±0.054	-0.283±0.052	-0.024±0.052	1.132			
	North	0.128±0.054	0.612±0.057	-0.152±0.055	0.083±0.056	1.519			
	Up	-3.674±0.227	2.743±0.239	-1.284±0.231	-0.528±0.233	5.758			
LAMA	East	0.092±0.018	-0.323±0.018	-0.071±0.018	-0.158±0.018	1.138	2007/11/17 -0.36±0.04		
	North	-0.265±0.020	0.288±0.020	0.084±0.020	0.339±0.020	1.081	2007/11/17 3.45±0.04		
	Up	1.196±0.078	-2.374±0.081	0.450±0.079	-0.101±0.079	4.863	2007/11/17 15.33±0.18		
LAMP	East	0.093±0.029	0.556±0.030	-0.292±0.029	-0.445±0.029	1.430			
	North	0.363±0.029	0.029±0.030	-0.340±0.029	-0.258±0.029	1.379			
	Up	1.674±0.126	3.324±0.132	0.520±0.128	0.124±0.127	5.278			
LASP	East	-0.168±0.026	0.169±0.028	-0.213±0.026	0.144±0.027	1.082			
	North	0.039±0.028	-0.002±0.030	0.051±0.028	0.064±0.029	1.188			
	Up	0.278±0.091	0.439±0.096	0.203±0.091	-0.617±0.094	3.854			
LATT	East	2.084±0.034	-0.548±0.036	0.037±0.035	0.172±0.036	2.306			
	North	-0.790±0.036	1.185±0.039	-0.289±0.037	-0.339±0.038	1.581			
	Up	0.625±0.158	1.998±0.169	-0.361±0.164	-0.617±0.165	6.815			

Station name	Component	Annual		Semi-annual		WRMS	Offsets		
		SIN [mm]	COS [mm]	SIN [mm]	COS [mm]	[mm]	yyyy/mm/dd [mm]	yyyy/mm/dd [mm]	yyyy/mm/dd [mm]
LEC1	East	-0.200±0.026	0.097±0.028	0.015±0.026	-0.041±0.026	1.284			
	North	-0.021±0.028	-0.656±0.031	-0.068±0.029	-0.158±0.028	1.519			
	Up	-0.708±0.097	-0.385±0.107	1.311±0.100	-0.174±0.097	5.143			
LEMN	East	0.439±0.045	-0.695±0.041	0.335±0.042	-0.588±0.042	1.234			
	North	0.908±0.047	0.441±0.043	-0.413±0.044	-0.037±0.044	1.552			
	Up	0.919±0.216	1.868±0.197	-1.523±0.204	-0.181±0.203	6.328			
LIDO	East	0.509±0.049	1.167±0.048	0.189±0.044	-0.473±0.039	1.999	2006/06/18-2006/10/03	-2.58±0.09	
	North	0.545±0.054	1.783±0.053	0.155±0.048	0.125±0.043	2.251	2006/06/18-2006/10/03	-1.47±0.10	
	Up	-0.083±0.244	1.902±0.241	1.069±0.218	-1.413±0.196	7.232	2006/06/18-2006/10/03	31.27±0.45	
LUZZ	East	0.671±0.036	-0.163±0.041	0.315±0.037	-0.676±0.038	1.340			
	North	0.766±0.039	1.493±0.045	-0.499±0.040	0.076±0.042	1.781			
	Up	-2.733±0.169	-2.487±0.192	0.104±0.172	-2.259±0.178	6.626			
M0SE	East	0.582±0.031	1.736±0.030	-0.562±0.028	-0.059±0.028	1.086	2007/06/19	-1.69±0.08	
	North	0.527±0.033	0.753±0.031	-0.068±0.029	0.019±0.030	1.267	2007/06/19	-1.10±0.08	
	Up	-1.750±0.119	-0.964±0.113	-0.767±0.106	-0.486±0.109	4.964	2007/06/19	9.84±0.30	
MALT	East	0.682±0.038	0.508±0.038	-0.075±0.038	-0.403±0.038	1.088			
	North	0.557±0.040	0.808±0.039	-0.450±0.040	-0.264±0.040	1.134			
	Up	1.015±0.179	1.775±0.176	-0.257±0.177	-0.144±0.177	4.363			
MAON	East	0.257±0.026	0.186±0.026	-0.179±0.026	0.053±0.026	0.962			
	North	0.274±0.027	0.127±0.027	0.020±0.027	-0.011±0.027	1.392			
	Up	0.802±0.096	0.479±0.094	0.571±0.095	-0.683±0.095	3.940			
MATE	East	0.259±0.018	1.240±0.019	-0.309±0.018	-0.067±0.018	1.394	2008/11/24	-5.54±0.04	
	North	0.035±0.020	0.753±0.020	-0.342±0.020	-0.157±0.020	1.408	2008/11/24	2.43±0.05	
	Up	0.154±0.082	1.691±0.085	-0.209±0.083	-0.670±0.082	4.243	2008/11/24	-2.77±0.20	
MEDI	East	1.598±0.017	-0.541±0.018	-0.292±0.017	0.228±0.017	2.118			
	North	-0.944±0.018	0.001±0.019	0.341±0.018	-0.345±0.018	1.806			
	Up	-1.652±0.058	-0.943±0.062	0.758±0.060	-0.365±0.060	3.473			
MILO	East	-0.786±0.029	-0.102±0.030	0.700±0.030	-0.144±0.029	1.887			
	North	1.006±0.029	0.514±0.031	-0.088±0.030	-0.268±0.030	1.790			
	Up	1.935±0.123	2.266±0.130	-0.684±0.126	-0.182±0.125	4.918			
MOCO	East	0.204±0.028	0.164±0.029	-0.069±0.028	-0.415±0.028	1.371			
	North	0.785±0.030	0.525±0.031	-0.502±0.031	-0.341±0.030	1.685			
	Up	-0.781±0.118	0.203±0.122	0.325±0.121	-0.522±0.120	6.094			
MODE	East	-0.397±0.026	-0.889±0.026	0.116±0.027	0.052±0.026	0.878			
	North	0.578±0.028	-1.022±0.028	-0.006±0.029	0.011±0.028	1.153			
	Up	-0.820±0.092	-3.401±0.091	0.066±0.094	-0.872±0.091	5.479			

Station name	Component	Annual		Semi-annual		WRMS	Offsets		
		SIN [mm]	COS [mm]	SIN [mm]	COS [mm]	[mm]	yyyy/mm/dd [mm]	yyyy/mm/dd [mm]	yyyy/mm/dd [mm]
MONC	East	-0.365±0.027	0.457±0.027	-0.152±0.027	-0.073±0.027	1.063			
	North	0.276±0.029	-0.767±0.029	0.110±0.029	0.029±0.029	1.187			
	Up	1.005±0.094	0.683±0.095	0.793±0.095	-0.623±0.095	4.525			
MOPS	East	-0.616±0.027	-0.771±0.028	0.000±0.028	-0.069±0.028	0.974			
	North	-0.047±0.029	0.378±0.030	0.004±0.031	-0.030±0.030	1.084			
	Up	-1.276±0.095	-4.581±0.098	-0.426±0.099	-0.982±0.096	5.555			
MRGE	East	-0.644±0.029	-0.179±0.033	-0.098±0.031	0.197±0.030	1.385			
	North	0.580±0.031	0.111±0.035	0.175±0.033	-0.216±0.032	1.408			
	Up	-0.587±0.104	0.761±0.117	0.228±0.111	-0.360±0.107	5.869			
MRLC	East	-0.061±0.025	-0.499±0.025	-0.178±0.025	-0.174±0.025	1.912			
	North	-0.568±0.027	-0.376±0.027	-0.162±0.027	-0.398±0.026	2.454			
	Up	-2.072±0.108	0.549±0.109	-0.357±0.109	-0.185±0.107	4.750			
MSEL	East	0.122±0.020	0.072±0.021	-0.186±0.020	-0.066±0.020	1.084			
	North	-0.546±0.022	-0.127±0.023	0.149±0.022	-0.055±0.022	1.163			
	Up	-0.423±0.071	-0.438±0.075	0.876±0.072	-1.028±0.072	4.007			
MSRU	East	-0.046±0.032	0.259±0.033	-0.221±0.032	-0.330±0.032	1.500			
	North	0.549±0.034	1.032±0.035	-0.215±0.035	-0.475±0.034	1.125			
	Up	-0.241±0.150	1.229±0.154	-0.613±0.151	-0.238±0.150	3.954			
MURB	East	-2.322±0.023	-0.857±0.023	0.110±0.023	0.267±0.022	1.659			
	North	2.252±0.025	2.082±0.024	-0.986±0.025	-0.521±0.024	2.050			
	Up	0.350±0.085	-0.050±0.083	0.537±0.085	-0.867±0.083	3.383			
NICO	East	0.187±0.044	-0.795±0.047	0.120±0.046	-0.414±0.045	2.231			
	North	0.658±0.040	1.892±0.043	0.148±0.042	-0.231±0.041	2.573			
	Up	2.814±0.186	4.765±0.201	-0.126±0.195	-1.132±0.190	6.559			
NOA1	East	-0.503±0.033	-0.816±0.035	0.475±0.035	-0.187±0.033	1.752			
	North	-0.075±0.036	0.479±0.038	0.080±0.038	-0.300±0.036	2.344			
	Up	2.192±0.169	4.096±0.176	-1.773±0.177	-1.044±0.169	6.188			
NOT1	East	0.839±0.024	0.207±0.026	-0.386±0.025	-0.363±0.025	2.095			
	North	1.000±0.026	0.668±0.027	-0.240±0.026	-0.398±0.026	1.557			
	Up	1.724±0.114	1.755±0.121	0.229±0.118	0.369±0.117	6.053			
NOVA	East	0.113±0.029	0.627±0.030	0.039±0.028	0.108±0.029	1.104			
	North	0.544±0.031	1.302±0.032	0.069±0.030	-0.108±0.031	1.208			
	Up	-0.836±0.099	-0.249±0.103	0.919±0.095	-0.177±0.099	3.412			
ORID	East	-0.451±0.019	-0.068±0.019	-0.069±0.019	-0.090±0.019	1.734	2008/11/06 -1.64±0.05		
	North	0.551±0.021	0.563±0.021	0.008±0.021	-0.043±0.021	1.402	2008/11/06 -4.76±0.05		
	Up	-0.872±0.089	2.615±0.090	0.332±0.088	-1.042±0.089	4.559	2008/11/06 2.33±0.23		

Station name	Component	Annual		Semi-annual		WRMS	Offsets		
		SIN [mm]	COS [mm]	SIN [mm]	COS [mm]	[mm]	yyyy/mm/dd [mm]	yyyy/mm/dd [mm]	yyyy/mm/dd [mm]
OROS	East	-0.451±0.017	-0.792±0.018	-0.291±0.017	-0.151±0.017	1.084	2007/06/08 7.05±0.04		
	North	0.541±0.019	0.543±0.019	0.121±0.019	-0.010±0.019	1.101	2007/06/08 -10.20±0.04		
	Up	0.090±0.061	-0.966±0.061	-0.446±0.061	-0.204±0.060	3.767	2007/06/08 -2.41±0.13		
OSJE	East	0.198±0.016	-0.377±0.017	-0.078±0.017	-0.037±0.017	0.839			
	North	0.522±0.018	-0.587±0.019	0.041±0.018	0.237±0.018	1.081			
	Up	0.235±0.058	-0.747±0.062	-0.084±0.060	-0.201±0.060	3.808			
PACA	East	0.050±0.030	-0.047±0.035	-0.199±0.033	-0.061±0.031	1.302			
	North	0.451±0.032	-0.466±0.038	0.030±0.036	0.005±0.033	1.628			
	Up	0.699±0.130	4.357±0.151	0.496±0.144	-0.209±0.134	8.662			
PADO	East	-0.717±0.017	-1.072±0.018	0.055±0.017	0.144±0.017	1.121			
	North	0.858±0.018	2.593±0.019	-0.189±0.018	-0.238±0.019	1.358			
	Up	0.838±0.057	-0.011±0.061	0.300±0.058	-0.069±0.060	3.906			
PARM	East	-0.520±0.026	-0.112±0.027	-0.249±0.027	0.020±0.026	1.037			
	North	1.167±0.028	1.478±0.029	-0.237±0.028	0.101±0.028	1.079			
	Up	3.781±0.090	-3.629±0.092	1.044±0.092	0.429±0.090	3.825			
PAVI	East	0.443±0.025	2.337±0.026	-0.648±0.025	0.104±0.025	1.284	2005/09/14 2.14±0.07		
	North	-0.095±0.027	-0.989±0.028	-0.012±0.027	-0.055±0.027	1.033	2005/09/14 6.19±0.08		
	Up	0.234±0.087	-0.829±0.091	0.654±0.086	-0.941±0.088	3.454	2005/09/14 -23.12±0.26		
PAZA	East	0.134±0.038	-0.263±0.039	0.494±0.038	-0.255±0.039	1.465			
	North	0.200±0.040	1.276±0.041	-0.624±0.040	-0.053±0.041	1.607			
	Up	-0.271±0.169	2.336±0.174	-1.699±0.169	-1.117±0.174	5.727			
PENC	East	0.210±0.014	0.254±0.014	-0.098±0.014	-0.073±0.014	1.005	2003/05/22-2007/06/25 0.64±0.02		
	North	0.331±0.015	0.181±0.016	-0.011±0.016	0.050±0.016	1.029	2003/05/22-2007/06/25 4.52±0.02		
	Up	-0.448±0.048	-0.758±0.049	0.094±0.048	0.183±0.048	3.979	2003/05/22-2007/06/25 -10.30±0.08		
PESH	East	0.379±0.038	-0.475±0.039	-0.074±0.037	0.035±0.037	1.860			
	North	0.916±0.041	0.792±0.043	-0.119±0.040	0.146±0.040	1.767			
	Up	1.529±0.176	3.361±0.185	2.088±0.170	-2.423±0.175	7.134			
POLV	East	-0.271±0.022	-0.402±0.022	-0.100±0.022	-0.014±0.022	0.974			
	North	0.489±0.022	0.241±0.023	0.096±0.023	0.051±0.023	0.759			
	Up	0.251±0.066	0.117±0.069	0.277±0.067	0.274±0.068	2.743			
PONT	East	0.495±0.039	0.091±0.045	0.579±0.041	-0.748±0.042	2.160			
	North	0.661±0.042	1.107±0.048	-0.956±0.045	-0.270±0.045	1.978			
	Up	0.750±0.197	2.835±0.226	-0.739±0.210	-0.631±0.212	7.147			
PRAT	East	0.418±0.019	0.587±0.019	-0.193±0.019	-0.195±0.019	1.194			
	North	-0.122±0.020	-0.542±0.021	0.065±0.020	0.136±0.020	1.172			
	Up	-0.332±0.067	-0.027±0.069	0.649±0.068	-0.413±0.067	3.910			

Station name	Component	Annual		Semi-annual		WRMS	Offsets		
		SIN [mm]	COS [mm]	SIN [mm]	COS [mm]	[mm]	yyyy/mm/dd [mm]	yyyy/mm/dd [mm]	yyyy/mm/dd [mm]
PRKV	East	0.991±0.046	-0.341±0.044	0.421±0.044	-0.497±0.043	1.572			
	North	0.561±0.048	0.561±0.045	-0.421±0.045	0.070±0.045	1.919			
	Up	-1.033±0.222	1.699±0.211	-1.482±0.211	-1.285±0.209	6.821			
PSAR	East	0.188±0.057	-0.124±0.056	-0.068±0.055	-0.535±0.053	1.730			
	North	0.771±0.063	1.665±0.062	-0.128±0.061	-0.347±0.059	1.917			
	Up	1.932±0.287	3.210±0.283	0.890±0.276	-0.143±0.265	7.015			
RLSO	East	-1.383±0.034	-0.981±0.034	0.628±0.034	-0.151±0.033	1.170	2008/06/09 -4.03±0.10		
	North	1.029±0.038	1.093±0.038	-0.475±0.037	-0.151±0.037	1.012	2008/06/09 7.44±0.11		
	Up	2.516±0.177	3.713±0.175	-1.096±0.174	-1.105±0.172	4.535	2008/06/09 13.23±0.53		
ROVE	East	-0.290±0.024	-0.102±0.024	0.264±0.024	0.226±0.024	1.259			
	North	-0.276±0.025	-1.233±0.025	0.106±0.025	0.191±0.026	1.181			
	Up	0.338±0.082	1.232±0.083	0.873±0.082	-0.685±0.084	4.692			
RSMN	East	0.707±0.023	1.392±0.023	-0.027±0.023	0.102±0.023	1.411			
	North	0.482±0.024	-0.096±0.025	0.362±0.024	0.069±0.024	1.315			
	Up	-0.960±0.081	1.804±0.083	0.685±0.081	-0.248±0.082	4.294			
RSTO	East	0.431±0.017	0.330±0.018	-0.372±0.018	0.011±0.018	1.278	2009/04/06 5.46±0.05		
	North	0.847±0.019	0.735±0.020	0.114±0.019	-0.115±0.019	1.281	2009/04/06 5.66±0.06		
	Up	1.214±0.068	1.342±0.072	-0.086±0.069	-0.148±0.069	3.324	2009/04/06 -0.92±0.21		
SAND	East	0.236±0.036	0.358±0.037	0.210±0.037	-0.236±0.036	1.439			
	North	0.773±0.039	0.769±0.039	-0.478±0.040	-0.552±0.038	1.615			
	Up	-0.666±0.169	2.943±0.169	-1.597±0.172	-0.407±0.166	6.118			
SARA	East	-1.766±0.399	0.215±0.285	-0.350±0.210	0.793±0.165	1.146			
	North	-1.336±0.453	0.865±0.325	-0.290±0.239	0.467±0.188	1.377			
	Up	-6.465±1.587	-5.006±1.214	-1.220±0.874	0.499±0.747	6.052			
SBPO	East	-0.113±0.024	-0.003±0.024	-0.127±0.024	-0.048±0.024	0.840			
	North	-0.105±0.026	-0.354±0.026	0.284±0.026	-0.076±0.026	0.969			
	Up	0.757±0.084	-0.294±0.083	0.074±0.084	-0.363±0.084	3.135			
SERS	East	-0.039±0.030	0.355±0.032	-0.066±0.032	-0.322±0.030	1.346			
	North	0.527±0.033	0.999±0.035	-0.324±0.035	-0.396±0.033	1.272			
	Up	-0.725±0.145	0.380±0.151	-0.264±0.152	0.110±0.145	4.460			
SGIP	East	0.086±0.025	0.466±0.024	-0.158±0.025	0.059±0.025	1.297			
	North	0.559±0.027	0.220±0.026	0.060±0.027	-0.194±0.027	1.456			
	Up	1.502±0.088	-0.127±0.086	1.040±0.089	-0.008±0.087	3.481			
SHKO	East	0.386±0.029	0.234±0.036	-0.221±0.032	-0.059±0.034	0.992			
	North	0.171±0.033	0.903±0.041	0.211±0.036	-0.051±0.039	1.388			
	Up	-0.256±0.135	2.984±0.170	0.393±0.147	0.305±0.160	5.508			

Station name	Component	Annual		Semi-annual		WRMS	Offsets		
		SIN [mm]	COS [mm]	SIN [mm]	COS [mm]	[mm]	yyyy/mm/dd [mm]	yyyy/mm/dd [mm]	yyyy/mm/dd [mm]
SOFA	East	0.335±0.040	-5.077±0.037	0.363±0.037	-0.168±0.036	2.011			
	North	0.285±0.042	3.043±0.040	-0.828±0.040	0.017±0.039	1.936			
	Up	-2.756±0.175	-1.301±0.164	-2.077±0.164	0.542±0.161	6.119			
SOFI	East	0.137±0.019	-0.133±0.020	0.103±0.019	0.128±0.019	1.722			
	North	0.588±0.020	0.346±0.021	-0.245±0.021	-0.174±0.021	1.512			
	Up	0.064±0.083	0.882±0.087	-0.754±0.085	-0.483±0.085	5.102			
SPAN	East	1.693±0.040	-1.424±0.041	0.686±0.039	-0.770±0.040	1.698			
	North	1.358±0.044	-0.877±0.045	-0.515±0.043	-0.611±0.044	2.007			
	Up	1.129±0.201	2.614±0.206	-1.938±0.198	-1.694±0.203	6.682			
SRJV	East	0.438±0.024	0.798±0.023	-0.203±0.023	0.022±0.023	1.374			
	North	0.720±0.026	1.066±0.025	-0.578±0.025	0.045±0.026	1.555			
	Up	-1.347±0.095	0.420±0.093	-0.030±0.093	-0.665±0.094	4.585			
STSV	East	0.654±0.032	0.271±0.034	-0.038±0.033	-0.207±0.032	1.154			
	North	0.635±0.034	1.006±0.037	-0.580±0.036	-0.478±0.035	1.609			
	Up	-1.049±0.151	0.974±0.160	-0.346±0.158	-0.379±0.153	6.478			
STUE	East	5.118±0.027	1.855±0.028	0.090±0.028	-1.671±0.028	2.080			
	North	-0.474±0.029	-0.203±0.030	-0.158±0.030	0.862±0.030	2.439			
	Up	1.375±0.099	1.592±0.101	1.099±0.101	-0.286±0.100	5.348			
SVIN	East	0.497±0.029	0.778±0.030	0.377±0.029	-0.279±0.029	2.135			
	North	0.091±0.031	0.419±0.032	-0.598±0.031	-0.090±0.031	1.810			
	Up	-0.188±0.136	4.044±0.140	-0.770±0.136	-0.361±0.133	5.025	2007/04/30 20.62±0.27	2008/01/01 360.69±0.30	
TEOL	East	-0.217±0.020	0.075±0.020	-0.070±0.020	0.109±0.020	0.931			
	North	0.444±0.022	-0.243±0.022	0.086±0.022	0.010±0.022	0.943			
	Up	0.423±0.070	-0.509±0.071	0.246±0.070	-0.731±0.071	3.348			
TIRA	East	-1.018±0.054	-0.090±0.043	0.522±0.041	0.379±0.044	2.218			
	North	0.915±0.059	0.931±0.048	0.224±0.046	0.226±0.049	1.759			
	Up	5.374±0.258	6.943±0.212	0.327±0.200	-1.789±0.211	7.591			
TOLF	East	2.746±0.024	1.973±0.027	-0.548±0.024	-0.239±0.025	1.521			
	North	-1.269±0.025	0.351±0.028	0.133±0.026	-0.434±0.026	1.233			
	Up	2.638±0.090	1.875±0.103	-0.288±0.093	-0.243±0.095	3.569			
TORI	East	0.348±0.019	1.580±0.020	-0.175±0.019	0.038±0.020	1.181			
	North	-0.171±0.020	-1.416±0.021	0.275±0.020	-0.047±0.021	1.318			
	Up	-0.408±0.066	-0.863±0.070	0.722±0.067	-0.528±0.069	4.171			
TRIZ	East	-1.156±0.027	-0.165±0.029	0.542±0.027	0.278±0.028	1.940			
	North	2.647±0.029	1.885±0.031	-0.528±0.030	-0.478±0.031	1.859			
	Up	0.969±0.134	3.576±0.146	0.895±0.137	-1.449±0.142	5.753			

Station name	Component	Annual		Semi-annual		WRMS	Offsets		
		SIN [mm]	COS [mm]	SIN [mm]	COS [mm]	[mm]	yyyy/mm/dd [mm]	yyyy/mm/dd [mm]	yyyy/mm/dd [mm]
TUBI	East	0.094±0.024	-0.469±0.025	-0.234±0.025	-0.061±0.025	1.599			
	North	0.507±0.024	1.230±0.025	-0.148±0.024	-0.120±0.024	1.351			
	Up	0.560±0.107	2.781±0.110	-0.326±0.108	-0.827±0.108	4.612			
TUC2	East	0.697±0.031	-0.472±0.033	0.005±0.032	-0.362±0.032	1.417			
	North	1.634±0.035	1.328±0.037	-0.448±0.036	-0.472±0.036	1.260			
	Up	2.025±0.166	3.967±0.173	-0.826±0.167	-0.856±0.169	5.107			
TVRN	East	-0.080±0.032	-1.537±0.032	0.403±0.032	-0.035±0.032	1.491			
	North	0.356±0.035	-0.615±0.034	-0.145±0.034	-0.202±0.034	1.502			
	Up	0.880±0.150	2.132±0.146	-0.415±0.148	-0.940±0.148	6.353			
UNFE	East	-0.736±0.022	-1.425±0.023	-0.139±0.023	0.136±0.022	1.253			
	North	-0.385±0.024	0.787±0.026	-0.445±0.025	-0.108±0.024	1.891			
	Up	-0.040±0.081	-2.111±0.085	0.402±0.083	0.132±0.081	4.470			
UNPG	East	0.181±0.017	1.017±0.018	-0.238±0.017	-0.174±0.017	1.485	2006/04/19 -4.42±0.05		
	North	-0.149±0.018	-0.219±0.019	0.047±0.018	0.116±0.018	1.293	2006/04/19 12.89±0.06		
	Up	-0.618±0.063	0.807±0.065	0.614±0.064	0.042±0.063	4.018	2006/04/19 -3.45±0.20		
UNTR	East	0.538±0.031	0.421±0.032	-0.146±0.032	-0.226±0.031	1.475			
	North	-0.512±0.033	-1.047±0.034	0.290±0.034	-0.279±0.033	2.259			
	Up	-2.060±0.116	-0.968±0.121	-0.623±0.121	-0.659±0.117	5.512			
USIX	East	0.223±0.035	0.370±0.034	-0.130±0.034	0.027±0.035	1.218			
	North	0.038±0.036	0.286±0.036	-0.376±0.036	-0.271±0.036	1.573			
	Up	-0.261±0.152	1.614±0.149	-0.736±0.151	0.266±0.151	6.274			
UZHL	East	-0.041±0.015	-0.005±0.015	0.008±0.015	0.064±0.015	0.992			
	North	0.201±0.016	0.556±0.016	-0.009±0.016	0.000±0.016	0.898			
	Up	0.244±0.050	-0.502±0.052	-0.333±0.051	-0.393±0.050	3.099			
VAGA	East	-3.484±0.028	1.201±0.033	-0.910±0.030	0.947±0.030	2.170			
	North	-5.713±0.030	1.527±0.035	-1.744±0.031	1.944±0.032	3.533			
	Up	0.189±0.117	-1.467±0.135	-0.689±0.121	-1.215±0.123	5.759			
VEAR	East	-0.611±0.034	-0.494±0.036	-0.136±0.033	0.116±0.032	0.821			
	North	-0.492±0.038	-1.141±0.040	0.100±0.036	-0.032±0.035	1.108			
	Up	2.595±0.132	6.300±0.137	-1.005±0.126	0.997±0.122	6.244			
VLSM	East	0.204±0.029	-0.239±0.033	-0.054±0.030	-0.200±0.031	1.911			
	North	0.939±0.033	1.888±0.036	-0.116±0.033	-0.349±0.034	1.616			
	Up	0.540±0.151	2.727±0.168	-0.763±0.156	-0.216±0.160	5.127			
VLUC	East	0.028±0.043	0.060±0.054	-0.667±0.047	0.669±0.045	3.585			
	North	1.046±0.047	2.878±0.059	0.412±0.051	0.323±0.049	2.966			
	Up	0.085±0.195	4.737±0.248	-3.491±0.213	-2.876±0.206	8.448			

Station name	Component	Annual		Semi-annual		WRMS	Offsets		
		SIN [mm]	COS [mm]	SIN [mm]	COS [mm]	[mm]	yyyy/mm/dd [mm]	yyyy/mm/dd [mm]	yyyy/mm/dd [mm]
WROC	East	0.272±0.016	0.577±0.016	-0.106±0.016	-0.069±0.016	1.145	2006/09/01-2007/04/13	-10.03±0.03	
	North	0.020±0.018	0.087±0.018	0.274±0.018	0.110±0.018	1.319	2006/09/01-2007/04/13	-2.24±0.04	
	Up	0.133±0.065	-1.822±0.067	-0.022±0.065	0.491±0.065	4.485	2006/09/01-2007/04/13	4.54±0.15	
WTZR	East	0.179±0.014	0.512±0.014	-0.021±0.014	0.036±0.014	0.885			
	North	-0.174±0.015	-0.028±0.015	0.007±0.015	0.061±0.015	1.107			
	Up	-0.315±0.051	-0.569±0.051	-0.585±0.051	0.043±0.051	2.866			
YUND	East	0.483±0.054	0.424±0.052	-0.097±0.051	0.027±0.052	1.204			
	North	1.210±0.057	0.675±0.054	-0.237±0.053	0.497±0.055	1.704			
	Up	-3.071±0.244	0.344±0.230	-1.444±0.227	-0.503±0.234	6.146			
ZIMM	East	0.258±0.017	-0.086±0.017	-0.037±0.017	0.009±0.017	1.044			
	North	-0.110±0.017	-0.010±0.018	0.026±0.017	0.054±0.017	0.966			
	Up	-0.424±0.057	-0.571±0.057	0.220±0.057	-0.710±0.057	2.737			
ZOUF	East	-0.663±0.015	-0.375±0.016	0.091±0.016	0.411±0.015	1.070			
	North	0.644±0.016	0.470±0.017	0.452±0.017	-0.179±0.016	1.385			
	Up	-0.422±0.052	-0.726±0.053	-0.148±0.053	0.323±0.052	3.820			

Appendix B

Position time series

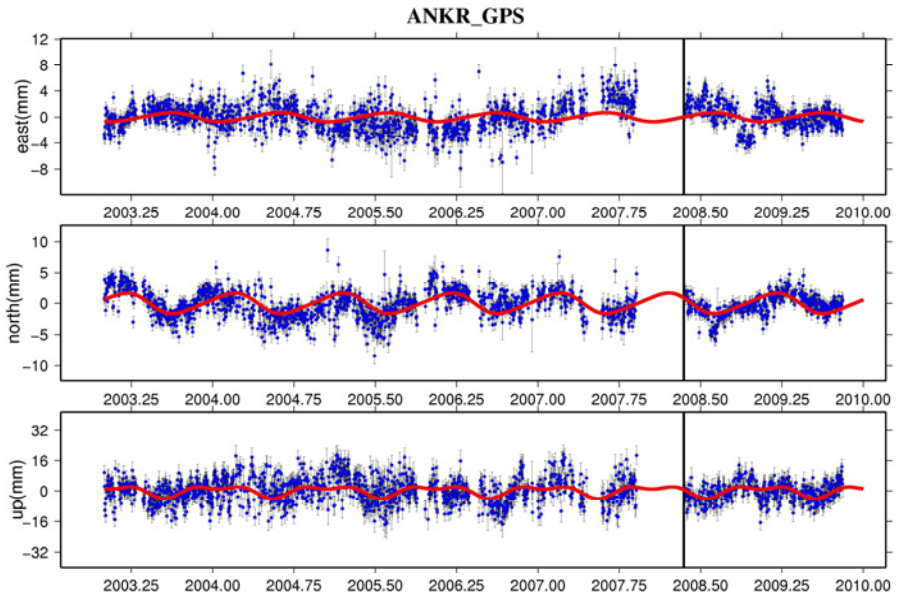
ANKR_GPS
east(mm)
north(mm)
up(mm)
2003.25 2004.00 2004.75 2005.50 2006.25 2007.00 2007.75 2008.50 2009.25 2010.00

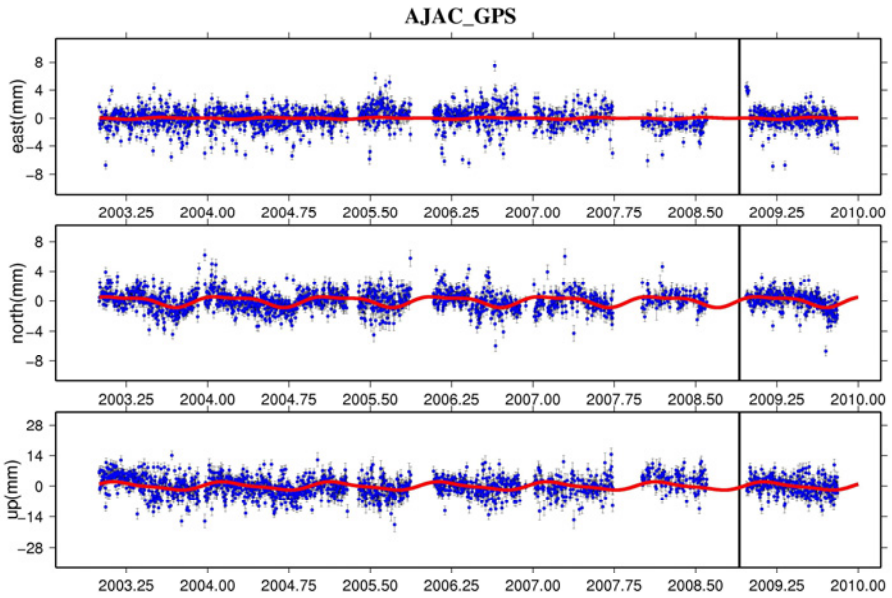
AJAC_GPS
east(mm)
north(mm)
up(mm)
2003.25 2004.00 2004.75 2005.50 2006.25 2007.00 2007.75 2008.50 2009.25 2010.00

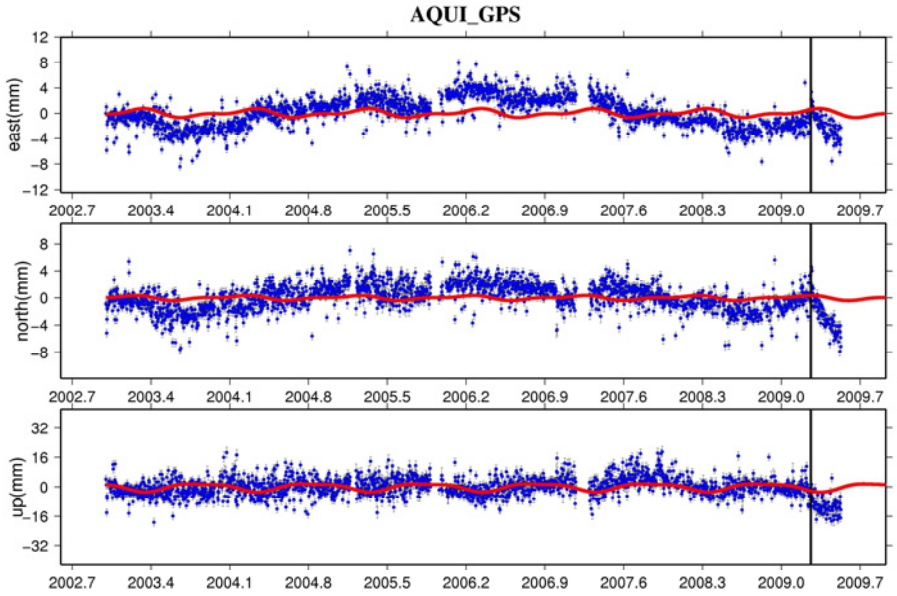
AQUI_GPS
east(mm)
north(mm)
up(mm)
2002.7 2003.4 2004.1 2004.8 2005.5 2006.2 2006.9 2007.6 2008.3 2009.0 2009.7

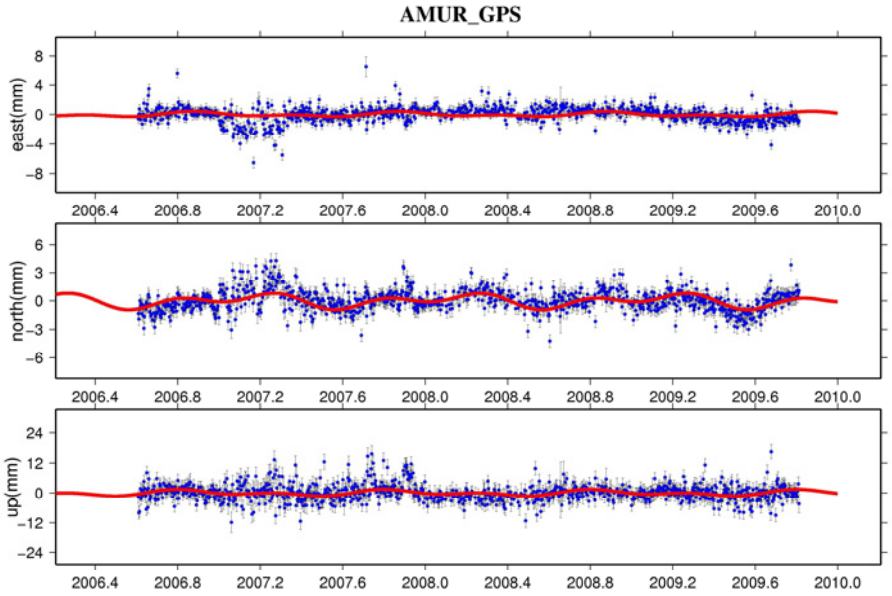
AMUR_GPS
east(mm)
north(mm)
up(mm)
2006.4 2006.8 2007.2 2007.6 2008.0 2008.4 2008.8 2009.2 2009.6 2010.0

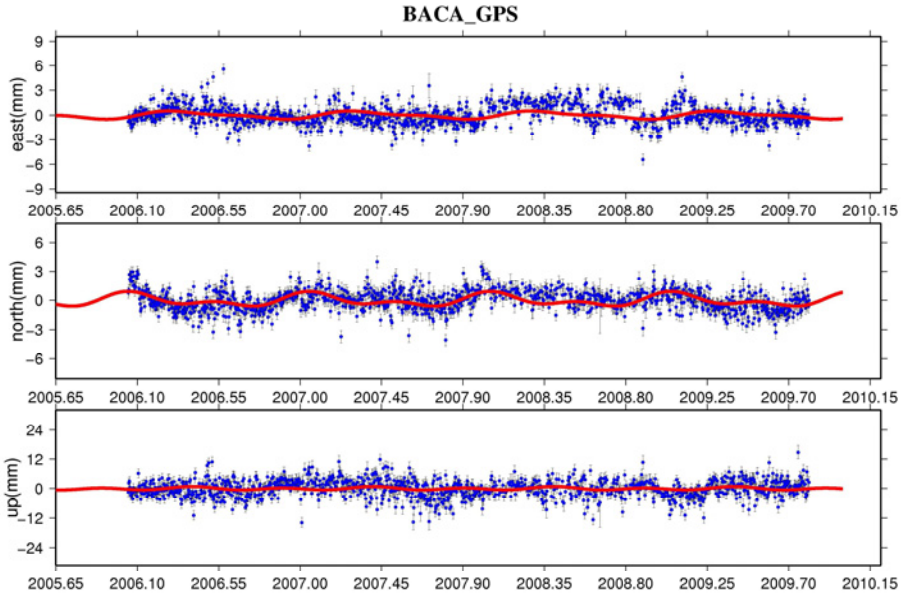
BACA_GPS
east(mm)
north(mm)
up(mm)
2005.65 2006.10 2006.55 2007.00 2007.45 2007.90 2008.35 2008.80 2009.25 2009.70 2010.15

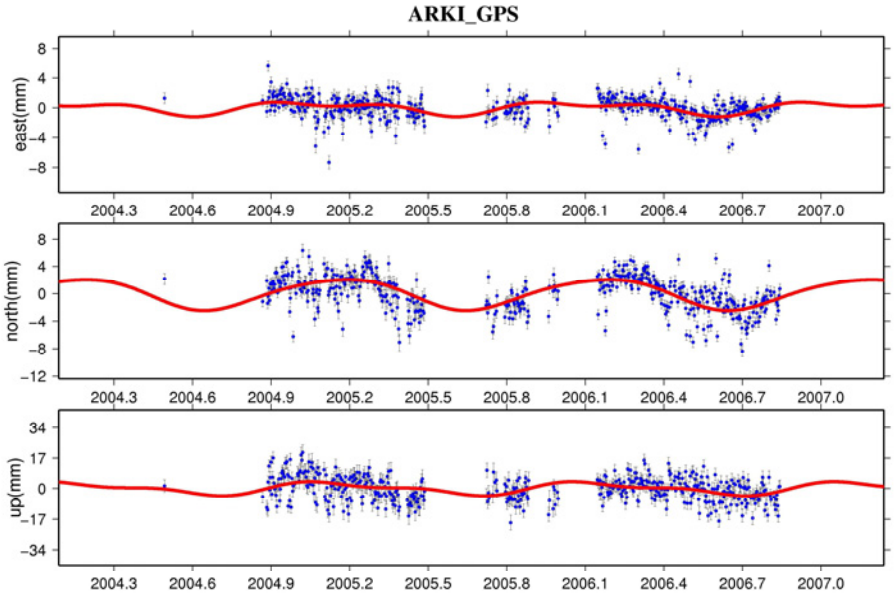
ARKI_GPS
east(mm)
north(mm)
up(mm)
2004.3 2004.6 2004.9 2005.2 2005.5 2005.8 2006.1 2006.4 2006.7 2007.0

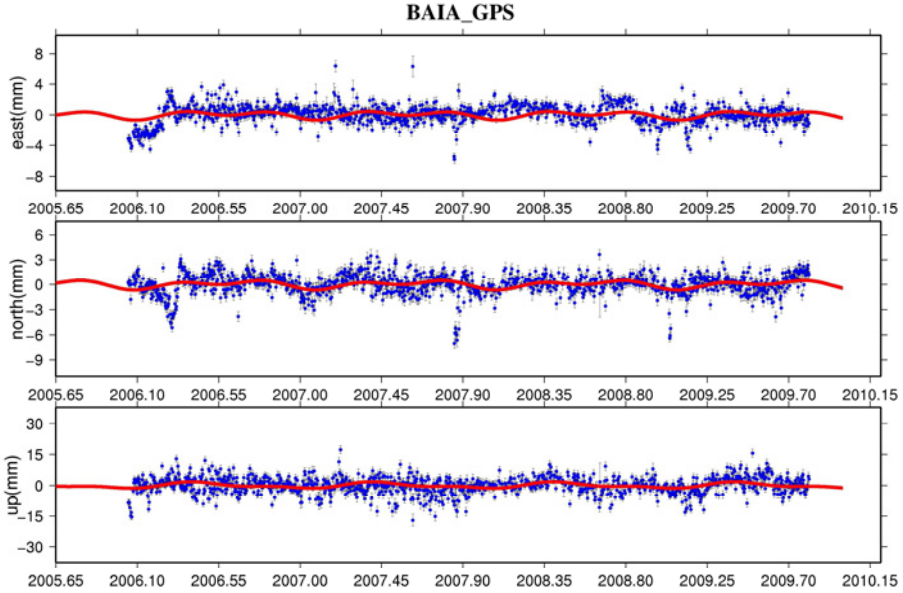
BAIA_GPS
east(mm)
north(mm)
up(mm)
2005.65 2006.10 2006.55 2007.00 2007.45 2007.90 2008.35 2008.80 2009.25 2009.70 2010.15

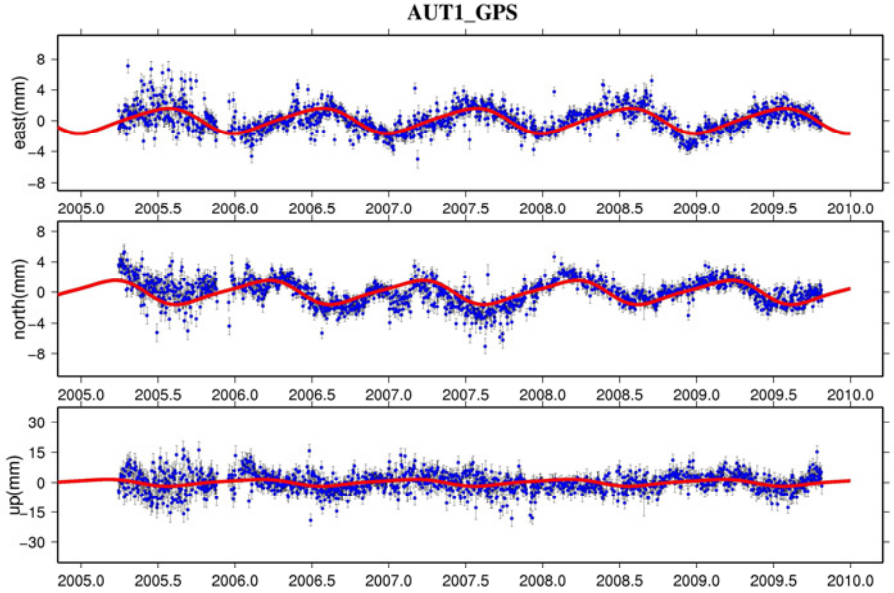
AUT1_GPS
east(mm)
north(mm)
up(mm)
2005.0 2005.5 2006.0 2006.5 2007.0 2007.5 2008.0 2008.5 2009.0 2009.5 2010.0

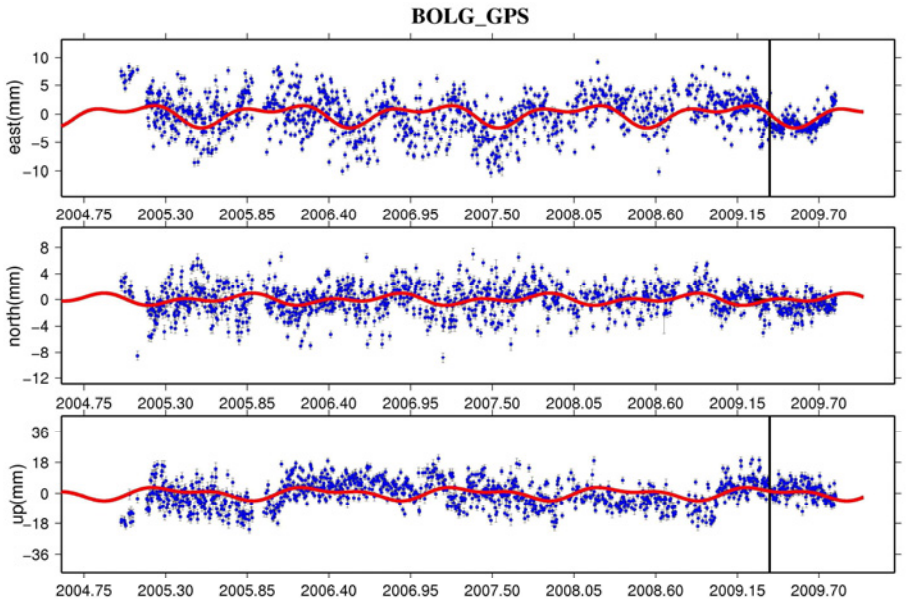
BOLG_GPS
east(mm)
north(mm)
up(mm)

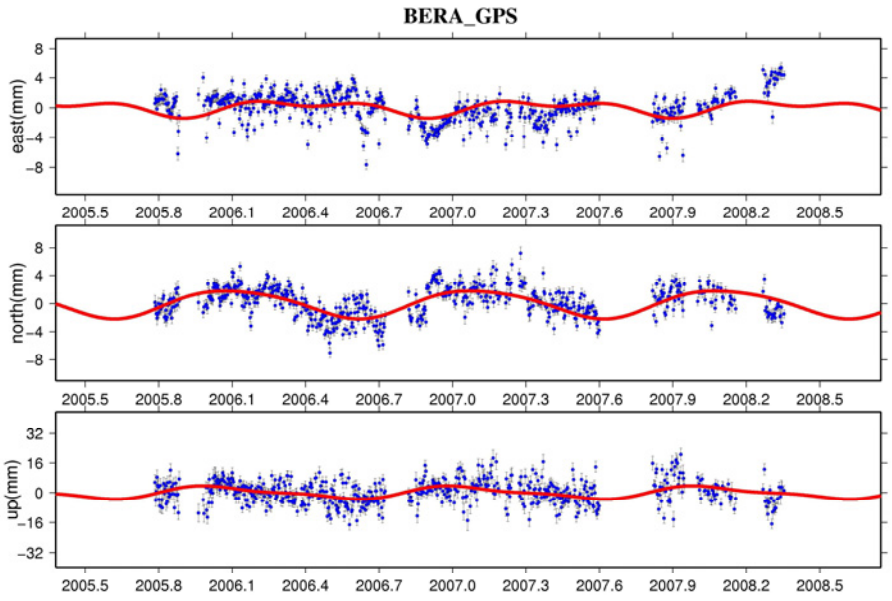
BERA_GPS
east(mm)
north(mm)
up(mm)

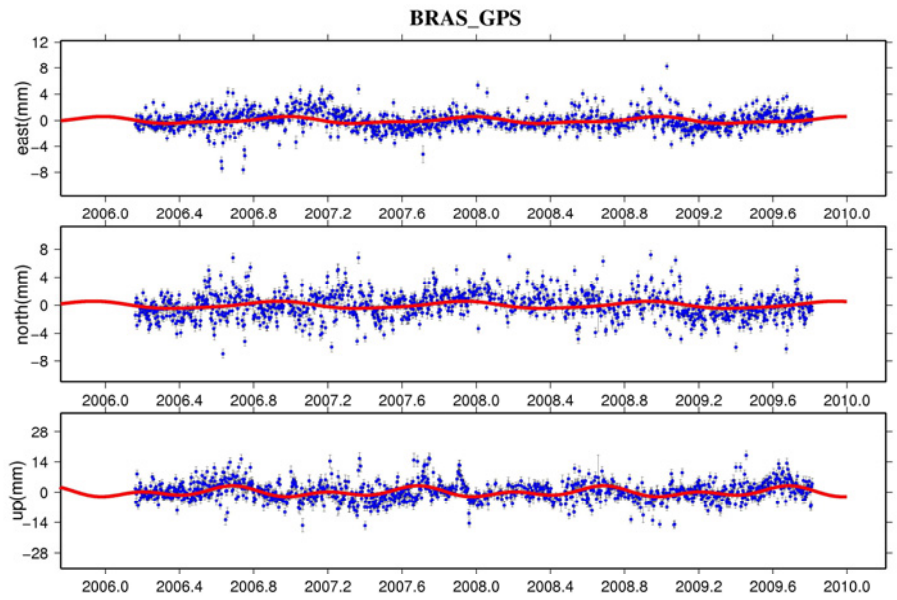
BRAS_GPS
east(mm)
north(mm)
up(mm)

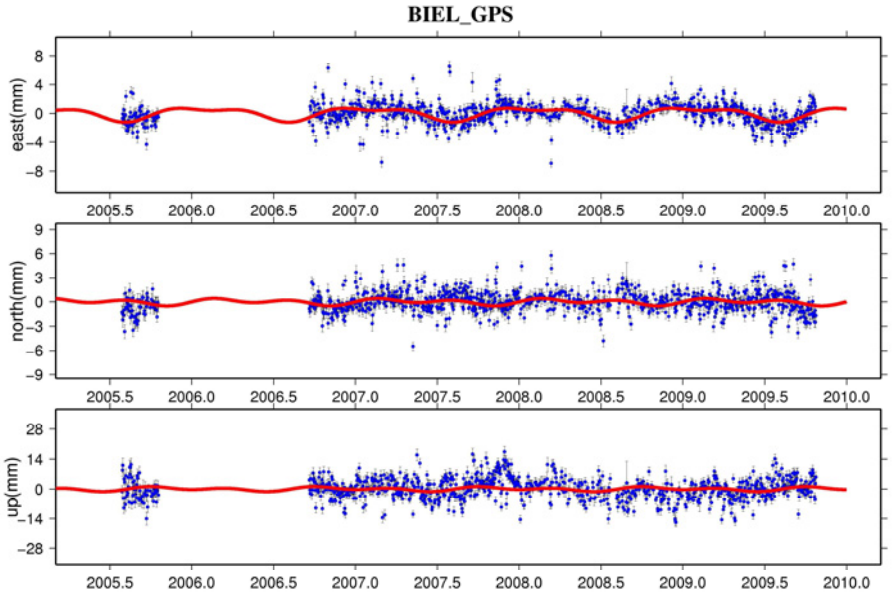
BIEL_GPS
east(mm)
north(mm)
up(mm)

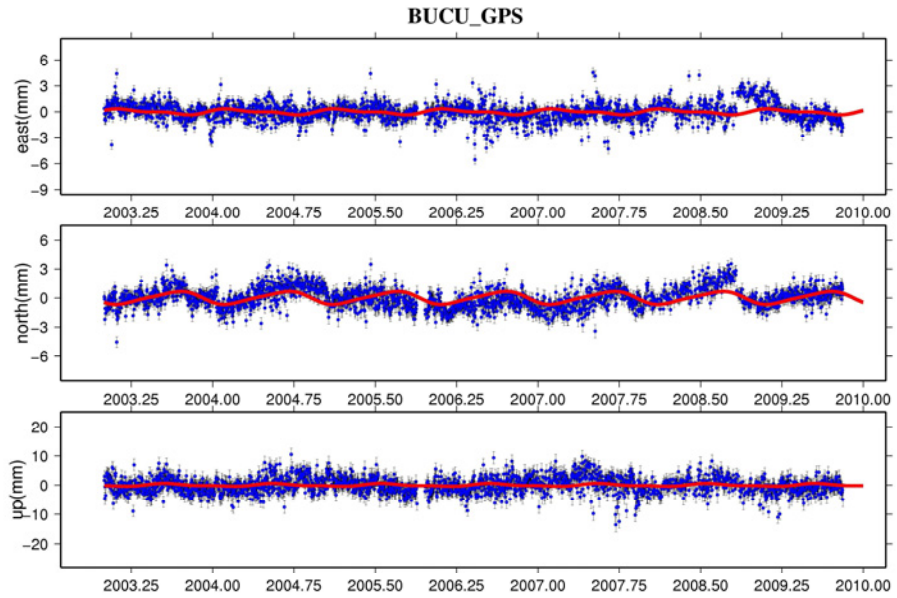
BUCU_GPS
east(mm)
north(mm)
up(mm)
2003.25 2004.00 2004.75 2005.50 2006.25 2007.00 2007.75 2008.50 2009.25 2010.00

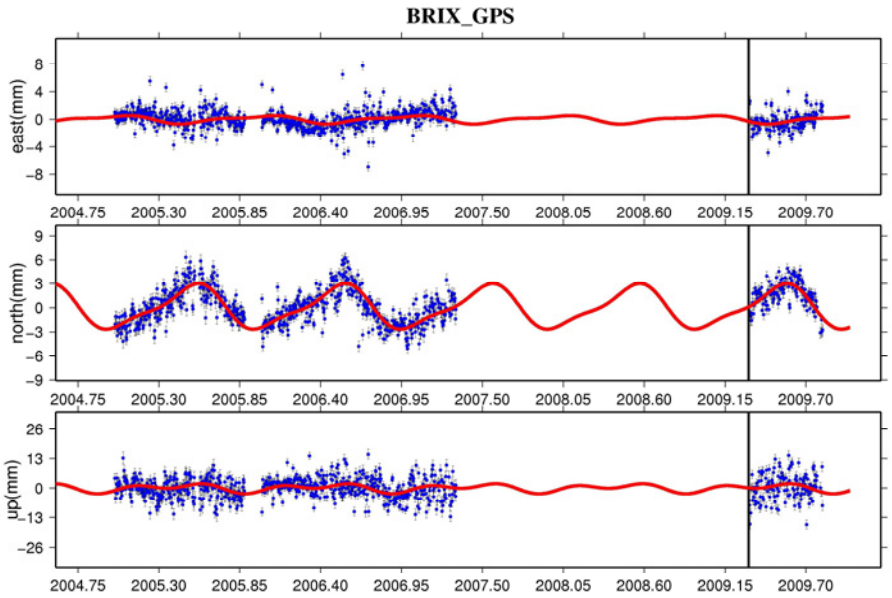
BRIX_GPS
east(mm)
north(mm)
up(mm)
2004.75 2005.30 2005.85 2006.40 2006.95 2007.50 2008.05 2008.60 2009.15 2009.70

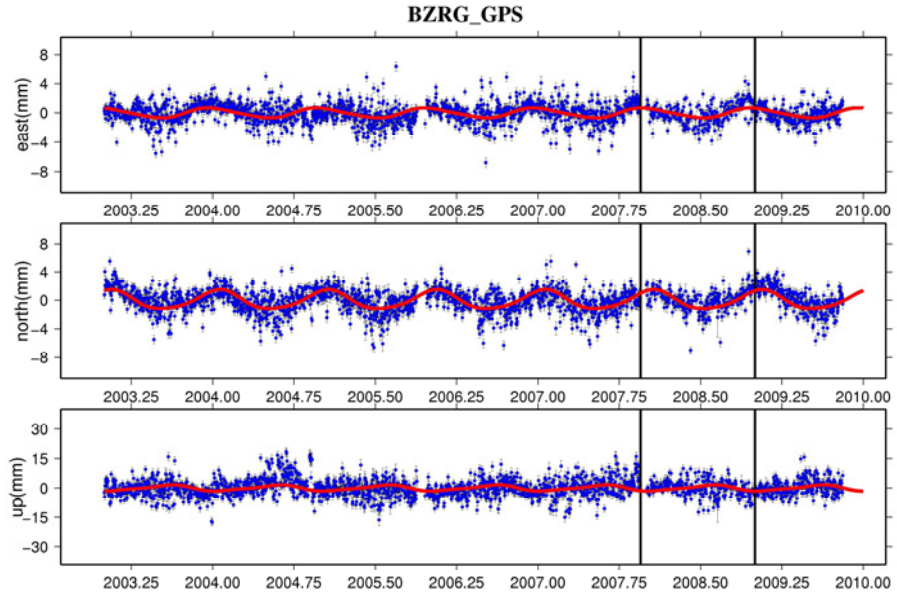
BZRG_GPS
east(mm)
north(mm)
up(mm)
2003.25 2004.00 2004.75 2005.50 2006.25 2007.00 2007.75 2008.50 2009.25 2010.00

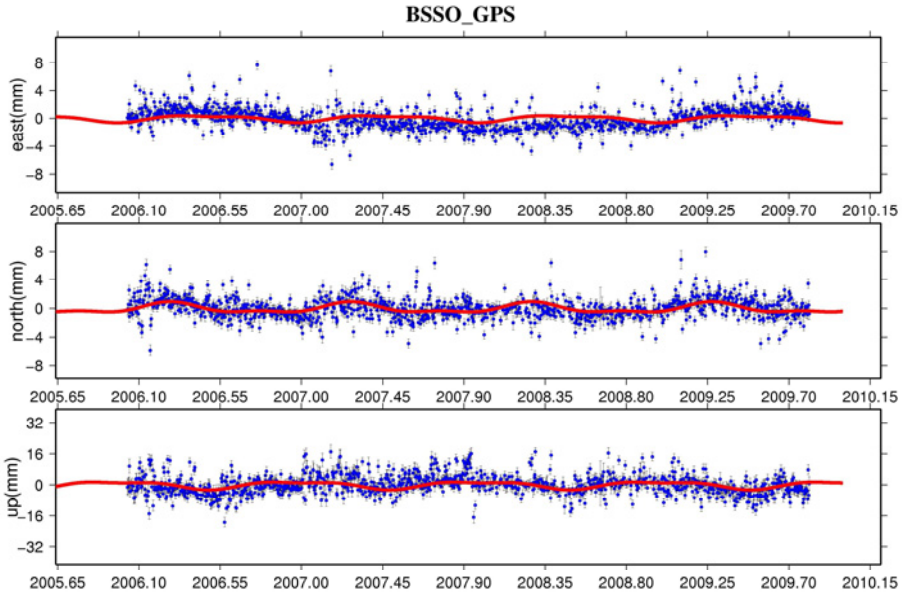
BSSO_GPS
east(mm)
north(mm)
up(mm)
2005.65 2006.10 2006.55 2007.00 2007.45 2007.90 2008.35 2008.80 2009.25 2009.70 2010.15

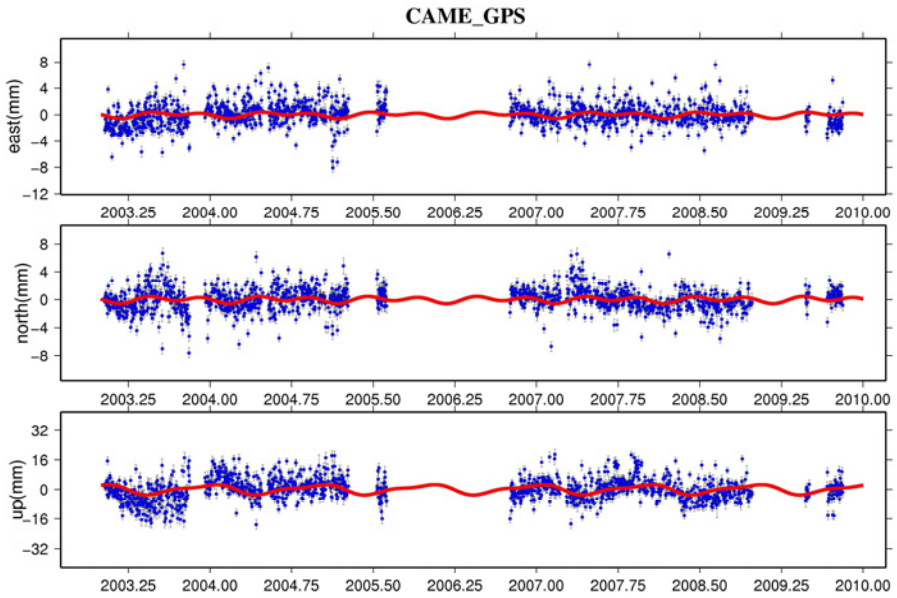
CAME_GPS
east(mm)
north(mm)
up(mm)
2003.25
2004.00
2004.75
2005.50
2006.25
2007.00
2007.75
2008.50
2009.25
2010.00

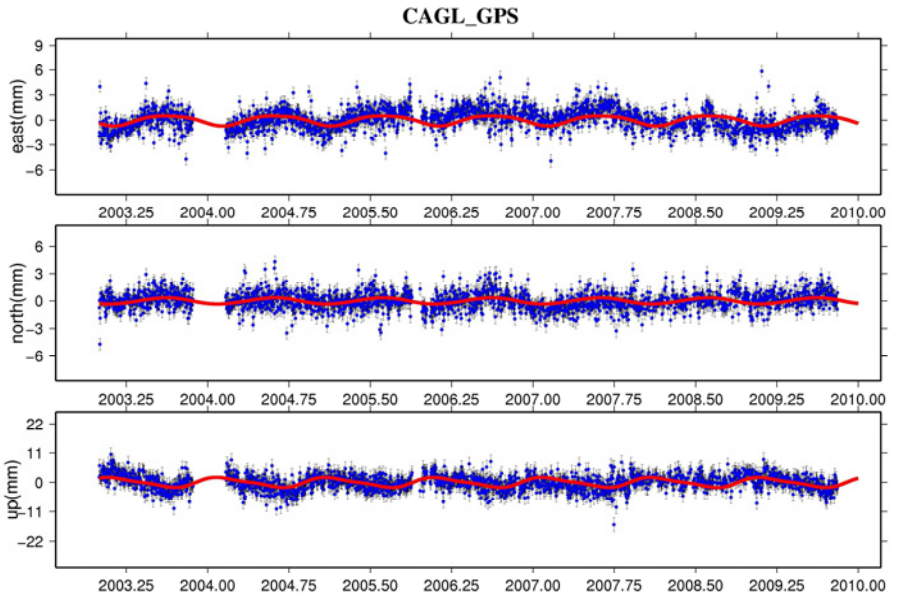
CAGL_GPS
east(mm)
north(mm)
up(mm)
2003.25
2004.00
2004.75
2005.50
2006.25
2007.00
2007.75
2008.50
2009.25
2010.00

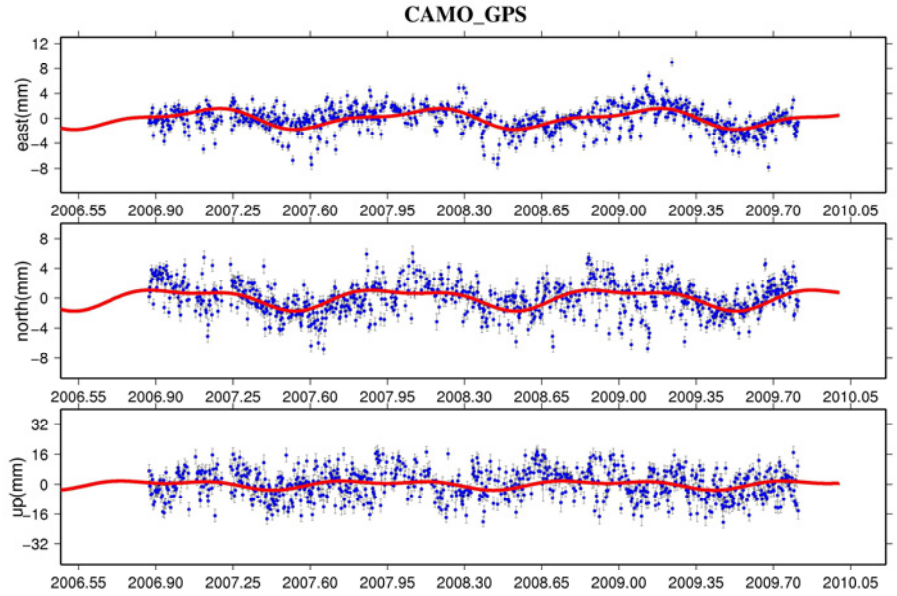
CAMO_GPS
east(mm)
north(mm)
up(mm)
2006.55
2006.90
2007.25
2007.60
2007.95
2008.30
2008.65
2009.00
2009.35
2009.70
2010.05

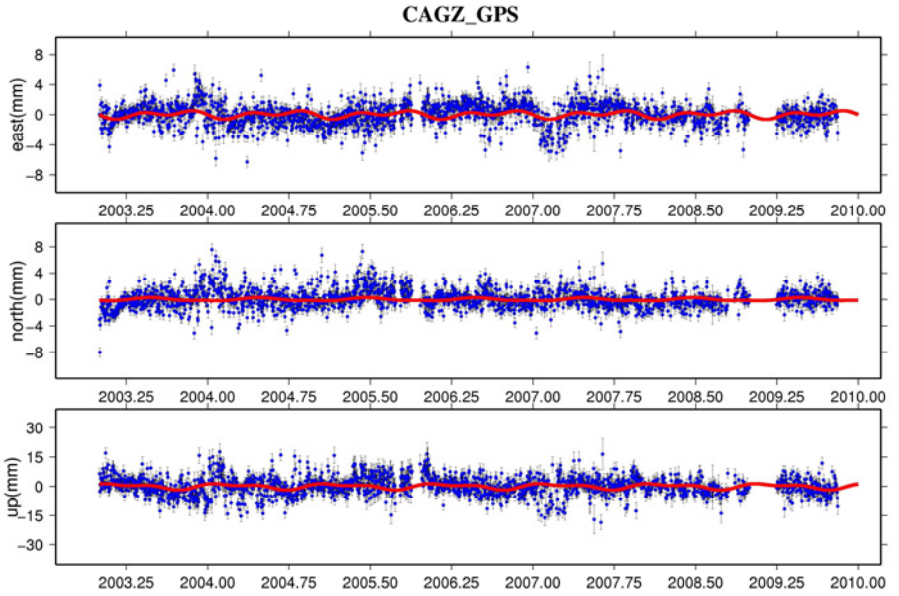
CAGZ_GPS
east(mm)
north(mm)
up(mm)
2003.25
2004.00
2004.75
2005.50
2006.25
2007.00
2007.75
2008.50
2009.25
2010.00

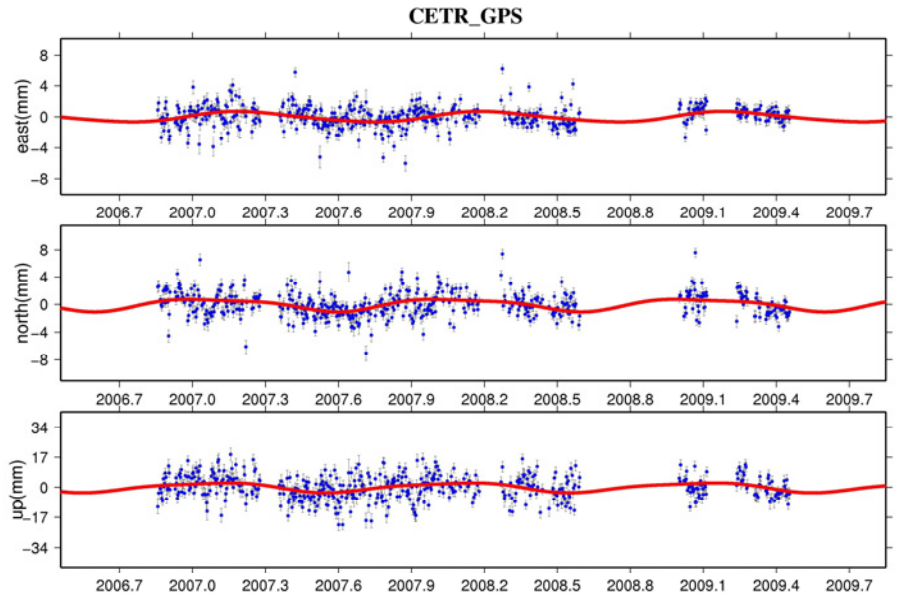
CETR_GPS
east(mm)
north(mm)
up(mm)

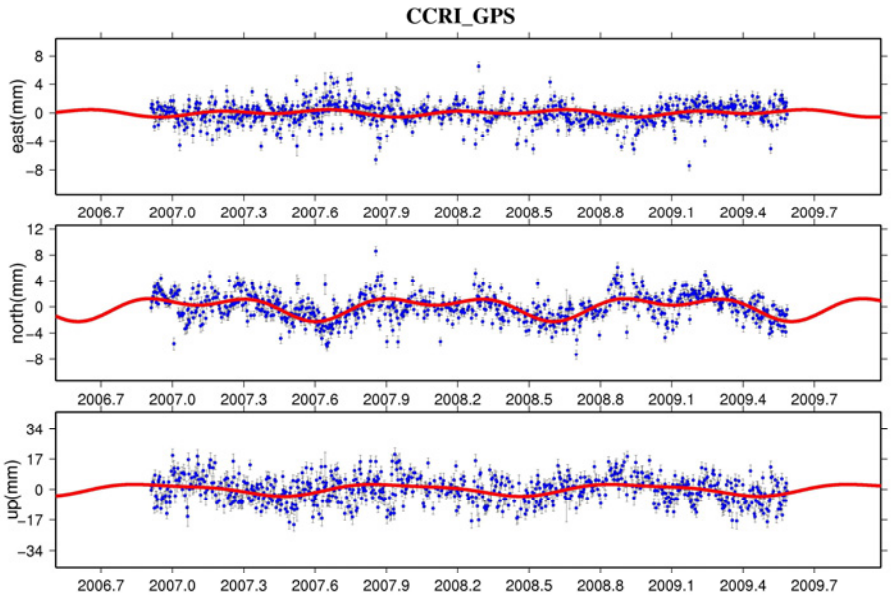
CCRI_GPS
east(mm)
north(mm)
up(mm)

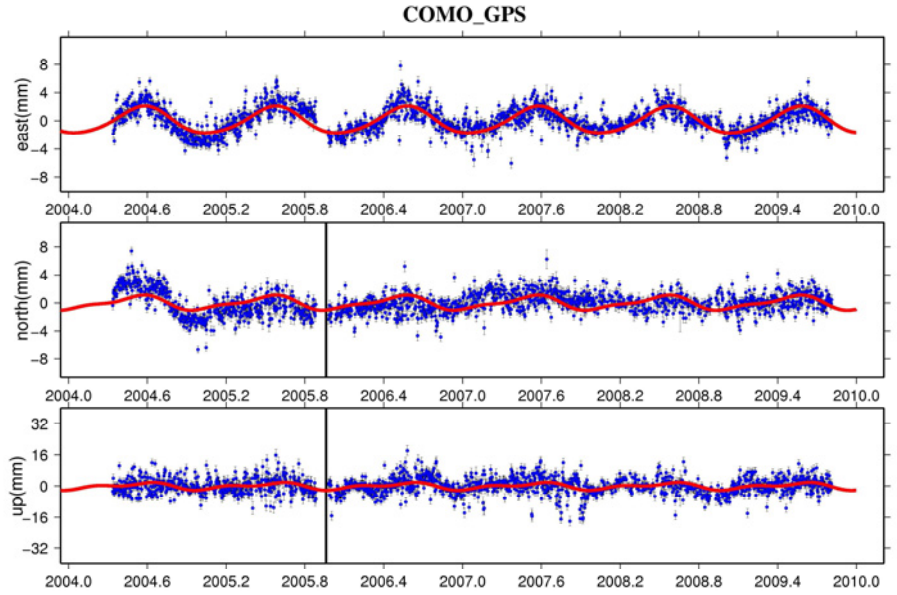
COMO_GPS
east(mm)
north(mm)
up(mm)

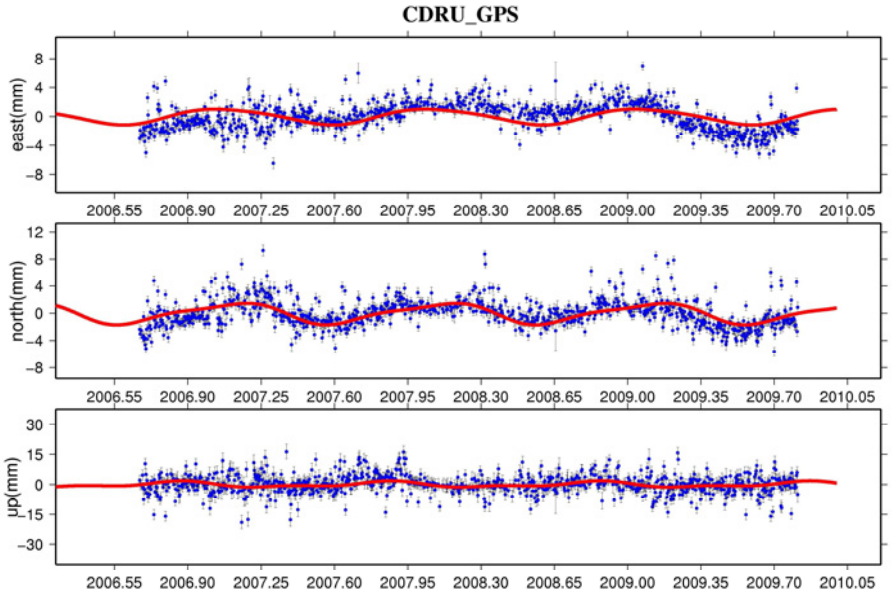
CDRU_GPS
east(mm)
north(mm)
up(mm)

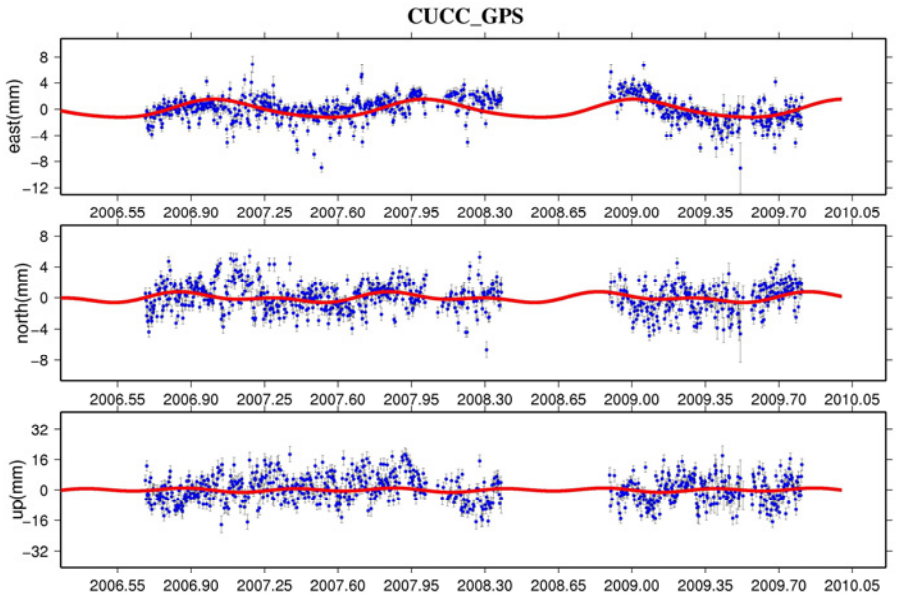
CUCC_GPS
east(mm)
north(mm)
up(mm)
2006.55 2006.90 2007.25 2007.60 2007.95 2008.30 2008.65 2009.00 2009.35 2009.70 2010.05

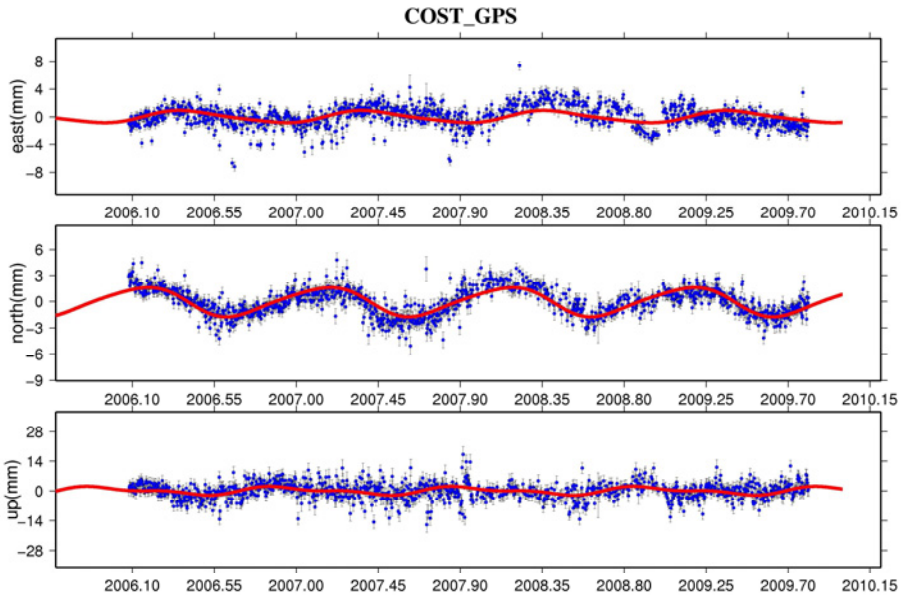
COST_GPS
east(mm)
north(mm)
up(mm)
2006.10 2006.55 2007.00 2007.45 2007.90 2008.35 2008.80 2009.25 2009.70 2010.15

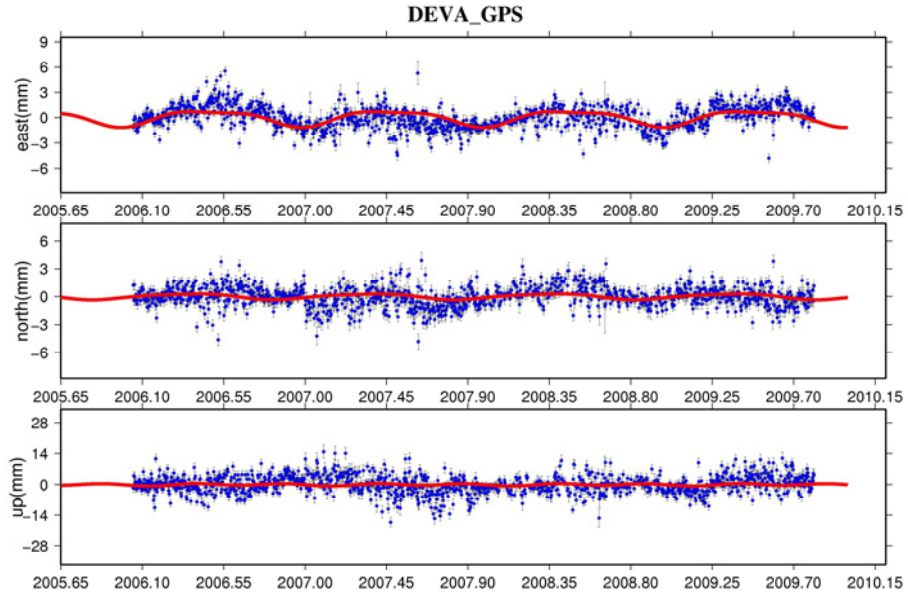
DEVA_GPS
east(mm)
north(mm)
up(mm)
2005.65 2006.10 2006.55 2007.00 2007.45 2007.90 2008.35 2008.80 2009.25 2009.70 2010.15

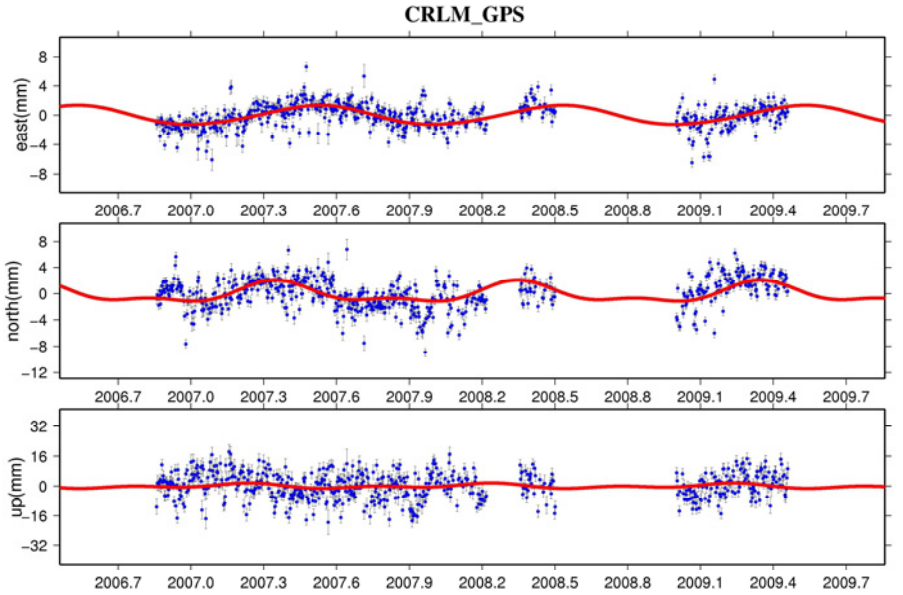
CRLM_GPS
east(mm)
north(mm)
up(mm)
2006.7 2007.0 2007.3 2007.6 2007.9 2008.2 2008.5 2008.8 2009.1 2009.4 2009.7

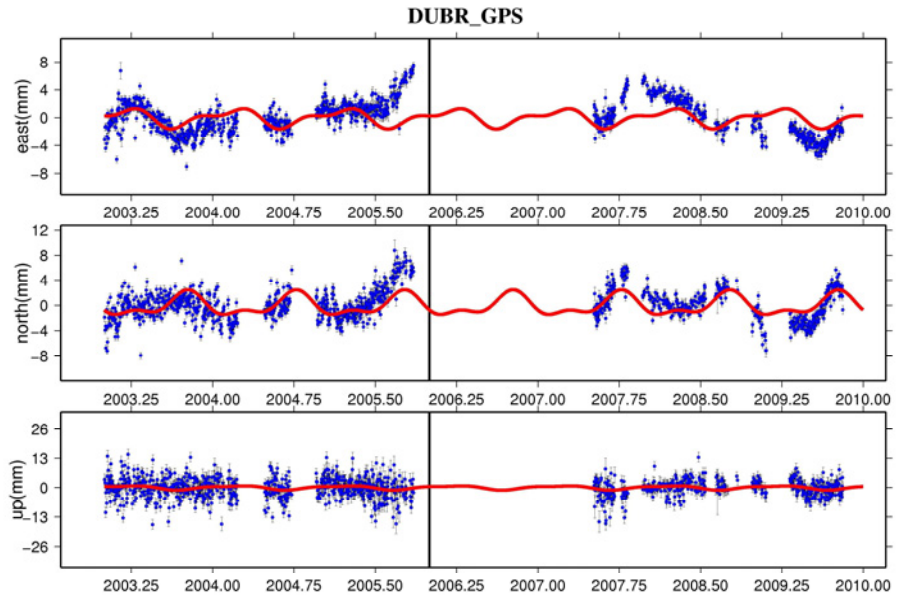
DUBR_GPS
east(mm)
north(mm)
up(mm)

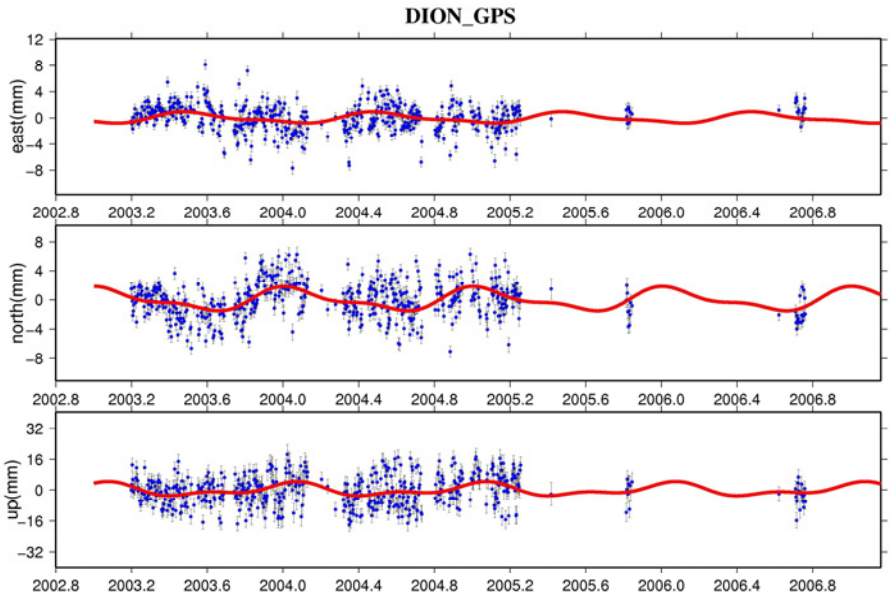
DION_GPS
east(mm)
north(mm)
up(mm)

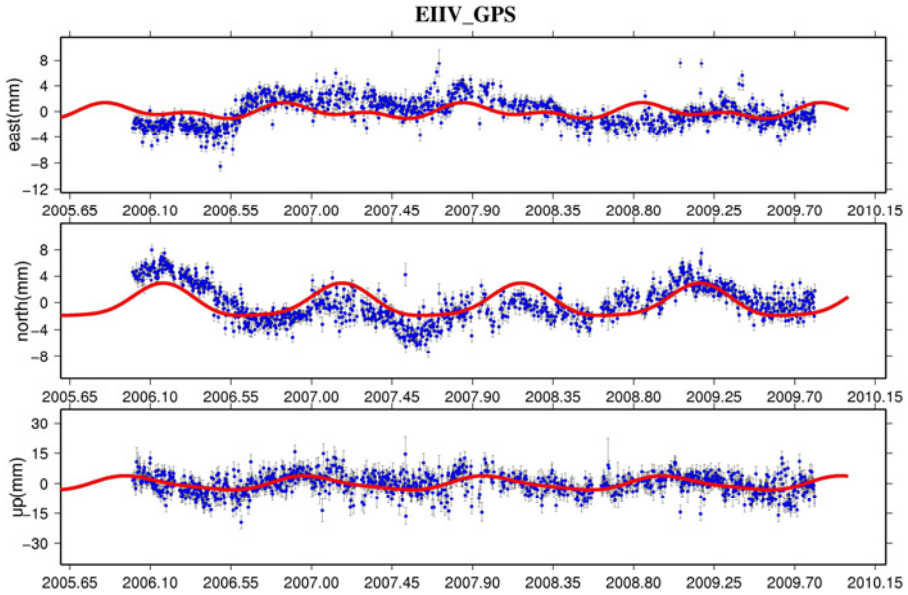
EIIV_GPS
east(mm)
north(mm)
up(mm)

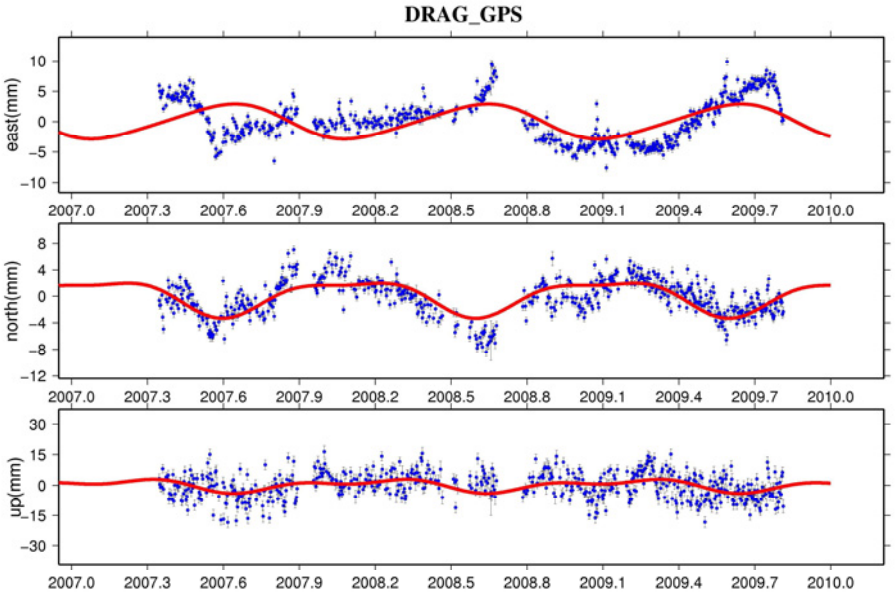
DRAG_GPS
east(mm)
north(mm)
up(mm)

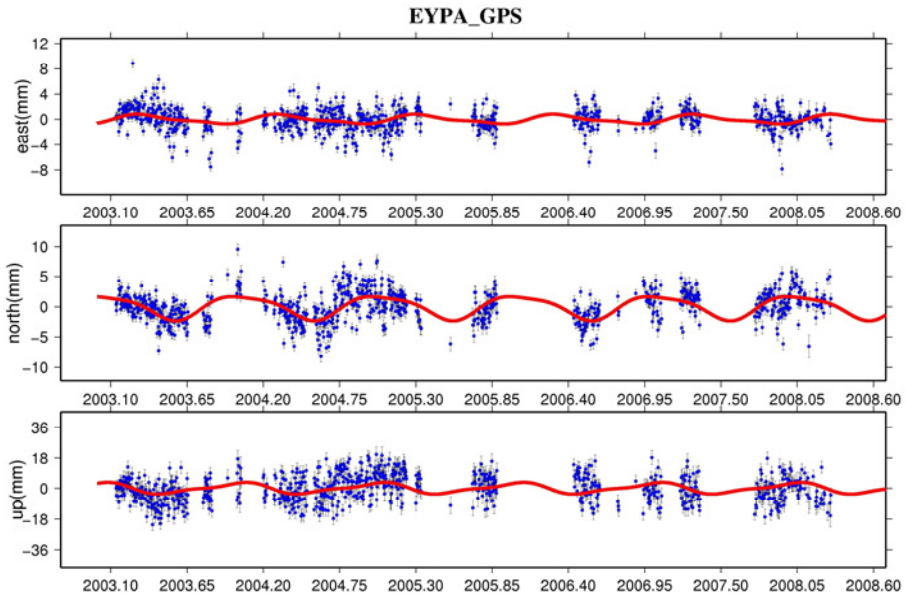
EYPA_GPS
east(mm)
north(mm)
up(mm)
2003.10 2003.65 2004.20 2004.75 2005.30 2005.85 2006.40 2006.95 2007.50 2008.05 2008.60

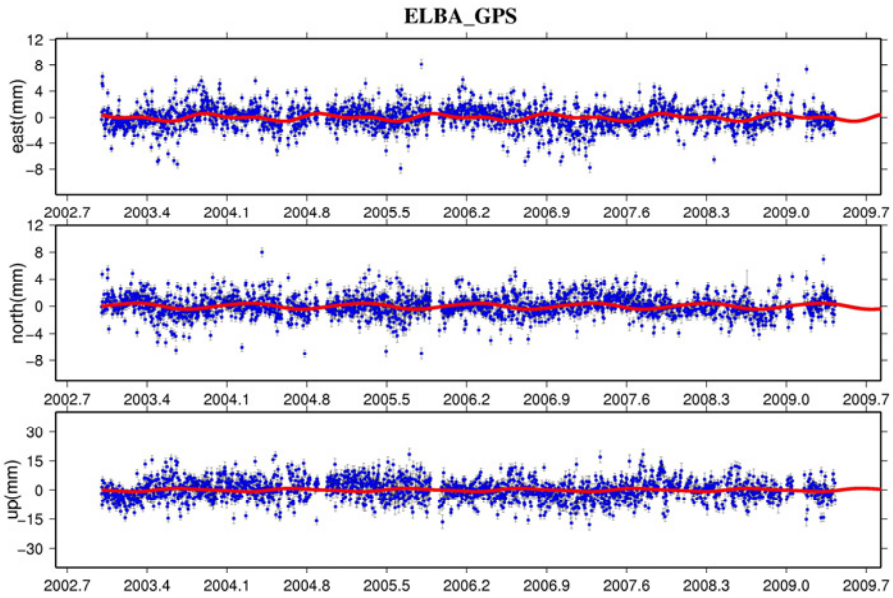
ELBA_GPS
east(mm)
north(mm)
up(mm)
2002.7 2003.4 2004.1 2004.8 2005.5 2006.2 2006.9 2007.6 2008.3 2009.0 2009.7

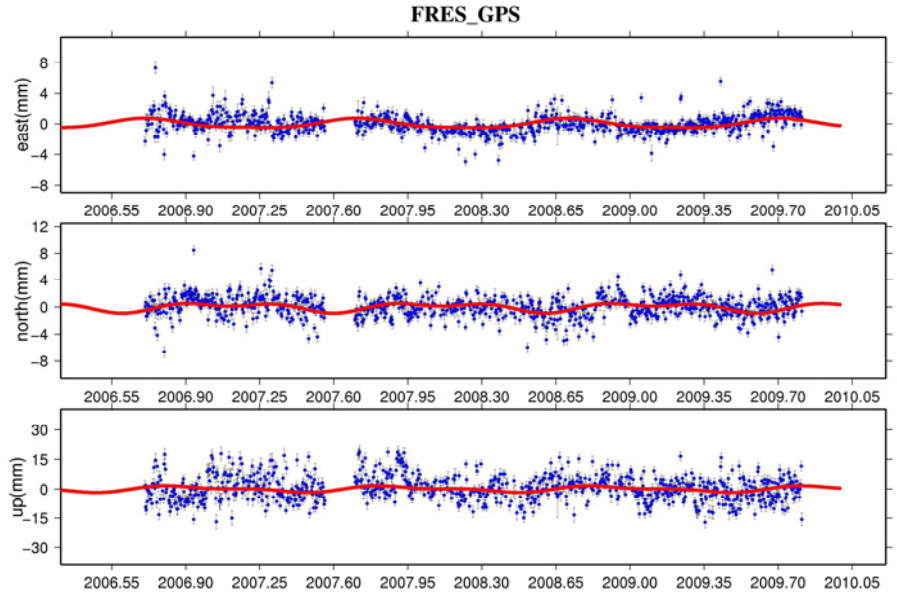
FRES_GPS
east(mm)
north(mm)
up(mm)
2006.55 2006.90 2007.25 2007.60 2007.95 2008.30 2008.65 2009.00 2009.35 2009.70 2010.05

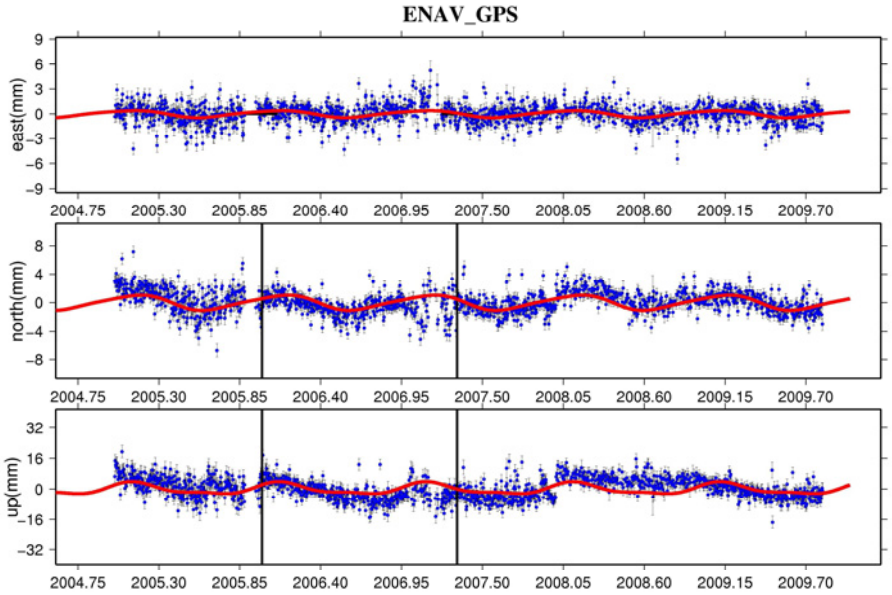
ENAV_GPS
east(mm)
north(mm)
up(mm)
2004.75 2005.30 2005.85 2006.40 2006.95 2007.50 2008.05 2008.60 2009.15 2009.70

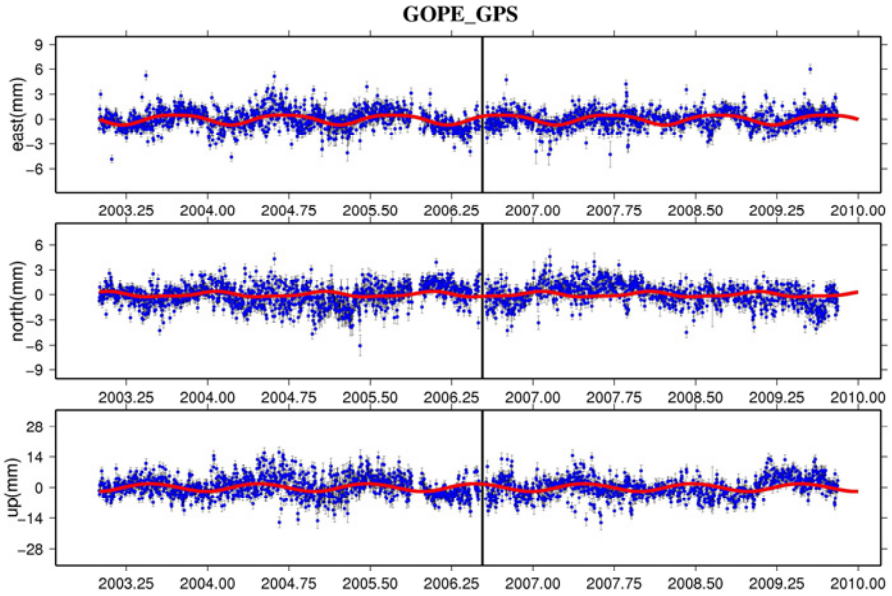
GOPE_GPS
east(mm)
north(mm)
up(mm)
2003.25
2004.00
2004.75
2005.50
2006.25
2007.00
2007.75
2008.50
2009.25
2010.00

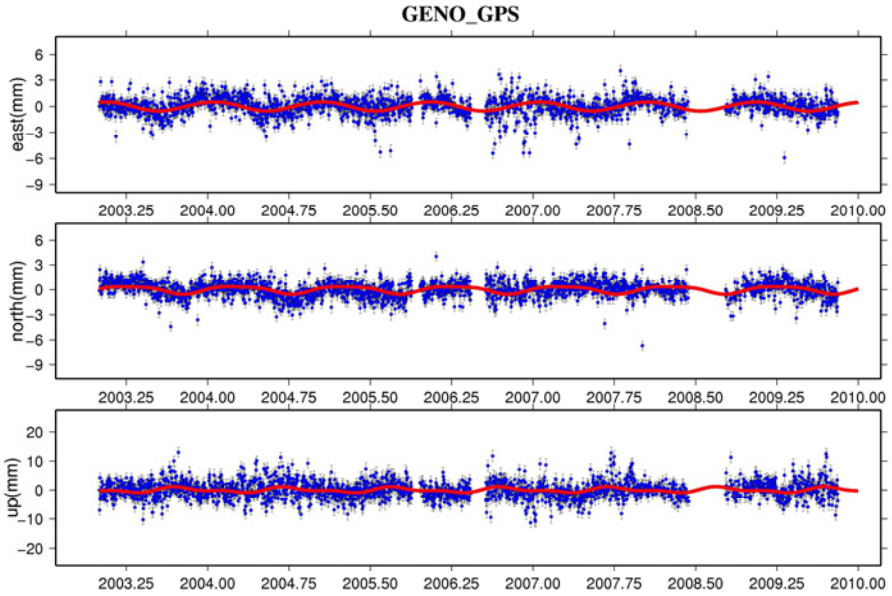
GENO_GPS
east(mm)
north(mm)
up(mm)
2003.25
2004.00
2004.75
2005.50
2006.25
2007.00
2007.75
2008.50
2009.25
2010.00

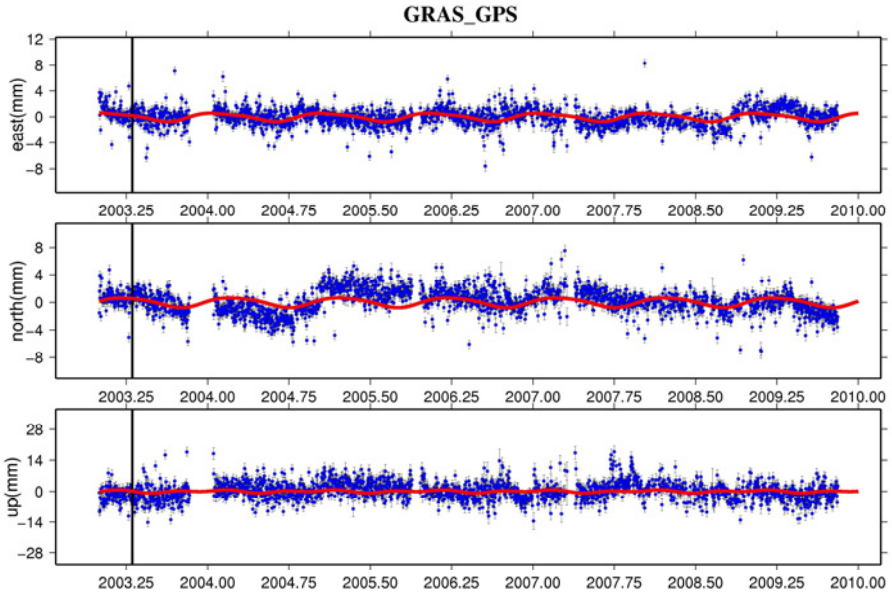
GRAS_GPS
east(mm)
north(mm)
up(mm)
2003.25
2004.00
2004.75
2005.50
2006.25
2007.00
2007.75
2008.50
2009.25
2010.00

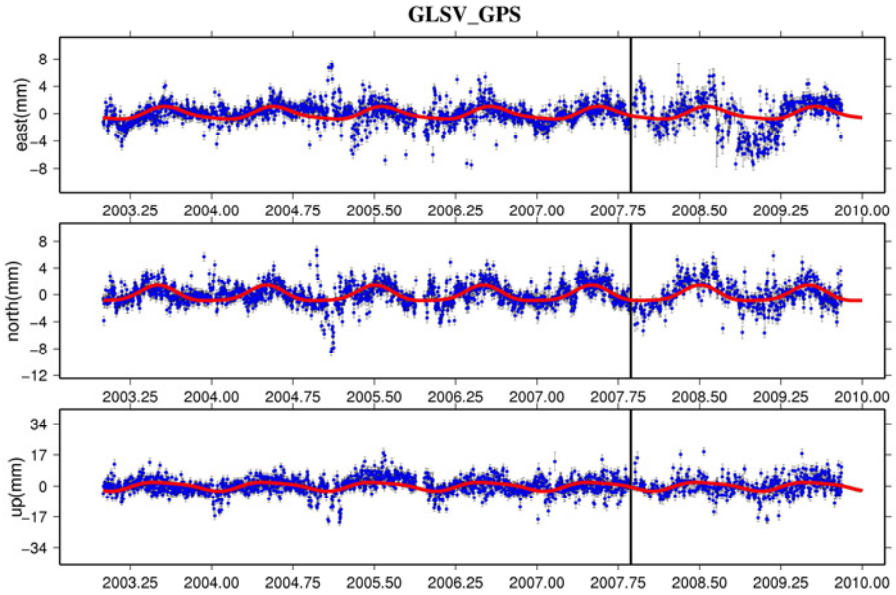
GLSV_GPS
east(mm)
north(mm)
up(mm)
2003.25
2004.00
2004.75
2005.50
2006.25
2007.00
2007.75
2008.50
2009.25
2010.00

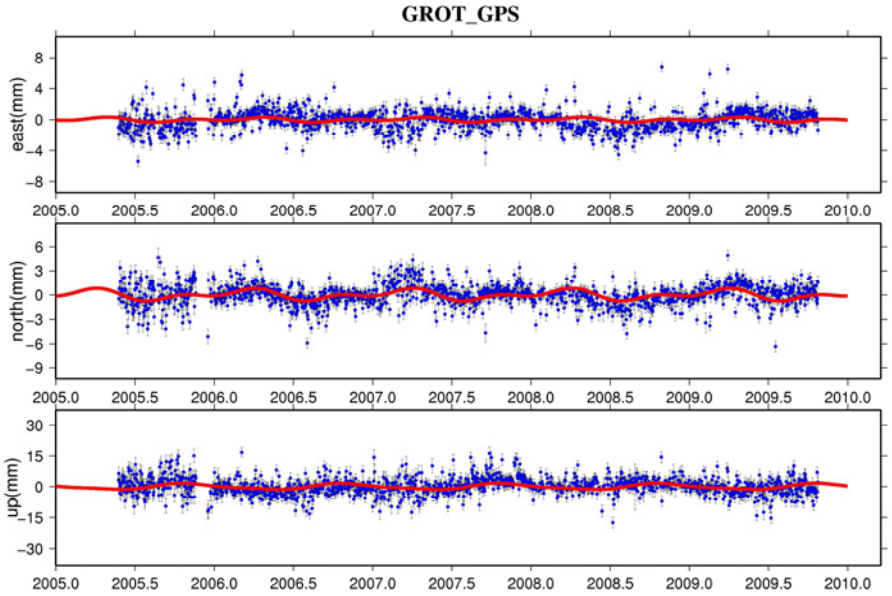
GROT_GPS
east(mm)
north(mm)
up(mm)

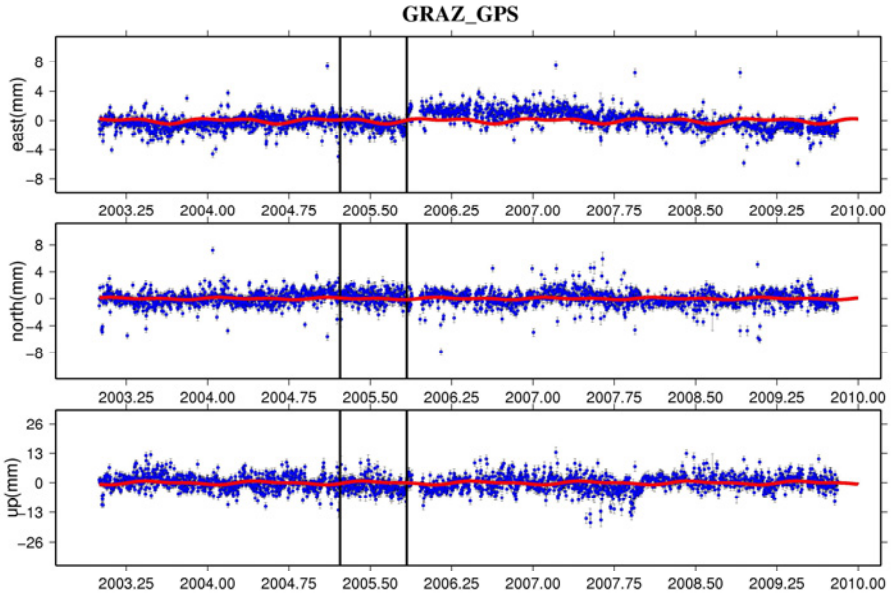
GRAZ_GPS
east(mm)
north(mm)
up(mm)

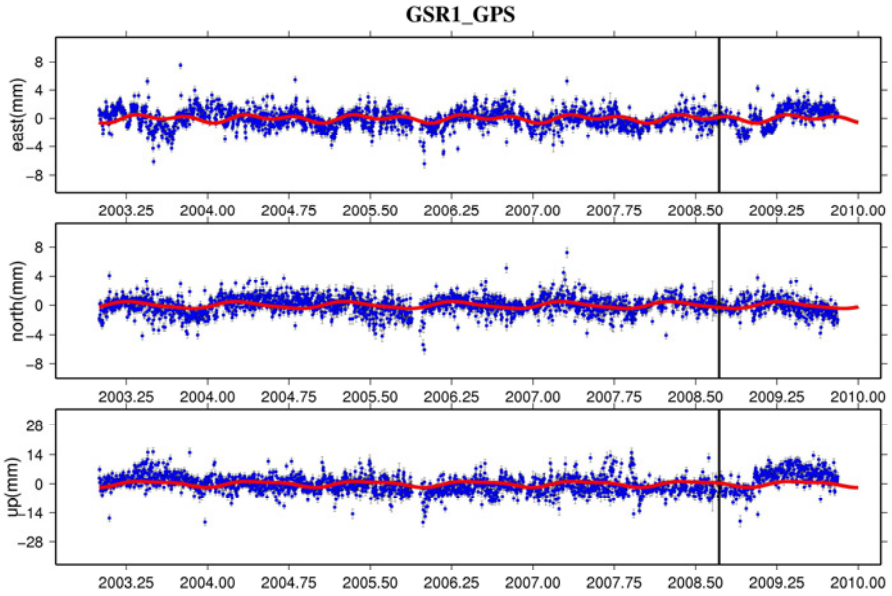
GSR1_GPS
east(mm)
north(mm)
up(mm)

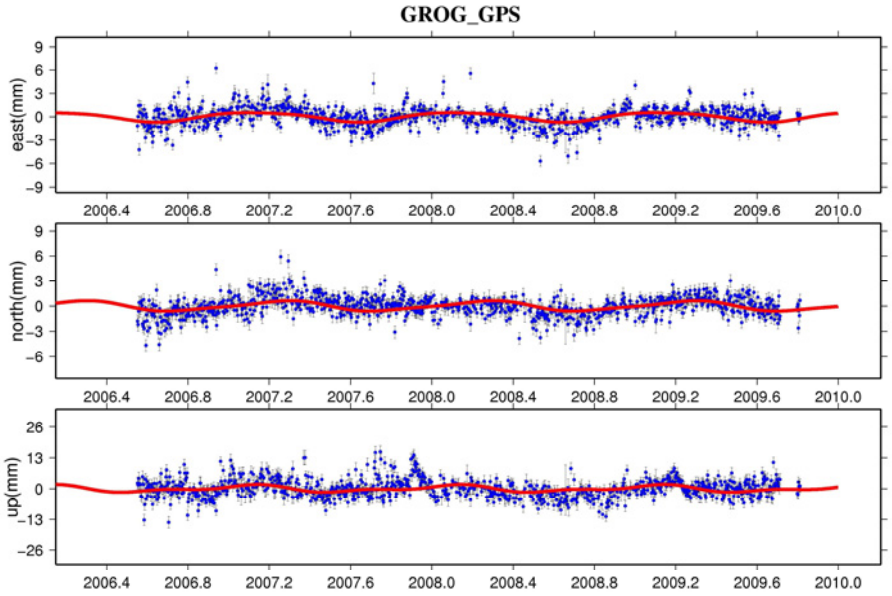
GROG_GPS
east(mm)
north(mm)
up(mm)

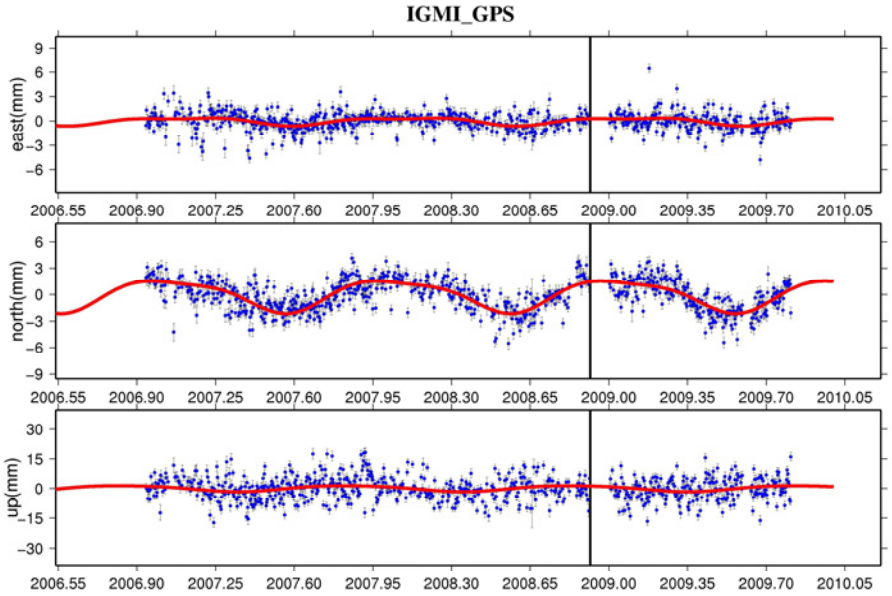
IGMI_GPS
east(mm)
north(mm)
up(mm)

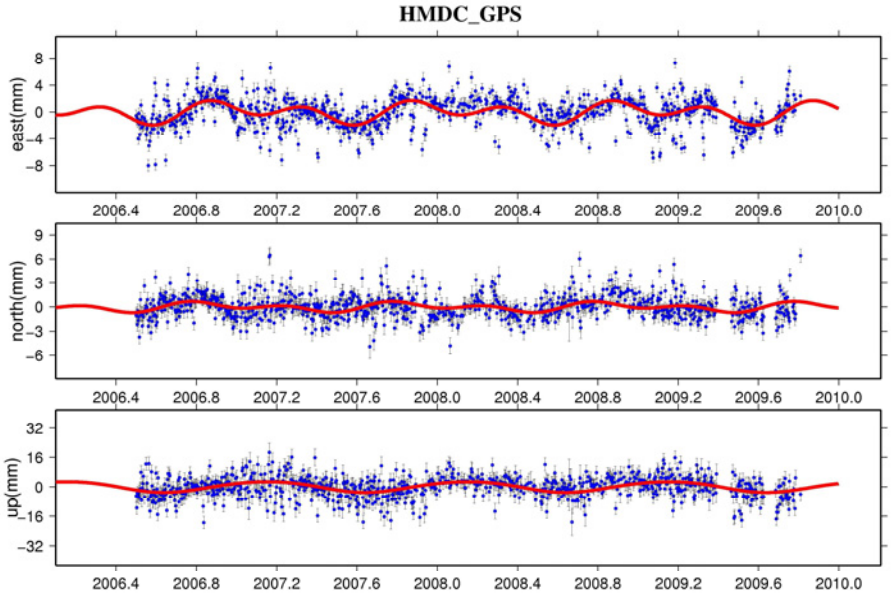
HMDC_GPS
east(mm)
north(mm)
up(mm)

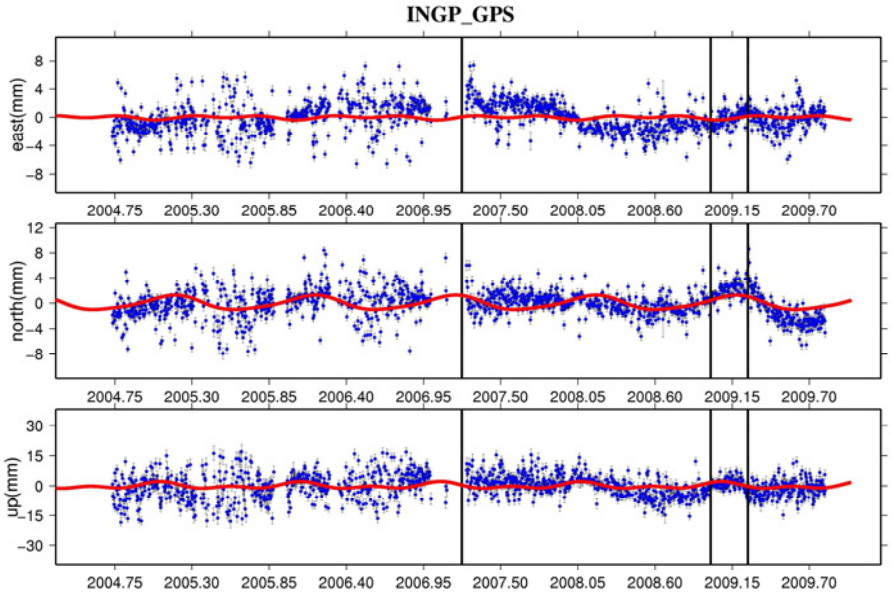
INGP_GPS
east(mm)
north(mm)
up(mm)

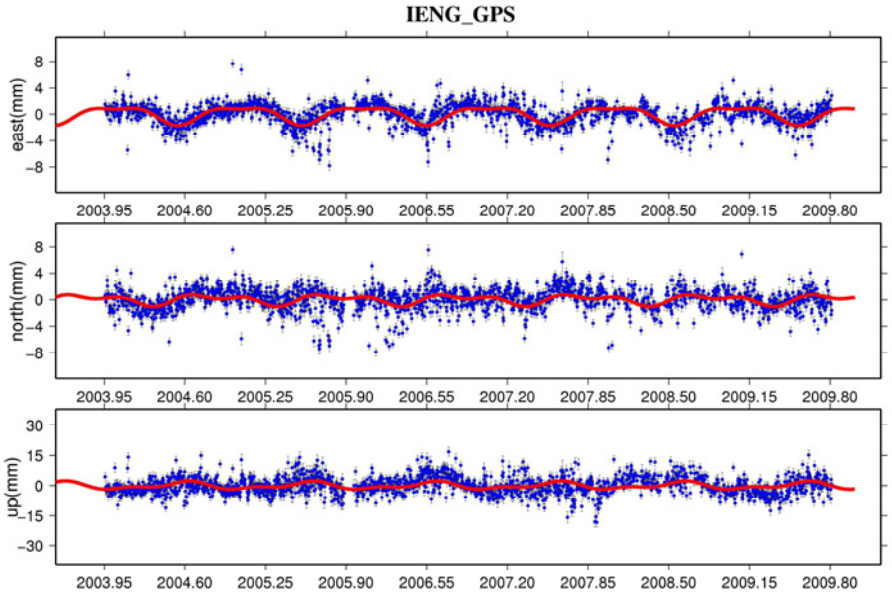
IENG_GPS
east(mm)
north(mm)
up(mm)

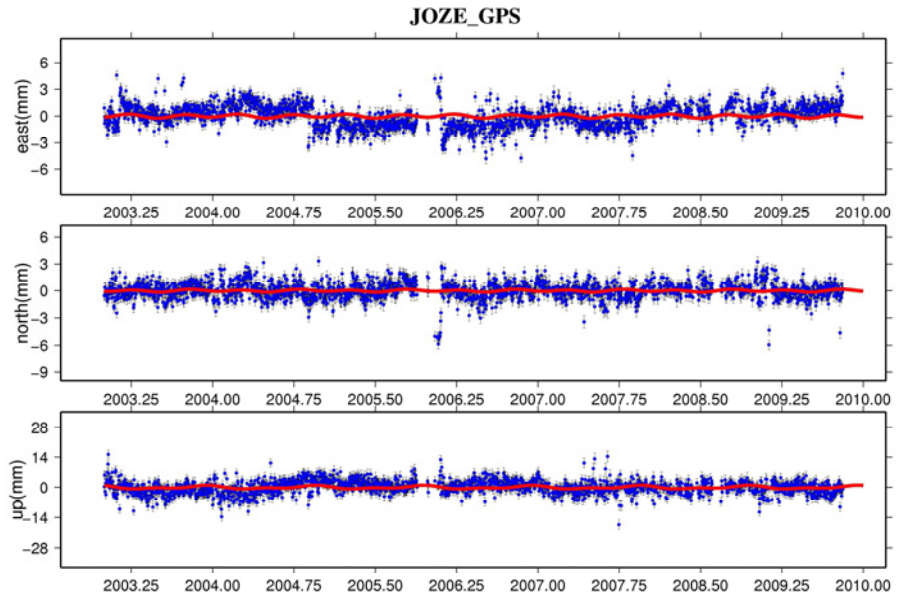
JOZE_GPS
east(mm)
north(mm)
up(mm)

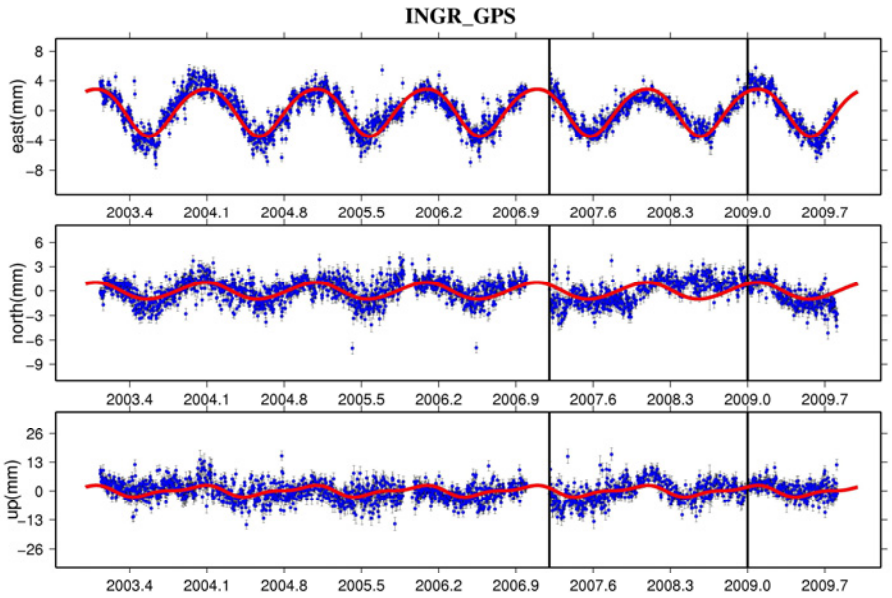
INGR_GPS
east(mm)
north(mm)
up(mm)

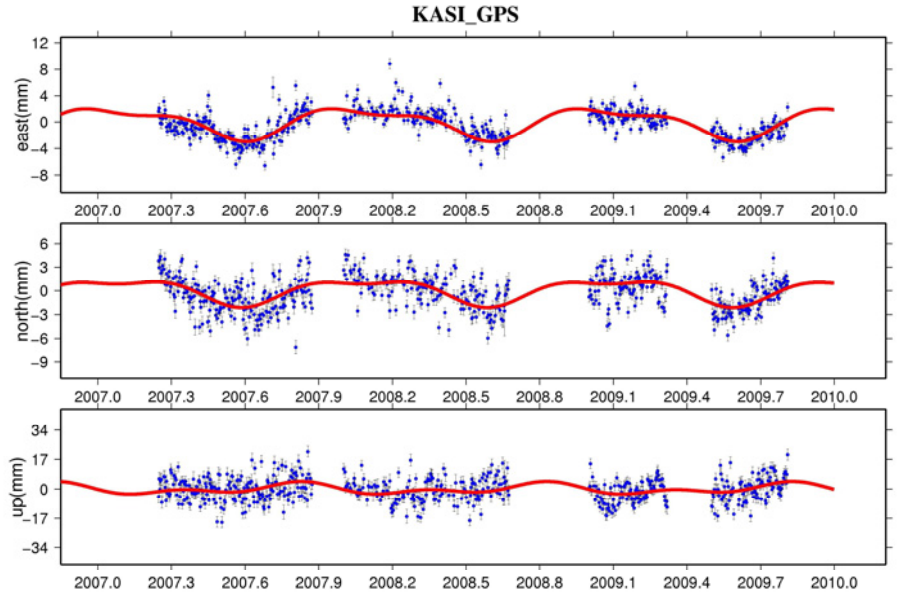
KASI_GPS
east(mm)
north(mm)
up(mm)

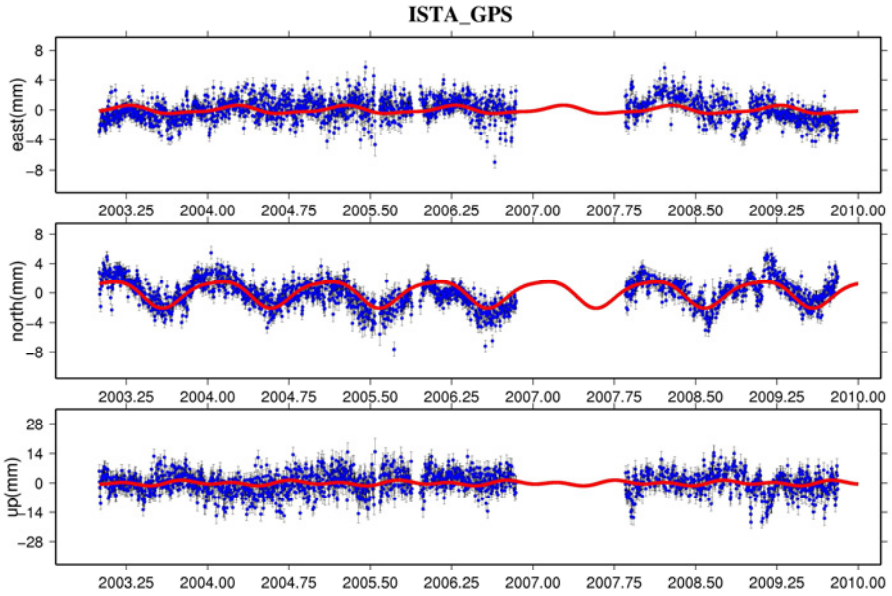
ISTA_GPS
east(mm)
north(mm)
up(mm)

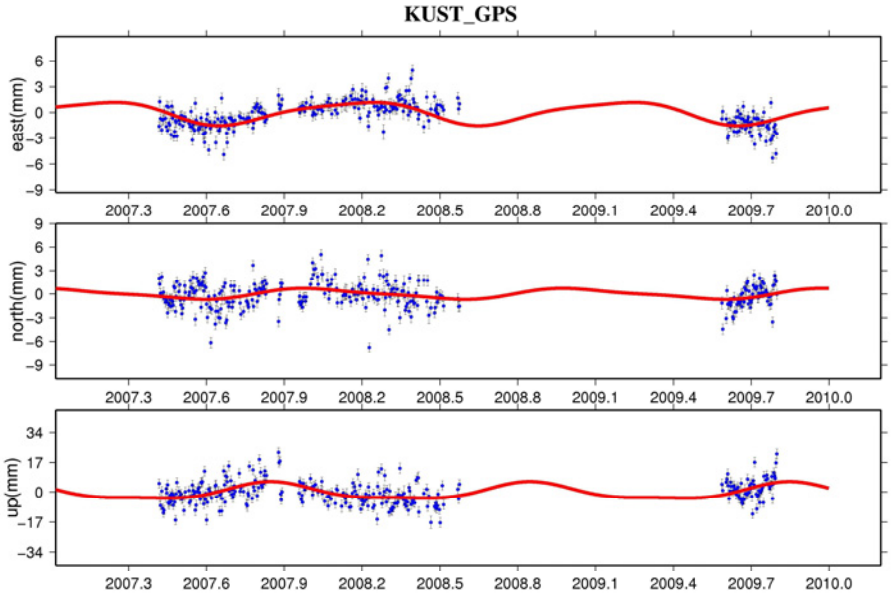
KUST_GPS
east(mm)
north(mm)
up(mm)

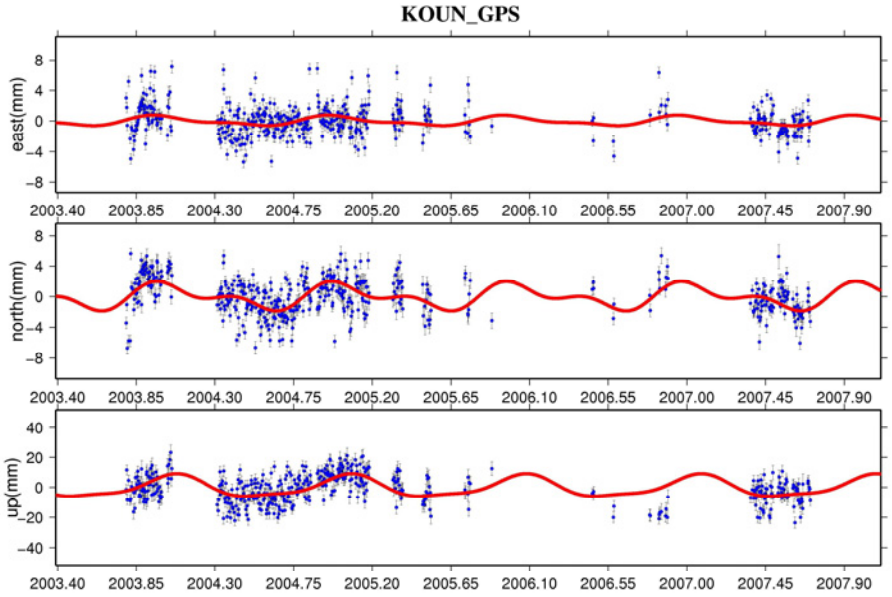
KOUN_GPS
east(mm)
north(mm)
up(mm)

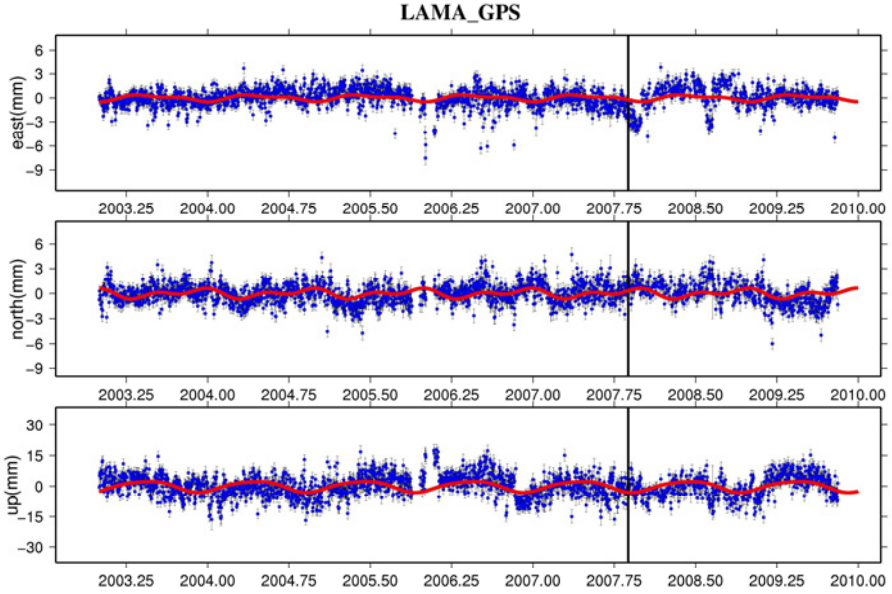
LAMA_GPS
east(mm)
north(mm)
up(mm)

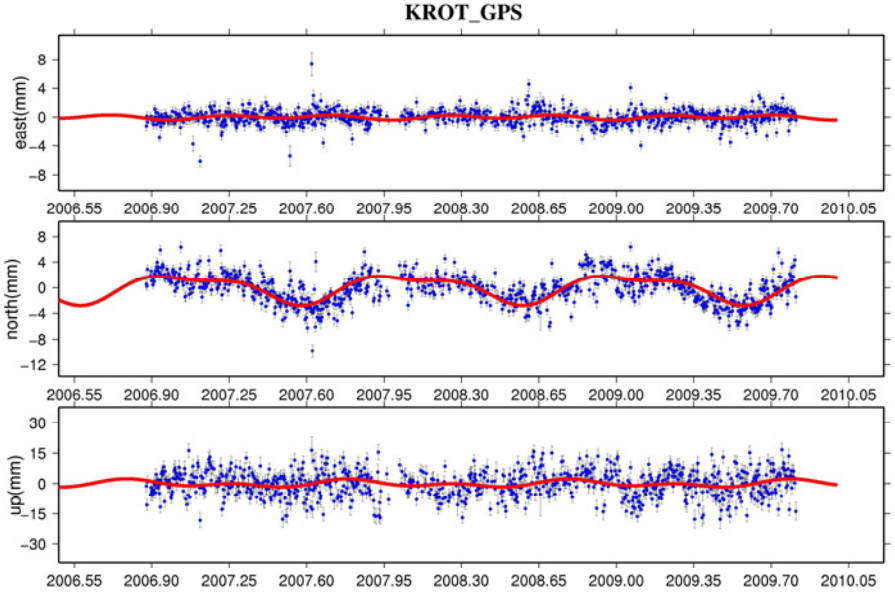
KROT_GPS
east(mm)
north(mm)
up(mm)

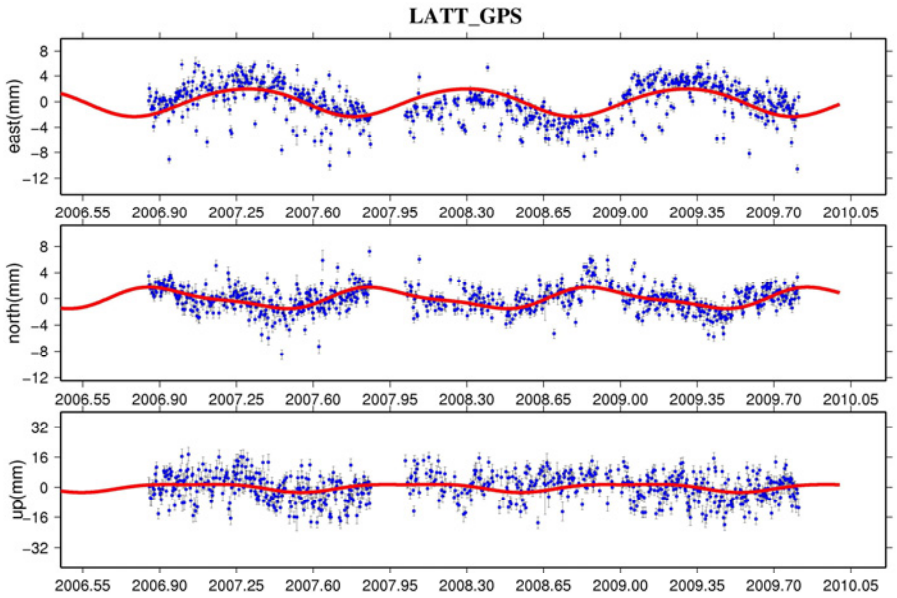
LATT_GPS
east(mm)
north(mm)
up(mm)

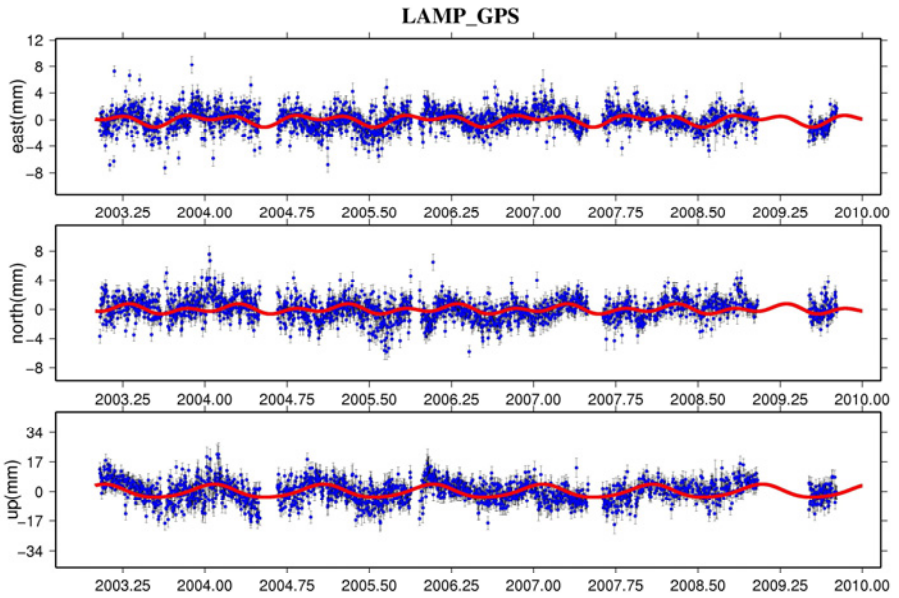
LAMP_GPS
east(mm)
north(mm)
up(mm)

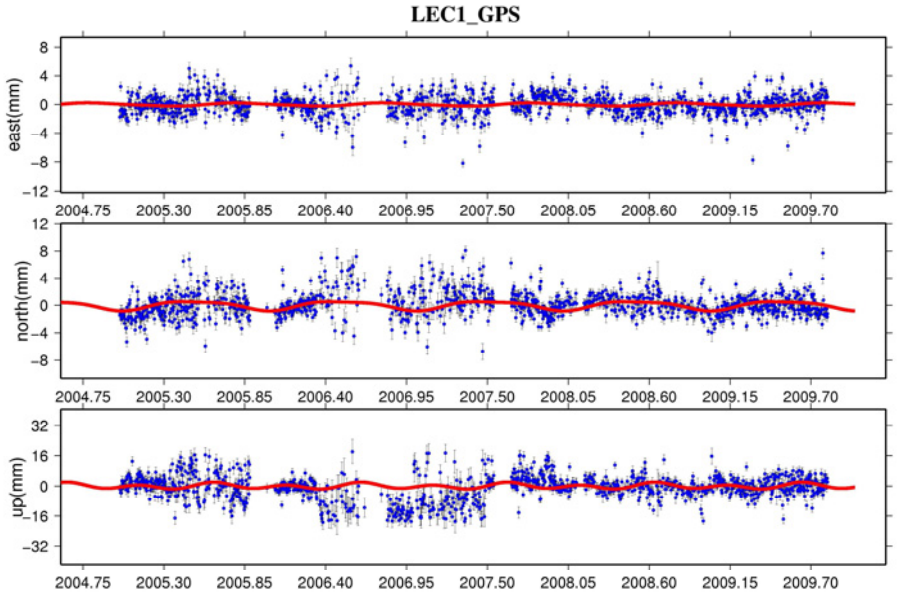
LEC1_GPS
east(mm)
north(mm)
up(mm)

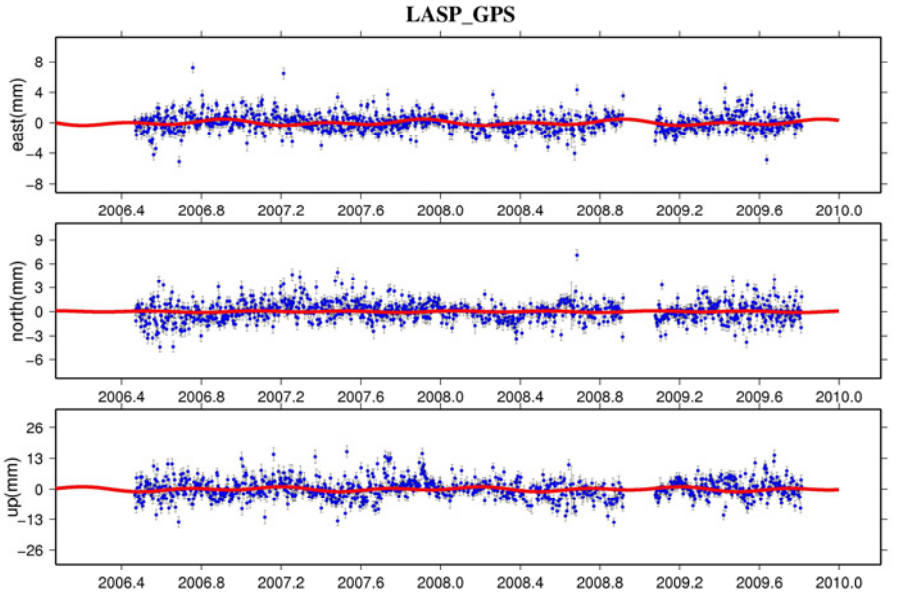
LASP_GPS
east(mm)
north(mm)
up(mm)

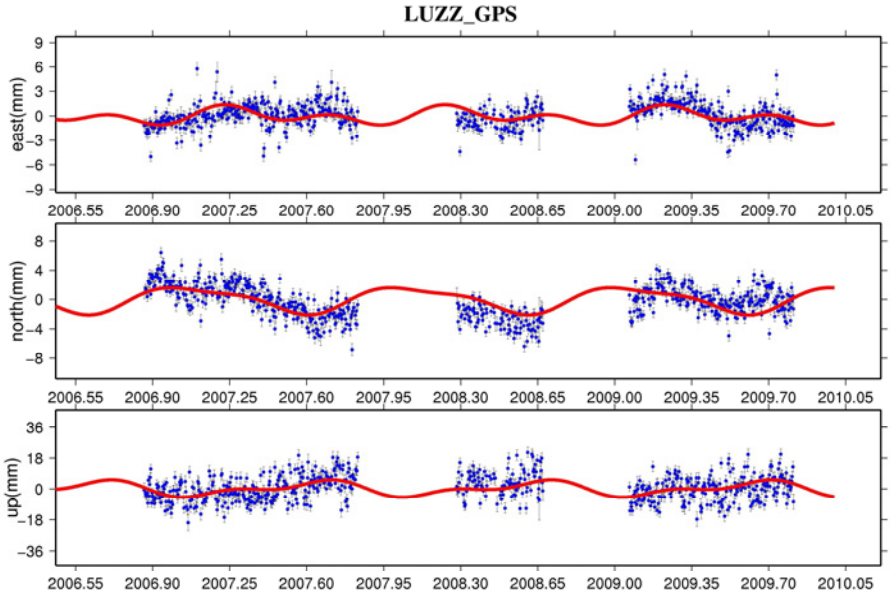
LUZZ_GPS
east(mm)
north(mm)
up(mm)

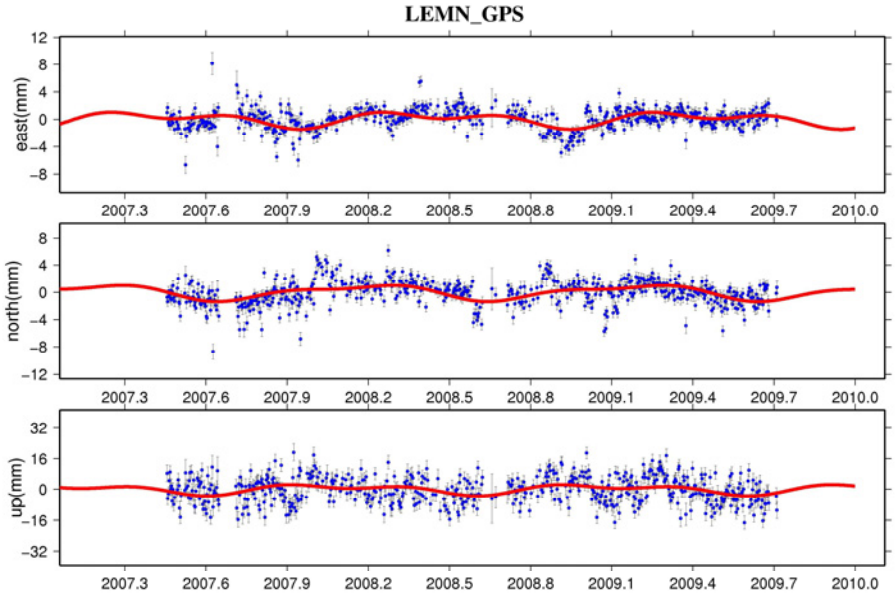
LEMN_GPS
east(mm)
north(mm)
up(mm)

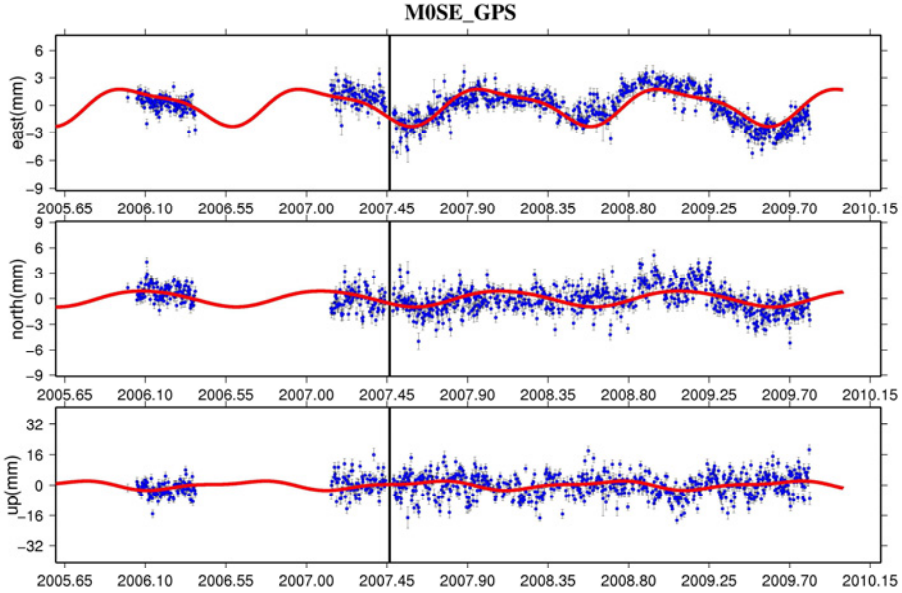
M0SE_GPS
east(mm)
north(mm)
up(mm)

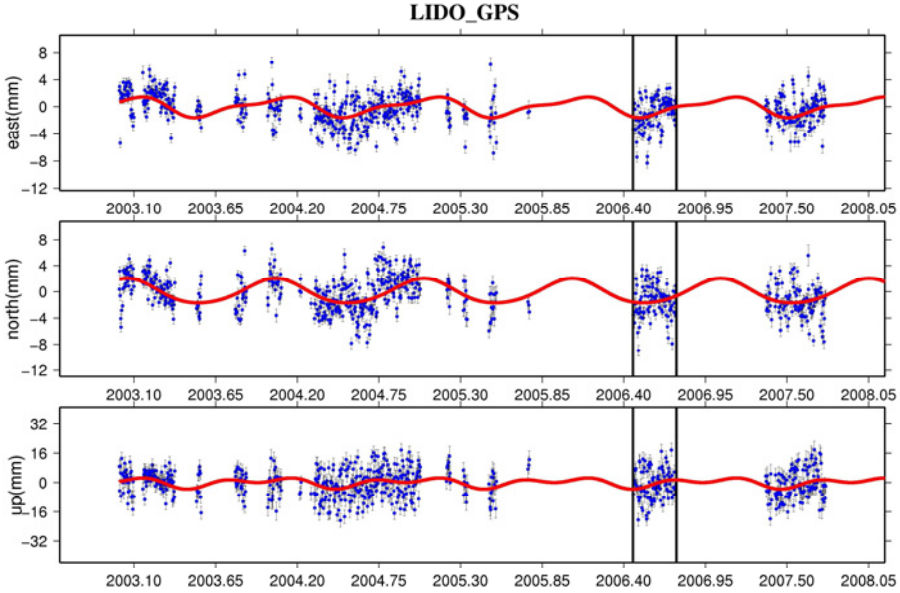
LIDO_GPS
east(mm)
north(mm)
up(mm)

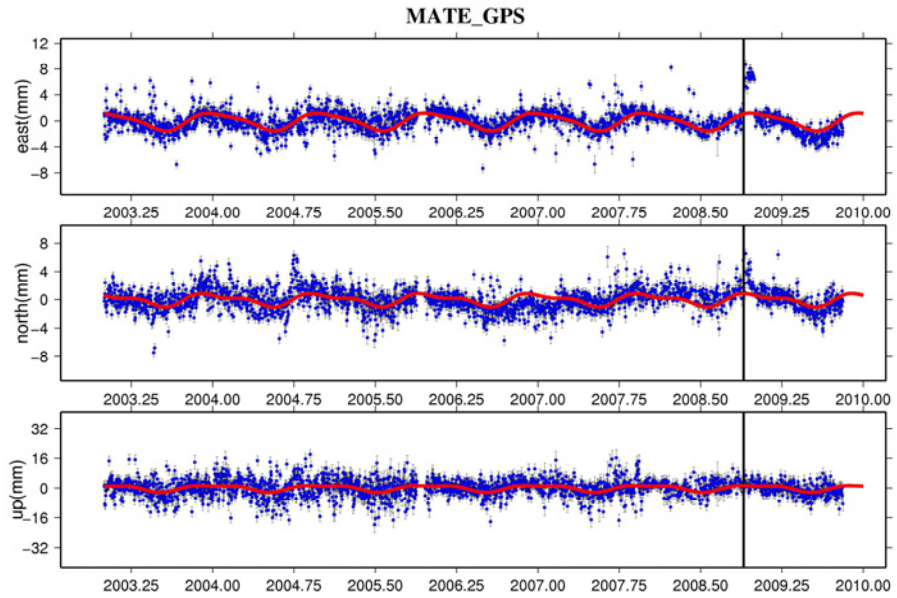
MATE_GPS
east(mm)
north(mm)
up(mm)
2003.25
2004.00
2004.75
2005.50
2006.25
2007.00
2007.75
2008.50
2009.25
2010.00

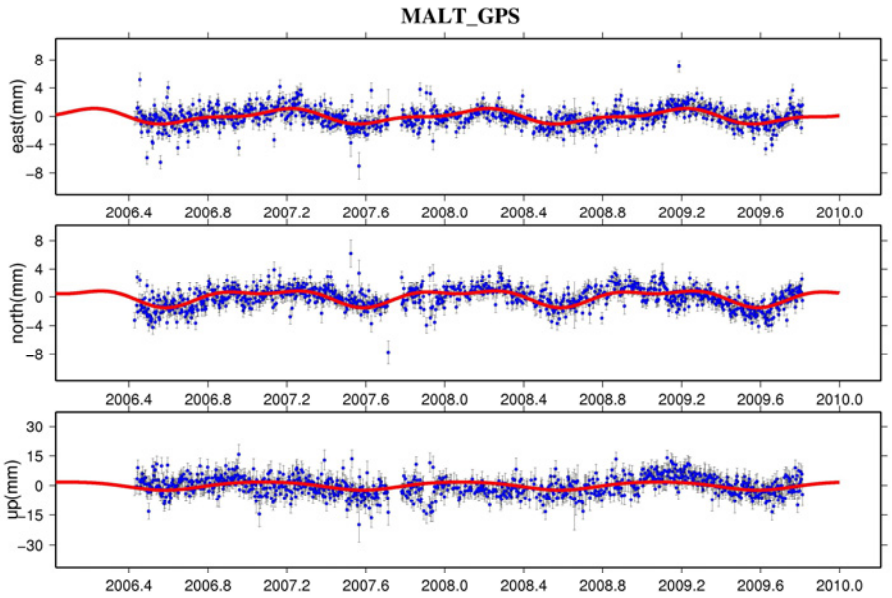
MALT_GPS
east(mm)
north(mm)
up(mm)
2006.4
2006.8
2007.2
2007.6
2008.0
2008.4
2008.8
2009.2
2009.6
2010.0

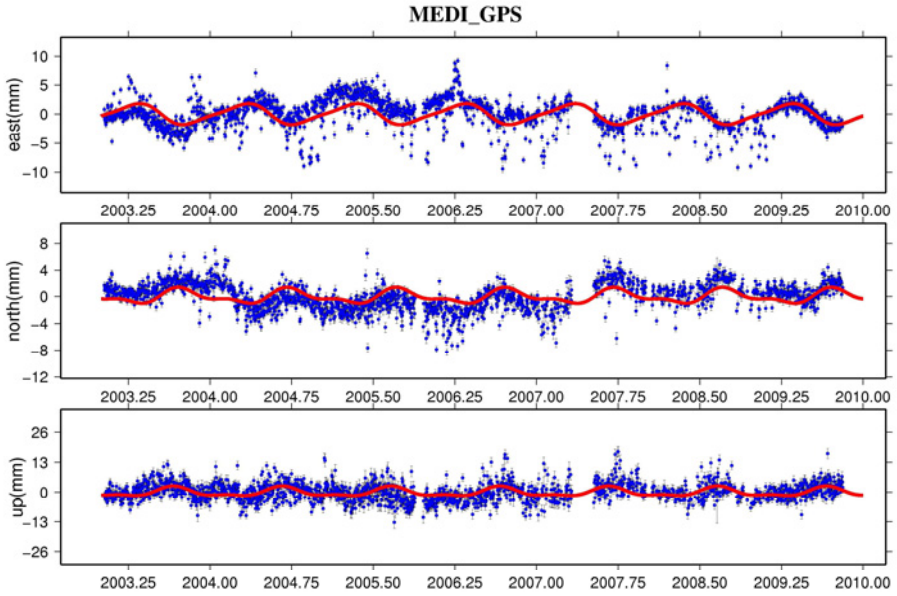
MEDI_GPS
east(mm)
north(mm)
up(mm)
2003.25
2004.00
2004.75
2005.50
2006.25
2007.00
2007.75
2008.50
2009.25
2010.00

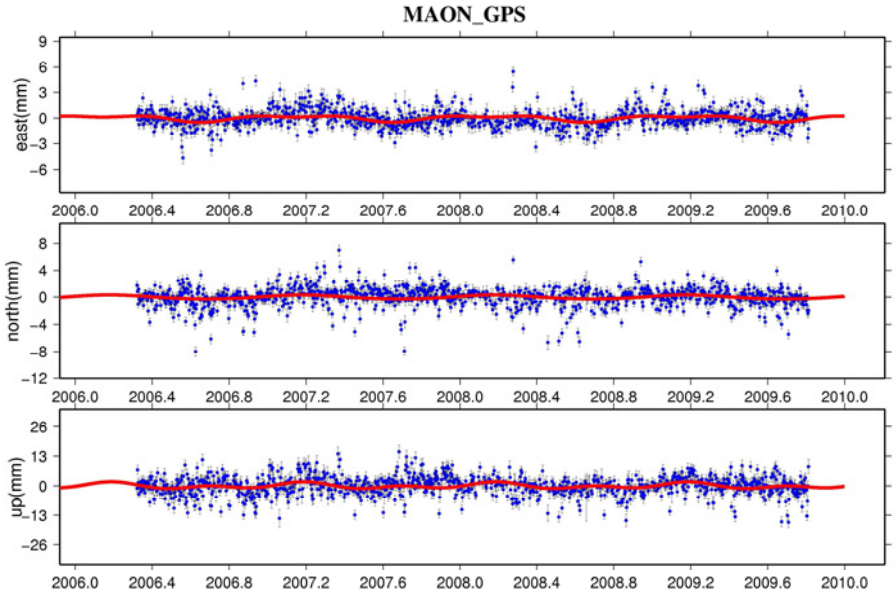
MAON_GPS
east(mm)
north(mm)
up(mm)
2006.0
2006.4
2006.8
2007.2
2007.6
2008.0
2008.4
2008.8
2009.2
2009.6
2010.0

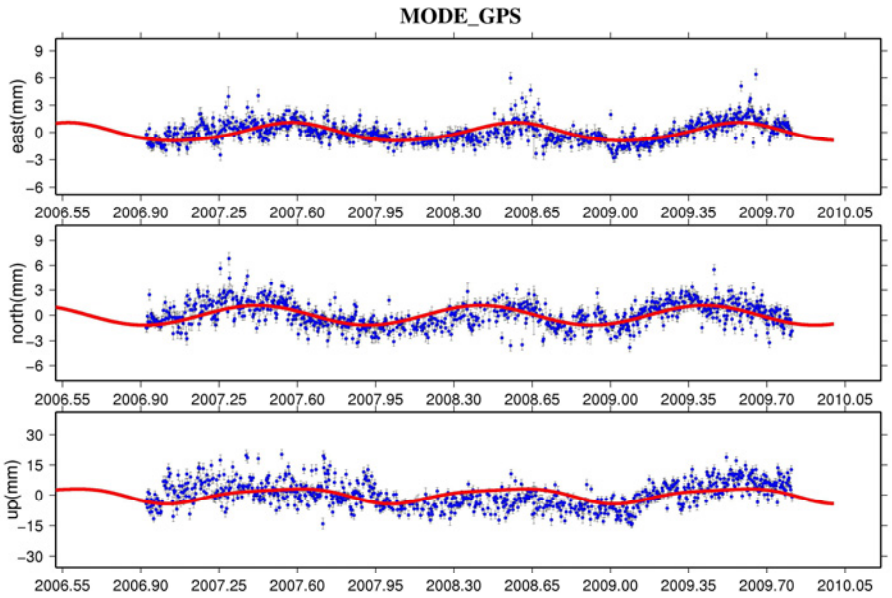
MODE_GPS
east(mm)
north(mm)
up(mm)

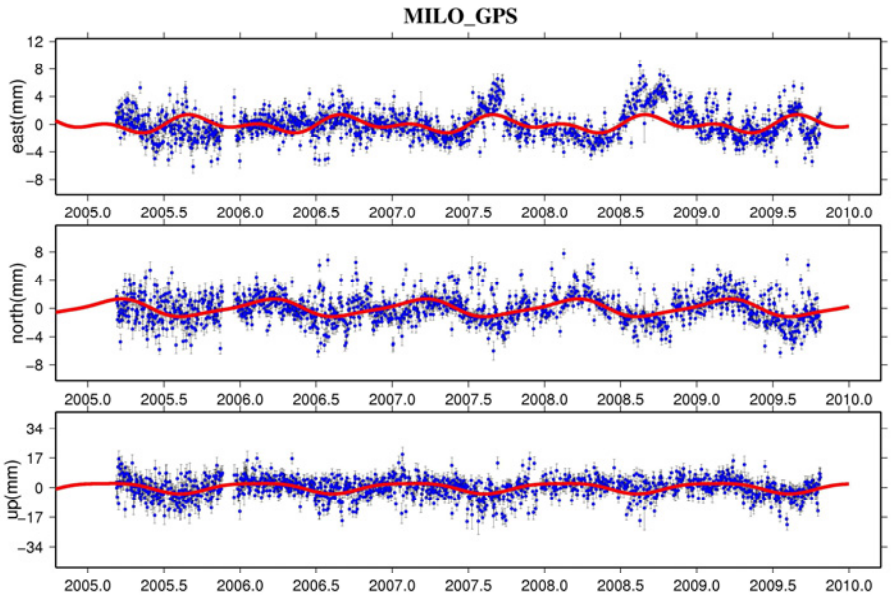
MILO_GPS
east(mm)
north(mm)
up(mm)

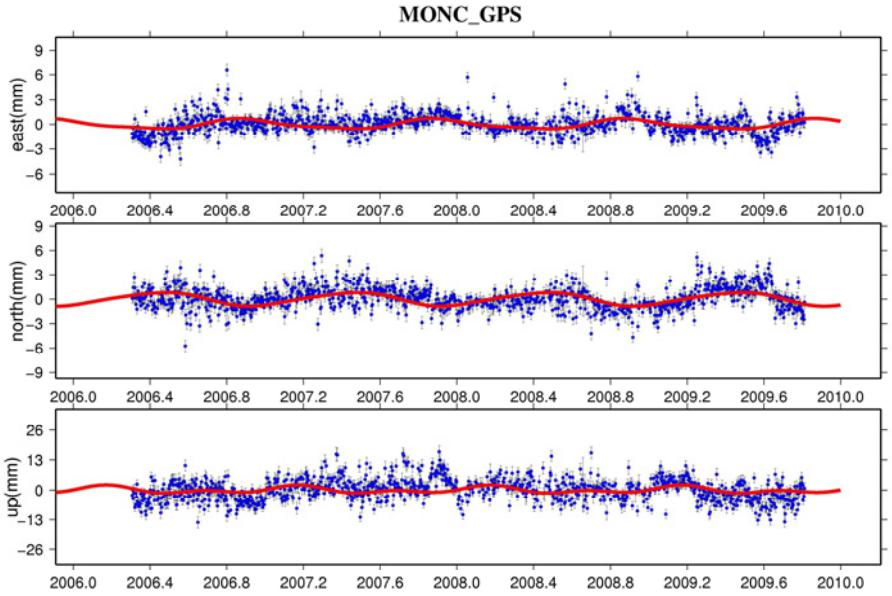
MONC_GPS
east(mm)
north(mm)
up(mm)

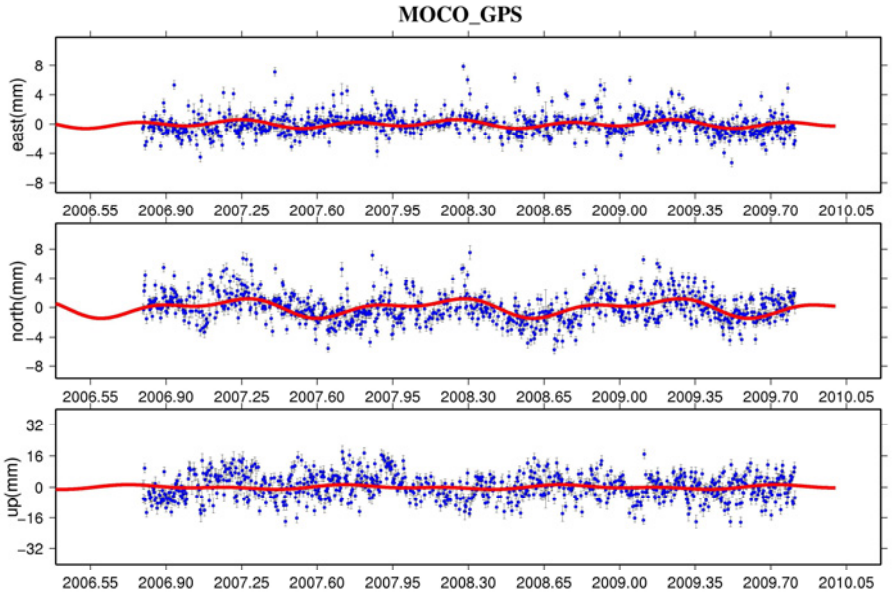
MOCO_GPS
east(mm)
north(mm)
up(mm)

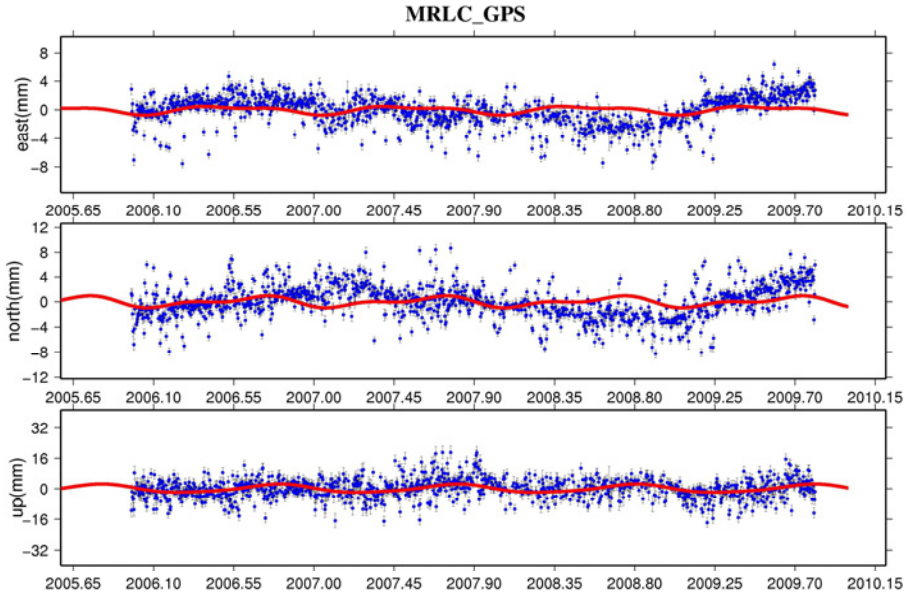
MRLC_GPS
east(mm)
north(mm)
up(mm)

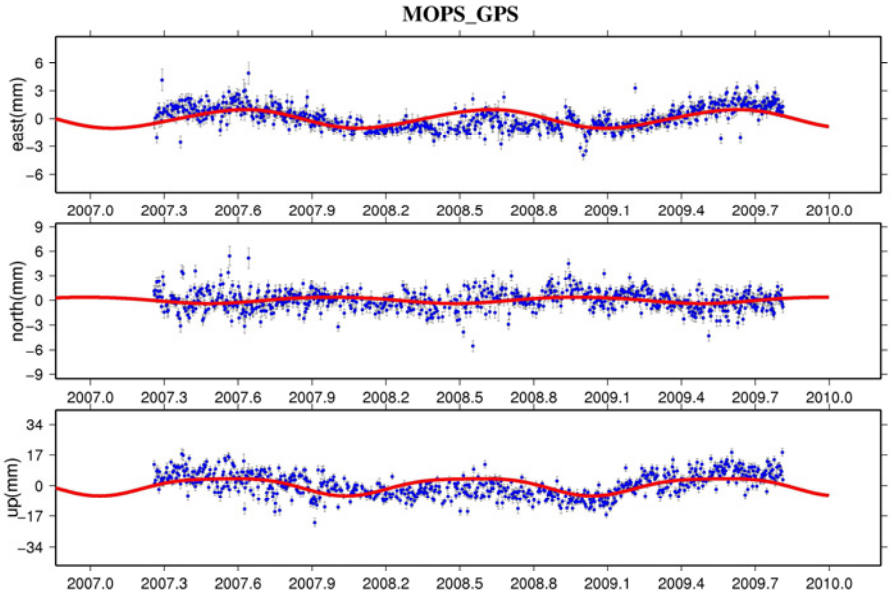
MOPS_GPS
east(mm)
north(mm)
up(mm)

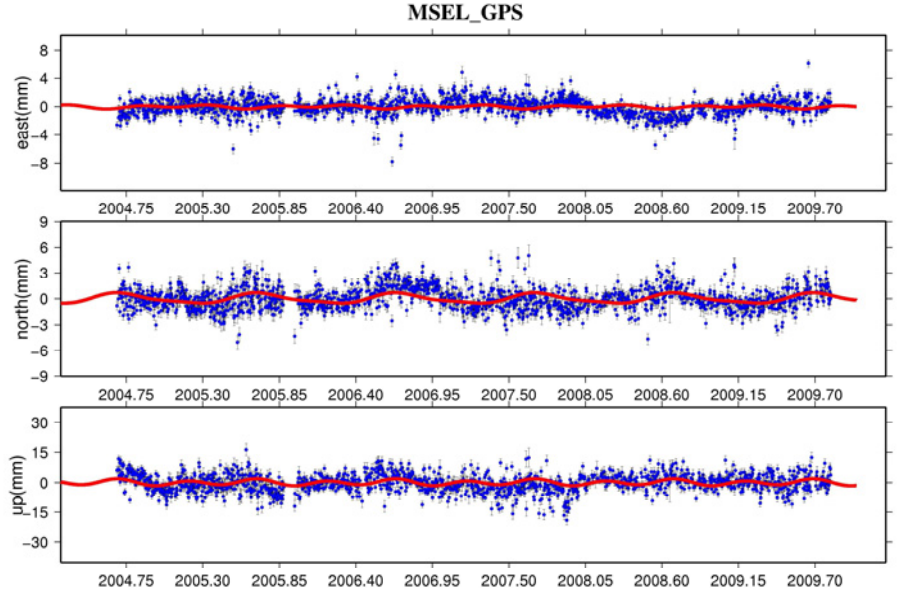
MSEL_GPS
east(mm)
north(mm)
up(mm)

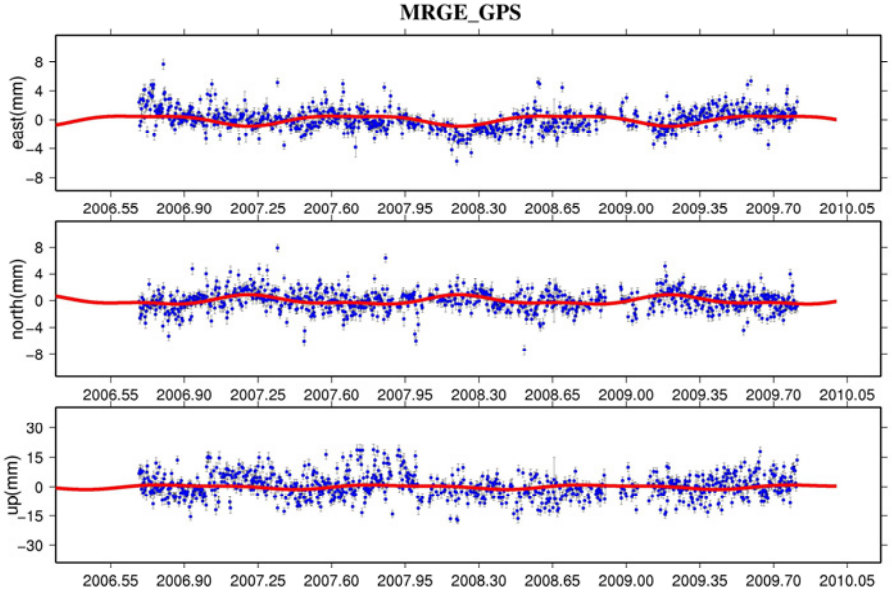
MRGE_GPS
east(mm)
north(mm)
up(mm)

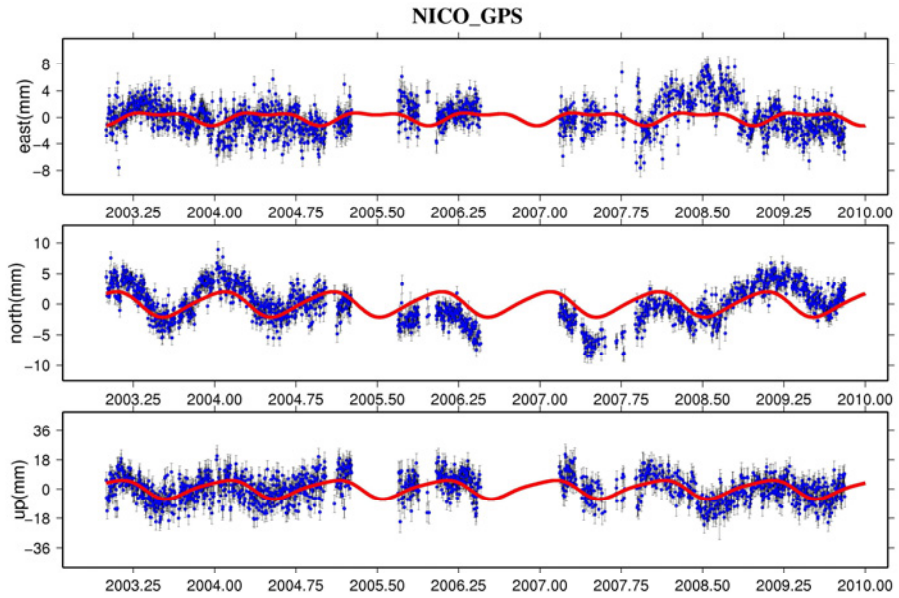
NICO_GPS
east(mm)
north(mm)
up(mm)

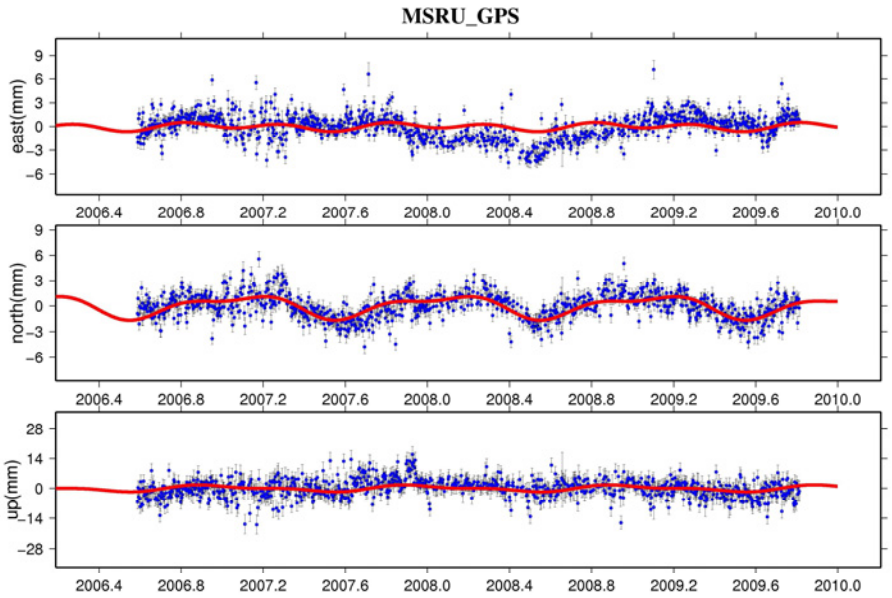
MSRU_GPS
east(mm)
north(mm)
up(mm)

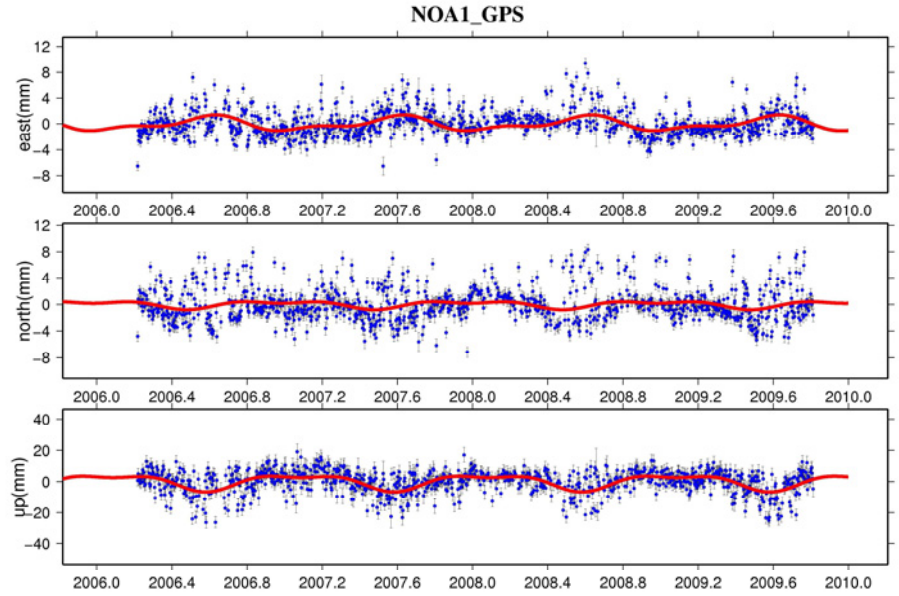
NOA1_GPS
east(mm)
north(mm)
up(mm)

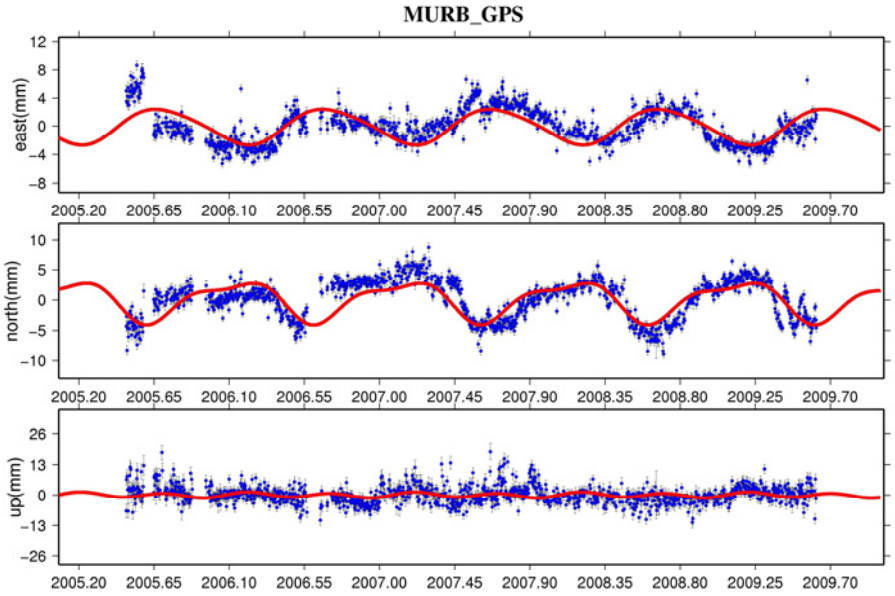
MURB_GPS
east(mm)
north(mm)
up(mm)

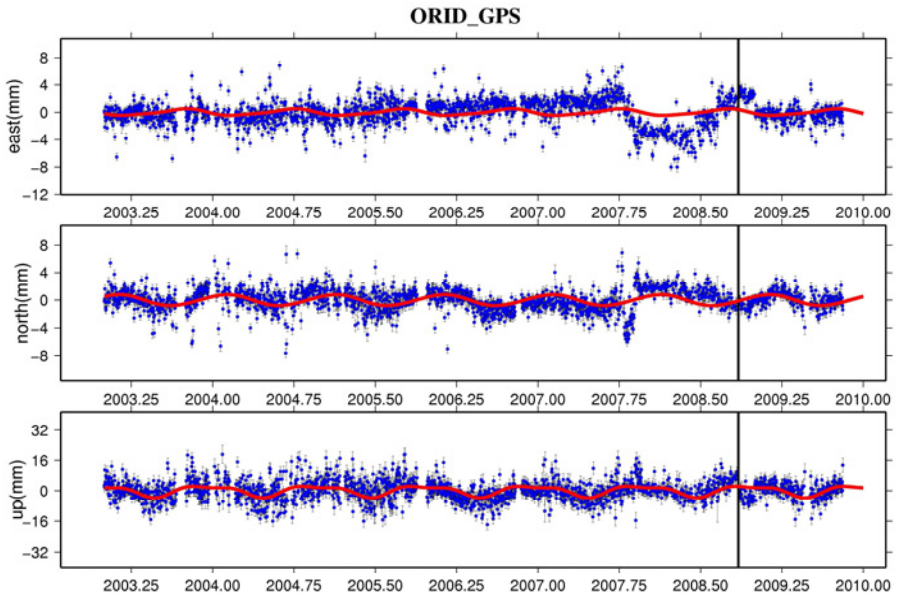
ORID_GPS
east(mm)
north(mm)
up(mm)
2003.25
2004.00
2004.75
2005.50
2006.25
2007.00
2007.75
2008.50
2009.25
2010.00

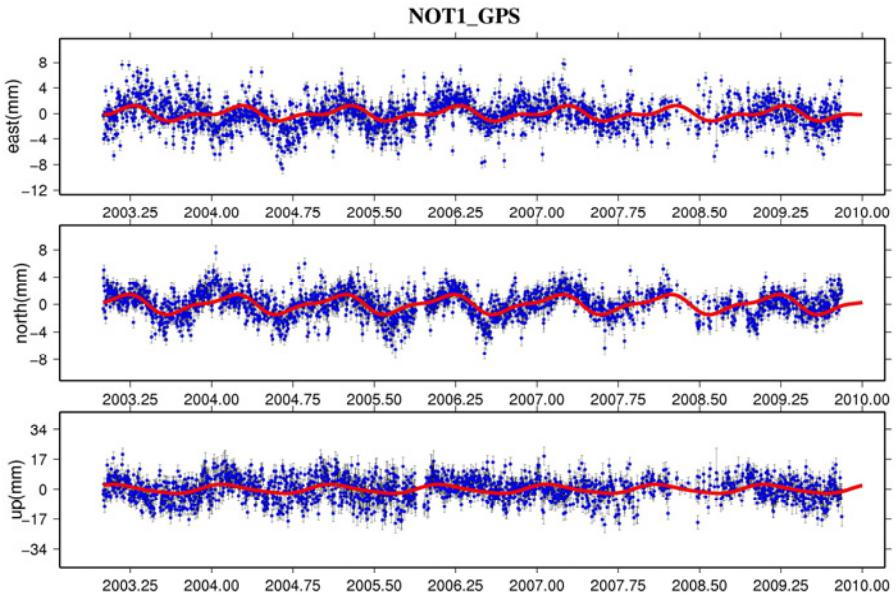
NOT1_GPS
east(mm)
north(mm)
up(mm)
2003.25
2004.00
2004.75
2005.50
2006.25
2007.00
2007.75
2008.50
2009.25
2010.00

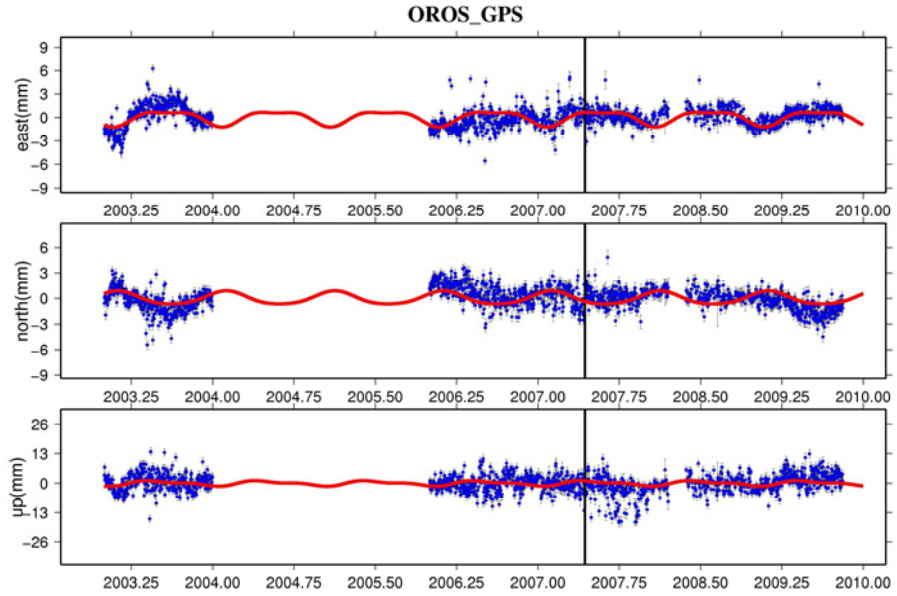
OROS_GPS
east(mm)
north(mm)
up(mm)
2003.25
2004.00
2004.75
2005.50
2006.25
2007.00
2007.75
2008.50
2009.25
2010.00

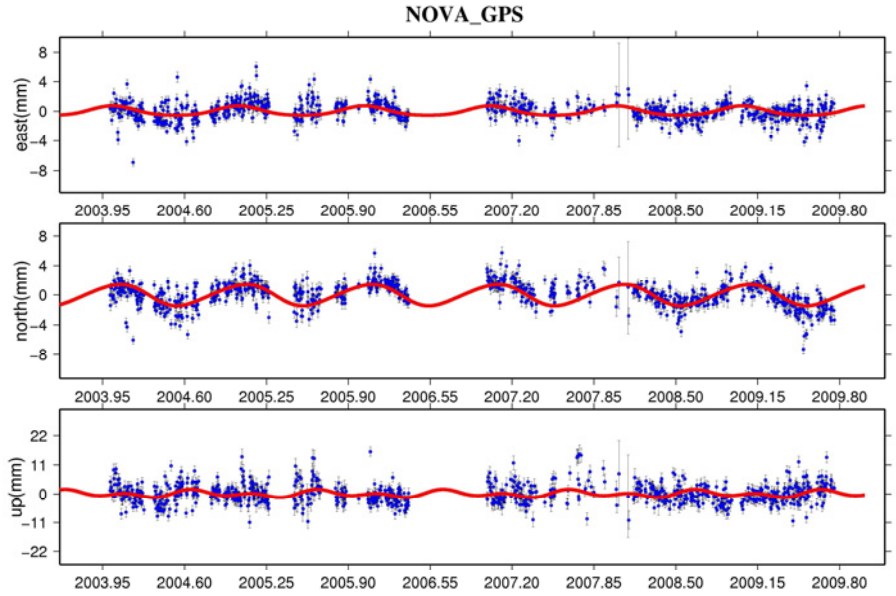
NOVA_GPS
east(mm)
north(mm)
up(mm)
2003.95
2004.60
2005.25
2005.90
2006.55
2007.20
2007.85
2008.50
2009.15
2009.80

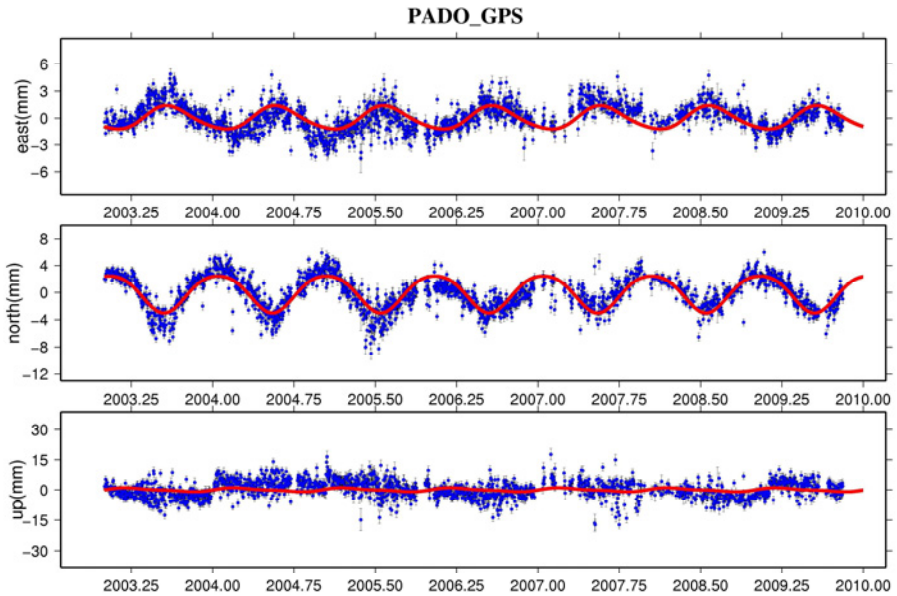
PADO_GPS
east(mm)
north(mm)
up(mm)
2003.25 2004.00 2004.75 2005.50 2006.25 2007.00 2007.75 2008.50 2009.25 2010.00

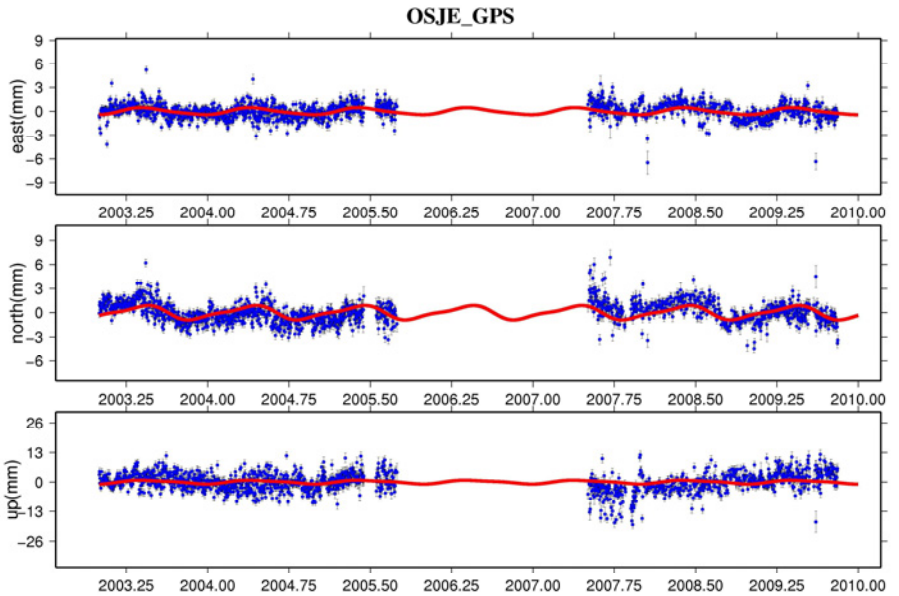
OSJE_GPS
east(mm)
north(mm)
up(mm)
2003.25 2004.00 2004.75 2005.50 2006.25 2007.00 2007.75 2008.50 2009.25 2010.00

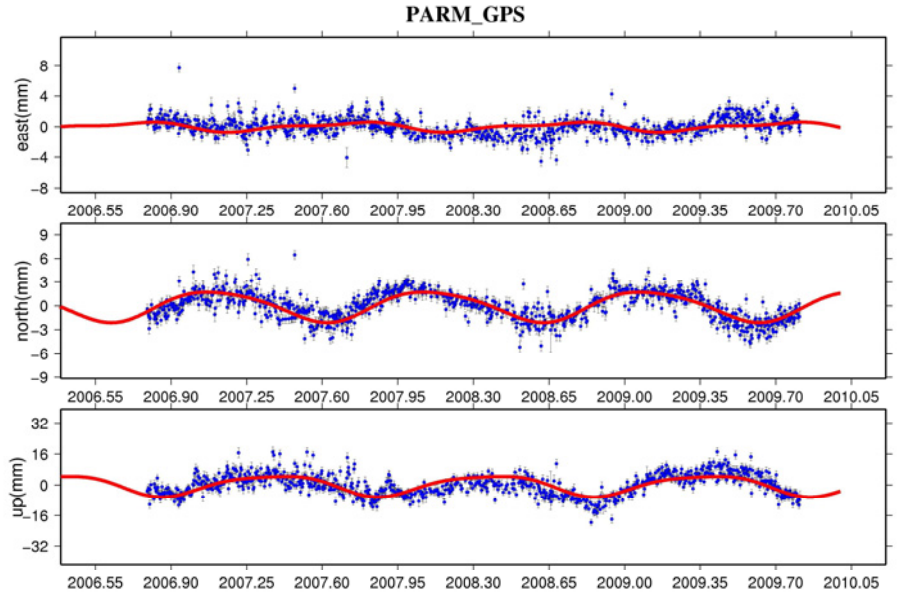
PARM_GPS
east(mm)
north(mm)
up(mm)
2006.55 2006.90 2007.25 2007.60 2007.95 2008.30 2008.65 2009.00 2009.35 2009.70 2010.05

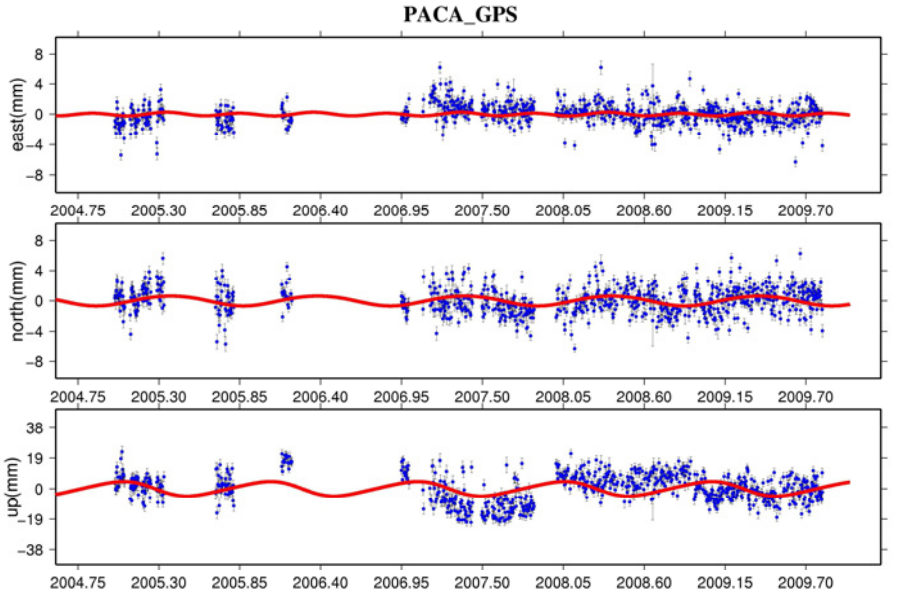
PACA_GPS
east(mm)
north(mm)
up(mm)
2004.75 2005.30 2005.85 2006.40 2006.95 2007.50 2008.05 2008.60 2009.15 2009.70

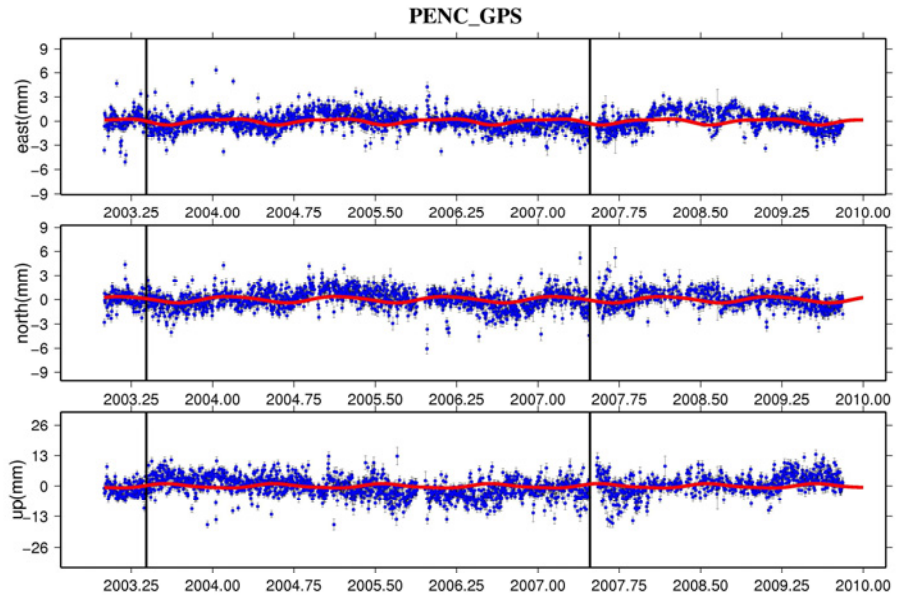
PENC_GPS
east(mm)
north(mm)
up(mm)
2003.25
2004.00
2004.75
2005.50
2006.25
2007.00
2007.75
2008.50
2009.25
2010.00

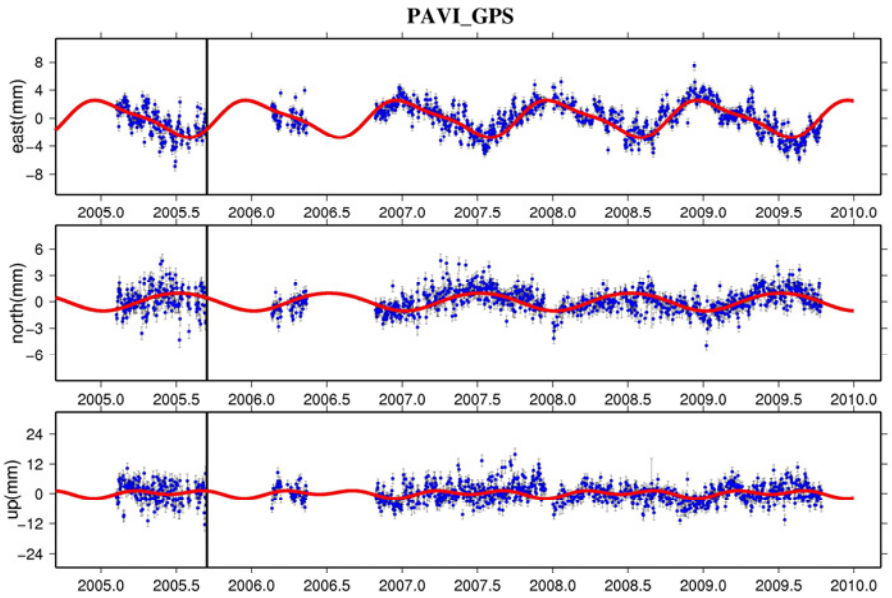
PAVI_GPS
east(mm)
north(mm)
up(mm)
2005.0
2005.5
2006.0
2006.5
2007.0
2007.5
2008.0
2008.5
2009.0
2009.5
2010.0

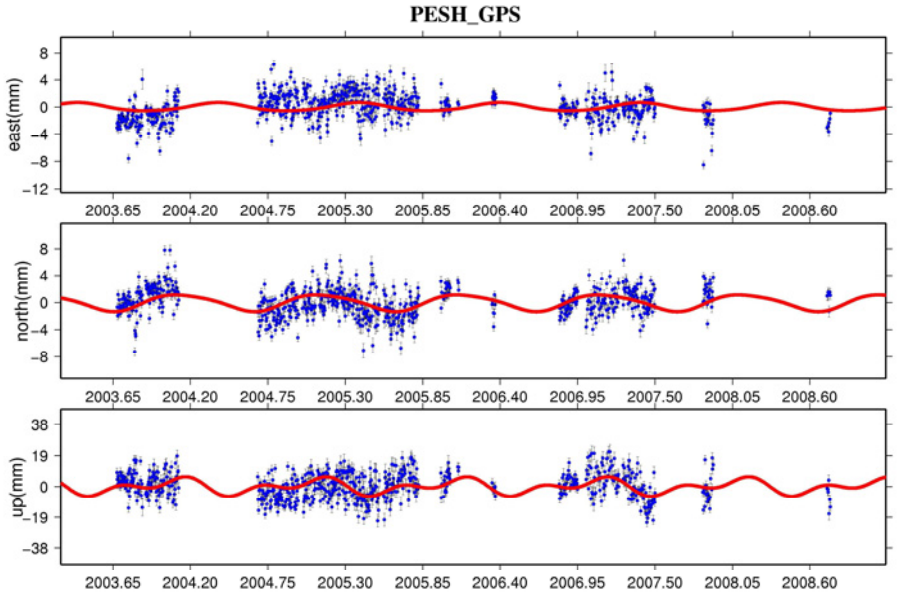
PESH_GPS
east(mm)
north(mm)
up(mm)
2003.65
2004.20
2004.75
2005.30
2005.85
2006.40
2006.95
2007.50
2008.05
2008.60

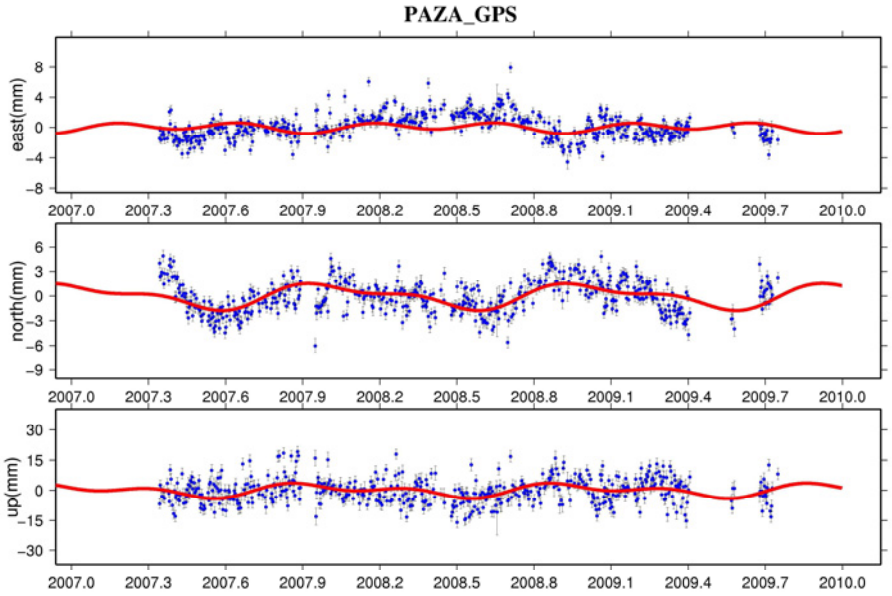
PAZA_GPS
east(mm)
north(mm)
up(mm)
2007.0
2007.3
2007.6
2007.9
2008.2
2008.5
2008.8
2009.1
2009.4
2009.7
2010.0

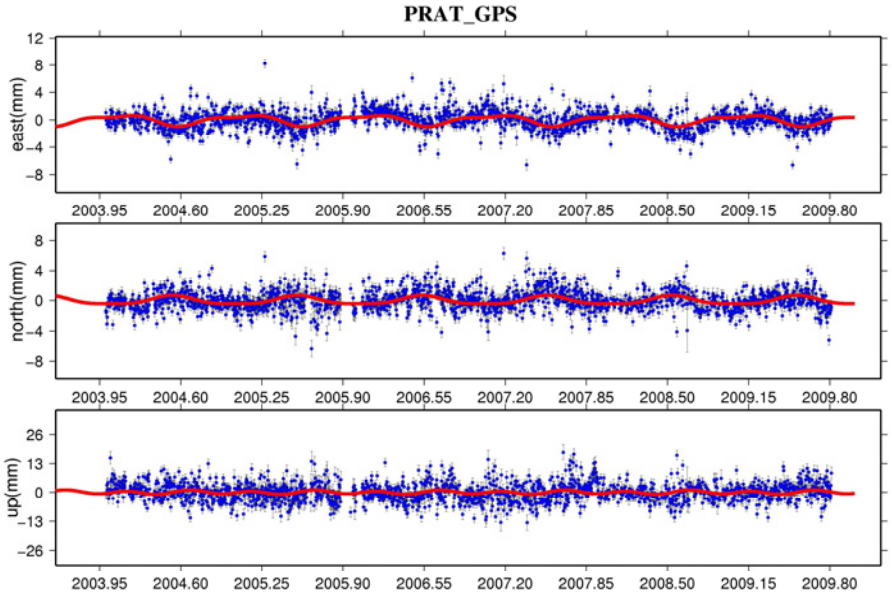
PRAT_GPS
east(mm)
north(mm)
up(mm)
2003.95
2004.60
2005.25
2005.90
2006.55
2007.20
2007.85
2008.50
2009.15
2009.80

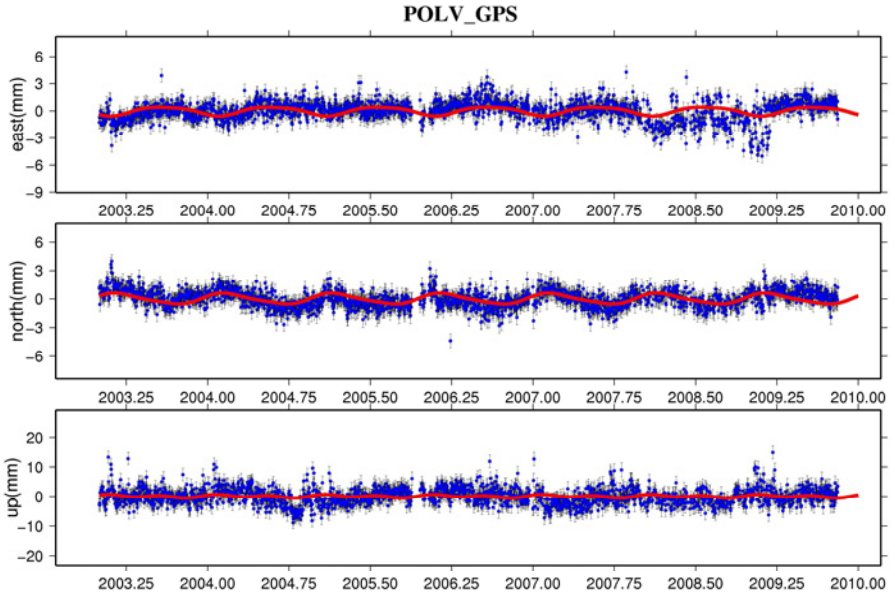
POLV_GPS
east(mm)
north(mm)
up(mm)
2003.25
2004.00
2004.75
2005.50
2006.25
2007.00
2007.75
2008.50
2009.25
2010.00

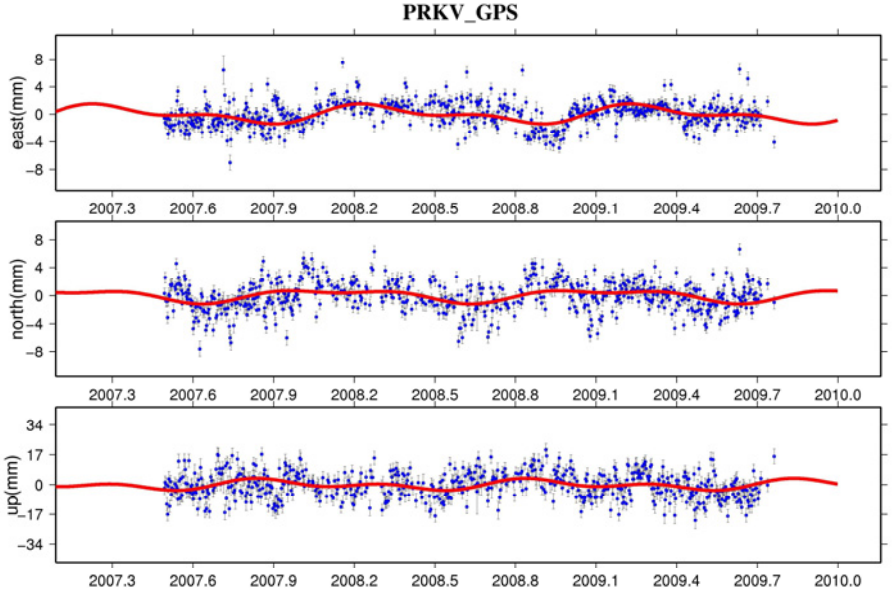
PRKV_GPS
east(mm)
north(mm)
up(mm)
2007.3
2007.6
2007.9
2008.2
2008.5
2008.8
2009.1
2009.4
2009.7
2010.0

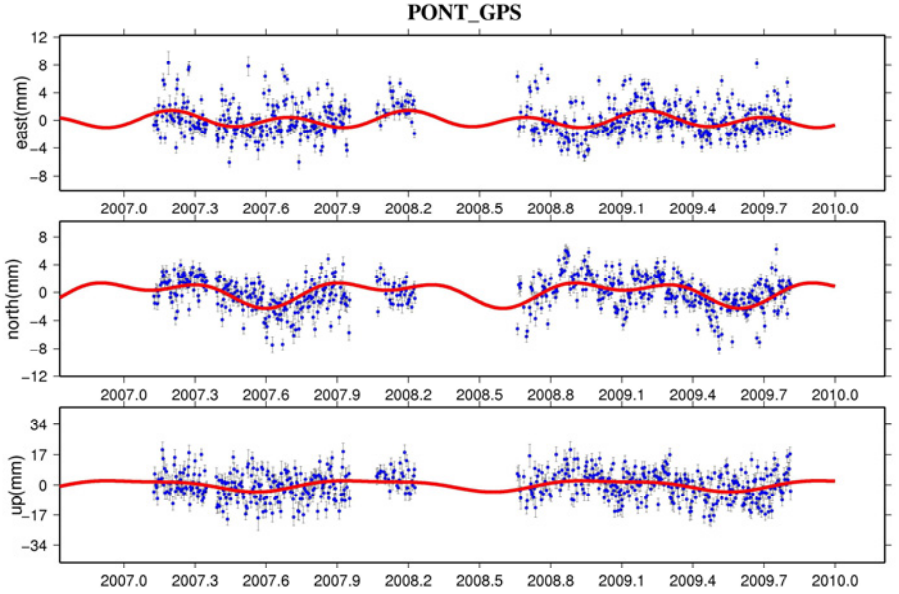
PONT_GPS
east(mm)
north(mm)
up(mm)
2007.0
2007.3
2007.6
2007.9
2008.2
2008.5
2008.8
2009.1
2009.4
2009.7
2010.0

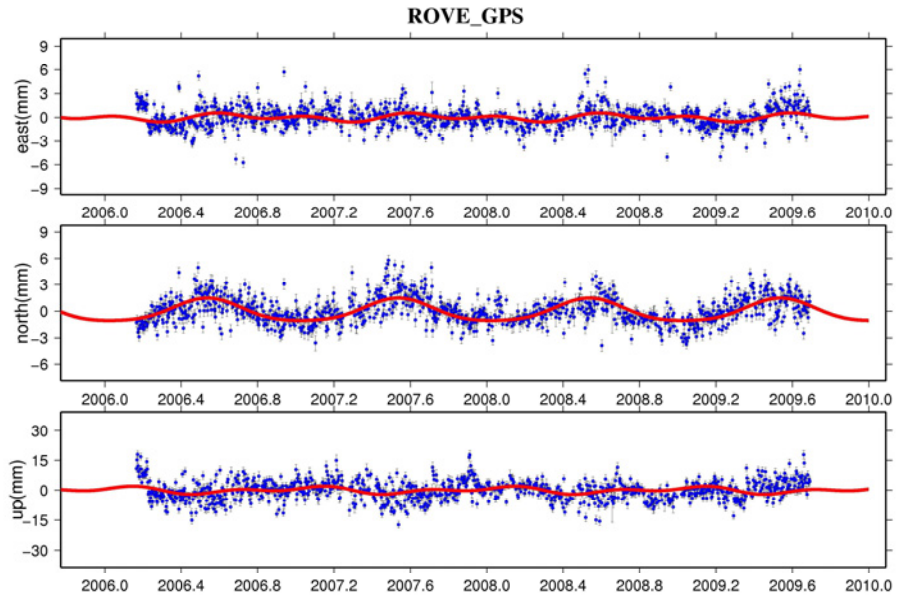
ROVE_GPS
east(mm)
north(mm)
up(mm)

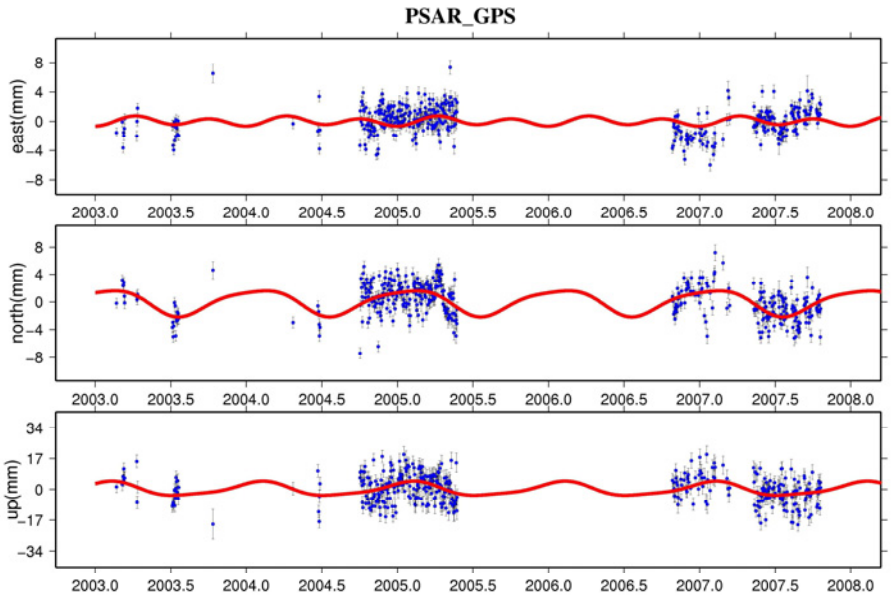
PSAR_GPS
east(mm)
north(mm)
up(mm)

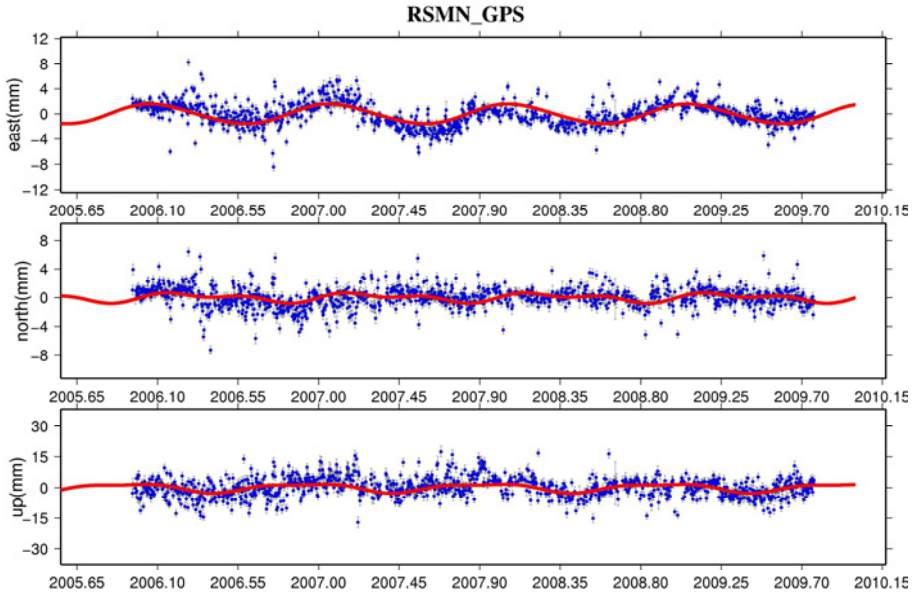
RSMN_GPS
east(mm)
north(mm)
up(mm)

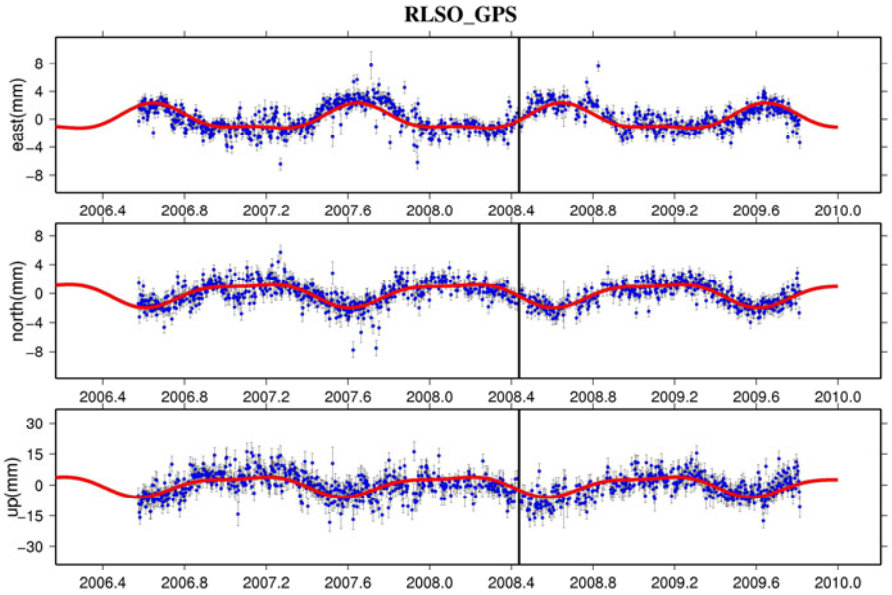
RLSO_GPS
east(mm)
north(mm)
up(mm)

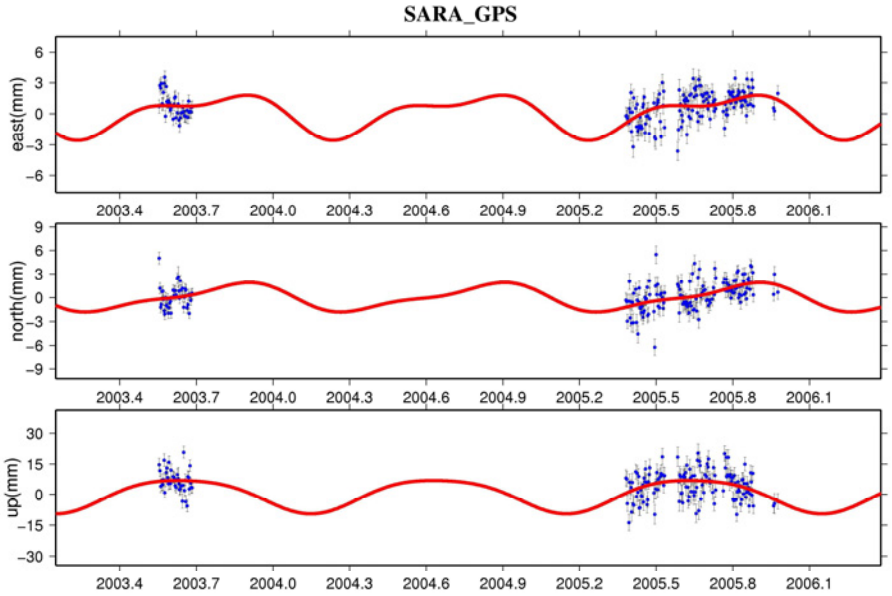
SARA_GPS
east(mm)
north(mm)
up(mm)

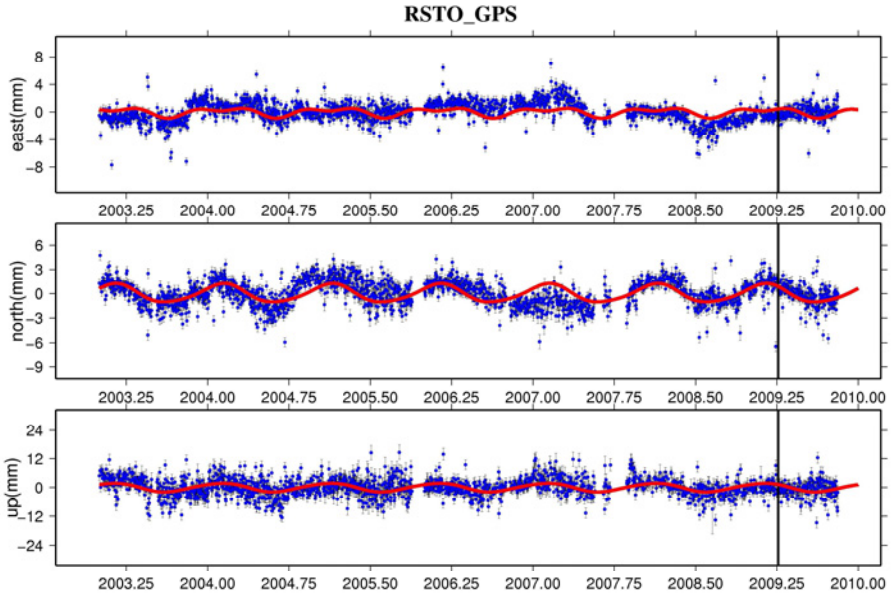
RSTO_GPS
east(mm)
north(mm)
up(mm)

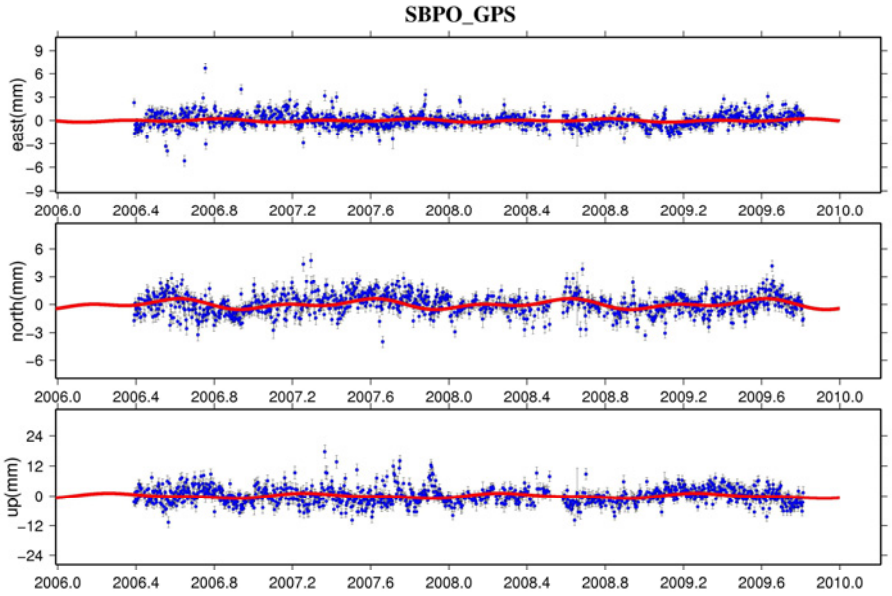
SBPO_GPS
east(mm)
north(mm)
up(mm)

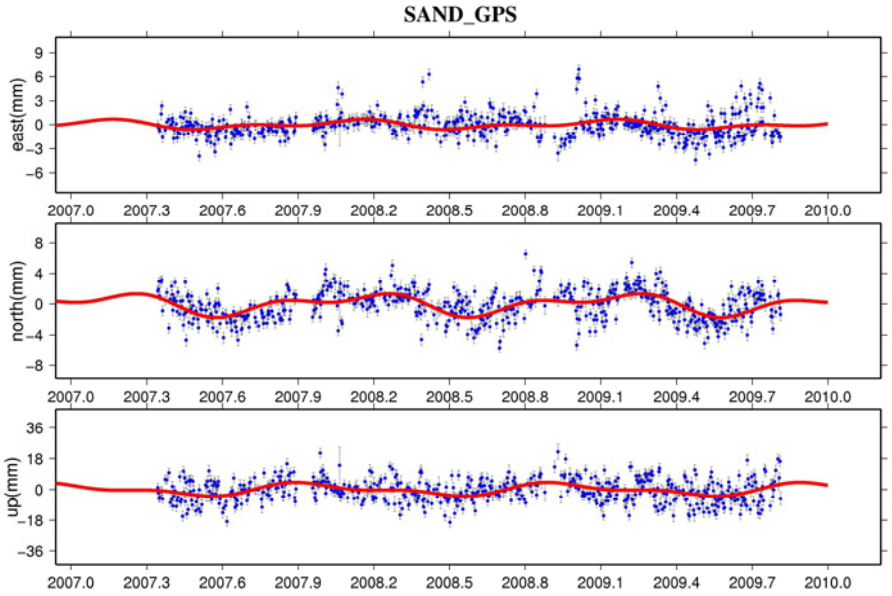
SAND_GPS
east(mm)
north(mm)
up(mm)

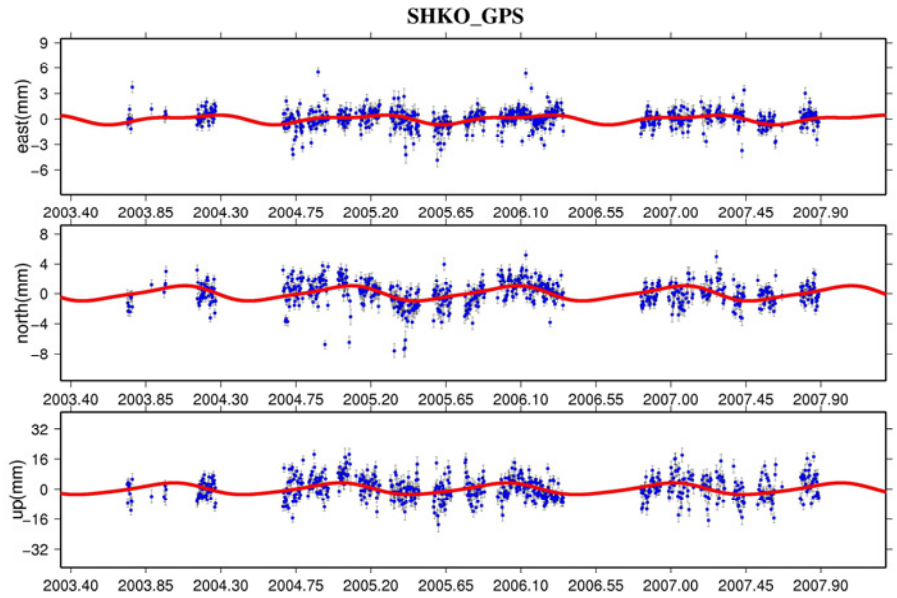
SHKO_GPS
east(mm)
north(mm)
up(mm)

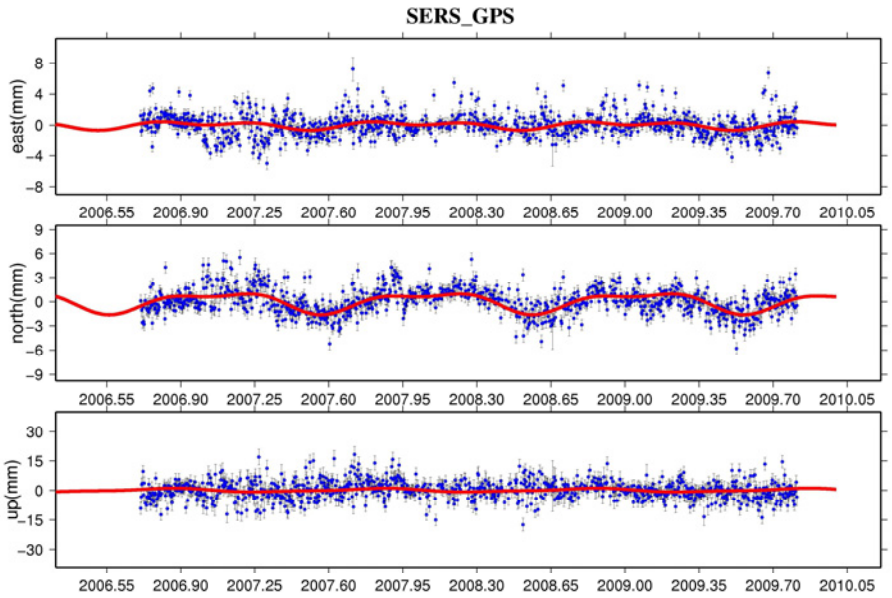
SERS_GPS
east(mm)
north(mm)
up(mm)

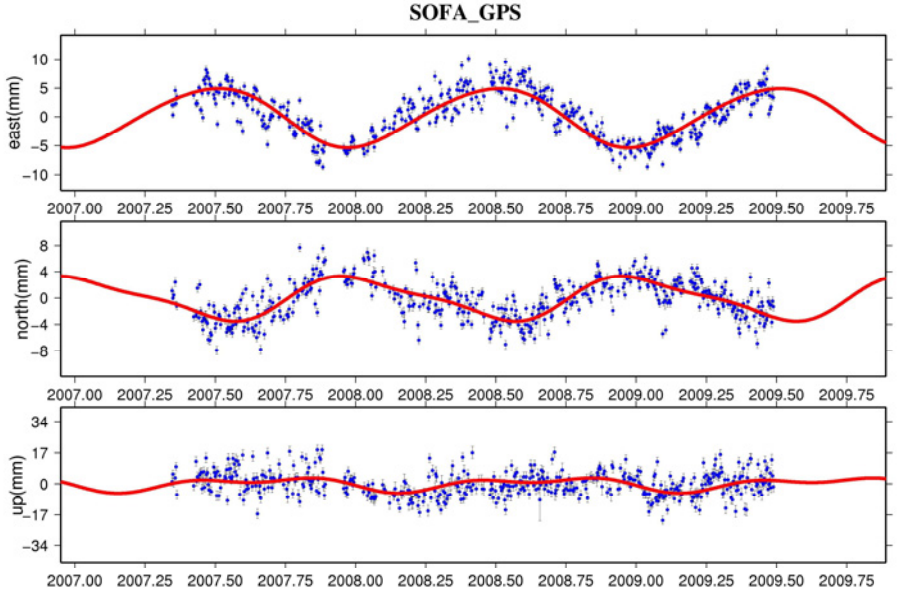
SOFA_GPS
east(mm)
north(mm)
up(mm)

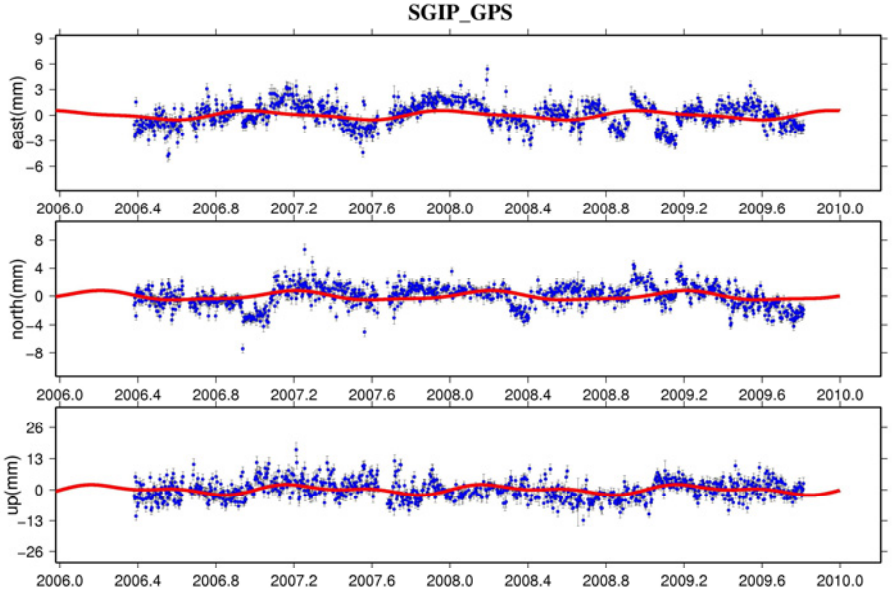
SGIP_GPS
east(mm)
north(mm)
up(mm)

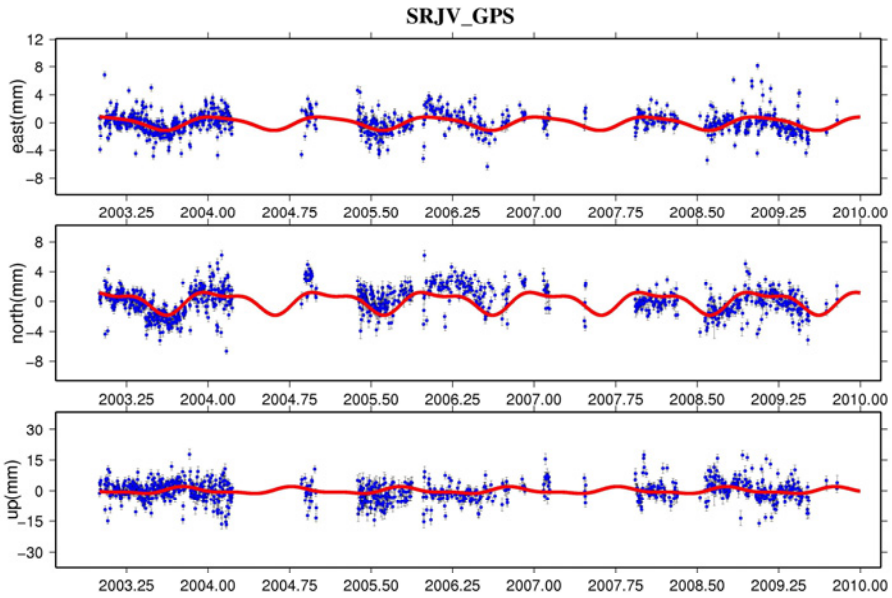
SRJV_GPS
east(mm)
north(mm)
up(mm)
2003.25 2004.00 2004.75 2005.50 2006.25 2007.00 2007.75 2008.50 2009.25 2010.00

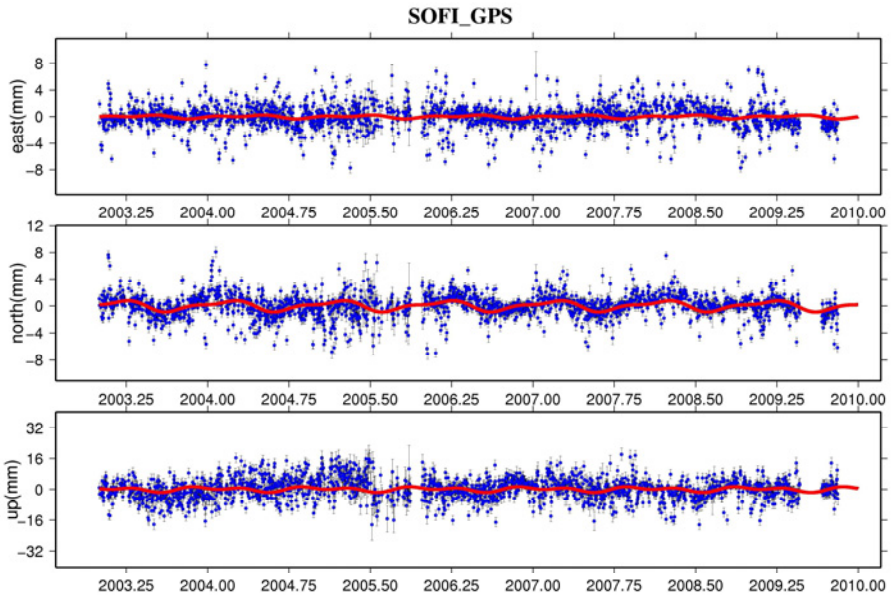
SOFI_GPS
east(mm)
north(mm)
up(mm)
2003.25 2004.00 2004.75 2005.50 2006.25 2007.00 2007.75 2008.50 2009.25 2010.00

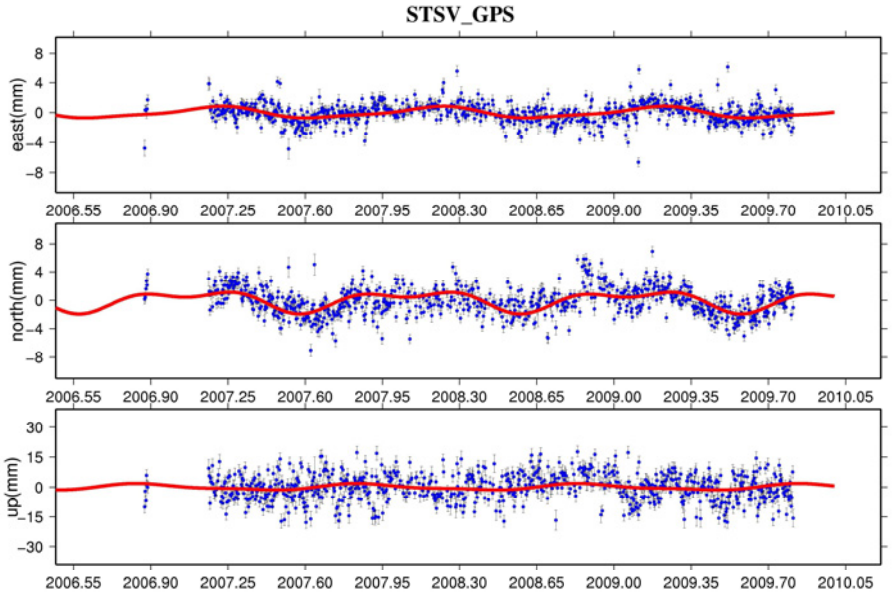
STSV_GPS
east(mm)
north(mm)
up(mm)
2006.55 2006.90 2007.25 2007.60 2007.95 2008.30 2008.65 2009.00 2009.35 2009.70 2010.05

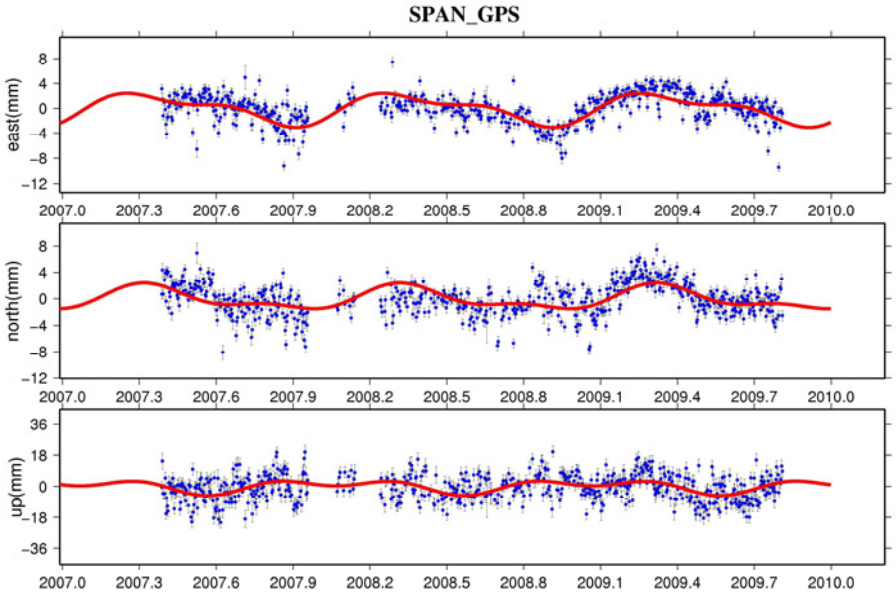
SPAN_GPS
east(mm)
north(mm)
up(mm)
2007.0 2007.3 2007.6 2007.9 2008.2 2008.5 2008.8 2009.1 2009.4 2009.7 2010.0

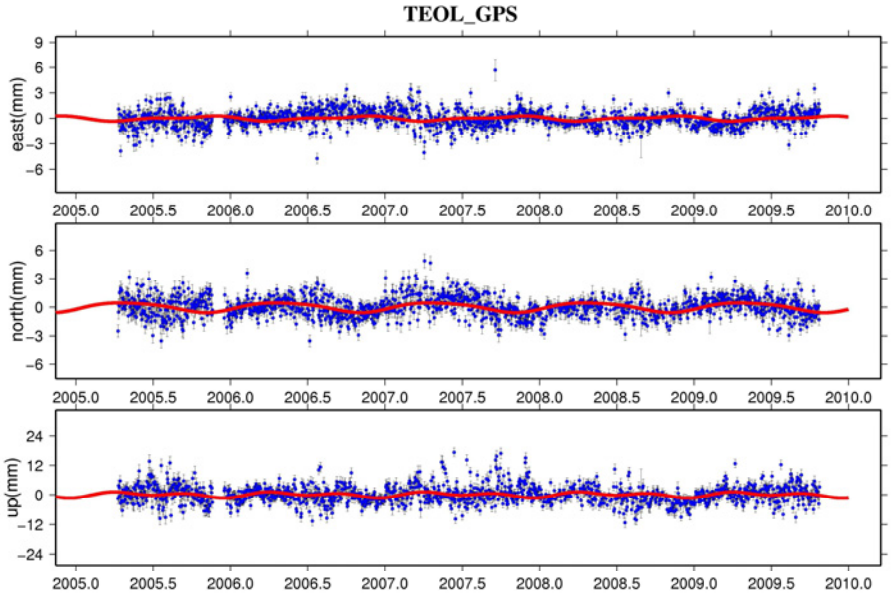
TEOL_GPS
east(mm)
north(mm)
up(mm)

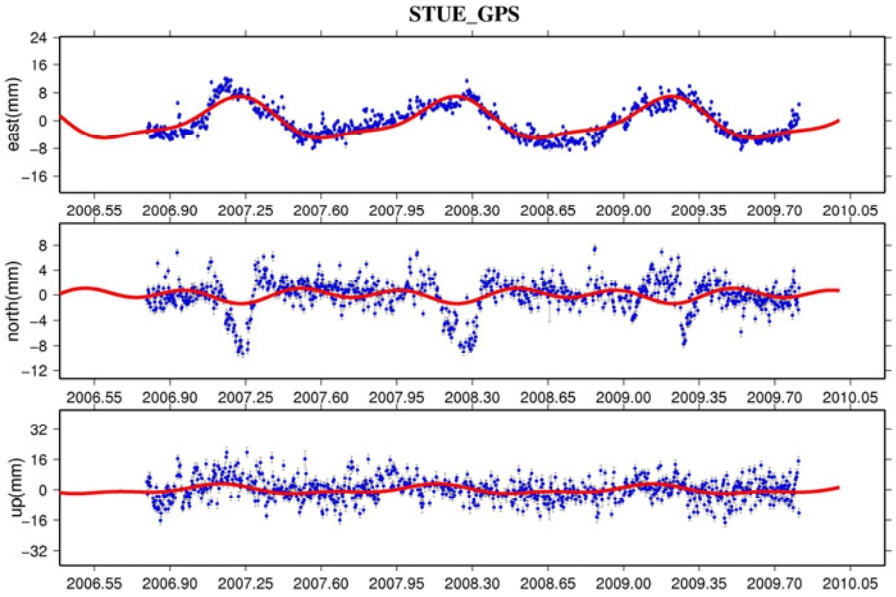
STUE_GPS
east(mm)
north(mm)
up(mm)

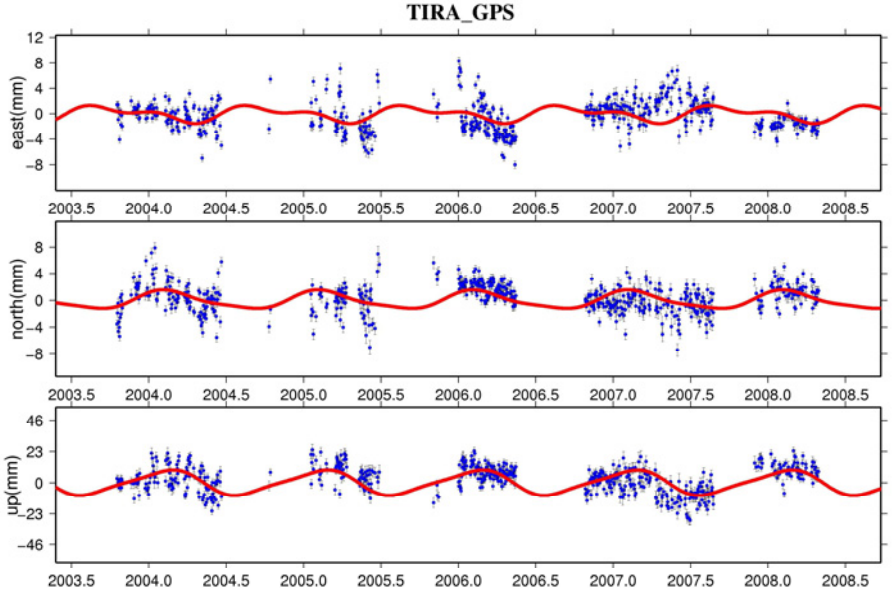
TIRA_GPS
east(mm)
north(mm)
up(mm)

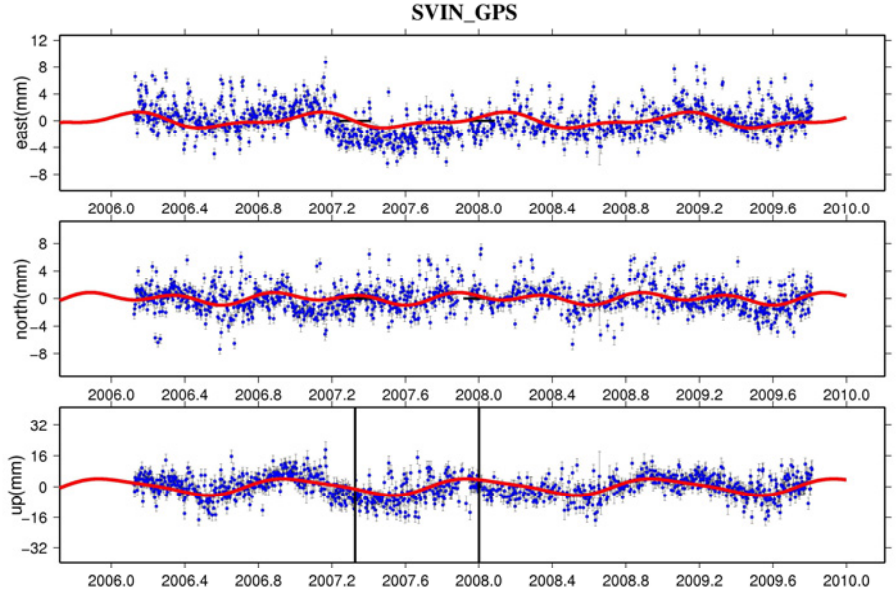
SVIN_GPS
east(mm)
north(mm)
up(mm)

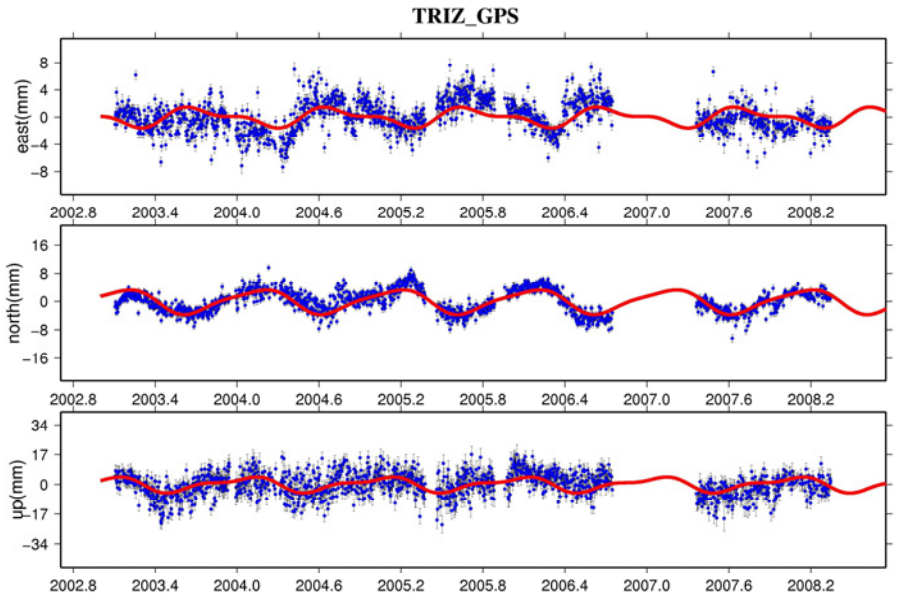
TRIZ_GPS
east(mm)
north(mm)
up(mm)

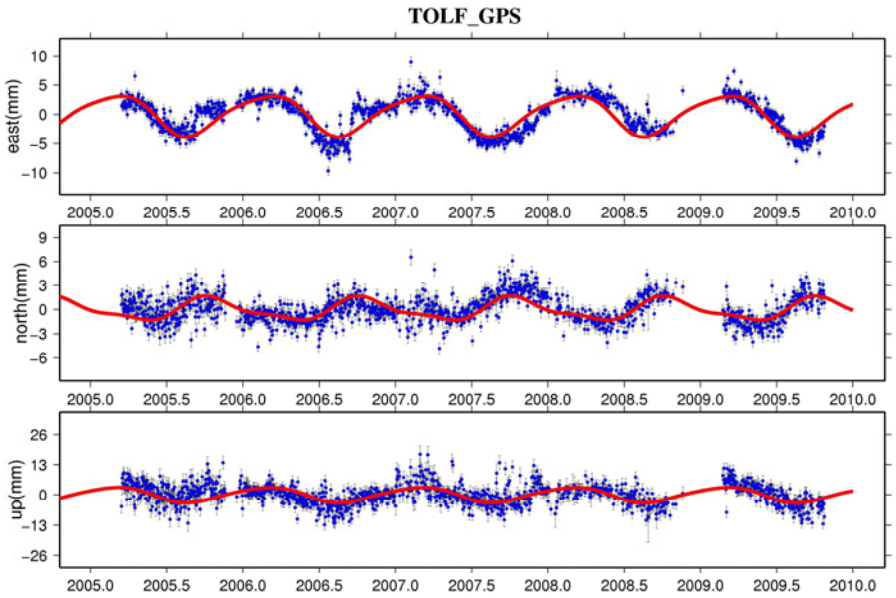
TOLF_GPS
east(mm)
north(mm)
up(mm)

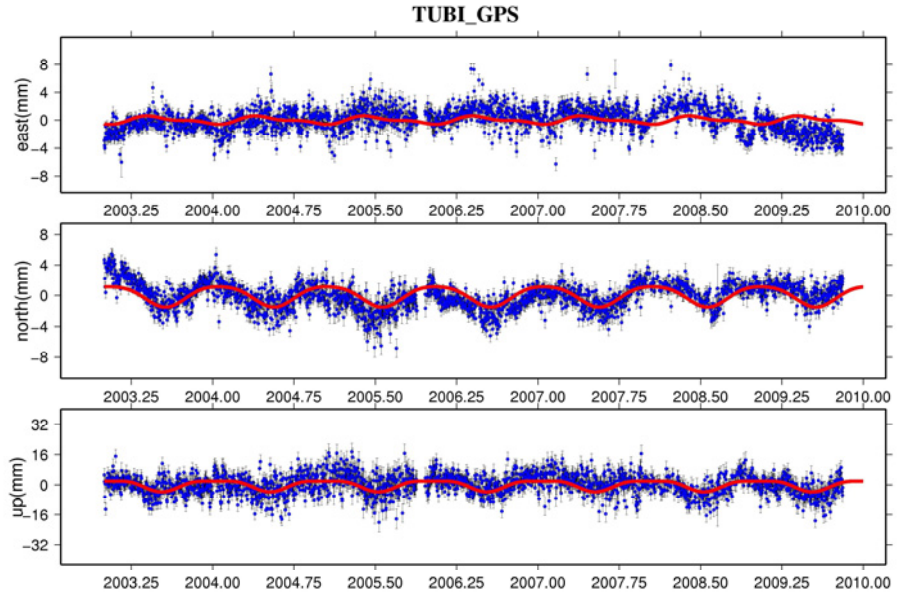
TUBI_GPS
east(mm)
north(mm)
up(mm)

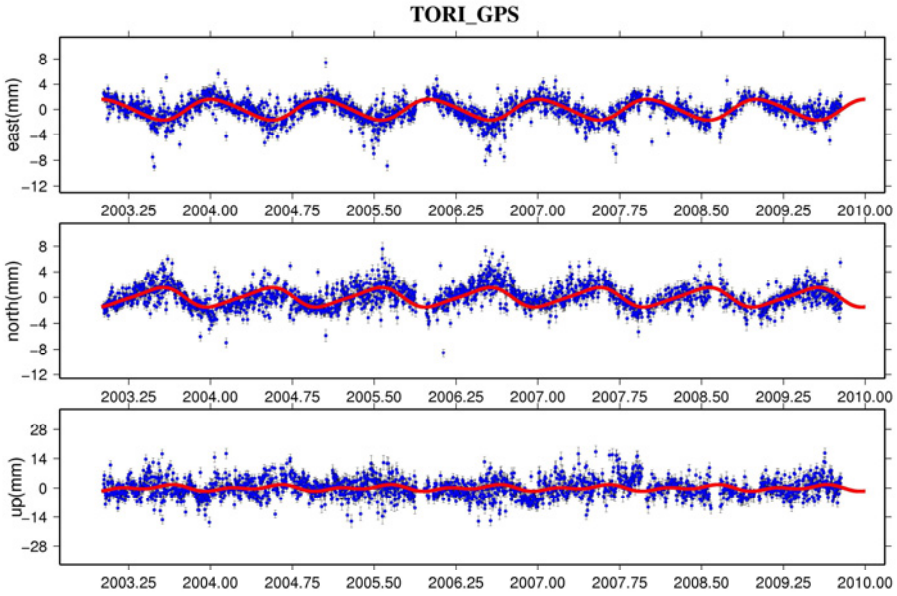
TORI_GPS
east(mm)
north(mm)
up(mm)

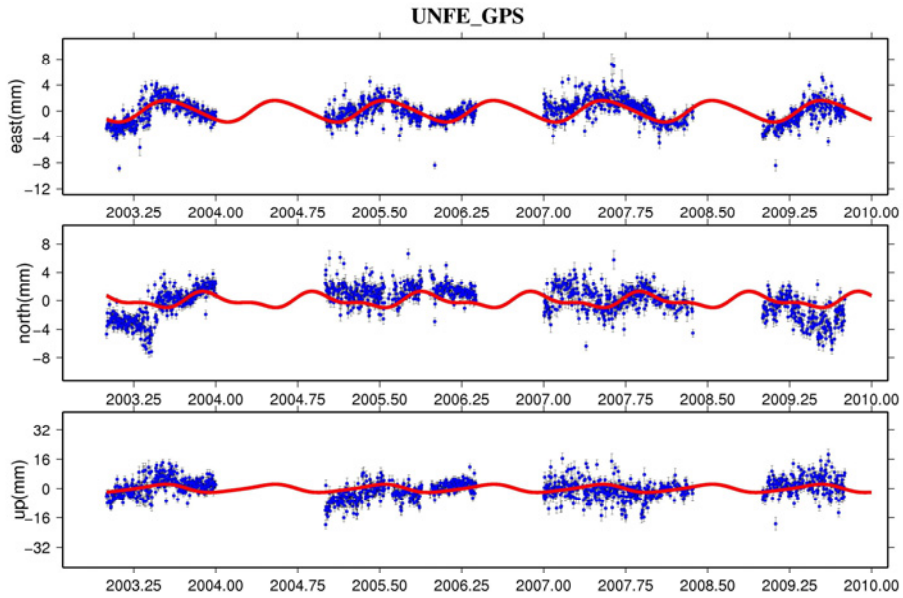
UNFE_GPS
east(mm)
north(mm)
up(mm)
2003.25
2004.00
2004.75
2005.50
2006.25
2007.00
2007.75
2008.50
2009.25
2010.00

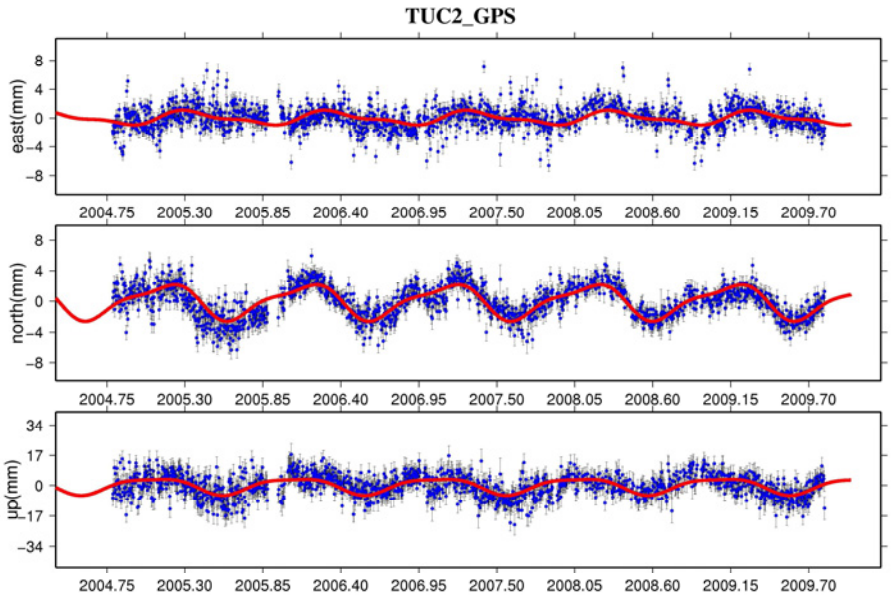
TUC2_GPS
east(mm)
north(mm)
up(mm)
2004.75
2005.30
2005.85
2006.40
2006.95
2007.50
2008.05
2008.60
2009.15
2009.70

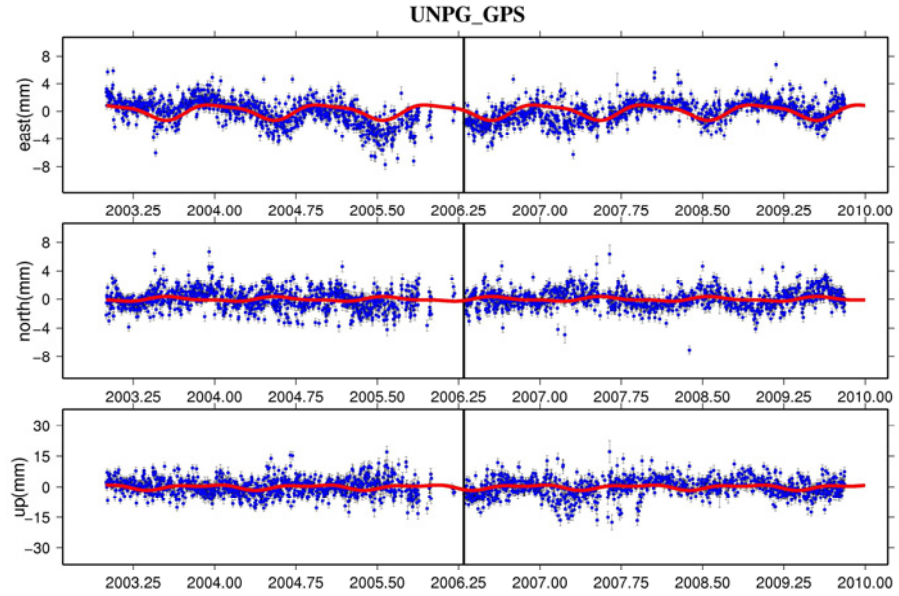
UNPG_GPS
east(mm)
north(mm)
up(mm)
2003.25
2004.00
2004.75
2005.50
2006.25
2007.00
2007.75
2008.50
2009.25
2010.00

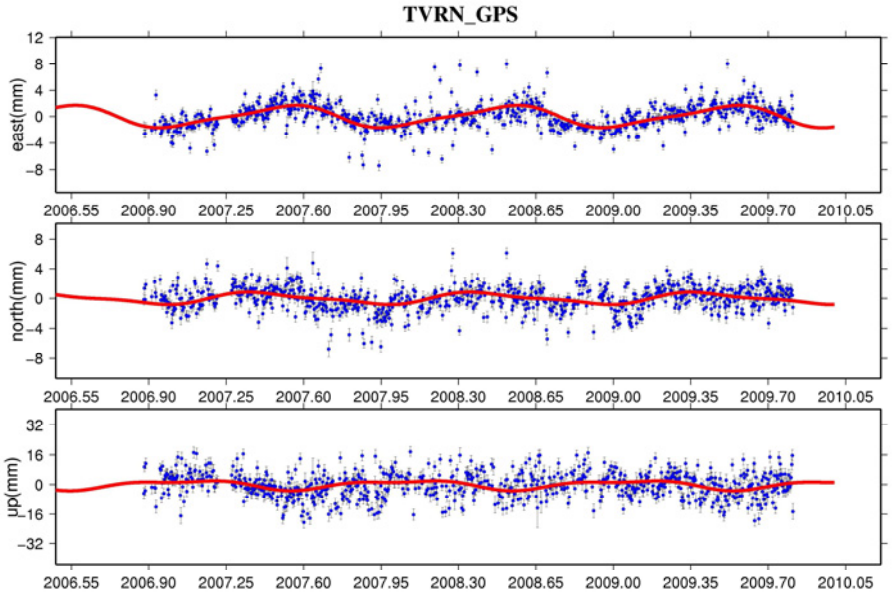
TVRN_GPS
east(mm)
north(mm)
up(mm)
2006.55
2006.90
2007.25
2007.60
2007.95
2008.30
2008.65
2009.00
2009.35
2009.70
2010.05

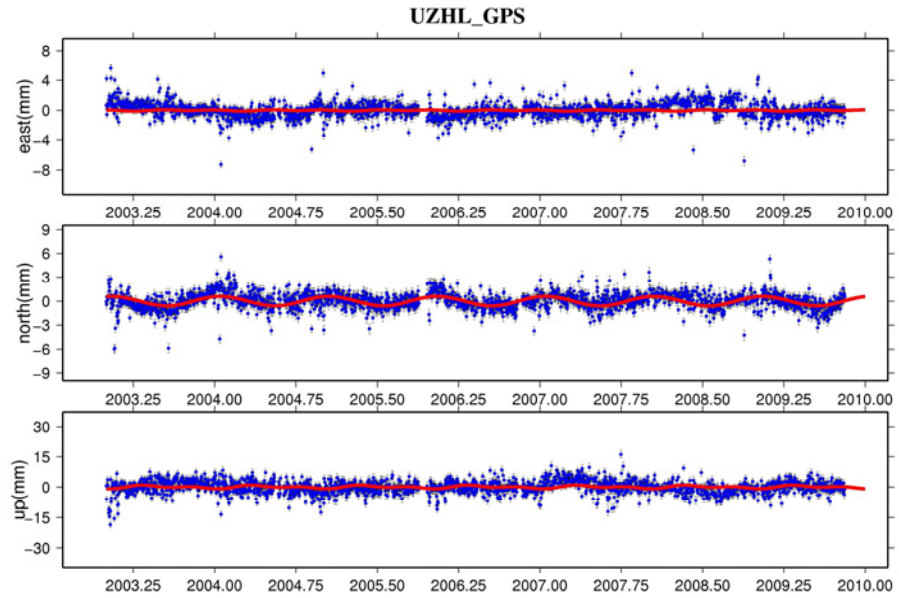
UZHL_GPS
east(mm)
north(mm)
up(mm)

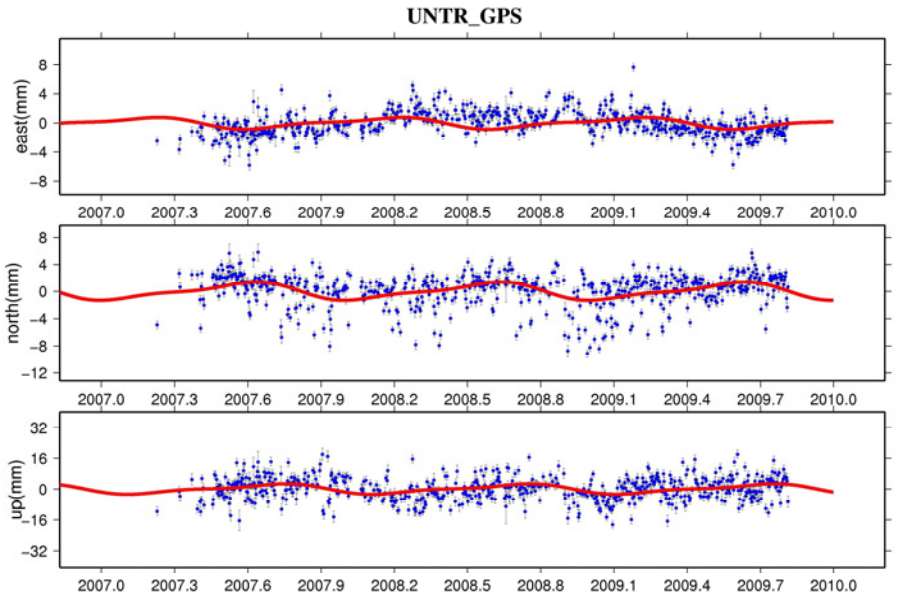
UNTR_GPS
east(mm)
north(mm)
up(mm)

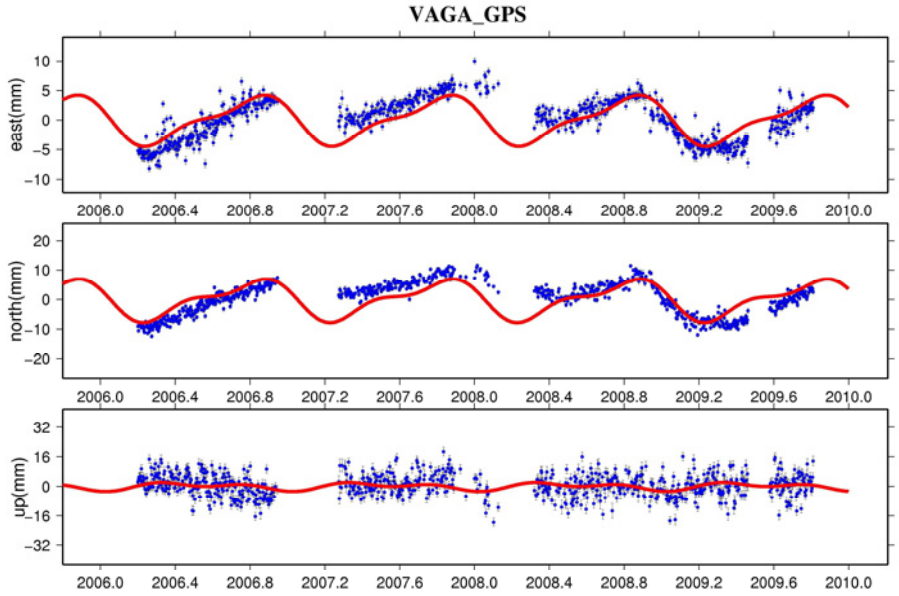
VAGA_GPS
east(mm)
north(mm)
up(mm)

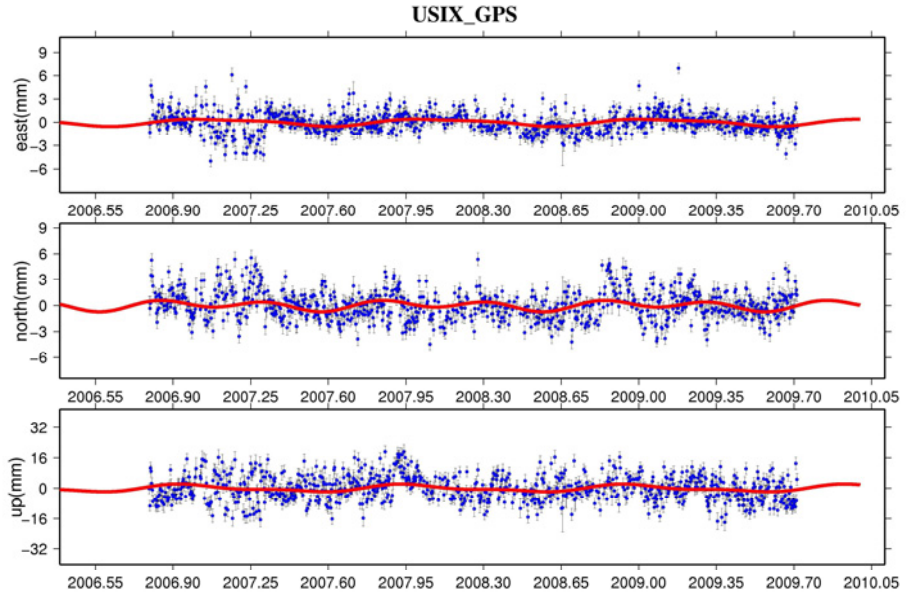
USIX_GPS
east(mm)
north(mm)
up(mm)

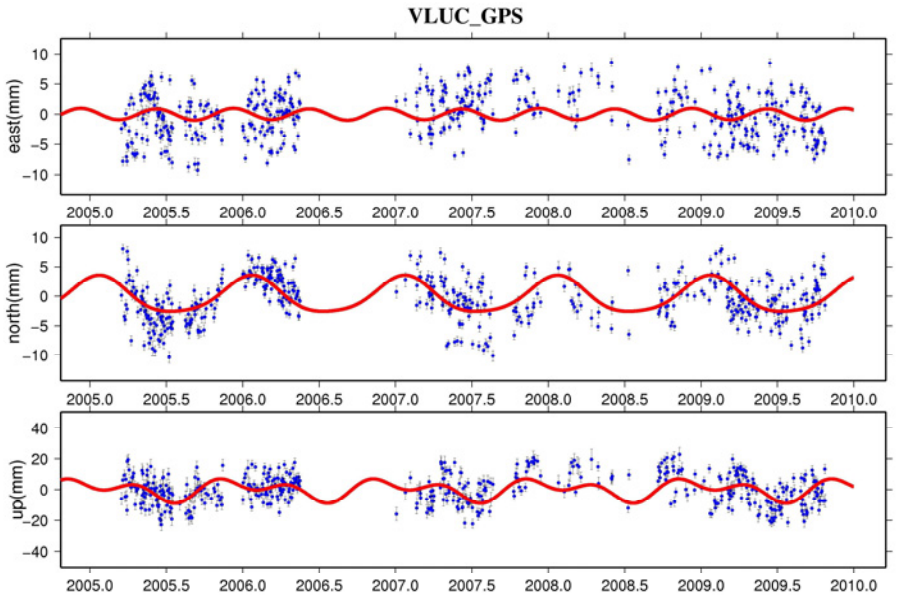
VLUC_GPS
east(mm)
north(mm)
up(mm)

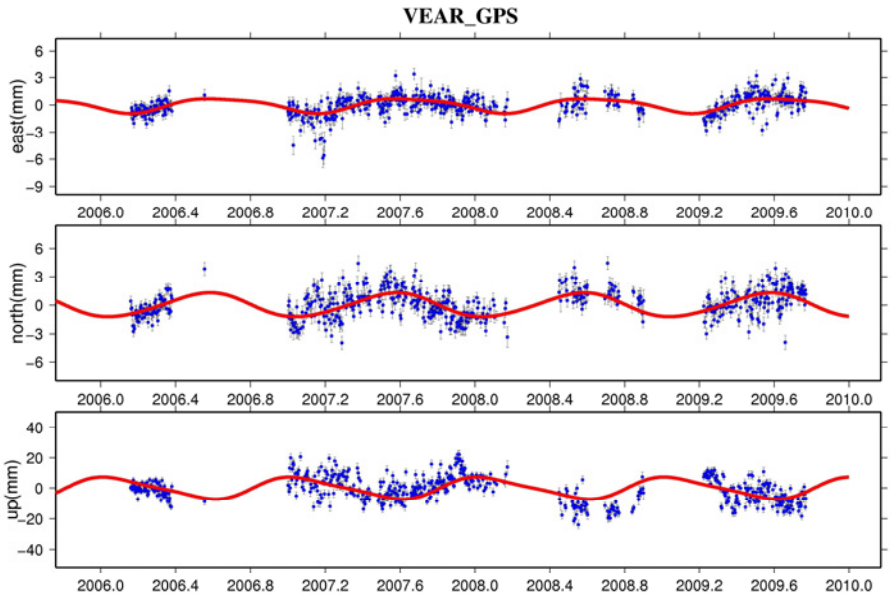
VEAR_GPS
east(mm)
north(mm)
up(mm)

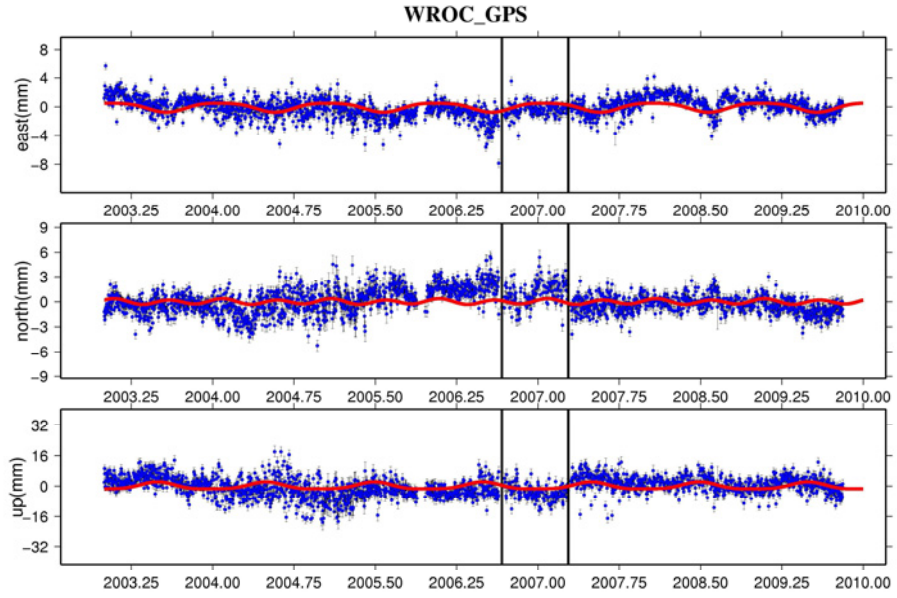
WROC_GPS
east(mm)
north(mm)
up(mm)

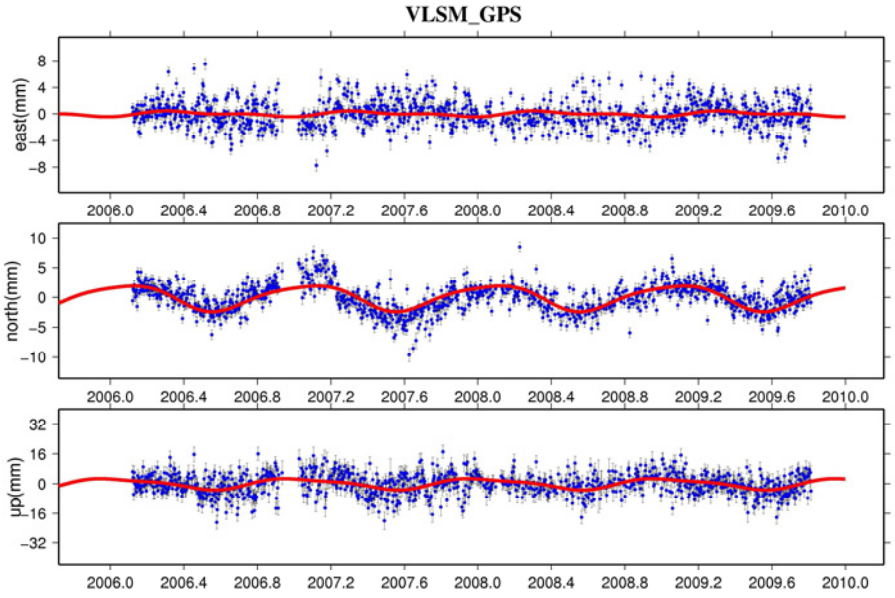
VLSM_GPS
east(mm)
north(mm)
up(mm)

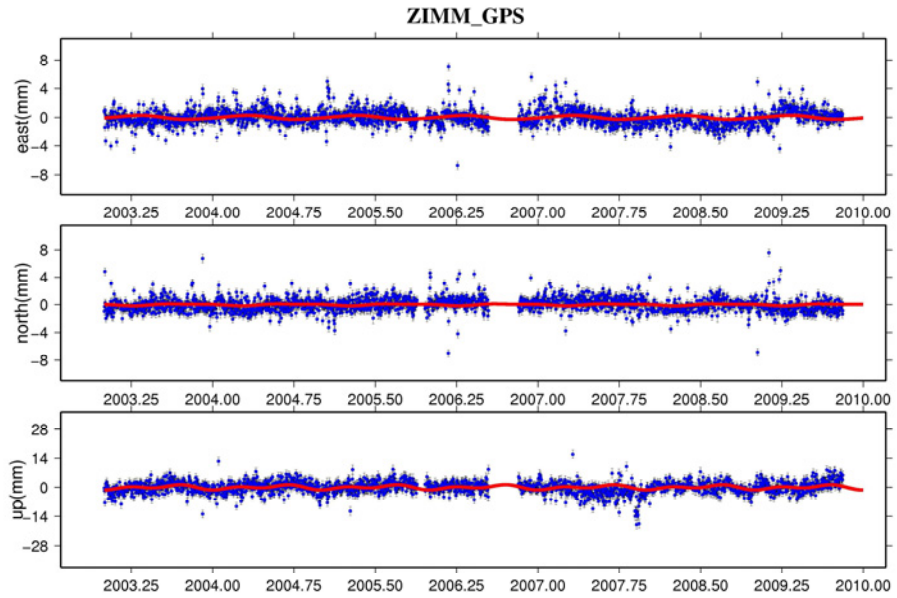
ZIMM_GPS
east(mm)
north(mm)
up(mm)
2003.25
2004.00
2004.75
2005.50
2006.25
2007.00
2007.75
2008.50
2009.25
2010.00

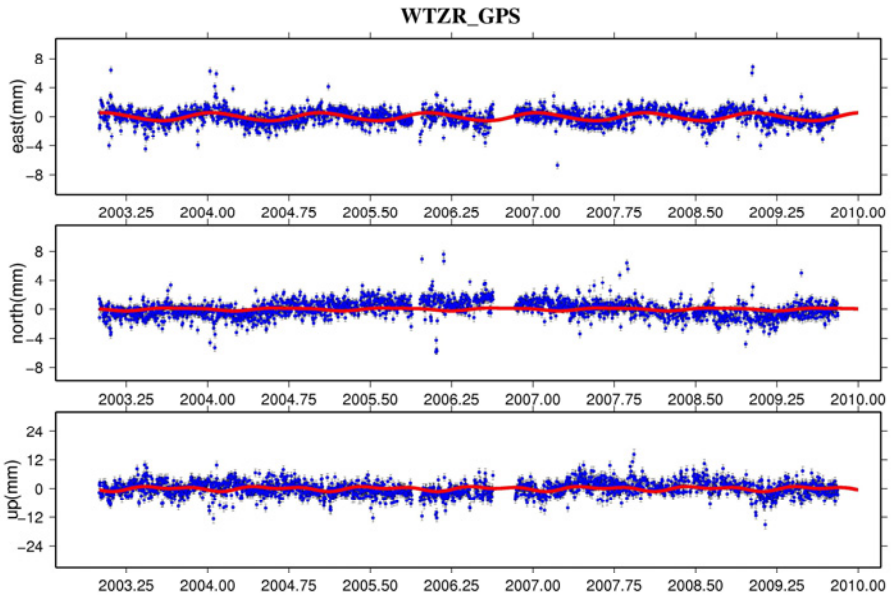
WTZR_GPS
east(mm)
north(mm)
up(mm)
2003.25
2004.00
2004.75
2005.50
2006.25
2007.00
2007.75
2008.50
2009.25
2010.00

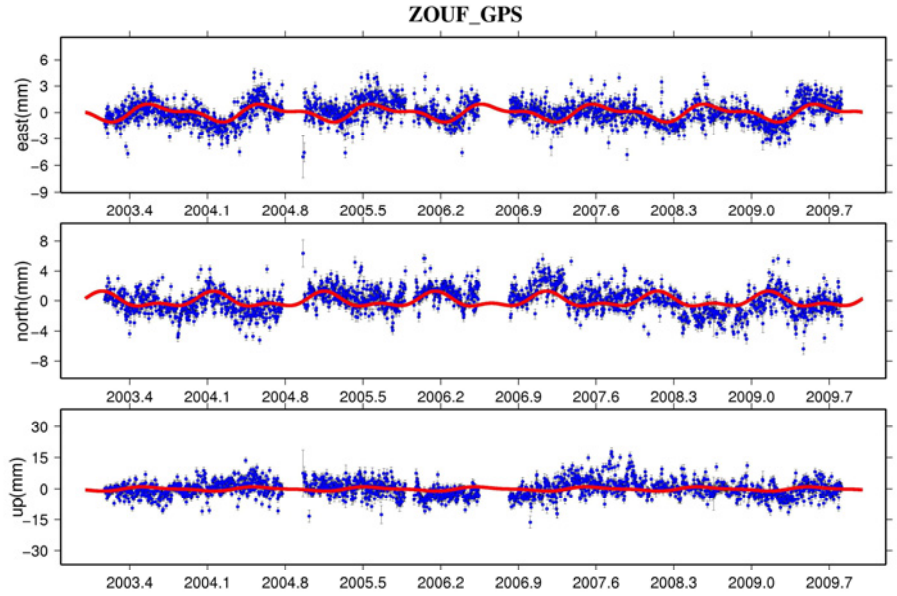
ZOUF_GPS
east(mm)
north(mm)
up(mm)
2003.4
2004.1
2004.8
2005.5
2006.2
2006.9
2007.6
2008.3
2009.0
2009.7

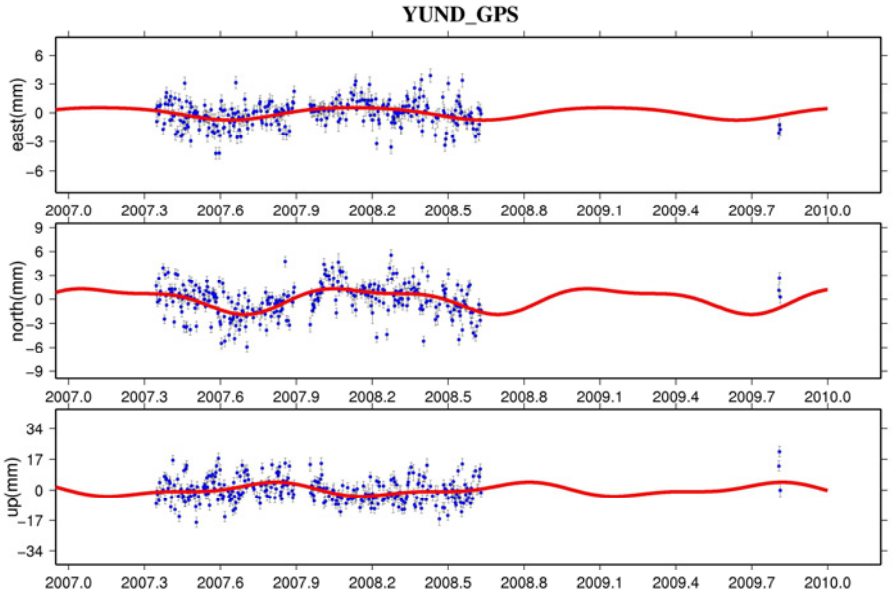
YUND_GPS
east(mm)
north(mm)
up(mm)
2007.0
2007.3
2007.6
2007.9
2008.2
2008.5
2008.8
2009.1
2009.4
2009.7
2010.0

Appendix C

Log files and photos

C.1 GPS permanent station VAGA

C.1.1 Photos

Figure C.1a. *Station monument of VAGA.*

Figure C.1b. *Station monument of VAGA.*

C.1.2. Log file of the GPS permanent station VAGA

VAGA Site Information Form (site log)
International GPS Service
See Instructions at:
ftp://igscb.jpl.nasa.gov/pub/station/general/sitelog_instr.txt

0. Form

Prepared by (full name) : Luigi_Zarrilli
Date Prepared : 2009-07-31T00:00Z
Report Type : DYNAMIC
If Update:
Previous Site Log :
Modified/Added Sections :

1. Site Identification of the GNSS Monument

Site Name : Valle Agricola
Four Character ID : VAGA
Monument Inscription : none
IERS DOMES Number : (A9)
CDP Number : NONE
Monument Description : Wyatt/Agnew drilled-braced
Height of the Monument : 1.2
Monument Foundation : steel rods
Foundation Depth : 1.5
Marker Description : Top of center support screw on SCIGN D3
Date installed : 2005-03-15T00:00Z

Geologic Characteristic : bedrock
Bedrock type : sedimentary
Additional Information :

2. Site Location Information

City or Town : Valle Agricola
State or Province : Campania
Country : Italia
Tectonic Plate : Nubia-Eurasia plate boundary
Approximate Position (ITRF)
X coordinate (m) : 4643697.8353
Y coordinate (m) : 1178022.4562
Z coordinate (m) : 4197656.6267
Latitude (N is +) : +412455.55651
Longitude (E is +) : +0141404.64330
Elevation (m, ellips.) : 791.20
Additional Information :

3. GNSS Receiver Information

3.1 Receiver Type : LEICA GRX1200PRO
Satellite System : GPS
Serial Number : 455305
Firmware Version : 1.52
Elevation Cutoff Setting : 10
Date installed : 2005-03-15T00:00Z
Date removed : 2005-04-07T00:00Z
Temperature Stabiliz. : 20° C +- 5°C
Additional Information :

3.2 Receiver Type : LEICA GRX1200PRO
Satellite System : GPS
Serial Number : 454410
Firmware Version : 1.52
Elevation Cutoff Setting : 10
Date installed : 2005-04-08T00:00Z
Date removed : 2008-03-30T00:00Z
Temperature Stabiliz. : 20° C +- 5°C
Additional Information : firmware upgrade

3.3 Receiver Type : LEICA GRX1200PRO
Satellite System : GPS
Serial Number : 454410
Firmware Version : 5.62
Elevation Cutoff Setting : 10
Date installed : 2008-03-31T00:00Z
Date removed : 2009-07-30T00:00Z
Temperature Stabiliz. : 20° C +- 5°C
Additional Information :

3.4 Receiver Type : LEICA GRX1200PRO
Satellite System : GPS
Serial Number : 461576
Firmware Version : 5.62
Elevation Cutoff Setting : 10
Date installed : 2009-07-30T00:00Z
Date removed : CCYY-MM-DDThh:mmZ
Temperature Stabiliz. : +-20°C
Additional Information :

3.x Receiver Type : (A20, from rcvr_ant.tab; see instructions)
Satellite System : (GPS/GLONASS/GPS+GLONASS)
Serial Number : (A5)
Firmware Version : (A11)
Elevation Cutoff Setting : (deg)
Date Installed : (CCYY-MM-DDThh:mmZ)
Date Removed : (CCYY-MM-DDThh:mmZ)
Temperature Stabiliz. : (none or tolerance in degrees C)
Additional Information : (multiple lines)

4. GNSS Antenna Information

4.1 Antenna Type : LEIAT504 SCIT
Serial Number : 102752
Antenna Reference Point : BPA
Marker->ARP Up Ecc. (m) : 0.0083
Marker->ARP North Ecc(m) : 0.0
Marker->ARP East Ecc(m) : 0.0
Alignment from True N : 0.0
Antenna Radome Type : SCIT
Radome Serial Number : 678
Antenna Cable Type :
Antenna Cable Length :
Date installed : 2005-03-15T00:00Z
Date removed : CCYY-MM-DDThh:mmZ
Additional Information :

4.x Antenna Type : (A20, from rcvr_ant.tab; see instructions)
Serial Number : (A*, but note the first A5 is used in SINEX)
Marker->ARP Up Ecc. (m) : (F8.4)
Marker->ARP North Ecc(m) : (F8.4)
Marker->ARP East Ecc(m) : (F8.4)
Alignment from True N : (deg; + is clockwise/east)
Antenna Radome Type : (A4 from rcvr_ant.tab; see instructions)
Radome Serial Number :
Antenna Cable Type : (vendor & type number)
Antenna Cable Length : (m)
Date Installed : (CCYY-MM-DDThh:mmZ)
Date Removed : (CCYY-MM-DDThh:mmZ)
Additional Information : (multiple lines)

8. Meteorological Instrumentation

8.1.x Humidity Sensor Model :
Manufacturer :
Serial Number :
Data Sampling Interval : (sec)
Accuracy : (hPa)
Height Diff to Ant : (m)
Calibration date : (CCYY-MM-DD)
Effective Dates : (CCYY-MM-DD/CCYY-MM-DD)
Notes : (multiple lines)

8.2.x Pressure Sensor Model :
Manufacturer :
Serial Number :
Data Sampling Interval : (sec)
Accuracy : (hPa)
Height Diff to Ant : (m)

Calibration date : (CCYY-MM-DD)
Effective Dates : (CCYY-MM-DD/CCYY-MM-DD)
Notes : (multiple lines)

8.3.x Temp. Sensor Model :
Manufacturer :
Serial Number :
Data Sampling Interval : (sec)
Accuracy : (hPa)
Aspiration : (UNASPIRATION/NATURAL/FAN/etc)
Height Diff to Ant : (m)
Calibration date : (CCYY-MM-DD)
Effective Dates : (CCYY-MM-DD/CCYY-MM-DD)
Notes : (multiple lines)

8.4.x Water Vapor Radiometer :
Manufacturer :
Serial Number :
Distance to Antenna : (m)
Height Diff to Ant : (m)
Calibration date : (CCYY-MM-DD)
Effective Dates : (CCYY-MM-DD/CCYY-MM-DD)
Notes : (multiple lines)

8.5.x Other Instrumentation : (multiple lines)

10. Local Episodic Effects Possibly Affecting Data Quality

11. On-Site, Point of Contact Agency Information

Agency : Istituto Nazionale di Geofisica e Vulcanologia Osservatorio di Grottaminarda
Preferred Abbrevation : INGV
Mailing Address : via Castello Aquino 13, 83035 Grottaminarda (AV)
Primary Contact
Contact Name : Antonio Avallone
Telephone (primary) : ++39-0825-421925
Telephone (secondary) :
Fax : ++39-0825-421937
E-mail : avallone@gm.ingv.it
Secondary Contact
Contact Name : Giulio Selvaggi
Telephone (primary) : ++39-06-51860410
Telephone (secondary) :
Fax : ++39-06-51860541
E-mail : selvaggi@ingv.it
Additional Information :

12. Responsible Agency (if different from 11.)

Agency :
Preferred Abbrevation :
Mailing Address :
Primary Contact
Contact Name :
Telephone (primary) :
Telephone (secondary) :
Fax :
E-mail :
Secondary Contact
Contact Name :

Telephone (primary) :
Telephone (secondary) :
Fax :
E-mail :
Additional Information :

13. More Information

Primary Data Center :
Secondary Data Center :
URL for More Information :
Hardcopy on File
Site Map : (Y or URL)
Site Diagram : (Y or URL)
Horizon Mask : (Y or URL)
Monument Description :
Site Pictures :
Additional Information : (multiple lines)
Antenna Graphics with Dimensions

LEIAT504 L1/L2 DORME MARGOLIN ANTENNA WITH CHOKE-RING

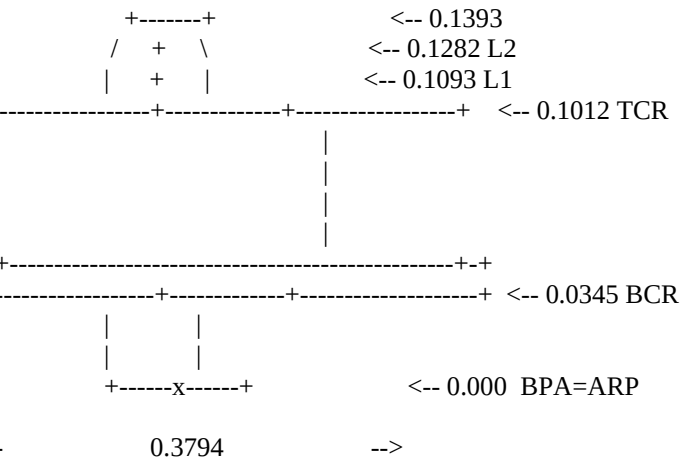

ARP: Antenna Reference Point
L1 : L1 Phase Center L2 : L2 Phase Center
TCR: Top of Chokering BCR: Bottom of Chokering
TGP: Top of Ground Plane BGP: Bottom of Ground Plane
TPA: Top of Preamplifier BPA: Bottom of Preamplifier
TOP: Top of Pole

All dimensions are in meters.

C.2 GPS permanent station SOFA

C.2.1 Photos

Figure C.2. *Station monument of SOFA*